

**TOWARDS IMPROVED ETHANOL
PRODUCTION FROM
LIGNOCELLULOSIC BIOMASS**

Cristian Fernando Triana

November 2016

**A thesis submitted for the degree of
Doctor of Philosophy of the University College London**

Department of Chemical Engineering

University College London

I, Cristian F. Triana, confirm that the work presented in this thesis is my own. Where information has been derived from other sources, I confirm that this has been indicated in the thesis.

Cristian F Triana C

ABSTRACT

Ethanol from biological feedstock has emerged as a promising alternative for the generation of energy from renewable sources in order to mitigate the damages caused by the gas emissions associated to the consumption of fossil fuels. In many countries, ethanol is already being produced at industrial scale from different biological raw materials. However, there are some technical issues related to this process that need to be addressed and one of the major problems is the high heat requirements which makes this process less competitive against well-established fuels.

This work proposes an optimisation methodology based on a dynamic approach to improve the overall efficiency of the process by considering new configurations and designs that allow the reduction of operating costs, usage of utilities, the size of units, etc. The work initially provides an introduction to the concept of fuels and the current global scenario regarding their production and consumption. Next, a general review of biofuels is given, in particular the production of ethanol from corn stover and the different units involved in this process. Additionally, mathematical formulations of the different units in the process are presented including detailed kinetic models and dynamic mass and energy balances. These models are first validated and then used in the construction of an overall model of the entire process which so far has not been available in open literature. This thesis also presents the development of an empirical mathematical model of an organophilic membrane for ethanol removal from aqueous solutions to increase the separation rates of ethanol in the process.

Finally, this work presents the optimisation of the ethanol production process considering the implementation of heat storage units to reduce the consumption of utilities such as steam and cooling water by reducing the Total Annualised Cost (TAC). The results obtained show that the implementation of heat integration in the process can achieve a reduction of 7 % in the TAC and 10 % in the total energy consumption. These results indicate that ethanol production from corn stover with the use of energy storage is a viable alternative for energy generation that can become part of the main market of the production of green technologies.

ACKNOWLEDGEMENTS

I would like to start this off by saying thanks to my family: My mom, my sister and my nephew. You have been the strength and the motivation to keep on working and doing what I am doing. You have shared my achievements and failures and never stopped supporting me and believing in me.

I would like to express my gratitude to my supervisors who supported, encouraged and contributed greatly in the development of this work and to my academic progress. First, to Professor Eric Fraga who helped me a lot during my application process to UCL and who always challenged me to be more confident about my work and how to present my results. And to Professor Eva Sorensen for her great support in many aspects related to education, especially, for introducing me to different scenarios in which I met great people, I saw great places and I was allowed to present my work to different audiences.

Special thanks to Professor Andrzej Górak and to Dr Philip Lutze for giving me the opportunity of working with them for 4 months at the Laboratory of Fluid Separations (FVT) at TU Dortmund. I would also like to thank Ms Kathrin Kissing and Dr Johannes Holtbrügge for the technical support provided during the development of my experimental work in Dortmund.

I would like to acknowledge the financial support of the Colombian Institute of Science and Innovation (COLCIENCIAS) and the Engineering and Physical Sciences Research Council (EPSRC) that made this research possible. Conference funding from UCL Graduate School and IChemE Fluid Separation Subject Group is also greatly acknowledged.

Finally, to my friends: Andres Calderon, Masha Koleva, Carlos Perez, Alexandros Adam, Adrian Aguirre, Joakim Beck, Harry Christodoulou, Ben Dercks, Alexa Duarte, Juan Carlos Uribe, Anna Kunze, Davide Bascone, David Lorenzo, Juan Pablo Mariscal, Sebastian Siegert, Dr. Javier Fontalvo, Euan Corral and all the funky crew from the Elephants Head and the IoE.

Table of contents

Abstract	4
Acknowledgements	5
List of tables	10
List of figures	14
Chapter 1 – Ethanol production process from lignocellulosic biomass	19
1.1 Introduction	19
1.2 Economics	20
1.3 Biofuels	23
1.4 Ethanol	25
1.5 Lignocellulosic biomass	26
1.6 Current outlook for biofuels	28
1.7 Summary	31
1.8 Aims	31
1.9 Organisation	31
Chapter 2 – Literature review	33
2.1 Introduction	33
2.2 General aspects of the ethanol production process from lignocellulosic biomass	34
2.3 Pretreatment	36
2.4 Detoxification	41
2.5 Enzymatic hydrolysis	42
2.5.1 Enzymatic activities	42
2.5.2 Enzymatic mechanism	43
2.6 Fermentation	45
2.7 Separation processes	50
2.8 Heat integration and heat storage	51
2.9 Summary and research statement	57
Chapter 3 – Mathematical models and model validation	60
3.1 Introduction	60
3.2 Process description	62
3.3 Dilute acid pretreatment	62

3.4	Evaporation	67
3.5	Detoxification	67
3.6	Simultaneous saccharification and co-fermentation (SSCF)	69
3.6.1	Enzymatic hydrolysis	69
3.6.2	Co-fermentation	71
3.7	Separation	74
3.7.1	Distillation	74
3.7.2	Membrane-based operation	74
3.8	Results	75
3.9	Pretreatment stage	76
3.10	Detoxification stage or Overliming	77
3.11	Enzymatic hydrolysis stage	77
3.12	Co-fermentation stage	80
3.13	Distillation stage	81
3.14	Pervaporation stage	81
3.15	Conclusions	81
Chapter 4 – Ethanol recovery from aqueous solutions using a PERVAP™ 4060 organophilic membrane		83
4.1	Introduction	83
4.2	Experimental materials and methods	85
4.2.1	Materials	86
4.2.2	Membrane and module	87
4.2.3	Gas chromatography	91
4.3	Experimental procedure	92
4.4	Modelling	94
4.4.1	Approach	94
4.4.2	Pure component and mixture property models	95
4.4.3	Models for permeance	95
4.5	Results	97
4.5.1	Model discrimination	98
4.6	Conclusions	111
Chapter 5 – Optimisation of the separation section of the ethanol production process		113

5.1	Introduction	113
5.2	Design of distillation columns	114
5.2.1	Shortcut methods	115
5.2.2	Group methods	115
5.2.3	Rigorous tray-by-tray optimisation models	116
5.3	Optimisation of a distillation system	116
5.3.1	Specifications of the distillation columns	123
5.3.2	Results of the optimisation of the distillation system	125
5.4	Optimisation of the pervaporation system using a PAN-B5 hydrophilic membrane	127
5.4.1	Specifications of the pervaporation network using a hydrophilic membrane	131
5.4.2	Results of the optimisation of the pervaporation network using a hydrophilic membrane	132
5.5	Optimisation of the pervaporation system using a PERVAPTM 4060 organophilic membrane	138
5.5.1	Specifications for the pervaporation network using an organophilic membrane	140
5.5.2	Results of the optimisation of the pervaporation network using an organophilic membrane	141
5.6	Optimisation of the complete separation section – Case study	150
5.6.1	Specifications of the separation section	150
5.6.2	Results of the separation sections	151
5.7	Sensitivity analysis	155
5.8	Conclusions	163
	Chapter 6 – Heat integration across an ethanol production process	166
6.1	Introduction	166
6.1.1	Direct heat integration (DHI)	167
6.1.2	Indirect heat integration (IHI)	168
6.1.3	Mixed direct-indirect heat integration (MDIHI)	169
6.2	Heat transfer fluids	169
6.3	Simulation procedure	172
6.3.1	Configuration of the ethanol process without heat storage	172

6.3.2	First superstructure of the ethanol production process with heat storage	179
6.3.3	Second superstructure of the ethanol production process with heat storage	183
6.4	Results	184
6.4.1	Specifications	184
6.4.2	Optimisation results – pretreatment stages	185
6.4.3	Optimisation results – separation section	190
6.4.4	Optimisation results – energy demand and economic analysis	195
6.5	Conclusions	196
Chapter 7 – Conclusions and future work		200
7.1	Conclusions	200
7.2	Future work	203
List of publications and events		206
REFERENCES		207
NOMENCLATURE		232
Appendix A – Kinetic models, mass and energy balances for the production of ethanol from corn stover		235
A.1	Pretreatment	235
A.2	Detoxification	237
A.3	Evaporation	238
A.4	Simultaneous saccharification and co-fermentation (SSCF)	239
A.4.1	Saccharification	239
A.4.2	Simultaneous saccharification and co-fermentation	240
A.5	Distillation column	244
A.5.1	Tray	244
A.5.2	Condenser	246
A.5.3	Drum	247
A.5.4	Reboiler	248
A.5.5	Tray section	249
A.6	Membrane system	251
A.6.1	Fibre side	251
A.6.2	Shell side	252

List of tables

Table 1.1: Energy densities for some biofuels (Drapcho et al., 2008)	25
Table 1.2: Cellulose, hemicellulose and lignin content in agricultural residues (% w/w dry basis)	29
Table 1.3: Cellulose, hemicellulose and lignin content in by-products of agricultural processes (% w/w dry basis)	29
Table 1.4: Cellulose, hemicellulose and lignin content in crops for energy generation (% w/w dry basis)	30
Table 2.1: Pretreatment methods for lignocellulosic materials	38
Table 2.2: Literature review on the pretreatment of lignocellulosic biomass for ethanol production	39
Table 2.3: Enzymes used in conversion of cellulose into glucose	44
Table 2.4: Use of enzymatic hydrolysis in the production of glucose and other reducing sugars from cellulose	46
Table 2.5: Microorganisms used in ethanol production	47
Table 2.6: Recent experimental works related to the implementation of the SSCF process in the production of ethanol from lignocellulosic biomass	48
Table 2.7: Separation methods used in the dehydration of ethanol	52
Table 3.1: Chemical characterisation of corn stover (dry basis % w/w) reported by Bhandari et al., (1984); Čuček et al., (2011); Esteghlalian et al., (1997) and Liu and Chen, (2016)	65
Table 3.2: Estimated ethanol purity for an ethanol feed concentration of 94% (w/w)	80
Table 4.1: Operating conditions used in the experiments	87
Table 4.2: List of components produced during the fermentation of lignocellulosic hydrolysates	89
Table 4.3: Specifications for the optimal operation of the PERVAP™ 4060 membrane (Sulzer Chemtech, 2014)	91
Table 4.4: Experimental results for the removal of ethanol from aqueous solutions using the PERVAP™ 4060 membrane	100
Table 4.5: Partial fluxes of ethanol and water under the influence of different impurities at 40 °C and a permeate pressure of 20 mbar	101

Table 4.6: Parameters of the mathematical model of the organophilic membrane	102
Table 4.7: Model validation using additional experimental data	105
Table 4.8: Lack-of-fit test for the parameter estimation of the membrane model	105
Table 4.9: Parameter estimation problem for the permeance of ethanol and water using Eq. 4.3	108
Table 4.10: Parameter estimation problem for the permeance of ethanol and water using Eq. 4.4	109
Table 4.11: Parameter estimation problem for the permeance of ethanol and water using Eq. 4.5	110
Table 5.1: Input variables used in the optimisation of the distillation systems	124
Table 5.2: Initial guesses and bounds used in the optimisation of the distillation systems	126
Table 5.3: Results of the optimisation of the distillation systems	126
Table 5.4: Input variables used in the optimisation of the pervaporation system using the PAN-B5 hydrophilic membrane	131
Table 5.5: Initial guesses and bounds used in the optimisation of the PAN-B5 hydrophilic membrane	132
Table 5.6: Optimal parameters for a minimum TAC in the PAN-B5 hydrophilic membrane system	135
Table 5.7: Input variables used in the optimisation of the pervaporation system using the PAN-B5 hydrophilic membrane	140
Table 5.8: Initial guesses and bounds used in the optimisation of the PAN-B5 hydrophilic membrane	140
Table 5.9: Optimal parameters for a minimum TAC in the PERVAP 4060TM organophilic membrane system	142
Table 5.10: Input variables used in the optimisation of the distillation column linked to the organophilic membrane system	143
Table 5.11: Results of the optimisation of the distillation systems using the permeate stream of the pervaporation system shown in Figure 5.15 as feed	144
Table 5.12: Initial guesses and bounds used in the optimisation of the PAN-B5 hydrophilic membrane in the configuration with the organophilic	146

membrane	
Table 5.13: Initial guesses and bounds used in the optimisation of the PAN-B5 hydrophilic membrane	147
Table 5.14: Optimal parameters for a minimum TAC in the pervaporation network using the distillate stream of the single distillation column shown in Figure 5.13	147
Table 5.15: Input variables used in the optimisation of the separation section with and without the organophilic membrane	150
Table 5.16: Results of the optimisation of the superstructures of the separation stages of the ethanol production process	154
Table 5.17: Case studies considered in the optimisation of the separation section	156
Table 5.18: Sensitivity analysis of the separation section	158
Table 6.1: List of heat transfer fluids (Vignarooban et al., 2015)	170
Table 6.2: List properties of Therminol 66 (Eastman, 2016)	173
Table 6.3: Initial guesses used in the optimisation of the process with and without heat integration	183
Table 6.4: Operating conditions for the reactors and evaporator	183
Table 6.5: Optimal results of the pretreatment stages for all the configurations	185
Table 6.6: Results of the optimisation of the pretreatment stages and composition of the process streams (% w/w)	188
Table 6.7: Results of the optimisation of the separation stages without heat storage (membrane area of 500 m ²)	191
Table 6.8: Results of the optimisation of the separation stages in Superstructure 1 (membrane area of 500 m ²)	191
Table 6.9: Results of the optimisation of the separation stages in Superstructure 2 (membrane area of 500 m ²)	192
Table 6.10: Energy requirements for the different configurations of the ethanol process (kW)	193
Table 6.11: Economic analysis for equipment used in the ethanol production process 1x10 ³ (US\$/year)	194
Table 6.12: Economic analysis for utilities and services used in the ethanol	194

production process 1×10^3 (US\$/year)

Table 6.13: Area and cost for heat exchangers in all configurations

195

List of Figures

Figure 1.1: Global oil consumption since 2004 (U.S. Department of Energy, 2015)	20
Figure 1.2: Spot crude prices since 2004 (BP, 2016a)	20
Figure 1.3: Global consumption and production of natural gas since 2004 (U.S. Department of Energy, 2016)	22
Figure 1.4: Global consumption and production of coal since 2004 (BP, 2016a, 2012; U.S. Department of Energy, 2015)	22
Figure 2.1: Standard configuration for ethanol production	35
Figure 2.2: Configuration of the ethanol production process from lignocellulosic biomass considering two fermentation stages	37
Figure 2.3: Configuration of the ethanol production process from lignocellulosic biomass considering co-fermentation of both pentoses and hexoses	37
Figure 2.4: Configuration of the ethanol production process from lignocellulosic biomass considering simultaneous saccharification and co-fermentation (SSCF)	37
Figure 2.5: Liquid-Vapour Equilibrium (VLE) calculated using ChemCAD for the mixture ethanol/water at 1 atm	50
Figure 3.1: Flowsheet of the ethanol production process from corn stover	64
Figure 3.2: Xylose remaining in the solid fraction in the hydrolysis of hemicellulose. The left side represents the results obtained with gPROMS. The right side is the experimental data presented by Esteghlalian et al., (1997)	78
Figure 3.3: Model validation for the detoxification of acid hydrolysates. The left side shows the results using gPROMS. The right side shows the experimental data obtained by Purwadi et al., (2004)	78
Figure 3.4: Validation of the kinetic model for enzymatic saccharification. The left side presents the results using gPROMS. The right side presents the experimental data presented by Kadam et al., (2004)	79
Figure 3.5: Validation of the fermentation model proposed by Leksawasdi et al., (2001). The left side presents the results using gPROMS. The right side	79

presents the experimental data	
Figure 3.6: Validation profile for liquid weight fraction of binary mixture ethanol/water using gPROMS and ChemCAD	80
Figure 4.1: Experimental design for the evaluation of the parameters of the mathematical model of the PERVAPTM 4060 membrane (C = feed concentration, T = feed temperature, P = permeate pressure)	87
Figure 4.2: Simplified flowsheet of the laboratory-scale set-up for pervaporation experiments. (1) Feed tank, (2) Heat exchanger, (3) Membrane module, (4) Thermal oven, (5) Cooling traps, (6) Vacuum pump, (7) Exhaust, (8) Heating cabinet and (9) Back-pressure regulator	88
Figure 4.3: Pervaporation plant	90
Figure 4.4: Membrane module	90
Figure 4.5: Thermal oven	90
Figure 4.6: Jacketed tank	90
Figure 4.7: Cooling traps	90
Figure 4.8: Partial flux for ethanol and water using the different formulations proposed in Equations 4.3 to 4.5	105
Figure 4.9: Parity plots with the fitted parameters for ethanol (top) and water (bottom) using: (a) Eq. 4.3, (b) Eq. 4.4, (c) Eq. 4.5, (d) Eq. 4.3, (e), Eq. 4.4, (f) Eq. 4.5	107
Figure 5.1: Sections of the distillation column used in the rigorous tray-by-tray optimisation	117
Figure 5.2: a) Rectification section with side reflux stream and b) stripping section with side boilup stream	117
Figure 5.3: Configurations for the distillation system considered in this work: a) single distillation column and b) double distillation system with mixed waste	119
Figure 5.4: Outer Approximation (OA) algorithm for the solution of the MINLP problem using gPROMS (Process System Enterprises, 2015)	124
Figure 5.5: Streams and concentrations in a single distillation column using the results of the optimisation presented in Table 5.3	128
Figure 5.6: Streams and concentrations in a double-column distillation system using the results of the optimisation presented in Table 5.3	128

Figure 5.7: Pervaporation network design using PAN-B5 hydrophilic membrane	129
Figure 5.8: Optimisation of the hydrophilic pervaporation system at different membrane areas for the system consisting of a single distillation column shown in Figure 5.5	133
Figure 5.9: Comparison of total annualised cost vs. energy consumption for three and four in-series pervaporation stages shown in Figure 5.8	134
Figure 5.10: Results of the optimisation of the pervaporation network using PAN-B5 hydrophilic membrane and a membrane area of 250 m ² for the distillation system shown in Figure 5.5	137
Figure 5.11: Pervaporation network design using PERVAP TM 4060 organophilic membrane	139
Figure 5.12: Results of the optimisation of the pervaporation network using PERVAP TM 4060 organophilic membrane and a membrane area of 20 m ² and 19 in-parallel modules	143
Figure 5.13: Results of the optimisation of the distillation column under the specifications presented in Table 5.10	145
Figure 5.14: Optimisation of the hydrophilic pervaporation system at different membrane areas for the system consisting of a single distillation column shown in Figure 5.13	145
Figure 5.15: Results of the optimisation of the pervaporation network using PAN-B5 hydrophilic membrane and a membrane area of 150 m ² for the distillation system shown in Figure 5.14	149
Figure 5.16: Superstructure of the separation section of the ethanol production process: a) single distillation and pervaporation network with PAN-B5 hydrophilic and b) pervaporation network with PERVAP TM organophilic membrane linked to a single distillation column and a pervaporation network with PAN-B5 hydrophilic membrane	149
Figure 5.17: Results of the optimisation of the separation section with a PAN-B5 hydrophilic membrane area of 250 m ²	152
Figure 5.18: Results of the optimisation of the separation section including a PERVAP TM 4060 organophilic membrane with 19 in-parallel membrane modules with an area of 20 m ² and a PAN-B membrane with a membrane	153

area of 150 m²

Figure 5.19: Case 1 - Results of the optimisation of the separation section of the ethanol production process with the PERVAP™ 4060 organophilic membrane considering a feed concentration of ethanol of 4 % (w/w)	160
Figure 5.20: Case 2 - Results of the optimisation of the separation section of the ethanol production process with the PERVAP™ 4060 organophilic membrane considering a feed concentration of ethanol of 6 % (w/w)	161
Figure 5.21: Case 3 - Results of the optimisation of the separation section of the ethanol production process with the PERVAP™ 4060 organophilic membrane considering a concentration of ethanol in the distillate stream of 90 % (w/w)	162
Figure 5.22: Evaluation of the minimum TAC of the separation section with and without the organophilic membrane considering different cases studies	163
Figure 6.1: Flowsheet of the ethanol production process from corn stover without heat integration	175
Figure 6.2: Superstructure 1 of the ethanol production process from corn stover with heat storage (using the bottom stream from the distillation column to heat the stream of Therminol 66)	182
Figure 6.3: Superstructure 2 of the ethanol production process from corn stover with heat storage using the heat released in the condenser to heat the stream of Therminol 66	186
Figure 6.4: Results of the simulation and optimisation of the pretreatment stages of the ethanol production process	187
Figure 6.5: Results of the optimisation of the separation stages without heat storage	182
Figure 6.6: Results of the simulation and optimisation of the separation stages with heat storage (Superstructure 1)	189
Figure 6.7: Results of the simulation and optimisation of the separation stages with heat storage (Superstructure 2)	190
Figure 6.8: Temperatures of heat transfer fluid Therminol 66 across Superstructure 1	198
Figure 6.9: Temperatures of heat transfer fluid Therminol 66 across Superstructure 2	199

Figure 7.1: Flowsheet of possible scenarios for the optimisation of the separation section	204
Figure A.1: Scheme of a jacketed reactor used in the formulation of the mass and energy balances	236
Figure A.2: Scheme of a jacketed reactor used in the formulation of the mass and energy balances	241
Figure A.3: Schematic of a distillation column tray	245
Figure A.4: Flowsheet of the top of the distillation column	246
Figure A.5: Schematic of a Kettle reboiler	247
Figure A.6: Schematic of the membrane module (Marriott and Sorensen, 2003; Marriott et al., 2001; Tsuyumoto et al., 1997)	251

Chapter 1 – Ethanol production process from lignocellulosic biomass

Abstract

This chapter presents a report on the production and consumption of fuels around the world. This information shows an increase in the consumption of traditional fuels in the last years by the countries of the Convention on the Organization for Economic Co-operation and Development (OECD). The elevated consumption of sources such as oil and coal has not only impacted global economy but also, the environment. This chapter presents a breakdown of the different biofuels that are currently produced around the world and the different raw materials used in their production, focusing mainly on the production of ethanol from lignocellulosic biomass.

1.1 Introduction

The population in this planet keeps on increasing at elevated rates and this only represents a challenge for world's leaders and their governments in the search for efficient paths to provide food, healthcare and services to their people. However, the ever-increasing populace not only denotes a problem in terms of food and healthcare but also in terms of the energy demand that is necessary to maintain the gears of development and industrialisation well-greased. Energy has become a priority in every country due to its great influence in the creation of jobs, the modernisation of infrastructure, military, politics, etc. (Cardona and Sánchez, 2007; Drapcho et al., 2008; Hoekman, 2009). Therefore, a summary of the current state of fuels is presented in this chapter and the trends in their prices and consumption throughout the years. This chapter will also include the production of biofuels as an alternative to conventional energy sources leading to the selection of ethanol as the fuel of choice for the development of this thesis. Finally, this chapter will cover the different raw materials used in the production of ethanol via fermentation and the different units involved therein (e.g. reactors, evaporators, distillation columns, etc.).

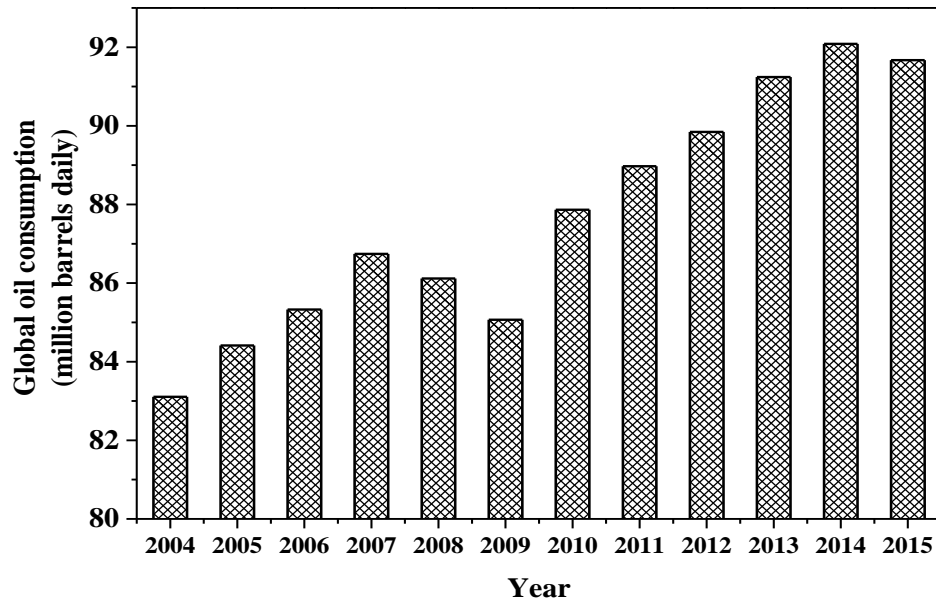


Figure 1.1: Global oil consumption since 2004 (U.S. Department of Energy, 2015)

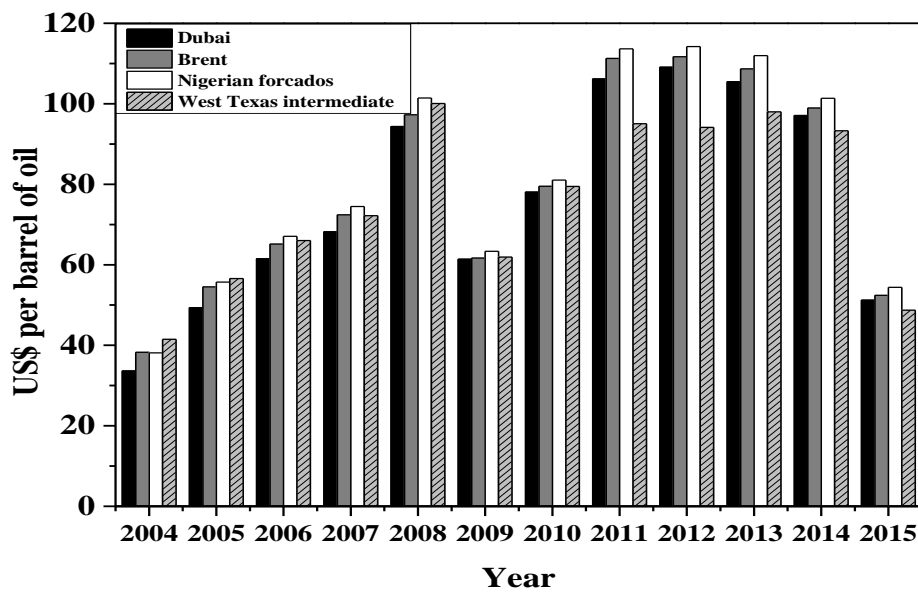


Figure 1.2: Spot crude prices since 2004 (BP, 2016a)

1.2 Economics

In emerging economies, the net energy consumption in 2015 increased significantly since 2004 (see Figure 1.1) with China alone accounting for 71% of global energy consumption growth. The consumption in the countries of the Convention on the Organization for Economic Co-operation and Development (OECD), which include EU countries, Canada, Turkey, Japan and the US, declined, led by a sharp drop in Japan which in volumetric terms was the world's largest decline (BP, 2012; U.S.

Department of Energy, 2015). The data reported by both BP and the U.S. Department of Energy suggest that the growth in global CO₂ emissions from energy use continued in 2015, but at a slower rate than back in 2010 (BP, 2016a; U.S. Department of Energy, 2015). Crude oil prices peaked in April 2011 following the loss of Libyan supplies and decreases of 9.7% were reported from 2013 to 2014. In 2015, the prices of oil plummeted approximately 47 % (BP, 2016a) (see Figure 1.2).

Natural gas prices in Europe and Asia – including spot markets and those indexed to oil – presented a noticeable increase along with oil prices, although movements within the year varied widely. North American prices reached record discounts to both crude oil and international gas markets due to continued robust regional production growth (Demirbas, 2007; Hoekman, 2009). Countries outside the OECD once again accounted for all of the net growth in global consumption. Chinese consumption growth, for instance, was below average but still recorded the largest increment to global oil consumption with 390,000 barrels/day (an increment of 2.1 % from 2013 to 2015). The global consumption of natural gas in 2015 increased only 0.4 % from 2013 and with an average price reduction in some OECD countries of 8.7 %. Figure 1.3 shows the global consumption and production of natural gas reported by the U.S. Energy Information Administration.

Global coal consumption fell by 1.8% in 2015, well below the 10-year average annual growth of 2.1% and the largest reported decline thus far (see Figure 1.4). The entire net decline was accounted for by the US (-12.7%, the world's largest volumetric decline) and China (-1.5%), partially offset by modest increases in India (+4.8%) and Indonesia (+15%). Coal's share of global primary energy consumption fell to 29.2%, the lowest share since 2005, (BP, 2016a)

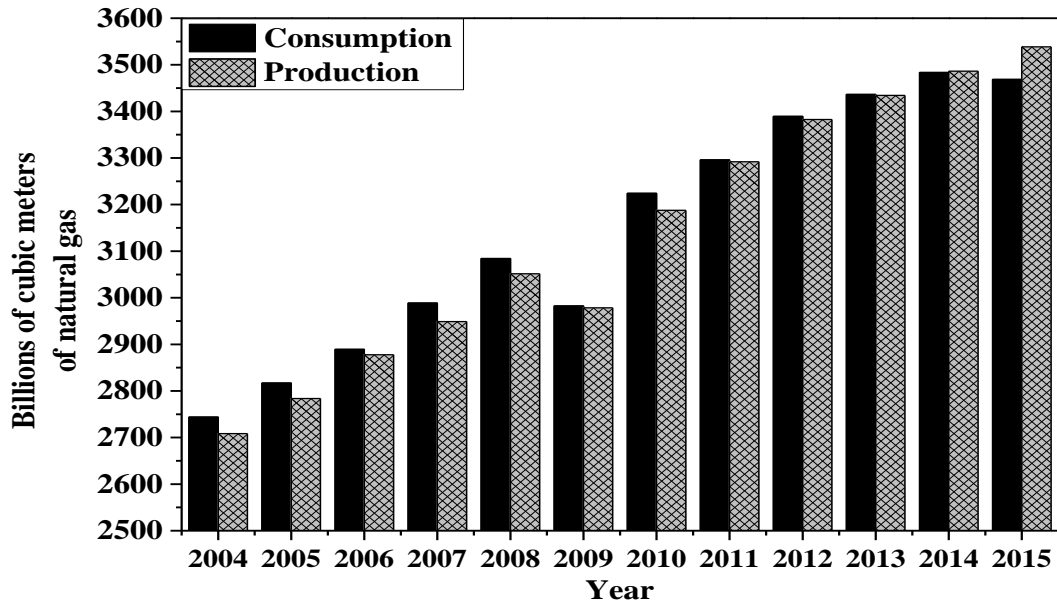


Figure 1.3: Global consumption and production of natural gas since 2004 (U.S. Department of Energy, 2016)

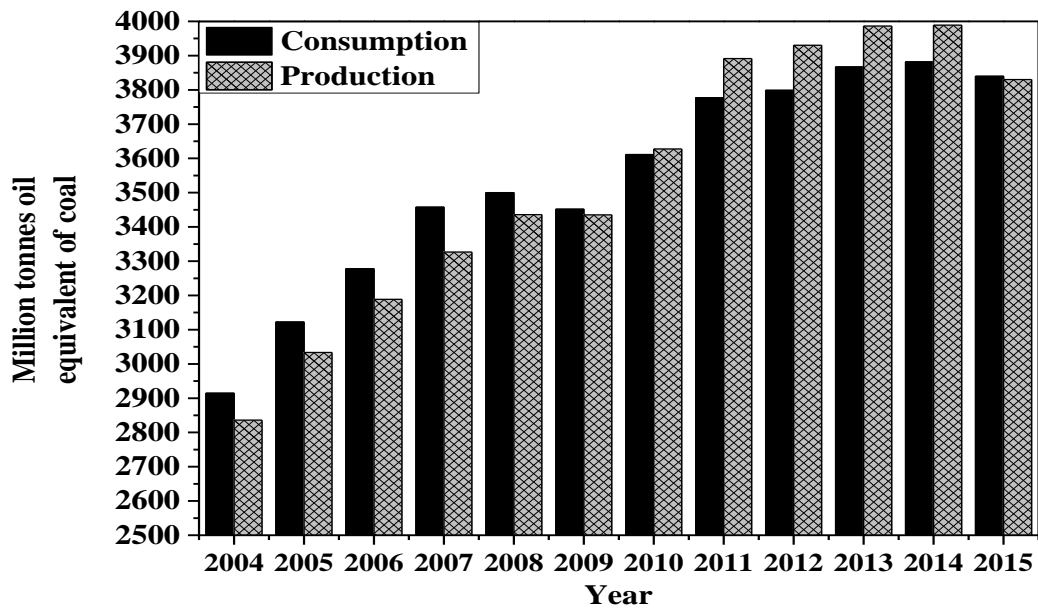


Figure 1.4: Global consumption and production of coal since 2004 (BP, 2016a, 2012; U.S. Department of Energy, 2015)

These statistics suggest that traditional energy sources (i.e. oil, natural gas, coal, etc.) are changing in unpredictable ways which directly impact several aspects of society (economics, foreign politics, culture, etc.). Also, the means to obtain these fuels and their consumption are believed to be detrimental to the environment. Several alternatives for the reduction of toxic gas emissions to the atmosphere have been proposed, but yet, fossil fuels are currently the most used energy sources in the world

(Escobar et al., 2009; Hoekman, 2009; Rašković et al., 2010). However, BP also refers to a global increase of 7% in the production of renewable sources in their report of June 2016 and an increase in the total world consumption of 11%, a trend that has persisted for the last 10 years (BP, 2016a; Koizumi, 2015; U.S. Department of Energy, 2015).

1.3 Biofuels

The production of biofuels has been proposed as a sustainable alternative for energy generation in order to reduce the usage of fossil fuels whose emissions are believed to be the main cause of global warming and the so-called “greenhouse effect” (Balat et al., 2008; Cardona et al., 2010; Demirbas, 2007). Biofuels make reference to the compounds whose origins are a manifestation of the capture and storage of solar energy through photosynthetic reactions (Raman et al., 2015). In the case of vegetable forms such as plants and algae, the oils are products of photosynthesis (Drapcho et al., 2008; Karlsson et al., 2014; Sánchez and Cardona, 2012). There are several forms of biofuels such as biodiesel which are a direct product of chemically transesterified oils, alcohols and alkanes which can be produced from organic substrates via anaerobic fermentation and biofuels like hydrogen that can be produced using chemical and biological routes (Cardona et al., 2010; Demirbas, 2007; Drapcho et al., 2008; Hoekman, 2009).

Biofuels are classified according to their source and type: primary and secondary biofuels. Primary biofuels are usually used in an unprocessed form, mainly for heating, cooking or electricity generation. These primary biofuels include hard and soft wood, wood chips and pellets, etc. (Drapcho et al., 2008; Escobar et al., 2009). They are often found as by-products in processes such as deforestation, agriculture, fishery products, municipal wastes, food industry and food services (Cardona et al., 2010; Drapcho et al., 2008; Felix and Tilley, 2009).

Secondary biofuels are the result of the conversion of biopolymers found in the raw material through biological paths such as anaerobic metabolism or fermentation (Siqueira et al., 2008; Sreenath et al., 2001; Sreenath and Jeffries, 2000; Triana et al., 2011). Secondary biofuels are further divided into first, second and third generation on the basis of raw material and technology used for their production (Bai et al.,

2008; Balat et al., 2008; Binod et al., 2010; Drapcho et al., 2008). The first generation refers to the biofuels obtained from seeds, grains and sugars via fermentation (e.g. ethanol from molasses or starch, and biodiesel from transesterified seed oils such as soybean oil). The second generation of secondary biofuels are obtained from lignocellulosic biomass (raw material mainly composed by cellulose, hemicellulose and lignin) to produce either ethanol via enzymatic hydrolysis and fermentation, or methane via anaerobic digestion (Balat et al., 2008; Petersson et al., 2007). Finally, the third generation comprises all the biofuels obtained from algae and sea weeds (Nigam, 2001).

Biofuels can be solids such as fuel wood, charcoal, and wood pellets; or liquid, such as ethanol, biodiesel and pyrolysis oils; or gaseous, such as biogas and hydrogen (Cardona and Sánchez, 2007; Drapcho et al., 2008; Nigam, 2001). Table 1.1 shows a comparative study between the different forms of biofuels in terms of the energy density. The information presented in Table 1.1 allows a better understanding about the energy potential that these components possess and how relevant their production is for industrial purposes and for social and economic growth. Hydrogen has the highest energy density of common fuels expressed on a mass basis. Other fuels such as gasoline and biodiesel have energy densities ranging from 40–46 kJ/g. Alcohols, on the other hand, present energy densities in the 20–30 kJ/g range but their combustion is complete (lower concentrations of toxic emissions) (Hoekman, 2009; Reijnders, 2006).

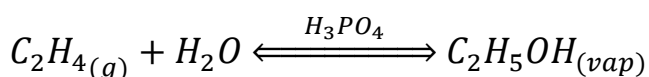
Liquid biofuels are primarily used to fuel vehicles, engines and energy cells for electricity generation. There are several reasons for biofuels to be considered as relevant technologies by both developing and industrialised countries (Hoekman, 2009; Koizumi, 2015; Su et al., 2015). For instance, biofuels represent a potential solution to energy security, environmental concerns, foreign exchange savings, and socioeconomic issues related to the rural sector (Demirbas, 2007; Koizumi, 2015). Additionally, all biofuels have very low sulphur levels and many of them have low nitrogen content which means that no SO_x and very low concentrations of NO_x gases are produced during combustion (Demirbas, 2007; Hoekman, 2009; Nigam, 2001).

Table 1.1: Energy densities for some biofuels (Drapcho et al., 2008)

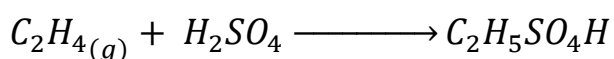
Fuel source	Energy density (kJ/g)
Hydrogen	143.0
Methane	54.0
Biodiesel	46.0
Gasoline	44.0
Soybean oil	40.2
Coal	35.0
Ethanol	29.6
Methanol	22.3
Soft wood	20.4
Hard wood	18.4
Bagasse	17.5

1.4 Ethanol

Ethanol will be considered in this study since it has a wide application in industry (e.g. pharmaceuticals, food and chemical industry). Table 1.1 presents the energy density of some biofuels of industrial application. Ethanol, for instance, shows an energy density of 29.6 kJ/g, which suggests that this biofuel has applicability and potential for a well-established fuel for engines, electricity generation, etc. One of the routes to produce ethanol is the hydration of ethylene in which excess of this gas gets in contact with high pressure and high temperature steam to produce ethanol in a reversible reaction catalysed by Phosphoric Acid (V), also known as synthetic ethanol (Roberts and Caseiro, 1977).



Another route, currently out of circulation for being considered obsolete due to its high energy consumption and low conversion of reactants is the hydration of ethylene using sulphuric acid (Roberts and Caseiro, 1977; Streitwieser and Heathcock, 1976).





Both of these routes are expensive and require high levels of energy (i.e. temperature 300 °C and pressure 60 – 70 atm) and product recovery (the removal of the catalyst and the outlet streams with low pH). Another route and the one that is currently receiving most of the attention is the production of ethanol via fermentation. This method allows the production of ethanol from substrates that mainly consist of reducing sugars such as hexoses and pentoses.

The importance of bioethanol as an alternative source of energy lies on the concept of clean energy which basically means that the production of ethanol should come from renewable sources that allow this technology to be sustainable and environmentally friendly (Fan et al., 2014; Karlsson et al., 2014; Raman et al., 2015; Su et al., 2015). To this date, many countries are producing biofuels. The main producers are USA with approximately 18.3 billion litres followed by Brazil with 17.5 billion litres and China with 1 billion litres on a yearly basis (Baeyens et al., 2015; García et al., 2013; Petrobras, 2016).

The current trend of these countries, and others, is an increasing interest in the use of particular renewable sources for energy generation purposes. The main raw materials for the ethanol production in these countries are sugar cane, molasses and corn, but there are also many other sources available (Hasunuma and Kondo, 2012; Kravanja et al., 2013; Triana et al., 2015a). In this work, the raw material considered for the ethanol production process is lignocellulosic biomass. The variety of lignocellulosic materials is vast, ranging from solid urban waste, agricultural residues, paper pulp, wood etc. However, none of these materials have a direct application in the production of high-added-value products, such as ethanol or other metabolites of industrial application. This work therefore aims to address the use of these materials as potential feedstock for the ethanol production process.

1.5 Lignocellulosic biomass

Traditionally, lignocellulosic biomass has been utilised for direct combustion. However, burning biomass still produces pollutants such as dust and acid rain gases

(e.g. sulphur dioxide and nitrogen oxides). Nevertheless, the amount of sulphur dioxide, for instance, produced during the combustion of biomass is 90% less than the amount produced by burning coal, and the concentration of atmospheric pollutants produced during this process are insignificant in comparison to other pollution sources (Chen and Zhang, 2015; Raman et al., 2015; Saxena et al., 2009). Lignocellulosic biomass comprises all the materials with high content of cellulose and hemicellulose trapped in the cellular walls by lignin. These materials are classified as follows (Drapcho et al., 2008; Escobar et al., 2009; Hahn-Hagerdal et al., 2006; Hoekman, 2009):

- Agricultural residues
- By-products of agricultural processes
- Crops for energy generation

Agricultural residues are the type of lignocellulosic biomass that is generated as a result of processes such as fruit harvesting, seeds, animal wastes and more. These materials are generated in large amounts, are easily accessible and also, fairly inexpensive than other sources of carbon such as molasses and starch (Ballesteros et al., 2004; Kadam et al., 2000; Palmqvist and Hahn-Hagerdal, 2000a). Some examples of these materials and their chemical composition are shown in Table 1.2.

By-products of agricultural processes are the result of processes carried out in order to harvest crops or to renew soil. Sugar cane bagasse is one the most used agricultural residues in ethanol production via fermentation, especially in South America where is being produced in large amounts (Aguilar et al., 2002; Avci et al., 2013). Some other materials are listed in Table 1.3. Crops for energy generation make reference to the crops that are meant to be used only for energy generation and not for human consumption. Table 1.4 shows some examples of these materials and their organic content. In general, the usage of biomass as a source of energy is of interest in the production of biofuels due to the following benefits:

- Lignocellulosic biomass is a renewable, potentially sustainable and relatively environmentally friendly source of energy due to its high organic content

(Abedinifar et al., 2009; Bai et al., 2008; Balat et al., 2008; Ballesteros et al., 2004)

- An increased use of biomass would extend the lifetime of diminishing crude oil supplies (Cardona et al., 2010; Cardona and Sánchez, 2007; Hahn-Hagerdal et al., 2006)
- Lignocellulosic materials are an energy source that could improve economies and energy security (Sanchez and Cardona, 2005; Saxena et al., 2009; Triana et al., 2011)
- The use of lignocellulosic biomass could lead to a reduction on the production and accumulation of carbon dioxide in the atmosphere (Cardona and Sánchez, 2007; Demirbas, 2007; Drapcho et al., 2008)

1.6 Current outlook for biofuels

The ethanol production from lignocellulosic biomass is a process that is still in an early stage of development and requires a great deal of investigation. When considering the implementation of the production of ethanol from lignocellulosic biomass, several aspects need to be taken into account. For example, one of these aspects is the availability of the raw material. Although many countries have functional plants of bioethanol from lignocellulosic biomass, not every country has access to the raw material and this can have a negative impact on the design of the plant as costs related to importation and transportation can increase (Mabee et al., 2011). Another relevant aspect in the design of an efficient plant of ethanol production is the chemical composition of the raw material. Differences in the chemical composition of the lignocellulosic material can affect the yield and the amount of substrate produced during the pretreatment stage, the size of the equipment and the energy requirements which later translates into lower yields of ethanol during fermentation (Hasunuma and Kondo, 2012; Triana et al., 2011).

When considering the applicability of the ethanol production process in industry, another aspect that should be considered is the operating conditions; in order to obtain high yields of ethanol, the enzymes require long periods of time (approximately 60 - 80 hours) to produce the necessary amount of reducing sugars for the subsequent fermentation (Avci et al., 2013; Cara et al., 2007; X. Zhang et al., 2009). Additionally, the fermentation stage also requires long residence times to

reach the desired concentration of the final product. In addition to the residence time, these two stages require pH and temperature conditions that guarantee the survival of the biological agent (Morales-Rodriguez et al., 2012, 2011). In the case of the pretreatment stage, this is one of the most problematic parts of the process, as large amounts of energy are needed to break down the lignin to release the cellulose and hemicellulose (Behera et al., 2010; Davis et al., 2005; Golias et al., 2002; Hahn-Hagerdal et al., 2006; Patle and Lal, 2008; Zhu and Pan, 2010).

Table 1.2: Cellulose, hemicellulose and lignin content in agricultural residues
(% w/w dry basis)

Material	Cellulose	Hemicellulose	Lignin	Reference
Barley straw	36 – 37	17 – 19	12 – 13	(Freer and Detroy, 1983)
Corn stover	36 – 39	21 – 22	19 – 20	(Drapcho et al., 2008; Mielenz et al., 2009)
Rice straw	32 – 47	19 – 27	5 – 24	(Binod et al., 2010; Drapcho et al., 2008; Karimi et al., 2006)
Wheat straw	15 – 40	25 – 35	<8	(Drapcho et al., 2008; Mielenz et al., 2009; Saha et al., 2005)

Table 1.3: Cellulose, hemicellulose and lignin content in by-products of agricultural processes
(% w/w dry basis)

Material	Cellulose	Hemicellulose	Lignin	Reference
Sugar cane bagasse	40 – 45	30 – 35	20 – 30	(Cardona et al., 2010; Carrasco et al., 2011)
Corn fibres	13 – 18	35 – 40	7 – 8	(Noureddini and Byun, 2010; Rasmussen et al., 2010)
Rice husk	15 – 36	12 – 35	8 – 16	(Saha & Cotta 2007; Saha & Cotta 2008)
Soy husk	20 – 51	10 – 20	1 – 4	(Mielenz et al., 2009)

Table 1.4: Cellulose, hemicellulose and lignin content in crops for energy generation
(% w/w dry basis)

Material	Cellulose	Hemicellulose	Lignin	Reference
Hybrid poplar	36 – 37	17 – 19	12 – 13	(Drapcho et al., 2008; H.-J. Huang et al., 2009)
Willow	36 – 39	21 – 22	19 – 20	(Drapcho et al., 2008; H.-J. Huang et al., 2009; Sassner et al., 2008, 2006)
Hay	32 – 47	19 – 27	5 – 24	(Drapcho et al., 2008; Xu et al., 2010)

Alternative configurations based on new technologies have arisen to improve the efficiency of the process. Several authors have suggested a configuration that comprises two saccharification stages (i.e. one to produce xylose from hemicellulose and another one to produce glucose from cellulose), whereas some other authors have considered one unit that combines the fermentation and the enzymatic saccharification (Agbogbo et al., 2006; Ballesteros et al., 2004). Current research is also focusing on the design of new and genetically modified strains, able to grow in the hydrolysates obtained on the stages of saccharification and new separation methods that allow to reduce energy consumption and increase product purity (Bai et al., 2008; Ballesteros et al., 2004; Cardona and Sánchez, 2007; Saxena et al., 2009).

Last but not least, energy consumption within the process has become a relevant aspect. As previously mentioned, most of the units of the process require large amounts of energy to guarantee either a high yield of substrate or a high concentration of the key product in the separation and purification stages. Energy reduction is therefore the main motivation behind this work. The aim is to determine the optimal configuration of the process which will distribute more effectively the required heat within the plant with minimum energy losses, and therefore, with minimum operating costs.

1.7 Summary

This chapter presented an introduction to the concept of energy generation and the different sources used for this purpose. The chapter also conveyed the idea that fossil fuels have become an intrinsic part of society and that their use is directly linked to development and industrialisation. However, as many studies have shown in the last decades, the usage of fossil fuels and the gas emissions associated to their consumption are leading to harmful effects on the ozone layer, which can be observed in the rise of the level of the seas, the melting of glaciers in the poles, droughts, among others. The objective of this chapter was to present a sustainable alternative for energy generation to contribute to the reduction in the utilisation of traditional fossil fuels. The production of ethanol from agricultural residues stands as an interesting proposal for clean energy since the combustion of this alcohol is complete and the concentration of toxic gas emissions significantly lower than in the cases of oil, carbon and natural gas.

1.8 Aims

The main objective of this thesis is to conduct a more comprehensive study based on rigorous optimisation methods to determine the optimal distribution of the heat sources within the ethanol production process considering aspects such as size of the plant, design of the different units and costs. This is a novel approach to reduce energy consumption which considers robust kinetic models, dynamic mass and energy balances, equations of state, activity models, etc. The deliverable of this work can be seen in Chapters 4 through 6.

1.9 Organisation

This thesis consists of seven chapters and an appendix and their organisation is the following:

- Chapter 1: Introduction to the concept of fuels and the current global scenario regarding production and consumption. Chapter 1 also presents a general review of biofuels leading to production of ethanol from lignocellulosic biomass.
- Chapter 2: Updated state-of-the-art for the some works related to the production of ethanol and the different units involved in the process. This

literature survey includes new technologies, methods of production, pretreatment techniques, new strains, etc.

- Chapter 3: Presentation of the mathematical models used in this work and their respective validation.
- Chapter 4: The development of an empirical mathematical model of an organophilic membrane for ethanol removal from aqueous solutions.
- Chapter 5: Optimisation of the separation stages (i.e. distillation and pervaporation) for the mixture ethanol/water.
- Chapter 6: Optimal distribution of the heat sources throughout the process to improve energy efficiency. This chapter presents heat integration of the units as a method to reduce the usage of utilities and therefore the reduction in the overall energy consumption within the process.
- Chapter 7: General conclusions of the thesis emphasising on the objectives achieved. Recommendations for future work are proposed in this chapter which have to show that the PhD work can have continuity and applicability.
- Appendix A: Detailed kinetic models applied to mass and energy balances of the units in the process.

Chapter 2 – Literature review

Abstract

Chapter 2 presents the main stages of the ethanol process and covers some of the most recent publications regarding pretreatment, overliming, enzymatic hydrolysis, fermentation and separation methods. Furthermore, a review of the different approaches on heat integration and optimisation of the ethanol production process will be introduced in order to establish what has already been explored and what is open for investigation.

2.1 Introduction

This chapter intends to convey the importance of a thorough literature review and how it can be useful to set the ground and the direction of modern applications and methodologies for the production of ethanol from lignocellulosic biomass. In this chapter, recent developments and new methods in the pretreatment of lignocellulosic biomass as well as the recent applications for detoxification, enzymatic hydrolysis and fermentation are presented. However, many of these works do not present an analysis of how this specific unit or units affect the entire plant or if they are economically feasible or not. The mathematical models for the reactors as well as for the hydrophilic membrane are taken from literature and modelled and simulated using gPROMS. The models of the distillation column, evaporator and heat exchangers are formulated by the author based on mass and energy balances with their respective correlations for heat transfer and VLE.

The standard configuration for ethanol production consists of four main stages: Pretreatment, enzymatic hydrolysis, fermentation and separation (Drapcho et al., 2008; Sanchez and Cardona, 2005; Sánchez and Cardona, 2012). This work also includes the review of hybrid processes and heat integration. Hybrid processes have emerged as an alternative to improve the efficiency of a plant and reduce costs.

The literature review conducted on this subject shows great advances and interesting results in terms of energy consumption, design and operating conditions in both simulation and experimentation. On the other hand, heat integration for the ethanol process has not been widely studied and few researchers have really focused their effort on this matter in order to improve not only the efficiency of the plant but also the design thereof. The different studies will be further discussed throughout this chapter. This chapter will conclude with the presentation of the research statement which will be useful to establish the deliverables of this thesis and its novelty.

2.2 General aspects of the ethanol production process from lignocellulosic biomass

Figure 2.1 shows the general series of steps in the ethanol production process for any raw material. In the case of ethanol production from lignocellulosic biomass, the raw material consists mainly of cellulose, hemicellulose and lignin. Lignin is a biopolymer whose bonds keep cellulose and hemicellulose trapped in the cellular walls of the material. The pretreatment stage (which usually operates at high temperatures and pressures) basically breaks said bonds and releases hemicellulose and part of cellulose making both biopolymers more susceptible to the action of chemical agents (e.g. acids, bases or enzymes) (Agbogbo et al., 2006; Esteghlalian et al., 1997). The content of the pretreatment reactor is then passed through a filter and divided into two streams: a liquid fraction (rich in reducing sugars) and a solid fraction (mainly unreacted cellulose and other biopolymers).

The solid fraction is then treated with specialised enzymes (e.g. cellulases and β -glucosidases) in order to degrade cellulose into cellobiose, glucose and other hexoses (Bezerra and Dias, 2005; Cara et al., 2007). In some cases and depending on the fermenting strain, other configurations for the ethanol production process can be considered.

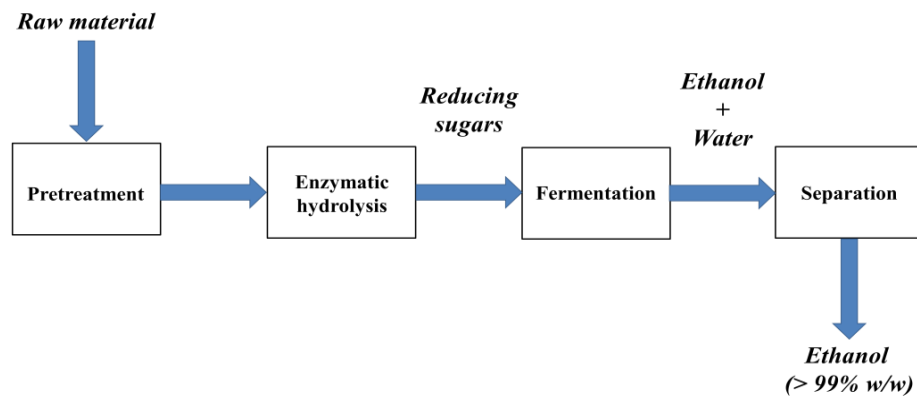


Figure 2.1: Standard configuration for ethanol production

Figure 2.2 shows an arrangement where two fermenters, one for hexoses and one for pentoses, are required (Agbogbo et al., 2006; Krishnan et al., 1999; Olofsson et al., 2008). In Figure 2.2, the fermenting microorganism is not necessarily the same in both fermenters since most natural strains are not capable of assimilating both hexoses and pentoses, simultaneously (Morales-Rodriguez et al., 2011; J. Zhang et al., 2009). Figure 2.3 shows an example of a configuration where specialised strains are utilised in the conversion of both reducing sugars and is known as *separate hydrolysis and fermentation (SHF)* (Abedinifar et al., 2009).

The ethanol production process from lignocellulosic biomass can also be approached by considering a configuration where enzymatic hydrolysis and co-fermentation are combined into a single unit in order to increase the yield of ethanol by reducing the inhibitory effects of substrate over the enzymes and product over the fermenting strains (Ballesteros et al., 2004; Kadar et al., 2004; Morales-Rodriguez et al., 2011). Figure 2.4 shows the configuration for the *simultaneous saccharification and co-fermentation* process (SSCF) (Jin et al., 2012; Su et al., 2012). This configuration is the one to be considered in this work since it combines two processes which already guarantees fewer units in the plant and also contributes to the reduction in the usage of utilities. Other units are also shown in Figure 2.4, including an evaporator which is used to concentrate xylose in the liquid fraction and a detoxification stage where the toxic by-products obtained during the pretreatment are degraded into insoluble salts to reduce their inhibitory effect on the fermenting strains (Purwadi et al., 2004).

Companies such as Petrobras (Brazil), INCAUCA (Colombia), BP (Brazil) use molasses and sugar cane bagasse to produce ethanol at continuous operation of the four main stages (i.e. including pretreatment, fermentation using yeast, two distillation columns and a dehydration section) (BP, 2016b; Incauca, 2016; Petrobras, 2016). The configurations presented in Figures 2.2 to 2.4 are proposed in several works but their implementation in industry still requires further investigation. These configurations also require an environmental analysis which determines the viability of this process and how its residual streams can be treated without causing further pollution.

2.3 Pretreatment

Every lignocellulosic material used in the production of ethanol has to be pretreated in order to reach high levels of conversion of the degradable biopolymers. The purpose of the pretreatment stage is to produce reducing sugars (e.g. glucose and xylose) from cellulose and hemicellulose. The pretreatment of the raw material has to meet the following requirements to guarantee high yields (Abedinifar et al., 2009; Drapcho et al., 2008; Freer and Detroy, 1982):

- Release of the main biopolymers such as cellulose and hemicellulose by degrading lignin
- Production of reducing sugars that can be assimilated by fermenting microorganisms
- Minimisation on the degradation or loss of usable carbohydrates

During the pretreatment, the cellular matrix of the lignocellulosic material is broken, releasing cellulose and hemicellulose. Additionally, the crystallinity of cellulose decreases, making it more susceptible to a further enzymatic attack and, at the same time, the hemicellulose is partially hydrolysed into pentoses (mainly xylose). Table 2.1 shows some of the most employed methods in the pretreatment of lignocellulosic biomass and the production of reducing sugars. The raw material considered in this work is corn stover, which is mainly composed of cellulose, hemicellulose, lignin and some other compounds such as protein and ashes. This raw material is very representative due to its organic content (i.e. the content of degradable biopolymers) and its availability in many countries around the world.

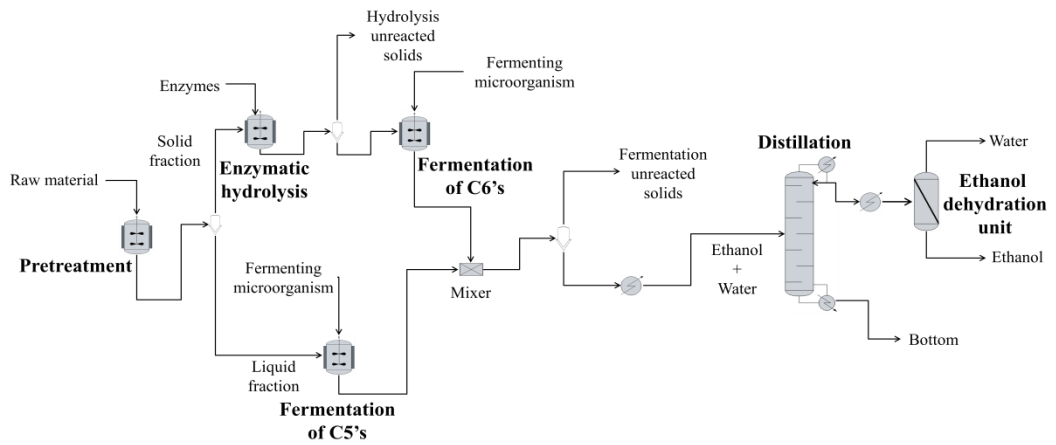


Figure 2.2: Configuration of the ethanol production process from lignocellulosic biomass considering two fermentation stages

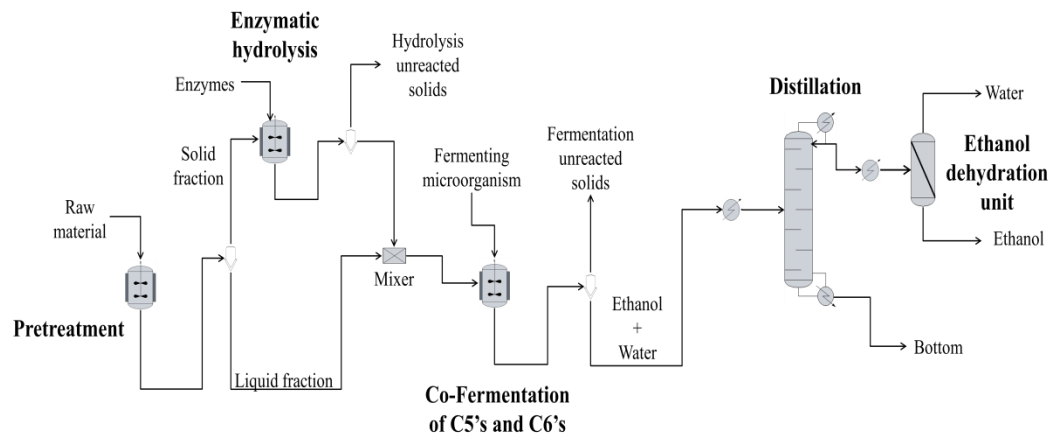


Figure 2.3: Configuration of the ethanol production process from lignocellulosic biomass considering co-fermentation of both pentoses and hexoses

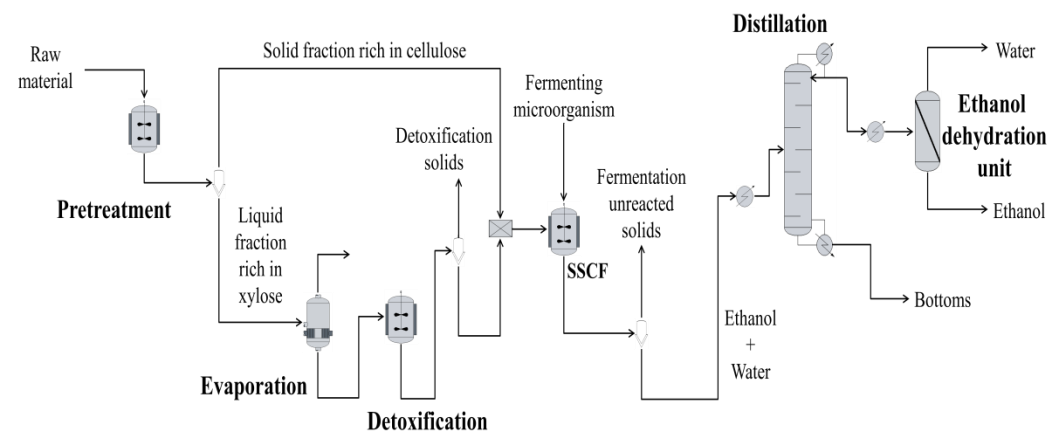


Figure 2.4: Configuration of the ethanol production process from lignocellulosic biomass considering simultaneous saccharification and co-fermentation (SSCF)

Table 2.1: Pretreatment methods for lignocellulosic materials

Pretreatment	Features	Reference
Concentrated acid (CA)	The raw material is treated with concentrated sulphuric acid at 121 °C for 4 hours.	(Abedinifar et al. 2009; Saxena et al. 2009)
Dilute acid (DA)	A 2 % (w/w) solution of H ₂ SO ₄ or HCl is mixed with the raw material and heated at 121°C for 3 to 4 hours.	(Mohagheghi et al. 2006; Saxena et al. 2009; Sukumaran et al. 2009)
Alkaline hydrolysis (AH)	A 2 % (w/w) solution of NaOH or KCl is mixed with the solid and heated at 121°C for 3 hours.	(Abedinifar et al. 2009; Saxena et al. 2009; Sukumaran et al. 2009)
Ammonia fibre explosion (AME)	The raw material gets in contact with ammonia in a ratio of 2 kg of NH ₃ per kg of solid at 90 °C for 30 min.	(Balat et al., 2008)
Ozonolysis (O)	The raw material is submitted to a reaction in presence of ozone at ambient temperature and pressure.	(Kim et al. 2008; Sanchez & Cardona 2005)
Liquid hot water (LHW)	The raw material is heated in water in a ratio of 1:10 at 220 °C for 2 min.	(Prasad et al., 2007)
Steam explosion (SE)	The raw material gets in contact with high pressure steam (5 – 10 bar) for residence times from 5 to 30 min. It is quickly depressurised so the expansion of the vapour can cause the break-up of the cellular matrix.	(Balat et al. 2008; Sanchez & Cardona 2005; Sassner et al. 2006)

All the techniques listed in Table 2.1 have shown promising results at laboratory scale. Pretreatment methods such as dilute-acid (DA), liquid hot water (LHW) and steam explosion (SE) are the most commonly used for lignocellulosic biomass. However, kinetic models for most of these pretreatments are not available in literature and a comparison of different methods is therefore not possible. For this work, the pretreatment technique considered is dilute-acid (DA) which is widely used in industry in the production of biofuels from molasses and sugar cane bagasse. The kinetic parameters for the mathematical model for corn stover are reported in literature by Esteghlalian et al., (1997). All kinetic models and parameters will be discussed later in Chapter 3.

Table 2.2: Literature review on the pretreatment of lignocellulosic biomass for ethanol production

Work	Description of the pretreatment	Characteristics	Reference
Steam explosion, organosolv, and sulfite pretreatment to overcome lignocelluloses recalcitrance (SPORL)	Three different pretreatment techniques for delignification and conversion of hemicellulose	Advantages for woody biomass conversion especially for softwood species; 30 min reaction time at 180 °C	(Zhu and Pan, 2010)
SPORL and dilute-acid (DA) pretreatments	High temperature and pressure operation for SPORL and DA pretreatments in the delignification of spruce	Production of reducing sugars with SPORL is 87.9 %, compared to 56.7 % with dilute acid	(Shuai et al., 2010)
Dilute mixed-acid pretreatment of sugarcane bagasse for ethanol production	Combination of sulphuric and acetic acid to improve the conversion of hemicellulose into xylose	The conversion of hemicellulose is 90 %. The solid ratio 1:10 showed the highest conversion and the lowest furfural concentration	(Jackson de Moraes Rocha et al., 2011)
Dilute acid (DA) pretreatment with phosphoric acid	Dilute H ₃ PO ₄ (0.0–2.0%, v/v) is used to pre-treat corn stover (10%, w/w)	Xylose (91.4% w/w) was obtained from corn stover pretreated with H ₃ PO ₄ 1% (v/v)	(Avci et al., 2013)

Pretreatment is one of the key stages of the ethanol production process from lignocellulosic biomass and many techniques have been investigated in order to improve the production of xylose by reducing the crystallinity of lignin and degrade its very intertwined structure (Avci et al., 2013; Jung et al., 2013). Table 2.2 shows some of the research on the pretreatment of lignocellulosic biomass and the key features and the results found therein.

All the methods presented in Table 2.2 not only seek to increase the production of monomeric sugars from the raw material but also to reduce the production of by-products such as furfural, HMF and organic acids which reduce pH in the growth

medium and raise the osmotic pressure of the cells during the fermentation (Diaz et al., 2015; Elgharbawy et al., 2016; Kumar et al., 2009; Liguori et al., 2015; Öhgren et al., 2007a).

Table 2.2: Literature review on the pretreatment of lignocellulosic biomass for ethanol production (cont.)

Work	Description of the pretreatment	Characteristics	Reference
Dilute sulfuric acid pretreatment of oil palm empty fruit bunches (EFB)	Optimised operating conditions for the pretreatment of oil palm to increase the production of ethanol in a microwave digester	Increase of ethanol yield from 52.5 % to 87.5 % when pretreated EFB slurry was treated with activated carbon before subjecting to fermentation	(Jung et al., 2013)
Pilot-scale steam explosion and diluted sulfuric acid pretreatments	Comparative study between steam explosion (SE) and dilute acid (DA) in sugarcane bagasse	Conversions of cellulose pulp of 90 % and 79 % were obtained from SE and DA pretreatment, respectively	(Rocha et al., 2015)
Utilisation of aqueous ammonia	Pretreatment of corn stover and rice husk using aqueous solutions of ammonia	The moderate temperature pretreatment with ammonia is suitable for high recovery of hexose and pentose during hydrolysis	(Swain and Krishnan, 2015)
Microwave-assisted pretreatment of lignocellulosic biomass	Microwave irradiation is applied to enhance enzyme hydrolysis of corn straw and rice husk immersed in water, aqueous glycerol or alkaline glycerol	23 % of lignin is removed when the material is pretreated in glycerol at 180 °C for 2 min	(Diaz et al., 2015)
Ionic liquid pretreatment	IL's have been increasingly exploited as solvents and/or reagents in many applications	The operation goes from temperatures between 100-120 °C and times between 1-5 h, depending on the raw material	(Elgharbawy et al., 2016)

2.4 Detoxification

The detoxification stage is used for the reduction on the concentration of toxic compounds produced during the pretreatment stage (i.e. furfural, hydroxymethylfurfural and some organic acids). Regardless of the pretreatment technique used to break down lignin and to degrade hemicellulose into reducing sugars, these toxic compounds are formed (Mohagheghi et al., 2006).

The detoxification or overliming stage consists of a reactor in which the liquid fraction coming out of the pretreatment stage is treated with a chemical agent to neutralise the acids in the hydrolysate solution and to convert the furfural and HMF into insoluble salts that can be separated by filtration. The operating conditions for this stage are usually between 30 – 60 °C, pH between 9 – 12 and residence time of 30 min. The most used agent for the detoxification of the acid hydrolysates produced during pretreatment is $\text{Ca}(\text{OH})_2$ showing good results in terms of conversion of furfural and organic acids and good applicability in industry (Chandel et al., 2007; Klasson et al., 2013; A. D. Moreno et al., 2013; Purwadi et al., 2004; Xie et al., 2015).

Purwadi et al., (2004) presented a very detailed experimental work for the detoxification of acid hydrolysates from Swedish spruce and the degradation of reducing sugars during this stage. Purwadi et al., (2004) also proposed a mathematical model to describe the reactions that would be more likely to take place during this stage. However, not many authors have decided to evaluate these parameters or try to obtain other kinetic models. Telli-Okur and Eken-Saracoglu, (2008) presented a similar approach as Purwadi et al., (2004) for the neutralisation and detoxification of the hydrolysates from sunflower seeds using $\text{Ca}(\text{OH})_2$ obtaining high rates of furan removal (41 – 68 %).

Klasson et al., (2013) presented an experimental work in which they performed a simultaneous detoxification, enzymatic hydrolysis and fermentation from milled switchgrass using biochar, seeking to reduce the inhibition of furfural and other by-products present in the hydrolysates. Similarly to Klasson et al., Xie et al., (2015) presented the experimental procedure to reduce the concentration of toxic by-products using amino acids. Five amino acids are considered in this work: cysteine,

histidine, lysine, tryptophan and asparagine. The results of this research showed a total conversion of furfural and other by-products. However, the authors have yet to estimate costs related to the utilisation of amino acids. In general, the overliming process applied to ethanol production has been very useful for the degradation of toxic compounds and its outcomes and operating conditions often go hand in hand with the performances in the pretreatment stage and the fermentation stage.

2.5 Enzymatic hydrolysis

The pretreatment stage produces two fractions: A liquid fraction rich in xylose and a solid fraction which is rich in unreacted cellulose and lignin. Different pretreatment techniques available, such as dilute-acid pretreatment, ozonolysis, steam explosion, among others, have high hemicellulose conversion during this stage (approx. 18 – 30 g/L of xylose) (Saha et al., 2005; Sreenath and Jeffries, 2000; Telli-Okur and Eken-Saracoglu, 2008). The remaining solid material, rich in cellulose, is then directed to a further stage of pretreatment in which the biopolymer is broken down into its basic structural units (mainly glucose and cellobiose) by the action of enzymes known as cellulases (Bansal et al., 2009; Bezerra and Dias, 2005; Kadam et al., 2004). This pretreatment stage is used in the production of substrate for the fermenting microorganisms, which is an important part in the ethanol production process and is also known as enzymatic hydrolysis. This reaction is widely used in industry reporting high yields in glucose production (approx. 15 – 30 g/L of glucose) (Bansal et al., 2009; Cara et al., 2007; J. Zhang et al., 2009).

2.5.1 Enzymatic activities

The mechanism to convert cellulose into glucose and cellobiose can make use of two different major groups of enzymes (Nigam, 2001; Sreenath et al., 2001):

1. Endoglucanases (1,4- β -D-glucanohydrolases).
2. Exoglucanases:
 - Cellodextrinases (1,4- β -D-glucan glucanohydrolases)
 - Cellobiohydrolases (1- β -D-glucan cellobiohydrolases)
 - β -Glucosidases (β -glucoside glucohydrolases)

Endoglucanases cut randomly in the amorphous sites of the polysaccharide chains of cellulose producing oligosaccharides of several lengths and consequently new ends of the chain. Exoglucanases act gradually over the reducing or non-reducing ends of the chains of cellulose releasing glucose (by the action of glucohydrolases) and cellobiose (by the action cellobiohydrolases) as products in major proportion. β -Glucosidases degrade the cellobiose into glucose in a parallel reaction (Mohagheghi et al., 2006; Telli-Okur and Eken-Saracoglu, 2008).

2.5.2 Enzymatic mechanism

The enzymatic hydrolysis takes place on the surface of cellulose and it has a complex nature which involves many more stages than any other reaction catalysed by enzymes. The different action mechanisms over the substrate are the following:

1. Adsorption of cellulase in the substrate (Jervis et al., 1997)
2. Location of a bond susceptible to hydrolysis on the surface of the substrate (formation of chain ends in the case of carbohydrolases and bond division in the case of Endogluconases) (Jervis et al., 1997)
3. Formation of the enzyme-substrate complex (Divne et al., 1998; Mulakala and Reilly, 2005)
4. Hydrolysis of the β -glucosidic bond followed by the simultaneous sliding of the enzyme along the chain of cellulose (Divne et al., 1998; Mulakala and Reilly, 2005)
5. Desorption of the cellulases from the substrate (Divne et al., 1998; Mulakala and Reilly, 2005)
6. Hydrolysis of cellobiose by the action of β -glucosidases and the subsequent inhibition of the enzyme by this product (Bezerra and Dias, 2005; Holtzapple et al., 1990; Xiao et al., 2004)

Enzymes commonly used in glucose production from cellulose are shown in Table 2.3. The most commonly used enzyme in industry, given its easy acquisition and low prices, is Celluclast 1,5 L.

Table 2.3: Enzymes used in conversion of cellulose into glucose

Cellulase	Yield (g of sugars /g of solid residues)	Reference
Celluclast 1,5L	0.11 – 0.26	(Cara et al. 2007; Zhang et al. 2009)
Mycotech	0.13 – 0.25	(Cara et al., 2007)
Genencor	0.17 – 0.30	(Cara et al., 2007)
Cellubrix	0.20 – 0.40	(Bansal et al. 2009; Petersson et al. 2007)

The enzymes reported in Table 2.3 require specific conditions of temperature and pH in order to ensure a high yield of glucose production and to avoid the formation of microbial agents that can cause inhibition. Some authors recommend supplementing the action of cellulases with β -glucosidases to further increase the production of glucose by degrading cellobiose (Beck et al., 1990; Palmarola-Adrados et al., 2005). Depending on the raw material and the cellulose crystallinity level, a cocktail of several enzymes is implemented in the production of reducing sugars as a way to increase the conversion of cellulose and other polymers that can be reduce to their monomeric units.

Table 2.4 shows the different works where enzymatic hydrolysis has been used in the production of hexoses from lignocellulosic biomass. The works presented in Table 2.4 are some of the most recent investigations on enzymatic hydrolysis of cellulose. Although the results reported in these works are promising in terms of the level of conversion and production of glucose, few publications have touched on the modelling and mathematical formulation.

Kadam et al., (2004) presented a model based on the Michaelis-Menten kinetics for the production of glucose, xylose and cellobiose taking into consideration inhibitory effects and loss of enzyme activity. This approach, unlike other publications, focuses on the different possible routes that can be measured during the enzymatic hydrolysis and the inhibitory effects of both substrate and product over the activity of the enzyme.

This work has been cited by over 90 authors, some of which include Kumar and Wyman, (2008), Engel et al., (2012), Gaykawad et al., (2012), Morales-Rodriguez et al., (2012), Cheng et al., (2015), Liguori et al., (2015), Niu et al., (2016), among others. The work of Morales has also been included in this thesis, as explained in the following chapters, since it merges both the kinetic model of the enzymatic hydrolysis with the model of co-fermentation of xylose and glucose using bacteria.

2.6 Fermentation

During the production of the reducing sugars (i.e. pentoses and hexoses), some by-products are also produced with inhibitory effects on the fermenting microorganisms (Chandel et al., 2007; Sreenath et al., 2001; Triana et al., 2011; Zhu et al., 2015). The fermentation stage is the step of the process in which the lignocellulosic hydrolysates are converted into ethanol via anaerobic metabolism. This is an important step in the process and most of the current research is focused on finding the optimal conditions of aspects such as new technologies and methodologies for growth, operating conditions and the design of new fermenting strains in order to achieve high ethanol yields by using all the available substrate (Baeyens et al., 2015; Carrasco et al., 2011; Liguori et al., 2015; Swain and Krishnan, 2015). Table 2.5 shows some of the most commonly employed strains in industry along with the ethanol yields.

The yields listed in Table 2.5 are calculated as *experimental ethanol yield/theoretical ethanol yield* (theoretical ethanol yield is 0.511 g of ethanol/g of available substrate) (Drapcho et al., 2008). Some researchers have developed new alternative configurations for this stage. Some of these alternatives include the recycling of the cells or the substrate, continuous fermentation with simultaneous saccharification or fermentation of only glucose, presenting good results. However, in the case of lignocellulosic biomass, most of the hydrolysates not only present hexoses but also pentoses. Some of the microorganisms in Table 2.5 are therefore considered when multiple-substrate fermentations are required to ensure higher yields of ethanol (Cho et al., 2010; Dien et al., 1998; Zhao et al., 2008).

Table 2.4: Use of enzymatic hydrolysis in the production of glucose and other reducing sugars from cellulose

Work	Enzyme	Characteristics	Reference
Simultaneous saccharification and fermentation (SSF) from woody and herbaceous materials	Celluclast 1.5 L	The raw material is pretreated with steam. SSF is carried out at 42 °C for 72 hours	(Ballesteros et al., 2004)
Hydrolysis of Japanese red pine	Celluclast 1.5 L and Novozyme 188	Enzymatic hydrolysis at 50 °C and 150 rpm for 72 h and at 2% (w/v) substrate concentration	(Kumar et al., 2009)
Enzymatic hydrolysis of corn stover for ethanol production	CPN cellulase and β -glucosidase Novo 188	Estimation of the kinetic parameters for a mathematical model that describes saccharification of cellulose	(Kadam et al., 2004)
SSF of lignocellulose to ethanol with thermotolerant yeast strains	Celluclast 1.5 L	Production of ethanol using coupled fermentation and enzymatic hydrolysis at 48 °C for 24 hours	(Hasunuma and Kondo, 2012)
Optimisation of saccharification of sweet sorghum bagasse using response surface methodology	Celluclast 1.5 L + β -glucosidase Novozyme 188	Lignocellulose rich sweet sorghum bagasse was used as a substrate for cellulolytic hydrolysis at 28 ± 2 °C for 8 days	(Saini et al., 2013)
Use of Cellulases from <i>Trichoderma reesei</i>	<i>T. reesei</i> cellulolytic cocktail for the saccharification of lignocellulosic feedstocks	Production of enzymes from <i>Trichoderma reesei</i> as means to optimise the saccharification of lignocellulosic biomass	(Berrin et al., 2014)
Biological pretreatments to increase the efficiency of the saccharification from <i>Spartina argentinensis</i>	β -glucosidase from almonds (49,290), hemicellulase from <i>A. niger</i> (H2125), cellulase from <i>A. niger</i> (C1184)	Production of ethanol from switchgrass with high content of C4 using Fungal supernatants.	(Larran et al., 2015)
SSCF for improving xylose conversion from steam-exploded corn stover	Cellulase Cellic CTec2	Steam-exploded corn stover for ethanol production using SSCF at 50 °C at high solid loading	(Liu and Chen, 2016)

Table 2.5: Microorganisms used in ethanol production

Microorganism	Substrates	Yield (%)	Reference
<i>Saccharomyces cerevisiae</i>	Glucose, Galactose, Maltose	43 – 87	(Behera et al., 2010; Siqueira et al., 2008)
<i>Pichia stipites</i>	Glucose, Xylose, Arabinose, Mannose	83 – 92	(Drapcho et al., 2008; Nigam, 2001)
<i>Candida shehatae</i>	Glucose, Xylose, Arabinose, Mannose	75 – 90	(Chandel et al. 2007; Huang et al. 2009)
<i>Candida lusitanae</i>	Glucose, Xylose, Sucrose, Cellobiose	70 – 85	(Freer & Detroy 1982; Sreenath et al. 2001)
<i>Candida tropicalis</i>	Glucose, Xylose, Sucrose, Cellobiose	76 – 85	(Jamai et al. 2007; Rattanachomsri et al. 2009)
<i>Escherichia coli</i>	Glucose, Glycerol	70 – 90	(Garcia et al.,2010; O'Brien et al., 2004)
<i>Zymomonas mobilis</i>	Glucose, Xylose, Fructose, Sucrose	80 – 92	(Behera et al., 2010; Leksawasdi et al., 2001)
<i>Klebsiella oxytoca</i>	Glucose, Fructose, Sucrose, Maltose	80 – 90	(Ji et al. 2009; Sanchez & Cardona 2005)
<i>Pachysolen tannophilus</i>	Glucose, Xylose, Glycerol	75 – 80	(Romero et al., 2007; Zhao et al., 2008)
<i>Clostridium thermocellum</i>	Glucose, Xylose	60 – 80	(Balusu et al., 2005)
<i>Kluyveromyces marxianus</i>	Glucose	70 – 80	(Kadar et al., 2004)

Publications related to this stage have explored different aspects such as operating conditions, growth media, fermenting microorganisms, and design of the reactor (Gaykawad et al., 2013; Kim et al., 2008; Öhgren et al., 2007a; Sanchez et al., 2004; Sasaki et al., 2015; Sreenath et al., 2001). However, current research is more focused on the fermenting microorganisms (e.g. yeast, bacteria or fungi) and how to obtain higher concentrations of ethanol with lower production of cells in a shorter residence time (Goliass et al., 2002; Tang et al., 2008; Tian et al., 2009; Zhu et al., 2015). In terms of the design of the reactor, research is also looking to couple other processes with the fermentation stage in order to increase ethanol yield and reduce the inhibitory effects of substrate, product and by-products over the performance of the microorganism (Kumar and Wyman, 2008; Palmqvist and Hahn-Hagerdal, 2000b; Ranjan et al., 2009; Xiao et al., 2004).

Some of these combinations include simultaneous saccharification and fermentation (SSF), simultaneous saccharification and co-fermentation (SSCF), removal of ethanol using selective membranes, genetically modified strains for specific substrates, etc. (Gaykawad et al., 2013, 2013; Huang et al., 2006; Niemisto et al., 2013; Tusel and Brüscke, 1985). Table 2.6 shows some of the works related to the production of ethanol from lignocellulosic hydrolysates.

Table 2.6: Recent experimental works related to the implementation of the SSCF process in the production of ethanol from lignocellulosic biomass

Work	Strain and enzyme	Characteristics	Reference
Two-step SSCF to convert AFEX-treated switchgrass to ethanol using commercial enzymes and <i>Saccharomyces cerevisiae</i> 424A(LNH-ST)	<i>S. cerevisiae</i> 424A(LNH-ST) + Spezyme CP and Novozyme 188	Ammonia fibre explosion is used to pretreat switchgrass and SSCF is carried out at 35 °C for 120 h	(Jin et al., 2010)
SSCF of AFEXTM pretreated corn stover for ethanol production using commercial enzymes and <i>Saccharomyces cerevisiae</i> 424A(LNH-ST)	<i>Saccharomyces cerevisiae</i> 424A(LNH-ST) + Spezyme CP (for cellulose conversion into glucose and cellobiose) + Novozyme 188 (for cellobiose conversion into glucose)	Conversion of glucose and xylose into ethanol from pretreated corn stover at 45 °C for 168 h	(Jin et al., 2012)
In situ laccase treatment of steam-exploded wheat straw in SSCF processes at high dry matter consistencies	<i>S. cerevisiae</i> F12 + Cellic CTec2 and Cellic Htec2	SSCF of laccase at 35 °C and pH 5.5 for 144 h	(A. D. Moreno et al., 2013)

Table 2.6: Recent experimental works related to the implementation of the SSCF process in the production of ethanol from lignocellulosic biomass (cont.)

Work	Strain and enzyme	Characteristics	Reference
High-Solid SSCF of alkaline-pretreated corncob using recombinant <i>Zymomonas mobilis</i> CP4	<i>Zymomonas mobilis</i> CP4 + cellulase (GC220) with 30 FPU/g cellulose and Multi-effect xylanase	The raw material is alkaline-pretreated Corncob. The operating conditions are pH = 5.5 and 30 °C for 96 h	(Su et al., 2012)
Fed-batch SSCF using steam-exploded wheat straw xylose-fermenting <i>Saccharomyces cerevisiae</i> strain: effect of laccase supplementation	<i>S. cerevisiae</i> KE6-12 + Cellic CTec2 and Cellic HTec2	All the experiments were run at 35°C and 180 rpm for 144 hours (batch SSCF) or 168 hours (fed-batch SSCF)	(A. Moreno et al., 2013)
SSCF of whole wheat in integrated ethanol production	<i>S. cerevisiae</i> TMB3400 + Cellulase (Celluclast 1.5 L) and b-glucosidase (Novozym 188)	Steam pretreated wheat. The operating conditions of the SSCF process are at 35 °C for 120 h	(Erdei et al., 2013)
Metabolic engineering of <i>Saccharomyces cerevisiae</i> PE-2 and CAT-1	<i>Saccharomyces cerevisiae</i> ethanol strains PE-2 and CAT-1 + Cellic Ctec2	Genetically modified <i>S. cerevisiae</i> for SSCF at 30 °C for 140 hours obtaining 92% of the theoretical yield	(Romaní et al., 2015)
SSCF by using xylose-fermenting <i>Saccharomyces cerevisiae</i>	<i>Saccharomyces cerevisiae</i> MN8140X/TF-TF + Cellic CTec2	SSCF for pretreated rice straw at 35 °C for 48 h reaching ethanol yield up to 74 % of the theoretical yield	(Sasaki et al., 2015)
SSCF of dry diluted acid pretreated corn stover at high dry matter loading	<i>S. cerevisiae</i> SyBE005 + Accellerase 1500 and Novozyme 188	Genetically modified <i>S. cerevisiae</i> for SSCF with 65% yield with 25% solid loading	(Zhu et al., 2015)
SSCF for steam-exploded corn stover at high solid loading	<i>Saccharomyces cerevisiae</i> IPE003 + Cellic CTec2	SSCF at different glucose/xylose ratios 30 °C, and 96 h with pH ranges from 4 to 5	(Liu and Chen, 2016)

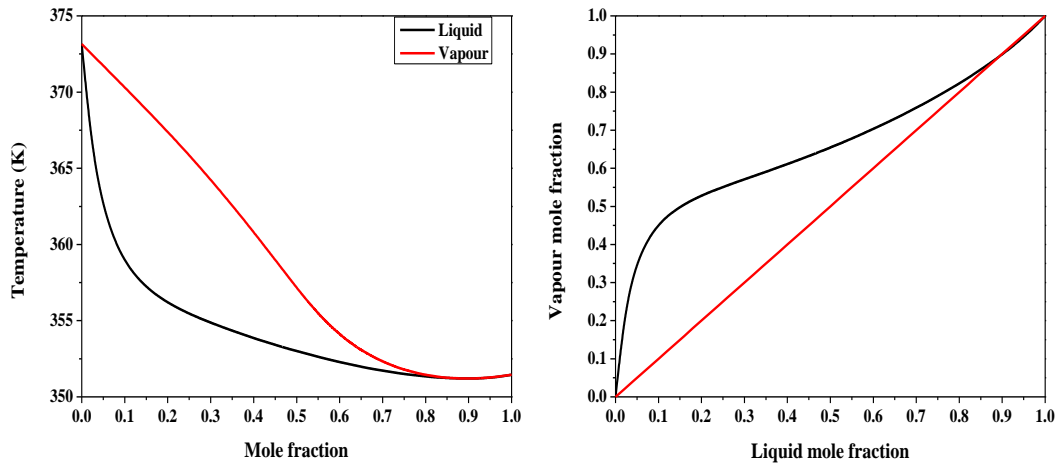


Figure 2.5: Liquid-Vapour Equilibrium (VLE) calculated using ChemCAD for the mixture ethanol/water at 1 atm

2.7 Separation processes

In the ethanol production process, the separation section or product recovery represents a challenge given the presence of a minimum boiling point azeotrope in the binary mixture ethanol/water (see Figure 2.5) using the NRTL method for the activity coefficients and Equation of State PSRK for the acentric factor. Since a high concentration of ethanol is required (approx. 99.5 % w/w) for fuel applications in engines or in any other machinery, high levels of energy are necessary to obtain a concentration close to the azeotrope (approx. 94% w/w) (Bai et al., 2008; Drapcho et al., 2008).

Separation methods such as distillation and adsorption have shown high rates of product recovery but with the energy-related costs in order to obtain concentrations of ethanol around 94 % (w/w), which is still not suitable for biofuel purposes (Balat et al., 2008; Lee et al., 2012). Alternative configurations to simple distillation include: extractive distillation, swing-pressure distillation, double-effect distillation, dividing wall distillation, etc. However, their implementation often entails additional expenses related to controllability and operation and, in the case of extractive distillation, solvent recovery (Kiss and Olujic, 2014; Le et al., 2015; Okoli and Adams, 2015).

Another alternative for ethanol dehydration is membrane-assisted distillation, in which membrane-based techniques are coupled with distillation systems to remove a

specific component or components from the feed mixture even beyond the barriers of an azeotrope with lower energy consumption (Koch and Gorak, 2014; Koltuniewicz, 2010; Kookos, 2003). In most membrane separations, the feed stream is split into two product streams: permeate and retentate. From which side the key product is removed depends highly on the nature of the membrane (Chovau et al., 2011; Fan et al., 2014; O'Brien et al., 2004; Valentinyi et al., 2013). The separation of the key product is mainly caused by the concentration or pressure gradient between both sides of the membrane. Since the membrane is highly selective, the key component permeates throughout the membrane from the feed stream and is then removed by the injection of an inert gas or by simply applying vacuum on the permeate side. Some cases of membrane-based separations include osmosis, pervaporation and vapour permeation (Koch and Gorak, 2014; Niemisto et al., 2013; Toth and Mizsey, 2015; Valentinyi et al., 2013). Table 2.7 presents some of the most recent works related to the purification of ethanol for fuel applications using different separation techniques.

2.8 Heat integration and heat storage

The optimisation of a process that includes heat exchange is an important step to improve the productivity and efficiency of a plant by reducing energy consumption and operating costs. It is for this reason that mathematical and thermodynamic methods are used to solve the optimisation problems by re-distributing the energy sources (i.e. utilities, process streams, etc.) (Baños et al., 2011; Biegler et al., 1999; Bryson and Ho, 1975; Rašković et al., 2010; Stuart and El-Halwagi, 2012a). Conventional methods for the optimisation of a heat exchange network can be classified into three general categories: Pinch point analysis, mathematic methods and metaheuristic methods (Hahn-Hagerdal et al., 2006):

1. **Pinch point analysis:** This analysis is a widely used method to determine the minimal demand for hot and cold duties supplied by utilities and to maximise heat recovery. The heat content of all the streams in the process and the initial and final temperatures must be known and then a heat exchange network (HEN) can be designed with minimum energy demand (Rašković et al., 2010; Stuart and El-Halwagi, 2012a). The process data is represented as a set of energy flows, or streams, as a function of heat load (kW) against temperature (°C). These data are combined for all the streams in the plant to give

composite curves, one for all hot streams (releasing heat) and one for all cold streams (requiring heat) (Baeyens et al., 2015; Fornell and Berntsson, 2012; Kravanja et al., 2013). The point of closest approach between the hot and cold composite curves is the pinch point (or just pinch) with a hot stream pinch temperature and a cold stream pinch temperature. This is where the design is most constrained.

Table 2.7: Separation methods used in the dehydration of ethanol

Work	Process	Characteristics	Approach	Reference
Control of an extractive distillation process to dehydrate ethanol using glycerol as entrainer	Extractive distillation process to produce anhydrous ethanol using glycerol as entrainer	Double distillation system. First column for the removal of ethanol (99.7 % w/w) and the second column for the recovery of glycerol	Simulation using ASPEN Plus	(Gil et al., 2012)
A new hybrid distillation–pervaporation process are combined in a single unit	The use of distillation and pervaporation for ethanol separation considering Membrane Dephlegmation	The membrane is placed inside the distillation column in order to remove ethanol beyond the azeotrope at different ratios and permeate rates	Simulation using ASPEN Plus	(Haelssig et al., 2012)
Innovative single step bioethanol dehydration in an extractive dividing-wall column	Extractive dividing-wall distillation using glycerol	Several configurations were taking into consideration obtaining concentrations of 99.8 % (w/w)	Simulation and optimisation using ASPEN Plus	(Kiss and Ignat, 2012)
Enhanced bioethanol dehydration by extractive and azeotropic distillation in dividing-wall columns	Bioethanol dehydration, using dividing-wall columns (DWC) extended to extractive distillation (ED) and azeotropic distillation	(ED) and (AD) used in DWC processes reach purities of bioethanol over 99.8 wt. %	Simulation and optimisation in ASPEN plus	(Kiss and Suszwalak, 2012)

Table 2.7: Separation methods used in the dehydration of ethanol (cont.)

Work	Process	Characteristics	Approach	Reference
Process analysis and optimisation of hybrid processes for the dehydration of ethanol	Combination of distillation, vapour permeation and adsorption	Ethanol dehydration process obtaining concentrations of 99.6 % (w/w) with lower capital costs	Simulation in ASPEN Plus supported with experiments	(Roth et al., 2013)
Ethanol recovery from fermentation broth with integrated distillation–membrane process	Membrane-assisted vapour stripping process	Distillate is sent to a membrane module to dehydrate ethanol in the retentate. Permeate is recycled to the column. Purity of ethanol 99 %	Experimentation	(Vane et al., 2013)
Azeotropic distillation and hybrid system for water–ethanol separation	Distillation column followed by hydrophilic NaA zeolite membrane	The hybrid process produces conc. of ethanol >99.4%wt. The hybrid system presents energy savings of 52.4% against azeotropic distillation	Experimentation	(Kunnakorn et al., 2013)
Logic hybrid simulation-optimisation algorithm for distillation design	Optimisation of hybrid processes with a hydrophilic membranes using a tray-by-tray optimisation approach	Reduction of energy consumption for process where two or more components are separated	Simulation using MatLab	(Caballero, 2015)
Ethanol recovery from fermentation broth with integrated distillation–membrane process	Membrane-assisted vapour stripping process	Distillate is sent to a membrane module to dehydrate ethanol in the retentate. Permeate is recycled to the column. Purity of ethanol 99 %	Experimentation	(Vane et al., 2013)

Hence, by finding this point and starting the design there, the energy targets can be achieved using heat exchangers to recover heat between hot and cold streams in two separate systems, one for temperatures above pinch temperatures and one for temperatures below pinch temperatures (Baños et al., 2011; Biegler et al., 1999; Bryson and Ho, 1975; Rašković et al., 2010; Stuart and El-Halwagi, 2012a; Yee et al., 1990a, 1990b; Yee and Grossmann,

1990). In practice, during the pinch analysis of an existing design, often cross-pinch exchanges of heat are found between a hot stream with its temperature above the pinch and a cold stream at temperatures below the pinch. Removal of those exchangers by alternative matching makes the process reach its energy target (Gorji-Bandpy et al., 2011). This method is flexible and provides a wide perspective to the designer in terms of configuration of the units and the solution. However, it is not possible to simultaneously minimise the price of the network and the amount of heat exchangers with this method (Gorji-Bandpy et al., 2011).

2. **Mathematical methods:** These methods make reference to the mathematical formulations which describe all the units and the system as a whole. This set of differential and algebraic equations includes the mass, momentum and energy balances and the solution of these models is usually carried out by using numerical methods (Gorji-Bandpy et al., 2011; Yee et al., 1990a, 1990b; Yee and Grossmann, 1990). For the optimisation of the process and the heat exchange network, some authors suggest methods such as:

- ***Linear programming (LP):*** linear programming is a technique for the optimisation of a linear objective function, subject to linear equality and linear inequality constraints. Its feasible region is a convex polyhedron, which is defined as the intersection of finitely many half spaces, each of which is defined by a linear inequality. Its objective function is a real-valued affine function defined on said polyhedron. A linear programming algorithm finds a point in the polyhedron where this function has the smallest (or largest) value if such a point exists (Biegler et al., 1999; Bryson and Ho, 1975; Vanderbei, 2010).
- ***Nonlinear programming (NLP):*** The problem is called a nonlinear programming problem if the objective function is nonlinear and/or the feasible region is determined by nonlinear constraints (Biegler et al., 1999; Yee et al., 1990a, 1990b; Yee and Grossmann, 1990).
- ***Mixed-integer linear programming (MILP):*** In a linear programming method, all the decision variables x are continuous variables which may

take on any positive value $Ax > b$ and $x > 0$. In MILP, the decision variables are integer values (Stuart and El-Halwagi, 2012b).

- **Mixed-integer nonlinear programming (MINLP):** It refers to mathematical programming method with continuous and discrete variables and nonlinearities in the objective function and constraints. The use of MINLP is a natural approach of formulating problems where it is necessary to simultaneously optimise the system structure (discrete) and parameters (continuous) (Bryson and Ho, 1975; Stuart and El-Halwagi, 2012a; Yee et al., 1990a, 1990b; Yee and Grossmann, 1990).

3. **Metaheuristics methods:** Metaheuristics are general algorithmic frameworks, often nature-inspired, intended to solve complex optimisation problems. In recent years, metaheuristic are emerging as useful alternatives to more classical approaches also for solving optimisation problems that include in their mathematical formulation uncertain, stochastic, and dynamic information, (Blum et al., 2005; Gendreau and Potvin, 2010). The metaheuristic algorithms have several advantages over the mathematical solvers. These methods are preferably used for complex spaces and since they do not use step sizes for solving, the objective function can be non-linear and non-continuous (Baños et al., 2011; Blum et al., 2005; Gendreau and Potvin, 2010). Some Metaheuristic methods include Simulated Annealing, Genetic Algorithm, Tabu Search Method, among others:

- **Simulated Annealing:** This is a multivariable combinatorial optimisation technique, based on an analogy with statistical mechanics. The basic principle of this method resemblances the annealing of solids in which the atoms are reorganized in order to obtain a minimum internal energy. For a given configuration, a random move is carried out by randomly picking a molecule and moving it in a random direction for a random distance (AN et al., 2008; Liu et al., 2013).
- **Genetic algorithms:** In a genetic algorithm, a population of candidate solutions (called individuals, creatures, or phenotypes) is evolved towards better solutions. Each candidate solution has a set of properties (its chromosomes or genotype) which can be mutated. Traditionally, solutions

are represented in binary as strings of 0s and 1s, but other encodings are also possible (Dieterle et al., 2003). The evolution usually starts from a population of randomly generated individuals and is an iterative process. The population in each iteration is also known as generation. In each generation, the fitness of every individual in the population is evaluated; the fitness is usually the value of the objective function in the optimisation problem being solved. The fittest individuals are stochastically selected from the current population, and each individual's genome is modified (recombined and possibly randomly mutated) to form a new generation. The new generation of candidate solutions is then used in the next iteration of the algorithm. Commonly, the algorithm terminates when either a maximum number of generations has been produced, or a satisfactory fitness level has been reached for the population (Rivera et al., 2006).

- **Tabu Search:** This is a heuristic approach for solving combinatorial optimisation problems by using a guided, local search procedure to explore the entire solution space without becoming easily trapped in local optimal. It has been shown to be effective for scheduling problems, traveling salesman problems, constraint satisfaction problems, as well as many engineering optimisation problems, such as general zero-one mixed integer programming problems (Teh and Rangaiah, 2003).

The main objective of this work is the integration of the heat sources within the ethanol production process in order to reduce the overall energy consumption. In order to achieve this goal, several aspects of the process need to be addressed. For instance, the design of the plant, the optimal operating conditions of the different units in the process, the evaluation of different alternatives that can improve the efficiency of the process, sustainability, economic feasibility, etc.

This project wants to show that the production of biofuels is an appealing alternative to the utilisation of fossil fuels and that they can also be implemented around the world. Several authors have explored different configurations and technologies in heat integration in the production of bioethanol from lignocellulosic biomass. Some

recent works include: Fornell and Berntsson, (2012), Grisales et al., (2008), Kravanja et al., (2013), Modarresi et al., (2012), Rašković et al., (2010), Čuček et al., (2011). These works are mainly focused on the implementation of the *Pinch Analysis* in the production of ethanol from biomass and savings of energy (Fornell and Berntsson, 2012; Grisales et al., 2008; Kiran and Jana, 2015; Rašković et al., 2010; Yee et al., 1990a, 1990b; Yee and Grossmann, 1990).

2.9 Summary and research statement

The literature review conducted in this chapter summarises the work done on design, experimentation, modelling and optimisation of the different units involved in the production of ethanol from lignocellulosic biomass. The main aspects and characteristics of the studies were highlighted. It can be seen that for the pretreatment, enzymatic hydrolysis and fermentation stages, current research is mainly dedicated to the improvement of the operating conditions and techniques used in the laboratory in order to achieve higher conversions. There is no economic analysis behind most of these studies and there is no implementation in industrial cases. However, this gap in literature can be advantageous and interesting to explore, especially the application of detailed mathematical models into more robust optimisation problems.

Mathematical models presented by Esteghlalian et al., (1997), Purwadi et al., (2004), Kadam et al., (2004) and Leksawasdi et al., (2001) are some of the most relevant and widely used kinetic models for pretreatment, detoxification, enzymatic hydrolysis and co-fermentation, respectively. These models take into account several aspects including inhibition by product, inhibition by by-product, inhibition by substrate, loss of activity, the influence of the operating conditions, etc. These kinetic models will be used in the simulation of the ethanol plant in gPROMS as described in the next chapters.

Most of the work that has been done on hybrid processes is focused on the design of systems with emphasis on simulation and optimisation. The majority of the work presented in literature contained some form of comparative analysis to conventional distillation processes (Kiran and Jana, 2015; Kiss and Olujic, 2014; Le et al., 2015; Sudhoff et al., 2015). These comparative studies highlighted the benefits of these

new technologies and sold the idea that their implementation can result in significant reductions in energy consumption and costs.

While previous works on hybrid processes have shown savings in costs, it should be noted that the extent of said savings may vary significantly between studies. Works by Kiss and collaborators have shown the benefits of different configurations for dividing wall and membrane-based operations using modelling, which allows the understanding of the theoretical flexibility of the system, as well as limitation of these processes compared to existing technologies (Kiss and Ignat, 2012; Kiss and Olujic, 2014; Kiss and Suszwalak, 2012). Publications by Górak and collaborators include simulation work in different separation systems, which have been validated against experimental studies in a pilot plant (Koch et al., 2013; Koch and Gorak, 2014; Roth et al., 2013; Sudhoff et al., 2015).

Research related to heat integration only made reference to the use of the *Pinch Analysis*, which is very helpful and widely recognised. However, this approach does not consider aspects such as the design of the plant and the configuration thereof or costs related to operation and equipment. The research group of Chemical, Catalytic and Biotechnological Processes (PQCB) led by Dr. Carlos Ariel Cardona has studied the production of bioethanol from different raw materials found in Colombia's rural areas. Their approach consists of using ASPEN Plus to simulate the process and evaluate the costs using the Economics tool known as Icarus developed by Aspen Tech. They also include in all of their publications an analysis for the environmental impact using the WAR algorithm which evaluates the toxicity of the outlet streams of the process based on their chemical composition (Grisales et al., 2008; Sanchez and Cardona, 2005; Sánchez and Cardona, 2012; Triana et al., 2011). Similarly, researchers such as Dr. Ricardo Morales-Rodríguez and collaborators from the University of Guanajuato in Mexico, have been working in the development of new configurations of the process using ASPEN Plus to reduce the production costs (Morales-Rodríguez et al., 2012, 2011).

The deliverable of this thesis is a practical methodology for the improvement of the ethanol production process from lignocellulosic biomass, considering aspects such as design and size of each unit within the plant, yield of ethanol, concentration of

ethanol at the end of the process, among other aspects. Other studies have used other packages to simulate the entire plant. However, most of these works only consider stoichiometric approaches for the reactors and none of them have focused on the optimisation of the distillation section and the pervaporation network as well as the minimisation of the total annualised costs for the whole process, which is something novel this thesis wants to deliver. The following chapters will present the results of the simulation and optimisation of the process as well as the implementation of heat integration.

Chapter 3 – Mathematical models and model validation

Abstract

This chapter presents the mathematical models of all the units involved in the production of ethanol from lignocellulosic biomass. The kinetic models of pretreatment, detoxification, simultaneous saccharification and co-fermentation (SSCF) and pervaporation are validated against experimental data found in literature. The models of evaporation and distillation are formulated from mass and energy balances. gPROMS is used for the simulation of all the units in the process and ChemCAD is used in the validation of the mathematical model for the distillation column.

3.1 Introduction

Simulations and modelling are often used in chemical engineering as tools to provide information regarding the operation and capacity of the plant, the energy required for its functioning and the concentration of the desired product. It is a cheaper way to predict the results of any process before engaging in any large-scale production. However, there must be sensible experimental data regarding the performance of the units in the process so the simulation can be compelling and reliable. This information usually comes from experimentation that has been done for a specific unit or mathematical formulations based on physical principles or both (Esteghlalian et al., 1997; Morales-Rodriguez et al., 2011; Phisalaphong et al., 2006).

Empirical models are obtained from experimental data usually at laboratory scale since the conditions at which the experiments are carried out can be easily controlled in order to get low margins of error. This also permits the reproduction of a specific experiment as many times as required to guarantee reliability in the final results. In the production of ethanol from biomass there are many mathematical models

available in literature and each one is derived from specific experiments for specific raw materials.

The ethanol production process from lignocellulosic biomass considers two main sections: a pretreatment section and a dehydration section as illustrated in Figure 3.1 (Bai et al., 2008; Balat et al., 2008; Karlsson et al., 2014; Wei et al., 2014). The pretreatment section comprises the pretreatment of the raw material using a chemical agent, the detoxification of the acid hydrolysates and the simultaneous saccharification and co-fermentation (SSCF) of the available substrate for the production of ethanol. For the pretreatment section, the kinetic models are derived from experimental data specifically obtained from different lignocellulosic materials.

Similarly, the kinetic models for detoxification, enzymatic hydrolysis and fermentation are derived from experimental data fitted into mathematical formulae. These models, however, are restricted to the operating conditions at which their parameters were obtained, meaning that if the parameters of a model were acquired in a temperature range between 10 and 20 °C, any results above or below this range cannot be trusted. The versatility of these models can be observed in their respective works showing an accurate description of the phenomena involved.

The dehydration section consists of the separation units where ethanol is recovered and purified. The aim of this chapter is to present reliable mathematical models that can accurately describe the different units of the ethanol process for both the distillation column and the pervaporation module. The distillation column is modelled using dynamic mass and energy balances considering aspects such as non-ideality of the mixture for a VLE approach. The set of algebraic-differential equations is solved using gPROMS and validated with simulation results using ChemCAD.

The mathematical models of the pervaporation systems presented in this work are also based on experiments which serve to calculate the molar flux through the membrane. This work presents two models: one for an organophilic membrane that separates volatile compounds on the permeate side and one model for a hydrophilic membrane that removes water to increase the concentration of ethanol on the

retentate side. This work will list the models that will be used in the simulation and optimisation of the ethanol production process from corn stover. These models will be implemented in the formulation of the mass and energy balances for each unit.

3.2 Process description

Figure 3.1 presents a configuration for the ethanol process using corn stover as raw material. This flowsheet has been proposed by other authors and considers SSCF as the method to produce ethanol, which represents savings in investment of equipment and the utilisation of services (Cardona and Sánchez, 2007; Grisales et al., 2008). Additionally, this method prevents the inhibition by substrate in the enzymatic hydrolysis and the inhibition by product in the fermentation (Morales-Rodriguez et al., 2012, 2011).

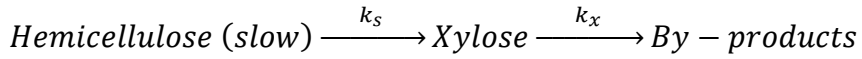
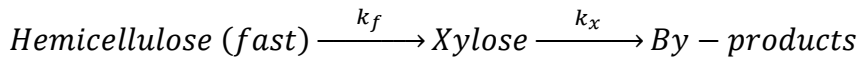
The separation section consists of a distillation system at atmospheric pressure in which the concentration of ethanol in the distillate stream will be close the azeotropic point and a set of pervaporation modules where ethanol is expected to be dehydrated up to concentrations higher than 99 % (w/w). The design of the pervaporation section presented in Figure 3.1 was proposed by Marriott and Sørensen, (2003).

3.3 Dilute acid pretreatment

The chemical characterisation of corn stover is shown in Table 3.1 (Esteghlalian et al., 1997; Rašković et al., 2010). The pretreatment stage consists of a reactor in which the raw material gets in contact with a chemical agent (e.g. acid, base or water) at high temperatures and pressures to degrade the lignin and to convert the hemicellulose into xylose and by-products (e.g. furfural, hydroxyl methyl furfural and organic acids) (Abedinifar et al., 2009; Drapcho et al., 2008; Mosier et al., 2005).

The pretreatment method of choice in this work is dilute-acid pretreatment. The application of this pretreatment method for lignocellulosic materials has shown promising results in industry in terms of lignin degradation, high hemicellulose conversion and xylose production (Demirbas, 2007; Drapcho et al., 2008; Esteghlalian et al., 1997; Mosier et al., 2005; Sreenath et al., 2001; Sreenath and Jeffries, 2000). The reactions that are considered in the work of Esteghlalian et al.,

(1997) and take place in the pretreatment of the lignocellulosic biomass are the following:



According to Esteghlalian et al., (1997), the percentage of fast hemicellulose in corn stover is 64.4 % and the rest is slow-reacting hemicellulose. The reason to choose this kinetic model is because it considers the effect of the concentration of sulphuric acid in the system, the reactivity of the raw material (which noticeably varies from on material to another (see Section 1.5)) and the effect of temperature in the reactor. This model assumes that the raw material consists of two fractions of hemicellulose: fast and slow. Fast hemicellulose refers to the part of the material that converts completely during the pretreatment and in a high reaction rate.

Slow hemicellulose refers to the fraction of the material whose reaction rate is very low due to the competitive nature of its counterpart. Equations 3.1 to 3.4 are the expressions of the reaction rates for fast hemicellulose, slow hemicellulose, xylose and by-products.

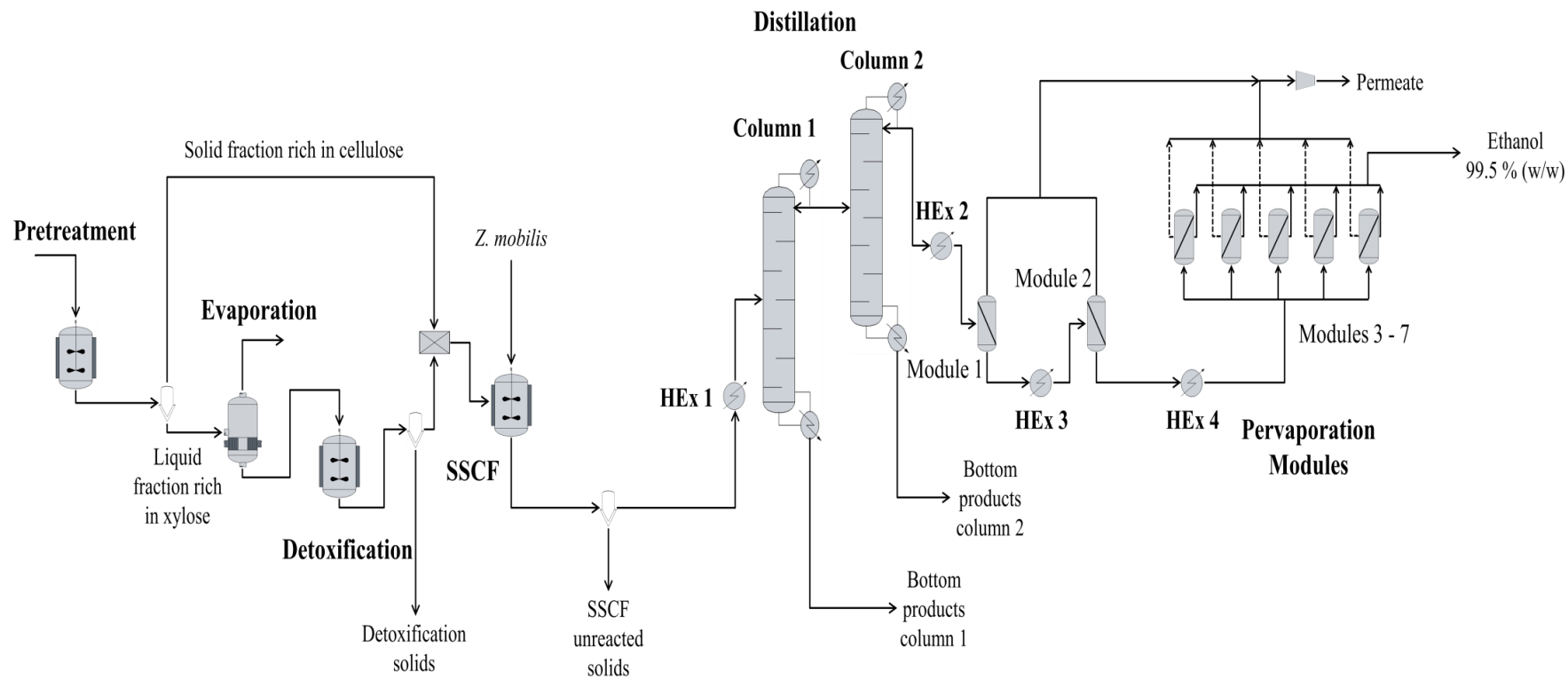


Figure 3.1: Flowsheet of the ethanol production process from corn stover

Table 3.1: Chemical characterisation of corn stover (dry basis % w/w) reported by Bhandari et al., (1984); Čuček et al., (2011); Esteghlalian et al., (1997) and Liu and Chen, (2016)

Component	Composition (% w/w)
Cellulose	36.0
Fast xylan	12.8
Slow xylan	7.00
Galactan	1.30
Arabinan	2.80
Lignin	19.7
Ash	7.20
Other	13.2

Equations 3.5 to 3.7 are Arrhenius-type equations for the reactions rate constants of the previous set of equations as functions of the operating temperature. Equation 3.8 is the actual concentration of sulphuric acid used in the pretreatment of corn stover (Esteghlalian et al., 1997). To summarise:

$$r_{hemi}^{fast} = -k_f C_{hemi}^{fast} \quad \text{Eq. 3.1}$$

$$r_{hemi}^{fast} = -k_s C_{hemi}^{slow} \quad \text{Eq. 3.2}$$

$$r_{xy} = k_f C_{hemi}^{fast} + k_s C_{hemi}^{slow} - k_x C_{xy} \quad \text{Eq. 3.3}$$

$$r_{bp} = k_x C_{xy} \quad \text{Eq. 3.4}$$

$$k_f = A_{fo} C_a^{1.5} \exp\left(-\frac{E_{fo}}{RT}\right) \quad \text{Eq. 3.5}$$

$$k_s = A_{so} C_a^{1.6} \exp\left(-\frac{E_{so}}{RT}\right) \quad \text{Eq. 3.6}$$

$$k_x = A_{2o} C_a^{0.5} \exp\left(-\frac{E_{xo}}{R T}\right) \quad \text{Eq. 3.7}$$

$$C_a = C - (0.1 \text{ Neutralizing ability of the raw material}) \quad \text{Eq. 3.8}$$

where:

A_{fo} : Pre-exponential factor for fast hemicellulose ($6.7 \times 10^{16} \text{ min}^{-1}$)

A_{so} : Pre-exponential factor for slow hemicellulose ($6.9 \times 10^{19} \text{ min}^{-1}$)

A_{xo} : Pre-exponential factor for xylose ($3.7 \times 10^{10} \text{ min}^{-1}$)

C : Real concentration of sulphuric acid in the reactor (mass fraction)

C_a : Actual concentration of sulphuric acid (mass fraction)

C_{fur} : Concentration of furfural produced during pretreatment (g/L)

C_{hemi}^{fast} : Concentration of fast hemicellulose (g/L)

C_{hemi}^{slow} : Concentration of slow hemicellulose (g/L)

C_{xy} : Concentration of xylose (g/L)

E_{fo} : Activation energy for fast hemicellulose conversion (129.8 kJ/mole)

E_{so} : Activation energy for slow hemicellulose conversion (167.6 kJ/mole)

E_{xo} : Activation energy for xylose degradation (98.4 kJ/mole)

k_f : Reaction rate constant for the conversion of fast hemicellulose (min^{-1})

k_s : Reaction rate constant for the conversion of slow hemicellulose (min^{-1})

k_x : Reaction rate constant for the conversion of xylose (min^{-1})

r_{hemi}^{fast} : Reaction rate of fast hemicellulose ($\text{g L}^{-1} \text{ min}^{-1}$)

r_{hemi}^{slow} : Reaction rate of slow hemicellulose ($\text{g L}^{-1} \text{ min}^{-1}$)

r_{xy} : Reaction rate of xylose ($\text{g L}^{-1} \text{min}^{-1}$)

r_{bp} : Reaction rate of by-products produced during pretreatment ($\text{g L}^{-1} \text{min}^{-1}$)

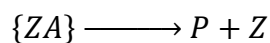
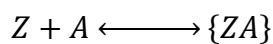
Although the kinetic model for the pretreatment using dilute acid considers several operating conditions involved in the reaction, it does not consider the formation of other by-products and other reducing sugars.

3.4 Evaporation

The outlet stream from the pretreatment reactor is filtered and divided into two streams: one liquid fraction (rich in xylose) and one solid fraction (rich in unreacted cellulose). The liquid fraction is evaporated with the main purpose of increasing the concentration of sugar and to remove some volatile components that can inhibit the performance of the fermenting strains (Binod et al., 2010; Kiran and Jana, 2015; Petersson et al., 2007; Wei et al., 2014, 2014). The mathematical model for the evaporation is formulated from the mass and energy balances which are unfolded in Appendix A.

3.5 Detoxification

The concentrated solution leaving the evaporation unit is treated with $\text{Ca}(\text{OH})_2$ in a process known as detoxification. This process is carried out, at constant temperature and pH, to reduce the concentration of furfural and other by-products, which have a high inhibitory effect on the performance of the fermenting microorganisms, by converting them into insoluble salts (Abedinifar et al., 2009; Bai et al., 2008; Ballesteros et al., 2004; Purwadi et al., 2004). The kinetic model of this unit and the mass balance are taken from Purwadi et al., (2004) and is based on a series of reactions that are assumed to take place during the detoxification of the hydrolysates and are represented as follows:



where:

Z : Concentration of Ca^{2+} cation (g/L)

A : Concentration of furfural (g/L)

P : Concentration of insoluble salts (g/L)

$\{ZA\}$: Concentration of Ca complex (g/L)

The reaction scheme above suggests the formation of a furan – Ca^{+2} complex that rapidly disassociates into insoluble salts and Ca^{+2} ions. In other words, $\text{Ca}(\text{OH})_2$ serves as a base in a neutralization reaction in which the acid hydrolysate is converted into salts. The mathematical model proposed by Purwadi et al., (2004) is an empirical model which was formulated taking into account pH and operating temperature. Unfortunately, this is the only model available in literature since current research only focuses in finding new experimental techniques for the detoxification of the lignocellulosic hydrolysates (see Section 2.3).

The limitations of this model in terms of temperature dependence will have a direct effect on the optimisation of the overall process since it will restrain the evaluation of different operating conditions. The equations of this model are presented as follows and the mass and energy balances are described in more detail in Appendix A. See Purwadi et al. (2004) for the values of the parameters of the model at pH values.

$$r_{fur} = -k_1 C_{fur} (C_{Z,0} - C_{ZA}) + k_2 C_{ZA} \quad \text{Eq. 3.9}$$

$$r_{ZA} = -(k_2 + k_3) C_{ZA} + k_1 C_{fur} (C_{Z,0} - C_{ZA}) \quad \text{Eq. 3.10}$$

$$r_P = -k_3 C_{ZA} \quad \text{Eq. 3.11}$$

The pH level is related to the initial amount of cation $C_{Z,0}$ as shown in Eq. 3.12:

$$C_{Z,o} = k_Z 10^{-(14-pH)} + C_{Z,0}^N \quad \text{Eq. 3.12}$$

where:

C_{fur} : Concentration of furfural (g/L)

C_P : Concentration of insoluble salts (g/L)

C_{ZA} : Concentration of Ca complex (g/L)

$C_{Z,0}^N$: Concentration of $\text{Ca}(\text{OH})_2$ to neutralise hydrolysates from acid state (g/L)

k_i : Reaction rate constants (min^{-1})

r_{fur} : Reaction rate of furfural ($\text{g L}^{-1} \text{min}^{-1}$)

r_P : Reaction rate of insoluble salts ($\text{g L}^{-1} \text{min}^{-1}$)

r_{ZA} : Reaction rate of Ca^{+2} complex ($\text{g L}^{-1} \text{min}^{-1}$)

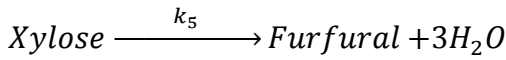
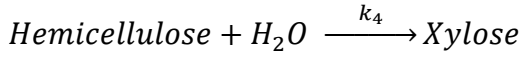
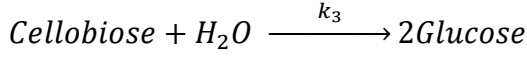
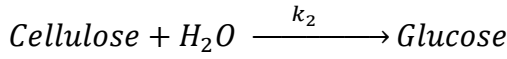
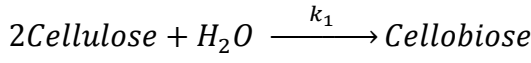
3.6 Simultaneous saccharification and co-fermentation (SSCF)

The stream leaving the detoxification stage is mixed with the solid fraction obtained during the pretreatment which will be later used as substrate in the production of ethanol. The simultaneous saccharification and co-fermentation (SSCF) stage comprises two operations: Enzymatic hydrolysis of cellulose and co-fermentation of both pentoses and hexoses. Both operations take place simultaneously in order to reduce the size of the plant and to further the production of ethanol by reducing the inhibitory effects over the activity of the enzymes and the metabolism of the fermenting strains (Kadam et al., 2004; Kadar et al., 2004; Leksawasdi et al., 2001; Morales-Rodriguez et al., 2011).

3.6.1 Enzymatic hydrolysis

The first operation is the enzymatic hydrolysis or saccharification where the unreacted cellulose from the pretreatment stage is degraded into cellobiose and glucose using cellulases (Bezerra and Dias, 2005; Kadam et al., 2004; Öhgren et al.,

2007b; Saha et al., 2005). The set of reactions for the enzymatic saccharification are listed below.



The kinetic model presented by Kadam et al., (2004) for the saccharification of cellulose using cellulase includes a term for absorption/desorption reaction K_{iad} and a term for the total concentration of enzymes as shown in Equations 3.13 and 3.14.

$$E_{iB} = \frac{E_{imax} K_{iad} E_{iF} C_{cell}}{1 + K_{iad} \cdot E_{iF}} \quad \text{Eq. 3.13}$$

$$E_{iT} = E_{iF} + E_{iB} \quad \text{Eq. 3.14}$$

$i = 1$ for cellulase; $i = 2$ for β -glucosidase

The reaction rates for cellulose, glucose and cellobiose are shown next. These models present the concentration of enzymes and a constant K_{inh} which represents the inhibition effect of the production of glucose, cellobiose and xylose over the activity of the enzymes. The reaction rates for each component are shown as follows:

$$r_{cell} = \frac{k_1 E_{1B} R_s C_{cell}}{1 + \frac{C_{Cb}}{K_{1.inh.Cb}} + \frac{C_{Gl}}{K_{1.inh.Cb}} + \frac{C_{Xy}}{K_{1.inh.Cb}}} \quad \text{Eq. 3.15}$$

$$r_{Gl} = \frac{k_2 (E_{1B} + E_{2B}) R_s C_{cell}}{1 + \frac{C_{Cb}}{K_{2.inh.Cb}} + \frac{C_{Gl}}{K_{2.inh.Cb}} + \frac{C_{Xy}}{K_{2.inh.Cb}}} \quad \text{Eq. 3.16}$$

$$r_{Cb} = \frac{k_3 E_{2F} R_s C_{Cb}}{K_{3M} \left(1 + \frac{C_{Gl}}{K_{3.inh.Gl}} + \frac{C_{Xy}}{K_{3.inh.Xy}}\right) + C_{Cb}} \quad \text{Eq. 3.17}$$

A variation for hemicellulose conversion into xylose and further degradation into furfural during the enzymatic hydrolysis has been proposed by Ballesteros et al. (2004).

$$r_{hemi} = k_4 C_{hemi} \quad \text{Eq. 3.18}$$

$$r_{Xy} = k_5 C_{Xy} \quad \text{Eq. 3.19}$$

3.6.2 Co-fermentation

The second operation is the co-fermentation of reducing sugars (e.g. xylose, glucose, cellobiose, etc.) into ethanol and other by-products (i.e. acetic acid, CO₂, cells, etc.) via anaerobic metabolism. The kinetic model presented by Leksawasdi et al., (2001) for recombinant bacterium *Zymomonas mobilis* ZM4(pZB5) includes the inhibition effect caused by the substrate, the main product and toxic by-products such as furfural. This mathematical approach is based on the Monod cell growth model. The mass and energy balances of the combined processes are summarized in Appendix A. The kinetic model for co-fermentation using bacteria is the following:

$$r_{X,Gl} = \mu_{max,Gl} \left(\frac{C_{Gl}}{K_{sx,Gl} + C_{Gl}} \right) \left(1 - \frac{C_{Eth} - C_{Eth,ix,Gl}}{C_{Eth,max,Gl} - C_{Eth,ix,Gl}} \right) \left(\frac{K_{ix,Gl}}{K_{ix,Gl} + C_{Gl}} \right) \quad \text{Eq. 3.20}$$

$$r_{X,Xy} = \mu_{max,Xy} \left(\frac{C_{Xy}}{K_{sx,Xy} + C_{Xy}} \right) \left(1 - \frac{C_{Eth} - C_{Eth,ix,Xy}}{C_{Eth,max,Xy} - C_{Eth,ix,Xy}} \right) \left(\frac{K_{ix,Xy}}{K_{ix,Xy} + C_{Xy}} \right) \quad \text{Eq. 3.21}$$

$$r_X = [\alpha r_{X,Gl} + (1 - \alpha) r_{X,Xy}] C_X \quad \text{Eq. 3.22}$$

$$r_{Gl} = \alpha q_{s,max,Gl} \left(\frac{C_{Gl}}{K_{ss,Gl} + C_{Gl}} \right) \left(1 - \frac{C_{Eth} - C_{Eth,is,Gl}}{C_{Eth,ms,Gl} - C_{Eth,is,Gl}} \right) \left(\frac{K_{is,Gl}}{K_{is,Gl} + C_{Gl}} \right) C_X \quad \text{Eq. 3.23}$$

$$r_{P,Gl} = q_{max,Gl} \left(\frac{C_{Gl}}{K_{sp,Gl} + C_{Gl}} \right) \left(1 - \frac{C_{Eth} - C_{Eth,ip,Gl}}{C_{Eth,mp,Gl} - C_{Eth,ip,Gl}} \right) \left(\frac{K_{ip,Gl}}{K_{ip,Gl} + C_{Gl}} \right) \quad \text{Eq. 3.24}$$

$$r_{P,XY} = q_{max,XY} \left(\frac{C_{XY}}{K_{sp,XY} + C_{XY}} \right) \left(1 - \frac{C_{Eth} - C_{Eth,ip,XY}}{C_{Eth,mp,XY} - C_{Eth,ip,XY}} \right) \left(\frac{K_{ip,XY}}{K_{ip,XY} + C_{XY}} \right) \quad \text{Eq. 3.25}$$

$$r_P = [\alpha r_{P,Gl} + (1 - \alpha) r_{P,XY}] C_X \quad \text{Eq. 3.26}$$

where:

- C_{cell} : Concentration of cellulose (g/L)
- C_{cb} : Concentration of cellobiose (g/L)
- C_{Eth} : Concentration of ethanol (g/L)
- $C_{Eth,ip,Gl}$: Threshold inhibition concentration of ethanol from glucose (g/L)
- $C_{Eth,is,Gl}$: Threshold conc. of ethanol from glucose that affects glucose uptake (g/L)
- $C_{Eth,ix,Gl}$: Threshold conc. of ethanol from glucose that causes inhibition (g/L)
- $C_{Eth,ip,XY}$: Threshold inhibition concentration of ethanol from xylose (g/L)
- $C_{Eth,is,XY}$: Threshold conc. of ethanol from xylose that affects xylose uptake (g/L)
- $C_{Eth,ix,XY}$: Threshold conc. of ethanol from xylose that causes inhibition (g/L)
- $C_{Eth,mp,Gl}$: Maximum inhibition concentration of ethanol from glucose (g/L)
- $C_{Eth,mp,XY}$: Maximum inhibition concentration of ethanol from xylose (g/L)
- $C_{Eth,ms,Gl}$: Maximum conc. of ethanol from glucose that affects glucose uptake (g/L)

$C_{Eth,ms,XY}$: Maximum conc. of ethanol from glucose that affects xylose uptake (g/L)
$C_{Eth,mx,Gl}$: Maximum conc. of ethanol from glucose that causes inhibition (g/L)
$C_{Eth,mx,XY}$: Maximum conc. of ethanol from xylose that causes inhibition (g/L)
C_{Gl}	: Concentration of glucose (g/L)
C_{hemi}	: Concentration of hemicellulose (g/L)
C_X	: Concentration of cells (g/L)
C_{XY}	: Concentration of xylose (g/L)
E_{iB}	: Bound concentration of enzymes on the substrate (g/L)
E_{iF}	: Concentration of free enzymes in solution (g/L)
E_{iT}	: Total enzyme concentration (g/L)
E_{imax}	: Maximum mass of active enzyme/substrate (kg of protein/kg of substrate)
K_{iad}	: Dissociation const. for absorption/desorption reaction i ($i=$ reactions 1, 2, 3 m ³ /kg of protein)
r_i	: Reaction rates for equation 16 – 28 (g L ⁻¹ min ⁻¹)
R_s	: Substrate reactivity
$K_{j:inh:k}$: Inhibition const. for the reactions $j = 1, 2, 3$. $k =$ cellobiose, glucose, xylose (g/L)

Equations 3.20 to 3.26 are the reaction rates for the consumption of xylose and glucose as well as the production of ethanol and cells during the co-fermentation stage. These equations are governed by two important aspects. The first one is the inhibition effect by both substrate and product which can be identified as K_{is} and K_{ip} ,

respectively. The second aspect is the maximum concentration of ethanol that can be produced without inhibiting the strain.

This is a detailed model that covers several aspects of the fermentation of reducing sugars and therefore will be used in the overall simulation of the ethanol production process (Morales-Rodriguez et al., 2011). The kinetic models for both enzymatic hydrolysis and co-fermentation are limited by the number of components that the authors investigated in their respective works. This issue is addressed later in this thesis in order to determine how these limitations affect the simulation and optimisation of the overall process.

3.7 Separation

Once the SSCF operation stops, the content of the reactor is filtered in order to remove cells and other solids. The liquid, consisting mainly of ethanol and water, is sent to a separation section where ethanol is purified to biofuel standard concentrations (>99% w/w.). The separation stage comprises two parts as described next.

3.7.1 Distillation

The first part of the separation stage is the removal of ethanol from the fermentation broth via distillation. A binary mixture of ethanol and water is recovered and purified to its azeotropic point. Two distillation columns are often used in order to reach this separation (Kiss and Olujic, 2014; Knapp and Doherty, 1992; Lutze and Gorak, 2013). The mass and energy balances and the assumptions used in this work are summarised in Appendix A.

3.7.2 Membrane-based operation

The second stage is the dehydration of the binary azeotropic mixture via membrane separation. This methodology is able to reach concentrations of ethanol of 99 % w/w or even higher. The membrane separation stage comprises different modules in parallel and/or in-series to increase the purity of ethanol with low energy consumption (Koch et al., 2013; Lutze and Gorak, 2013; Roth et al., 2013;

Valentinyi et al., 2013). The model used in this work to simulate the pervaporation module is the one introduced by Tsuyumoto et al., (1997). The mass and energy balances for the fibre side and the shell side are shown in Appendix A. Eq. 3.27 presents the partial molar flux of ethanol as a function of the pressure gradient between feed and permeate and also the mole composition in the feed stream.

$$J_{Ethanol} = 1.72 \times 10^{-10} x_{Ethanol} (P_{feed} - P_{permeate}) \quad \text{Eq. 3.27}$$

Eq. 3.28 is the partial molar flux for water permeating through the membrane. This is a more complex formulation as it includes the activity between the vapour phase and the liquid phase. This equation is a function of feed temperature, permeate pressure, mole fraction of water in feed, mole fraction of water in permeate, the thickness of the membrane. Tsuyumoto et al., (1997) and (1995) obtained the parameters of this model for permeate pressures between 10 and 10,000 Pa, temperatures between 40 and 70 °C and concentrations of ethanol in feed between 99 and 99.5 % (w/w).

$$J_{Water} = \frac{8.086 \times 10^6 \exp\left(-\frac{11500}{T}\right)}{\delta_m} \left(\gamma_{feed} x_{water} - \frac{P_{permeate}}{P_{Water}^{sat}} Y_{water} \right) + \frac{3.441 \times 10^{-3} \exp\left(-\frac{3390}{T}\right)}{2\delta_m} \left((\gamma_{feed} \cdot x_{water})^2 - \left(\frac{P_{permeate}}{P_{Water}^{sat}} y_{water} \right)^2 \right) \quad \text{Eq. 3.28}$$

3.8 Results

The mass and energy balances and other equations used in this work (and outlined in Appendix A) are solved using gPROMS (Process System Enterprises, 2015). In order to solve the models and validate their formulation, a revision of the algorithms and solvers used in gPROMS should be introduced. gPROMS presents two mathematical solvers for the simultaneous solution of differential and algebraic (DA) systems: DASOLV and SRADAU. Both are very effective in the solution of DA systems but they differ from each other in the method of integration. DASOLV uses *Backward Finite Differences* (BFD) whereas SRADAU uses a 4th order *Runge-Kutta* method. The stability and effectiveness of these models depends on discontinuities

and oscillations in the system. In this work, DASOLV is used since computational times with this method are substantially shorter than with SRADAU (5 sec shorter) (Process System Enterprises, 2015). Both solvers automatically adjust the integration step so the criterion shown in Eq. 3.29 can be met. The difference in CPU times is

$$\sqrt{\frac{1}{n_d} \sum_{i=1}^{n_d} \left(\frac{\epsilon_i}{a + r|x_i|} \right)^2} \quad \text{Eq. 3.29}$$

where:

- n_d : The number of differential variables in the problem
- I : The solver's estimate for the local error in the i^{th} differential variable
- x_i : The current value the i^{th} differential variable
- a : Absolute error tolerance
- r : Relative error tolerance

Each model is validated against experimental results (in the case of the reactors and the pervaporation modules) and ChemCAD (for the distillation columns).

3.9 Pretreatment stage

The pretreatment stage is validated against the experimental results obtained by Esteghlalian et al., (1997) and this is shown in Figure 3.2. The results in this figure initially suggest good concordance for the percentage of xylose remaining in the raw material between the experimental data and the mathematical model. Figure 3.2 also shows the effect of temperature in the pretreatment as the conversion of hemicellulose. Higher temperatures not only increase the conversion of hemicellulose but also reduce the reaction time as hemicellulose degrades more quickly than as seen in the curves of 140 °C and 180 °C for a concentration of sulphuric acid of 0.6 % (w/w). Conversely, the concentration of sulphuric acid in the reaction also contributes to the fast degradation of hemicellulose into xylose. Figure 3.2 indicates a reduction of the amount of xylose remaining in the material as the

concentration of sulphuric acid doubles up. According to Esteghlalian et al., (1997), yields of xylose above 80 % from corn stover can be reached at temperatures of 180 °C and concentrations of sulphuric acid of 1.2 % (w/w).

3.10 Detoxification stage or Overliming

The overliming model proposed by Purwadi et al., (2004) has been compared with experimental results at 30 °C for different pH levels. As seen in Figure 3.3, the concentration of furfural in the hydrolysates decreases as pH increases, suggesting a faster neutralisation of the acid hydrolysates. The experimental data obtained by Purwadi et al. (2004), are close to the trend predicted by the mathematical model which justifies the implementation of this model into the main process. However, this model is restricted to the operating configurations at which the parameters were obtained. The parameters for the detoxification model are available in the work Purwadi and collaborators at an operating temperature of 30 °C.

3.11 Enzymatic hydrolysis stage

During the enzymatic hydrolysis of cellulose, cellulases cut the chain of the biopolymer to produce monomeric units known as glucose and cellobiose. For the formulation of the model and therefore the estimation of its parameters, it is required to measure the concentration of most of the species involved in the reaction.

In the case of the work presented by Kadam et al., (2004), the only components that could be measured in laboratory were glucose and cellobiose. These sugars are usually quantified in laboratory using instrumental analysis or colourimetry (Najafpour and Shan, 2003; Saini et al., 2013; Xiao et al., 2004).

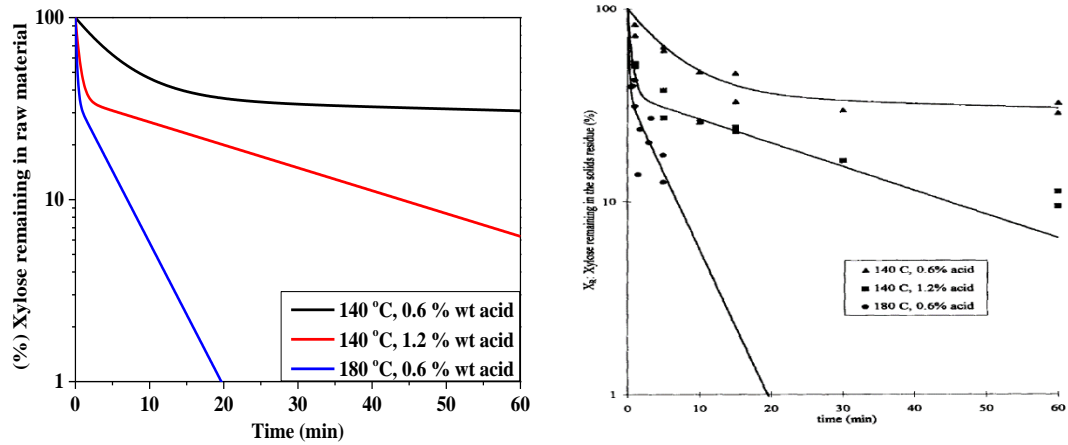


Figure 3.2: Xylose remaining in the solid fraction in the hydrolysis of hemicellulose. The left side represents the results obtained with gPROMS. The right side is the experimental data presented by Esteghlalian et al., (1997)

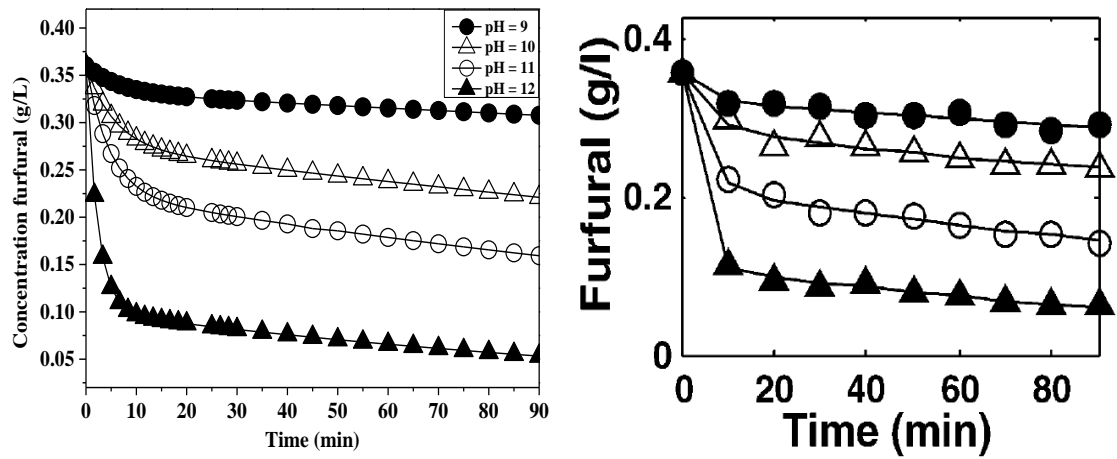


Figure 3.3: Model validation for the detoxification of acid hydrolysates. The left side shows the results using gPROMS. The right side shows the experimental data obtained by Purwadi et al., (2004)

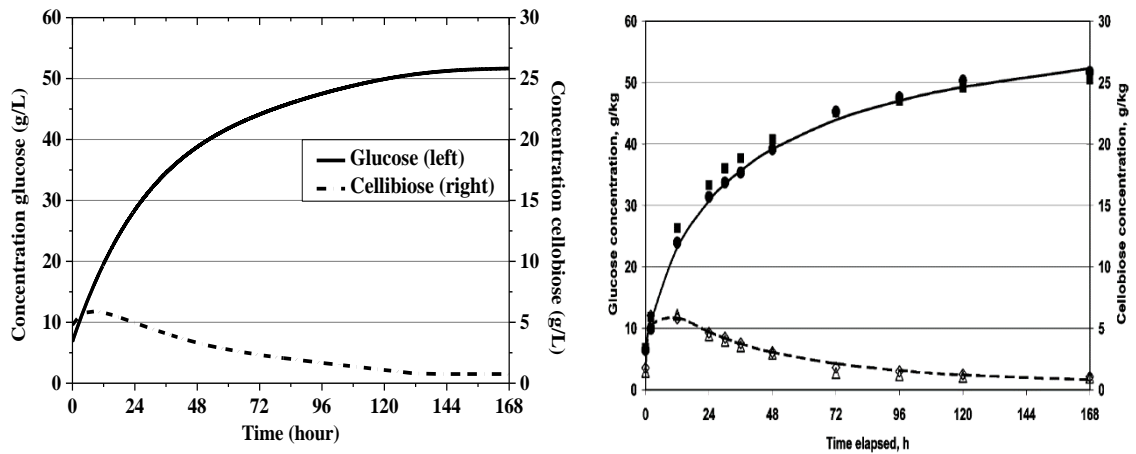


Figure 3.4: Validation of the kinetic model for enzymatic saccharification. The left side presents the results using gPROMS. The right side presents the experimental data presented by Kadam et al., (2004)

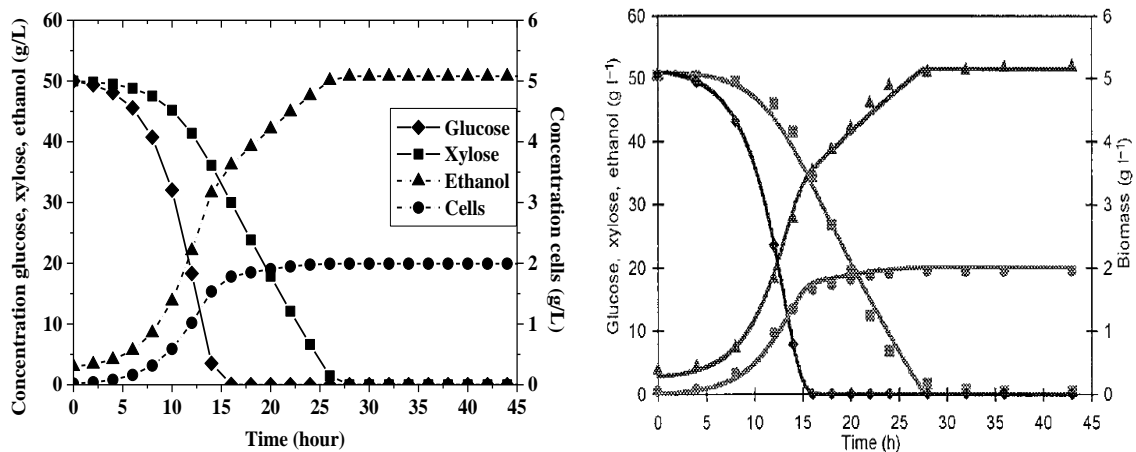


Figure 3.5: Validation of the fermentation model proposed by Leksawasdi et al., (2001). The left side presents the results using gPROMS. The right side presents the experimental data

The experimental results in Figure 3.4 were obtained using 10% w/w corn stover solids with no added background sugars at 45 °C and, as seen in Figure 3.4, the production of glucose and the production and subsequent conversion of cellobiose in the enzymatic hydrolysis take place in a period of 168 h. The kinetic model proposed by Kadam et al., 2004 is chosen in this work because it considers inhibition by xylose, a major sugar in hemicellulose-derived hydrolysates. Other models not only neglect the effect of the concentration of xylose in the production of glucose but also do not consider the benefits of supplementing the reaction medium with β -glucosidase for higher yields of glucose.

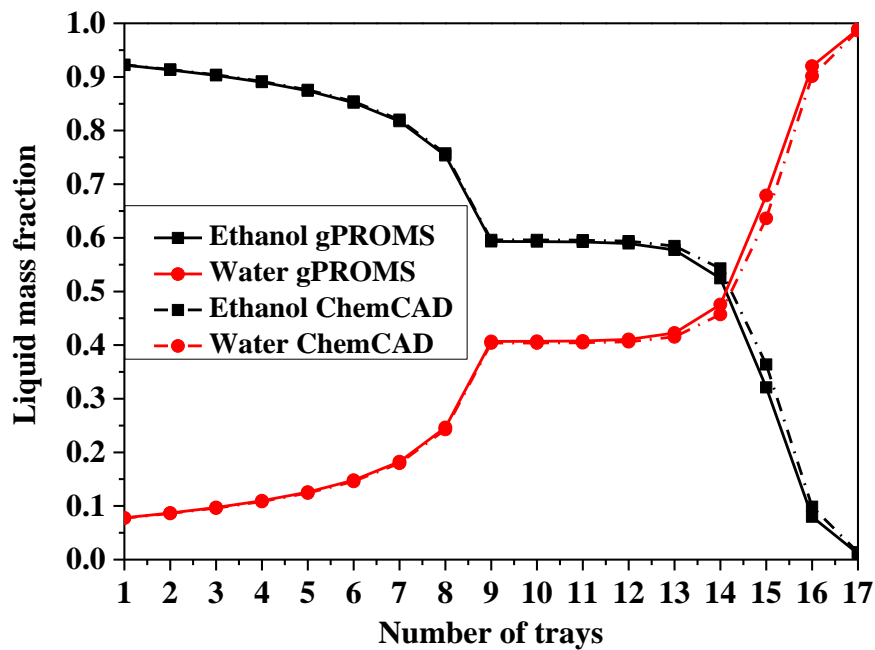


Figure 3.6: Validation profile for liquid weight fraction of binary mixture ethanol/water using gPROMS and ChemCAD

Table 3.2: Estimated ethanol purity for an ethanol feed concentration of 94% (w/w)

Feed flow rate (kg/h)	Ethanol concentration (% w/w)		
	Tsuyumoto et al., (1997)	Marriott and Sorensen, (2003); Marriott et al., (2001) (3D model)	This work
44.9	97.20 (Experimental data)	97.30	97.18 (Calculated)

3.12 Co-fermentation stage

Figure 3.5 presents the validation of the co-fermentation model proposed by Leksawasdi et al., (2001). This model describes the fermentation of both xylose and glucose into ethanol using a recombinant bacterium known as *Zymomonas mobilis* ZM4 (*pZB5*). The results of the kinetic model show agreement with the experimental data obtained by Leksawasdi et al., (2001). It is also clear that by using this microorganism, a higher conversion of both xylose and glucose and lower production of cells can be expected in comparison to conventional strains often used in industry.

3.13 Distillation stage

The distillation column system has also been validated. The results of the dynamic model for a distillation column are compared against ChemCAD when the column has reached steady-state. For the simulation, a flow rate of 1.18 kg/sec (or 50 mol/sec) of a solution 20 % mole of ethanol is fed into a distillation column consisting of 15 trays, one total condenser and one reboiler. The number of stages is determined with the Fenske-Underwood-Gilliland (FUG) approach using ChemCAD's shortcut model. The activity model used in both simulations is NRTL and the Equation of State is PSRK for the evaluation of thermodynamic properties. As seen in Figure 3.6, the results using the MESH equations in gPROMS for the distillation column follow a similar trend as the profiles obtained using ChemCAD.

3.14 Pervaporation stage

Table 3.2 shows the validation of the model for the pervaporation module against the experimental results obtained by Tsuyumoto et al., (1997). It also shows the results reported by Marriott and Sorensen which consider radial and axial distribution of ethanol and water inside the membrane module as well as the operation time. The concentration of ethanol in the retentate obtained in this work considers a plug-flow approach inside the membrane module and is very similar to the results obtained with the 3D approach (a difference of 0.12 %). This suggests that a more robust formulation does not necessarily increase accuracy or even required and often incurs in longer computational times due to the complexity that entails solving partial differential equations. Although radial and axial distributions are important for a thorough design of the module and the performance of the membrane, this work will not consider this approach since the main objective is to integrate all the sources of energy in the process for a more efficient and profitable production of ethanol.

3.15 Conclusions

This chapter presented the different models that describe the different units involved in the production of ethanol from corn stover. The empirical models used for the pretreatment, detoxification, enzymatic hydrolysis and fermentation were validated against experimental data used for their own formulation which are available in the

respective publications. These comparisons were made in order to guarantee an accurate depiction of the reactions that take place in the production of ethanol. However, it is important to notice that these models are restricted to a range of operating conditions and this can limit the opportunities to explore different designs and arrangements of the process with higher efficiencies. The system of equations that described the distillation process was developed from dynamic mass and energy balances and the results of the simulation were compared to licensed software giving similar trends in the profiles of the mass fractions along the column. The mathematical formulation of the distillation column using gPROMS considered the non-ideality of the mixture ethanol/water as well as the implementation of equations of state to predict thermodynamic properties.

The model for the pervaporation using a hydrophilic membrane proposed by Tsuyumoto et al., (1997) has been used in several works since it considers the effect of the different operating conditions in the system as well as the concentration of ethanol in the feed. Some of these works have considered a more complex formulation of the distribution of the species inside the membrane module. However, the results obtained in this work have shown that a more simplistic focus on the simulation of the membrane was as effective as a more rigorous and detailed approach. In other words, a plug-flow formulation gave similar results in the concentration of ethanol to the 3D model. The following chapters will present the incorporation of all these models into an overall simulation of the ethanol production process leading to the heat integration thereof.

Chapter 4 presents the development of a mathematical model based on experimentations of an organophilic membrane for the removal of ethanol from aqueous solutions. This model will be used in the simulation of the complete process in order to determine the viability in terms of separation rates, energy consumption and total annualised cost.

Chapter 4 – Ethanol recovery from aqueous solutions using a PERVAP™ 4060 organophilic membrane

Abstract

Pervaporation is one of the most investigated and most applied membrane-based methods for ethanol dehydration in industry as it generally is less energy intensive than distillation. This work presents the formulation of a model that can describe the performance of a PERVAP™ 4060 organophilic membrane used for the separation of ethanol from a fermentation broth in order to reduce the energy consumption of the separation stages in the ethanol production process.

4.1 Introduction

The literature review presented in Chapter 2 showed a variety of works using different techniques to recover ethanol from aqueous solutions. Most of these works included membrane-assisted methods to overcome the azeotrope and reduce energy consumption (Cho et al., 2010; Golias et al., 2002; Sánchez and Cardona, 2012; Siqueira et al., 2008).

Alternative technologies for fluid separations include membrane-based operations such as pervaporation, reverse osmosis and vapour permeation (Gaykawad et al., 2013, 2012; Wei et al., 2014). Membrane-based operations can be implemented as stand-alone processes or in combination with other units (i.e. hybrid separation processes) to complete a separation task (Kreis and Górak, 2006). Currently, membrane separations are seldom considered as stand-alone operations since they have a low throughput and require larger membrane areas, resulting in high investment and operating costs. If large streams or high purities are required, membrane separations are best applied within hybrid processes which are membrane

systems coupled with thermal and/or extractive separation technologies (e.g. distillation, absorption, esterification reactors, etc.) (Lutze and Gorak, 2013).

Some of the benefits of using hybrid processes (e.g. membrane-assisted distillation processes) include: large flexibility (the system can deal with a wide range of operating conditions, feed concentrations, capacity and purity requirements), improvement in energy efficiency (the separation stages can achieve high separation rates with low energy inputs) and the reduction of the size of some of the units in the process (Koch et al., 2013; Lutze and Gorak, 2013; Valentinyi et al., 2013).

This work will considered a system consisting of a distillation column coupled with a membrane-based operation to remove ethanol from the fermentation broth. Pervaporation is one of the most potentially interesting types of membrane-assisted separation methods used for solvent dehydration, organic solvents removal, breaking azeotropes, etc. Pervaporation consists of two steps: (a) permeation of one or more of the components of the feed through the membrane due to the gradient in the chemical potential because of pressure and concentration differences between the permeate and the retentate side and (b) evaporation into the vapour phase on the permeation side of the membrane (Yakovlev et al., 2013).

Configurations for the dehydration of ethanol often include a distillation system followed by a pervaporation network with hydrophilic membranes (Baker, 2012; Roth et al., 2013). The distillate stream of the distillation system leaves the column with a concentration close to the azeotrope and is passed through a hydrophilic membrane network where water is removed in the permeate side and ethanol reaches concentrations higher than 99 % (Marriott and Sorensen, 2003; Nagasawa et al., 2016; Tsuyumoto et al., 1997).

This chapter proposes the inclusion of a pervaporation module into the separation stage using a selective membrane to remove ethanol from the fermentation broth through the permeate side. The pervaporation module will be located between the

fermentation stage and the distillation column and is expected to operate at the same temperatures as the fermentation tank.

A polymeric membrane PERVAPTM 4060 will be considered in this work. This particular membrane removes volatile organic components through the permeate side instead of removing water as in the case of hydrophilic membranes. The PERVAPTM 4060 organophilic membrane has been studied for the removal of butanol, benzaldehyde, ethanol, heptane, 1-octen-3-ol from aqueous solutions (Ben Soltane et al., 2013; Claes et al., 2010; Martinez et al., 2013).

In order to assess the effectiveness of the implementation of the PERVAPTM 4060 organophilic membrane into the ethanol production a mathematical model of the system ethanol/water, based on experimentation, is required. However, there are no publications regarding the formulation of an empirical mathematical model of this specific system at the operating conditions expected to be obtained from a fermentation reactor. This chapter presents the formulation of an empirical model for the pervaporation of ethanol through an organophilic membrane. The membrane used in this work is a PERVAPTM 4060 polymeric membrane provided by Sulzer (Holtbruegge et al., 2013; Koch and Gorak, 2014). The operating conditions and the experimental procedure are explained in more detail in Sections 4.2 and 4.3, respectively. Sections 4.4 and 4.5 present the parameter estimation of the mathematical model using the experimental data and the statistical analysis thereof.

4.2 Experimental materials and methods

In order to estimate the parameters of a model that describes the permeation of ethanol, experimental data are required. This set of experiments is obtained in collaboration with the Laboratory of Fluid Separations at Technische Universität Dortmund, Germany. The mathematical model of the membrane has to be able to determine the permeance and partial fluxes of ethanol and water through said membrane when feed concentration, feed temperature and permeate pressure are specified.

The model also needs to show good fit with the experimental data given that its formulation is purely empirical. Additional experiments are carried out in order to evaluate the influence of some common fermentation by-products over the performance of membrane since these components may affect the performance of the pervaporation module.

4.2.1 Materials

The feed concentration of ethanol for the set of experiments presented in Table 4.1 is the range of concentrations that can be obtained after the filtration of the unreacted solids from the fermentation stage (Baeyens et al., 2015; Fan et al., 2014; Gaykawad et al., 2012). The range of feed temperatures includes the operating temperatures at which the microorganisms and the enzymes can simultaneously perform without compromising their activity and metabolism (Haelssig et al., 2012; O'Brien et al., 2004).

The range of operation for permeate pressure is between 400 and 3500 *Pa* and as Holtbruegge et al., 2013 have demonstrated, the optimal operating costs can often be found at maximum pressure differences between the feed and the permeate side. Table 4.1 summarises the operating conditions used in the estimation of the parameters of the mathematical model. Figure 4.1 shows the experimental design proposed for the development of the mathematical model. This experimental set-up considers a number of experiments that will cover the different operating conditions in order to guarantee a good fit of the parameters. The chemical system consists mainly of ethanol and water which are obtained after the fermentation stage (Erdei et al., 2013). However, during the fermentation of lignocellulosic hydrolysates, other by-products such as organic acids, glycerol, CO₂, can also be produced, although in lower concentrations (Sánchez and Cardona, 2012). Table 4.2 presents some of the most common by-products in the fermentation of lignocellulosic hydrolysates.

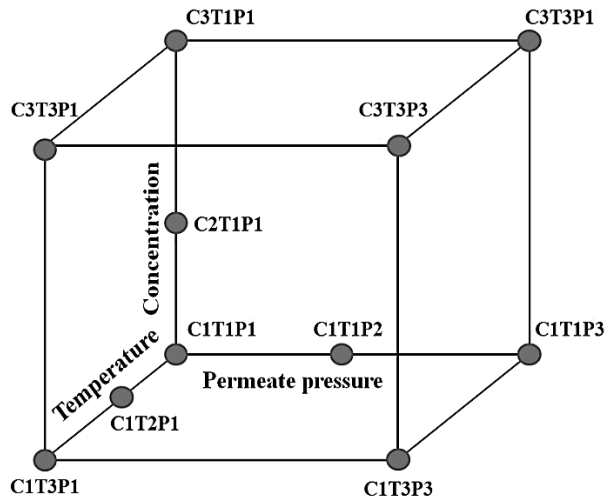


Figure 4.1: Experimental design for the evaluation of the parameters of the mathematical model of the PERVAP™ 4060 membrane (C = feed concentration, T = feed temperature, P = permeate pressure)

Table 4.1: Operating conditions used in the experiments

Point	Ethanol feed conc. (% w/w)	Feed temperature (°C)	Permeate pressure (mbar)
1	5 (C1)	30 (T1)	4 (P1)
2	7 (C2)	40 (T2)	20 (P2)
3	13 (C3)	50 (T3)	35 (P3)

4.2.2 Membrane and module

Figure 4.2 shows the flowsheet for the pervaporation module used in the Laboratory of Fluid Separations at TU Dortmund. The pervaporation plant (Figures 4.2 and 4.3) consists of a membrane module (3) inside of a thermal oven (4) that controls the temperature of the system and a jacketed tank (1) where the mixture is fed, completely insulated in order to avoid heat losses (see Figures 4.4 to 4.6).

The plant also features a set of cooling traps (5) (see also Figure 4.7) in which the condensate of the vapour that permeates through the membrane is collected for further measurements. The system initially operates in a loop in order to guarantee the steady-state conditions prior to the measurement of concentration in the samples. Once these conditions have been reached, the sampling can commence.

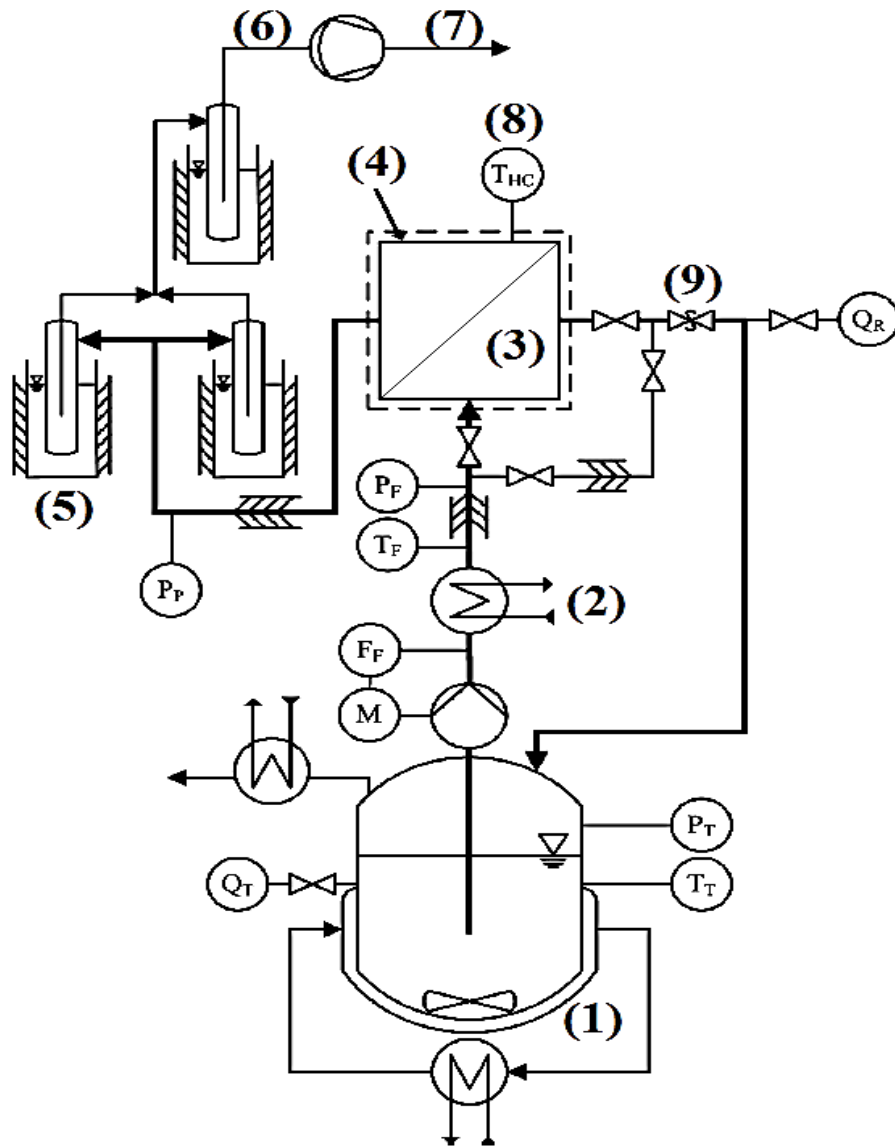


Figure 4.2: Simplified flowsheet of the laboratory-scale set-up for pervaporation experiments. (1) Feed tank, (2) Heat exchanger, (3) Membrane module, (4) Thermal oven, (5) Cooling traps, (6) Vacuum pump, (7) Exhaust, (8) Heating cabinet and (9) Back-pressure regulator

Table 4.2: List of components produced during the fermentation of lignocellulosic hydrolysates

Raw material	Pretreatment	Microorganism	Ethanol (g/L)	Acetic acid (g/L)	Glycerol (g/L)	Glucose (g/L)	Xylose (g/L)	Reference
Whole wheat	Steam explosion	<i>Saccharomyces cerevisiae</i> TMB3400	27 – 35	2.1 - 3	3.7- 4.3	0.3 - 0.7	15 - 17	(Erdei et al., 2013)
Whole wheat	Steam explosion + Amyloglucosidases	<i>Saccharomyces cerevisiae</i> TMB3400	44 – 45	2.1 - 3	4.7- 4.8	0.9 - 1	14 - 17	(Erdei et al., 2013)
Wheat straw	Steam explosion	<i>Saccharomyces cerevisiae</i> F12	22	5.6 - 5.7	-	0 - 5	15 - 16	(A. Moreno et al., 2013)
Paja brava	Steam explosion	<i>Saccharomyces cerevisiae</i> TMB3400	35 - 40	2.9 - 3.5	3.5- 4	<0.1	8 – 8.5	(Carrasco et al., 2011)
Hydrolysate	Dilute acid	<i>Yeast CGMCC 2661</i>	20 - 30	-	-	<0.5	<0.5	(Tian et al., 2009)
Sugar cane Bagasse	Dilute acid	<i>E. coli</i> SL100	20 - 30	-	-	<0.5	4.0 - 6	(Geddes et al., 2011)
Hydrolysate	Dilute acid	<i>Mucor indicus</i>	15 - 20	-	1.0 - 2	<0.5	2.0 - 4	(K Karimi et al., 2006)
Barley straw	Concentrated acid	<i>Saccharomyces cerevisiae</i> CEN.PK113-7D	21 - 30	2.04	-	<0.5	-	(Gaykawad et al., 2012)
Willow wood chips	Mild alkaline	<i>Saccharomyces cerevisiae</i> CEN.PK113-7D	8.0 - 12	5.43	-	<0.5	-	(Gaykawad et al., 2012)
Barley straw	Mild alkaline	<i>Saccharomyces cerevisiae</i> CEN.PK113-7D	13 - 19	4.75	-	<0.5	-	(Gaykawad et al., 2012)
Prepared Mixture	-	-	30 - 40	-	1	5	5	(Chovau et al., 2011)
Corn fibre	Dilute acid	<i>E. coli strain KO 11</i>	30 - 40	<0.5*	-	<0.5	5.0 - 10	(O'Brien et al., 2004)
Spruce chips	SO ₂ impregnation and exposed to a pressure of 22 bar	<i>Saccharomyces cerevisiae</i> (commercial)	51 - 52	9.6 - 9.8 *	-	1.5	3.7	(Ishola et al., 2013)

*After detoxification and neutralisation



Figure 4.3: Pervaporation plant



Figure 4.4: Membrane module



Figure 4.5: Thermal oven

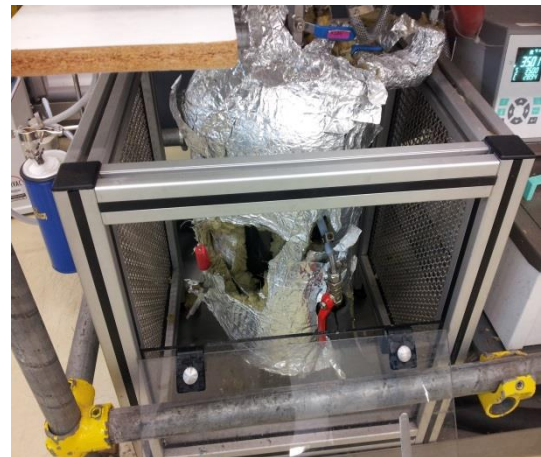


Figure 4.6: Jacketed tank



Figure 4.7: Cooling traps

Table 4.3: Specifications for the optimal operation of the PERVAP™ 4060 membrane
(Sulzer Chemtech, 2014)

Item	Value
Max concentration in feed	
Organic components	90 % (w/w)
Organic acids	<1 % (w/w)
Inorganic acids	<0.1% (w/w)
Maximum temperature	
Short operating times	85 °C
Long operating times	80 °C

The PERVAP™ 4060 membrane uses an active polyvinyl alcohol separating layer (the idealised formula $[\text{CH}_2\text{CH}(\text{OH})]_n$), differently cross-linked to adapt the membrane separation performance to different operating conditions and components in the feed stream (Ben Soltane et al., 2013; Claes et al., 2010; Sulzer Chemtech, 2014). The PERVAP™ 4060 membrane is mainly used to selectively separate volatile organic components (VOC's) such as benzene, benzaldehyde, ethanol, isobutanol, methanol, among others showing high separation rates with smaller membrane areas (Claes et al., 2012, 2010; Setlhaku et al., 2013; Yakovlev et al., 2013). The membrane area used in these experiments is 124.6 cm² which fits in the membrane module provided by TU Dortmund. The specifications for an optimal operation of this membrane are shown in Table 4.3.

4.2.3 Gas chromatography

A gas chromatograph (Shimadzu GC14A with software GCSolution) equipped with a flame ionisation detector (FID) is used to analyse feed, retentate and permeate samples. It has a column Restek RTX 5 which uses diphenyl dimethyl polysiloxane as a stationary component for sampling using an internal standard component. The specifications of the GC column are the following (RESTEK, 2016):

- Length = 30 mm
- Internal diameter = 0.25mm
- Film diameter = 1µm

The mass fractions of organic compounds are obtained directly from the evaluation of the chromatogram based on single-component calibration curves using acetonitrile as the internal standard. Each sample is analysed three times and average values are used for further estimation of the parameters taking into account the standard deviation of each experiment (Koch and Gorak, 2014; Roth et al., 2013). The quality of the GC analysis is validated during the experiments by the analysis of test mixtures with known compositions. The FID detector used in the GC analysis is able to analyse only the mass fraction of organic components such as ethanol and acetonitrile in the samples. The mass fraction of water is calculated from the mass fractions of ethanol and acetonitrile determined by the GC analysis using a total mass balance. The operating conditions of the Shimadzu GC14A, used in this work, are presented next:

- Helium as carrier gas with pressure of 65 *kPa*
- Split around 1:80 1 μ l injection-volume
- Detector: FID (with synth. Air and Hydrogen)

Temperature programme:

- Detector: 300 °C
- Injection-temperature: 275 °C
- Column: (only Ethanol) 80 °C hold for 3.5 min at constant temperature
- Column: (with Acetic Acid) 80 °C hold for 3.2 min heat up with 30 °C/min to 150 °C hold for 0.5 min

4.3 Experimental procedure

The experimental procedure implemented in this work is as follows:

1. Open the bypass valves and close the valves that feed the membrane module (3) to circulate the mixture during the stabilisation of the process (see Figure 4.2).
2. Open the valves of the feed tank (1).

3. Turn on the control system of the thermal oven (3) and set the desired temperature.
4. Switch on the vacuum pump and set the permeate pressure at which the separation will take place.
5. Switch on the pump used for the feed (1) and circulation of the mixture at a flow rate of 50 L/h. The feed flow rate has to be high since in this experiment what is being determined is only the flux through the membrane and the concentration in permeate. The concentration in retentate is expected to be the same as in the feed.
6. Turn on the control system for the temperature and set a feed temperature.
7. Set the feed concentration of the mixture by adding ethanol or water to the feed tank (GC analysis is used here in order to determine the feed concentration).
8. When the temperature has reached the set point and is no longer changing, the feed valve of the membrane module is opened and the bypass is closed. It is recommendable to wait for 30 more minutes after steady-state has been reached in order to guarantee reliable data.
9. Place the empty cooling traps (5) (previously weighed) in the containers with liquid nitrogen and open the valve for the vacuum pump to collect the sample.
10. Samples of the feed and retentate are taken at time 0 min. The sampling time for feed, permeate and retentate is every 10 minutes or even longer depending on the operating conditions and the mass of permeate collected, (some operating conditions require longer times in order to collect sufficient permeate for the GC analysis). The experiment stops once three samples of permeate have been collected. Average time per experiment: 30 minutes.
11. The same procedure is carried out using different fermentation by-products at different concentrations. In this work, glucose, xylose, glycerol and acetic acid are considered. Although furfural is usually found in the ethanol production process from lignocellulosic biomass, this work does not contain any experiment with this component since its handling requires high safety conditions due to its high toxicity.

The experimental procedure presented above consists of a series of steps which allows regulating and fully operating the pervaporation plant in order to guarantee reliable experimental data. The operating flow rate of the feed is set at 50 L/h in order to secure the same concentration in both feed and retentate since the idea of this experiment is to determine the flux and the concentration of ethanol through the membrane not to evaluate the rates of separation in the retentate side. The experimental procedure also seeks to minimise losses of ethanol in the sampling and in the feed tank by constantly checking the concentration of the feed tank and the other outlet streams as well as the stability in the measurement of both temperature and permeate pressure.

4.4 Modelling

The experimental procedure previously outlined helped to obtain the different experimental results that will be used in the estimation of the parameters of the mathematical model. This section presents the methodology and tools implemented in the estimation of the parameters of an empirical mathematical model used to describe the pervaporation of aqueous solutions of ethanol under different operating conditions. The approach for the parameter estimation in the model uses the weight of permeates, the concentration of ethanol, the time of collection of samples and the area of the membrane to determine the partial fluxes of the components through the membrane. All calculations are carried out using gPROMS v. 4.1.0 (Process System Enterprises, 2015).

4.4.1 Approach

The driving force for mass-transfer of one or more components between two phases is given by their differences in the chemical potentials (DF_i) (Holtbruegge et al., 2013). For pervaporation, the driving force for mass transfer is commonly expressed as the difference in fugacities between the feed and the permeate side of the membrane as shown in Eq. 4.1 (Valentinyi et al., 2013):

$$DF_i = (x_i^{feed} \gamma_i P_i^{sat} \varphi_i^{sat}) - (x_i^{perm} P_{perm} \varphi_i^{vap}) \quad i = 1, 2, \dots, NC \quad \text{Eq. 4.1}$$

The partial flux of component i is evaluated from the experimental data as the relation between the mass of permeate, the membrane area and the time of the collection of the samples. The permeance of ethanol and water Q_i ($\text{g m}^{-2}\text{s}^{-1}\text{Pa}^{-1}$) can be calculated from Eq. 4.2. The number of components NC is two (i.e. only ethanol and water are considered).

$$J_i = Q_i DF_i \quad i = 1, 2, \dots, NC \quad \text{Eq. 4.2}$$

4.4.2 Pure component and mixture property models

The thermodynamic properties of all components (including fermentation by-products) are evaluated using Multiflash 4.1.43 (Infochem, 2013). NRTL is used for the calculation of the activity coefficients of the components in the mixture. The PSRK equation of state is used to evaluate the fugacity coefficients and Antoine's equation is used for the calculation of vapour pressures.

4.4.3 Models for permeance

This work introduces three equations for the permeance of the membrane in order to conduct a comparative study between different formulations for the calculation of the partial fluxes. This analysis will determine if the number of experiments and the number of parameters are relevant factors for an accurate depiction of the pervaporation of ethanol through the membrane and if the model is suitable to be implemented in the main process.

Eq. 4.3 is taken from the work presented by Koch and Gorak, (2014). This equation represents the variation of the permeance as a function of the feed temperature T with an Arrhenius-type equation along with the influence of the feed concentration $W_{feed,i}$. However, the effect of the variation of the permeate pressure is not considered for this particular formulation. According to the work of Koch and Gorak, (2014), the approach presented in Eq. 4.3 has been found to accurately describe systems of binary mixtures since it incorporates two operating conditions that have great influence over the process.

$$Q_i = Q_{0,i} \text{EXP} \left(-\frac{E_i}{R} \left(\frac{1}{T} - \frac{1}{T_0} \right) \right) W_{feed,i}^{A_i} \quad i = 1,2, \dots NC \quad \text{Eq. 4.3}$$

Another variation of Eq. 4.3 can be used to obtain the parameters of the mathematical model taking into consideration the effect of the permeate pressure and vapour pressure. This approach has been presented in the work of Holtbruegge et al., (2013).

$$Q_i = Q_{0,i} \text{EXP} \left(-\frac{E_i}{R} \left(\frac{1}{T} - \frac{1}{T_0} \right) \right) W_{feed,i}^{A_i} \left(\frac{P_{perm}}{P_i^{sat}} \right)^{B_i} \quad i = 1,2, \dots NC \quad \text{Eq. 4.4}$$

Eq. 4.5 is a variation of the work presented by Holtbruegge et al., (2013). The approach presented in Eq. 4.5 presents a different form of the term that includes the permeate pressure and the vapour pressure and also features an additional parameter:

$$Q_i = Q_{0,i} \text{EXP} \left(-\frac{E_i}{R} \left(\frac{1}{T} - \frac{1}{T_0} \right) \right) W_{feed,i}^{A_i} \left(\frac{(P_i^{sat} - P_{perm}) + C_i}{(P_i^{sat} - P_{perm}) + D_i} \right)^i \quad i = 1,2, \dots NC \quad \text{Eq. 4.5}$$

The mathematical model will have the feed temperature T , the permeate pressure P_{perm} and the feed mass concentration of ethanol $W_{feed,i}$ as input variables to calculate the permeance Q_i of each component in the system (Equations 4.3 to 4.5). The molar fraction of ethanol in the permeate side x_i^{perm} is determined as follows:

$$x_i^{perm} = \frac{J_i}{\sum_{i=1}^{NC} J_i} \quad i = 1,2, \dots NC \quad \text{Eq. 4.6}$$

With the mole fractions of the permeate and feed sides and the temperature of the feed, the driving forces DF_i can be estimated using Eq. 4.1 and the partial fluxes with Eq. 4.2. The parameters to be fitted from the experimental data are listed next:

- $Q_{0,i}$: Pre-exponential permeance value for the Arrhenius-type equation for the influence of feed temperature in the performance of the separation. ($\text{g m}^{-2}\text{s}^{-1}\text{Pa}^{-1}$)
- E_i : Activation energy. ($\text{J mol}^{-1}\text{K}^{-1}$)
- A_i, B_i, C_i, D_i : Constants

4.5 Results

Table 4.4 presents the measured data and the calculated data from the set of experiments previously outlined using Eq. 4.2. The results reported in Table 4.4 show that the operating conditions have a direct influence over the performance of the membrane and therefore the partial fluxes of ethanol and water. When feed concentration of ethanol increases (from 5% to 13% w/w ethanol) at constant feed temperature (30 °C) and permeate pressure (400 Pa) the partial fluxes increase too (59 % increase for ethanol and 27% for water).

Similarly, when the temperature increases from 30 °C to 50 °C at constant feed concentration (5% w/w ethanol) and permeate pressure (400 Pa), the partial fluxes increase 56 % and 61 % for ethanol and water, respectively. Conversely, when the permeate pressure increases from 400 Pa to 3500 Pa, the partial fluxes tend to decrease as reported by Marriott and Sorensen (2003), Roth et al., (2013) and Wei et al., (2014). The decrease of the partial fluxes (see Table 4.4) at constant T (30 °C) and W_{feed} (5% w/w ethanol) is reported to be 71 % for ethanol 80 % for water. The results of the experiments suggest that permeate pressure is an operating condition that has a significant impact in the amount of material passing through the membrane and should be taken into consideration for the formulation of the mathematical model. This analysis also indicates that, within the range of operating conditions, higher fluxes and higher separation rates of ethanol through the membrane can be achieved.

Table 4.5 presents the results of the partial fluxes of ethanol and water at different concentrations of impurities. These are the by-product concentrations expected to be

obtained after the fermentation stage. To investigate the influence of different fermentation by-products, first a pure ethanol/water mixture is subjected to pervaporation experiments, which will serve as a reference for the comparative analysis.

The operating conditions for the pure mixture ethanol/water are: 40 °C, 2000 Pa and a feed concentration of ethanol of 5 % (w/w). For components that exhibit low vapour pressure, driving forces such as pressure gradient and concentration gradient are very low. Hence, these components (i.e. glycerol, glucose, xylose) can be considered as impermeable and should not be detected in the permeate stream (Chovau et al., 2011). However, an increase of the total flux through the membrane is observed when these components are introduced into the mixture.

Acetic acid is detected in the permeate stream and an increase in the flux of ethanol of approximately 40% can be observed. However, and as previously mentioned, higher concentrations of organic acids can compromise the membrane in its structure and its durability in the long term (Sulzer Chemtech, 2014).

4.5.1 Model discrimination

This work compares three empirical models of the PERVAP™ 4060 membrane taking into account different approaches in the formulation of the equation for permeance of each component. The parameters of these models are adjusted from the experimental data shown in Table 4.4. The parameter estimation model using gEST and gPROMS considers a solver of Maximum-Likelihood Estimation (MLE) for complex models using both dynamic and steady-state experimental data (Process System Enterprises, 2015). gPROMS attempts to determine values for the uncertain physical and variance model parameters that maximise the probability that the mathematical model will predict the measurement values obtained from the experiments.

Table 4.5 presents the results of the experiments with the membrane using by-products often found in the fermentation of hydrolysates of lignocellulosic biomass.

The calculations featured in this work are carried out using Dell OptiPlex 9010 Intel® Core™ i7-3770 CPU @3.40 GHz and 16 GB RAM running Windows 7® Enterprise (64-bit operating system). The results of the parameter estimation for equations 4.3 to 4.5 are presented in Table 4.6.

Table 4.4: Experimental results for the removal of ethanol from aqueous solutions using the PERVAP™ 4060 membrane

Sample	Measured data							Calculated data			
	Ethanol feed (w/w)	Water feed (w/w)	Ethanol permeate (w/w)	Water permeate (w/w)	Temp (°C)	Permeate pressure (mbar)	Mass permeate (g)	Ethanol flux ($g\ m^{-2}\ s^{-1}$)	Water flux ($g\ m^{-2}\ s^{-1}$)	Permeance ethanol 10^5 ($g\ m^{-2}\ s^{-1}\ Pa^{-1}$)	Permeance water 10^5 ($g\ m^{-2}\ s^{-1}\ Pa^{-1}$)
C1T1P1	0.06±0.003	0.94±0.003	0.25±0.01	0.75±0.01	30.53±0.03	4.35±0.15	2.59±0.07	0.058±0.002	0.173±0.008	5.63±0.28	4.42±0.20
C1T1P=10	0.06±1x10 ⁻⁴	0.94±1x10 ⁻⁴	0.26±0.01	0.74±0.01	30.60±0.10	9.70±0.01	2.10±0.01	0.055±0.002	0.151±0.002	5.61±0.20	4.37±0.08
C1T1P2	0.05±0.001	0.95±0.001	0.27±0.01	0.73±0.01	30.34±0.05	19.8±0.13	1.6±1x10 ⁻⁴	0.04±4x10 ⁻⁴	0.11±4x10 ⁻⁴	5.20±0.35	4.15±0.03
C1T1P=28	0.06±2x10 ⁻⁴	0.94±2x10 ⁻⁴	0.29±0.01	0.71±0.01	30.42±0.01	28.3±0.22	1.69±0.04	0.033±0.001	0.080±0.003	4.99±0.17	4.39±0.02
C1T1P3	0.05±0.003	0.95±0.003	0.33±0.01	0.67±0.01	30.58±0.03	34.8±0.27	0.6±0.005	0.017±0.001	0.034±0.001	4.11±0.37	2.43±0.12
C2T1P1	0.07±6x10 ⁻⁴	0.93±6x10 ⁻⁴	0.3±0.004	0.7±0.004	30.63±0.02	4.33±0.27	2.94±0.11	0.078±0.002	0.184±0.008	5.85±0.19	4.71±0.20
C1T2P1	0.04±5x10 ⁻⁴	0.96±5x10 ⁻⁴	0.23±0.02	0.77±0.02	40.21±0.07	4.08±0.21	2.56±0.05	0.080±0.007	0.262±0.009	5.81±0.61	3.75±0.10
C1T3P1	0.04±3x10 ⁻⁴	0.96±3x10 ⁻⁴	0.23±0.02	0.77±0.01	49.71±0.06	4.63±0.23	4.29±0.03	0.131±0.004	0.442±0.001	5.25±0.19	3.83±0.46
C1T3P3	0.05±0.001	0.95±0.001	0.27±0.01	0.73±0.01	49.79±0.05	34.8±0.28	3.34±0.16	0.122±0.001	0.326±0.021	5.58±0.05	3.62±0.24
C3T1P1	0.13±0.002	0.87±0.002	0.38±0.01	0.62±0.01	30.37±0.16	4.09±0.21	4.24±0.08	0.142±0.001	0.236±0.006	6.62±0.15	6.15±0.15
C3T3P1	0.13±0.003	0.87±0.003	0.44±0.02	0.56±0.02	50.32±0.27	3.98±0.18	6.56±0.10	0.382±0.018	0.495±0.012	6.05±0.36	4.01±0.16
C3T1P3	0.13±0.001	0.87±0.001	0.44±0.02	0.56±0.02	30.58±0.02	35.4±0.13	2.44±0.08	0.09±4x10 ⁻⁴	0.121±0.076	6.81±0.17	8.16±0.80
C3T3P3	0.14±0.004	0.86±0.004	0.4±0.001	0.6±0.001	50.11±0.26	35.24±0.44	7.83±0.47	0.290±0.017	0.408±0.026	4.90±0.10	4.53±0.28

C = concentration of ethanol in the feed stream, T = feed temperature, P = permeate pressure. 1, 2, and 3 represent the points shown in Figure 4.1. P = 10 and 28 mbar represent intermediate points taken to improve the fit of the parameters of the model. The uncertainty of the results is obtained as the mean of the standard deviation of all the experiments used for each point.

Table 4.5: Partial fluxes of ethanol and water under the influence of different impurities at 40 °C and a permeate pressure of 20 mbar

By-product	Concentration (g/L)	Ethanol feed (% w/w)	Water feed (% w/w)	By-product feed (% w/w)	Ethanol permeate (% w/w)	Water permeate (% w/w)	By-product permeate (% w/w)	Ethanol flux (g m⁻²s⁻¹)	Water flux (g m⁻²s⁻¹)	By-product flux (g m⁻²s⁻¹)	Total flux (g m⁻²s⁻¹)
No by-product	0	0.050±0.001	0.950±0.001	-	0.26±0.011	0.74±0.011	-	0.076±0.002	0.217±0.007	-	0.293±0.009
Glucose	1	0.051±0.001	0.947±0.001	0.002±0.001	0.24±0.003	0.76±0.003	-	0.071±0.002	0.226±0.002	-	0.297±0.004
Glucose	2	0.05±1x10 ⁻⁴	0.95±1x10 ⁻⁴	0.004±1x10 ⁻⁴	0.26±0.007	0.74±0.003	-	0.074±0.002	0.210±0.002	-	0.284±0.004
Xylose	5	0.047±0.001	0.948±0.001	0.005±0.001	0.25±0.002	0.75±0.002	-	0.076±0.005	0.235±0.015	-	0.311±0.020
Xylose	10	0.048±0.001	0.942±0.001	0.010±0.001	0.25±0.006	0.75±0.006	-	0.081±0.002	0.250±0.006	-	0.328±0.008
Glycerol	3	0.057±3x10 ⁻⁴	0.94±3x10 ⁻⁴	0.003±3x10 ⁻⁴	0.28±0.013	0.72±0.013	-	0.092±0.001	0.242±0.013	-	0.332±0.014
Glycerol	6	0.050±1x10 ⁻⁴	0.944±1x10 ⁻⁴	0.006±1x10 ⁻⁴	0.26±0.007	0.74±0.007	-	0.088±0.001	0.249±0.006	-	0.337±0.007
Acetic acid	1	0.046±5x10 ⁻⁴	0.953±5x10 ⁻⁴	0.001±1x10 ⁻⁴	0.228±0.003	0.685±0.002	0.088±0.001	0.138±0.003	0.414±0.008	0.053±0.001	0.605±0.012
Acetic acid	2	0.051±1x10 ⁻⁴	0.947±1x10 ⁻⁴	0.002±0.001	0.269±0.011	0.648±0.012	0.083±0.002	0.121±0.006	0.291±0.003	0.037±0.001	0.499±0.010

Table 4.6: Parameters of the mathematical model of the organophilic membrane

Parameter	Ethanol		
	Eq. 4.3	Eq. 4.4	Eq. 4.5
$Q_{o,i} (10^5)$	7.40±1.72	6.98±1.650	7.67±0.78
E_i	-1883±752	-4420±1520	-3640±825
$A_i (10^3)$	9.60±0.75	10.6±0.750	10.2±0.77
B_i	-	-0.045±0.03	-
C_i	-	-	8.57±2.31
D_i	-	-	-85.4±20.7
	Water		
$Q_{o,i} (10^5)$	3.46±0.73	3.51±0.80	3.45±0.17
E_i	-11399±4774	-8550±3240	-9640±1042
A_i	-5.24±1.87	-5.26±1.85	-4.88±2.09
B_i	-	0.037±0.01	-
C_i	-	-	26.6±8.74
D_i	-	-	-2.68±0.60

Table 4.6 present the results of the parameter estimation of the different approaches for the evaluation of the permeance of each component. From this table, it can be seen the similarities in the values of the pre-exponential term $Q_{o,i}$ in each equation for both ethanol and water. For ethanol, for example, the values go from 6.98×10^{-5} to $7.67 \times 10^{-5} \text{ g m}^{-2} \text{ s}^{-1} \text{ Pa}^{-1}$ (a difference of approximately 10%).

On the other hand, the activation energy terms (E_i) exhibit differences that can go up to 57 % for ethanol and 25 % for water. The power term A_i , which is also found in all the approaches, exhibits values that go from 0.096 to 0.106 for ethanol (approx. 9%) and from -5.26 to -4.88 for water (approx. an increment of 7%). The results of the parameter estimation indicate that all the parameters are susceptible to changes when a different formulation is implemented or when additional operating conditions (i.e. permeate pressure) are considered.

From the previous section it can be seen that fermentation by-products influence the performance of the organophilic membrane. However, their contribution in the mathematical model is not considered in this work since most of these components are either degraded during the pretreatment or the overliming or present low

concentration in the feed stream of the separation section. Additional experiments are conducted using different fermentation by-products in order to assess their effect over the membrane performance. The influence of temperature over partial fluxes using the parameters of equations 4.3 to 4.5 is shown in Figure 4.8.

As seen in Table 4.4, the partial fluxes increase with temperature as the result of the increase of the driving force and the vapour pressures (Marriott and Sorensen, 2003; Roth et al., 2013; Wei et al., 2014). It can also be seen that Eq. 4.5 has a better fit of the experimental data as curves for ethanol and water are closer to the experimental data also plotted in Figure 4.8. From this figure, it can also be concluded that a good adjustment of the experimental data can be obtained when the number of parameters in the model is higher.

An additional experiment, only for the binary mixture ethanol/water, was conducted in order to validate the mathematical model using a point that was not included in the parameter estimation. This experimental point consists of a feed concentration of 7 % (w/w) of ethanol, a feed temperature T of 40 °C and a permeate pressure of 2000 Pa. Using the additional set of experiments (C2T2P2), the mathematical model using Eq. 4.5 can be validated.

The results of the model verification presented in Table 4.7 show a good fit between experimental data and predicted results reporting errors of ± 4.4 % in the concentration of ethanol in the permeate side. Figure 4.9 shows the parity plots for the mathematical model of the organophilic membrane and the experimental values. The standard deviation between the experimental data and the predicted values of the permeance for ethanol and water are $6.9 \times 10^{-6} \text{ g m}^{-2} \text{ s}^{-1} \text{ Pa}^{-1}$ and $1.32 \times 10^{-5} \text{ g m}^{-2} \text{ s}^{-1} \text{ Pa}^{-1}$, respectively. The closing of the mass and component balances for these experiments can be quite difficult, because all measured variables are inevitably corrupted by experimental errors.

Given that errors are inevitable during experimentation, a statistical analysis is required in order to quantify said errors and determine the reliability of the

mathematical model and how it differs from the experimental data. Tables 4.8 to 4.9 show the error analysis of the estimation of the parameters in the mathematical model for the membrane using Equations 4.3 to 4.5. The Lack-of-fit test, which is commonly used for testing independence and goodness of fit between observed and expected values, is considered in this work. This chapter will use the Pearson's chi-square test which is the most used method for the assessment of accuracy in the estimation of parameters for empirical models. Equation 4.7 defines the difference between the expected outcome frequencies and the observed ones:

$$\chi^2 = \sum_{k=1}^n \frac{(O_k - E_k)^2}{E_k} = N \sum_{k=1}^n \frac{\left(O_k/p_i - p_i \right)^2}{p_i} \quad \text{Eq. 4.7}$$

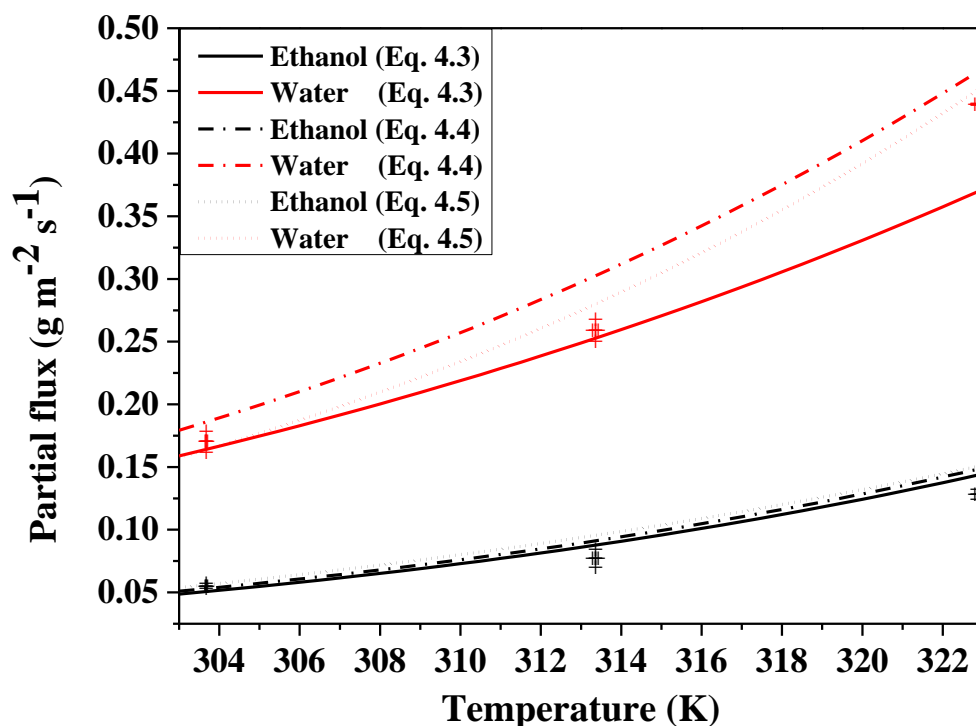


Figure 4.8: Partial flux for ethanol and water using the different formulations proposed in Equations 4.3 to 4.5

Table 4.7: Model validation using additional experimental data

Operating Conditions	Experimental			Predicted		
	$W_{Permeate}^{Ethanol}$	$J_{Ethanol}$ ($g\ m^{-2}\ s^{-1}$)	J_{Water} ($g\ m^{-2}\ s^{-1}$)	$W_{Permeate}^{Ethanol}$	$J_{Ethanol}$ ($g\ m^{-2}\ s^{-1}$)	J_{Water} ($g\ m^{-2}\ s^{-1}$)
T = 40.4 °C P= 20.05 mbar	0.339±0.029	0.115±0.013	0.224±0.004	0.324	0.115	0.223

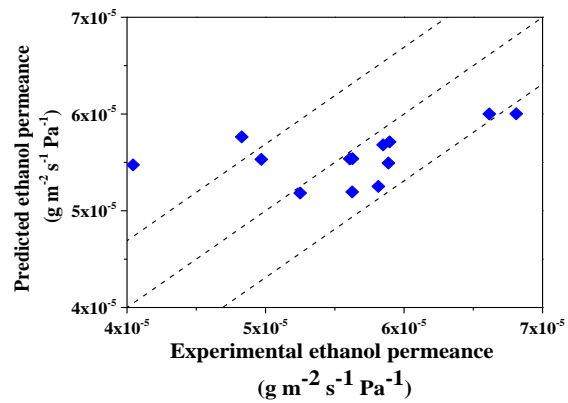
Table 4.8: Lack-of-fit test for the parameter estimation of the membrane model

Equation	Weighted Residual (χ)	χ^2 - value (95 %)
4.3	15.04	31.41
4.4	13.34	28.87
4.5	15.42	26.30

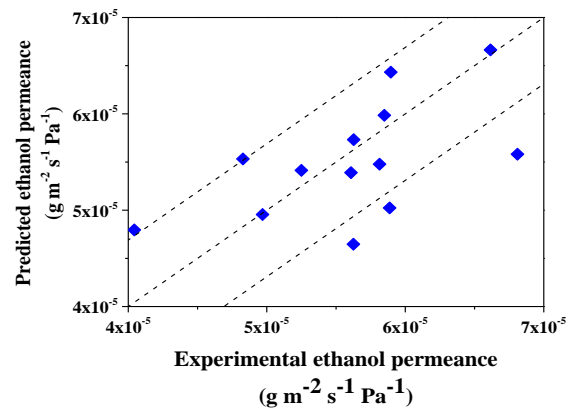
Table 4.8 shows the results of the statistical analysis of the experimental data using the Pearson's chi-square method described in Eq. 4.7. Here O_k is the observed frequency for bin k , E_k is the expected (theoretical) frequency for bin k and n is the number of bins used in the analysis. The Pearson's chi-square test states that when the χ^2 -value (at 95%) $\geq \chi^2$ for a p -value of 0.95 (or 95 %), the mathematical model can be concluded at a significance level of confidence of 95% to be a good representation of the experimental process and the parameters are well-adjusted. Conversely, χ^2 -value (at 95%) $\leq \chi^2$ rejects the null hypothesis that the model is representing the observed data.

The results of the lack-of-fit test show that all the models have a good fit against the experimental data, which indicates that the number of experiments is enough to predict the permeance for either component at the range of operating conditions. Tables 4.9 to 4.11 show the error analysis of the mathematical model of the membrane using equations 4.3 to 4.5.

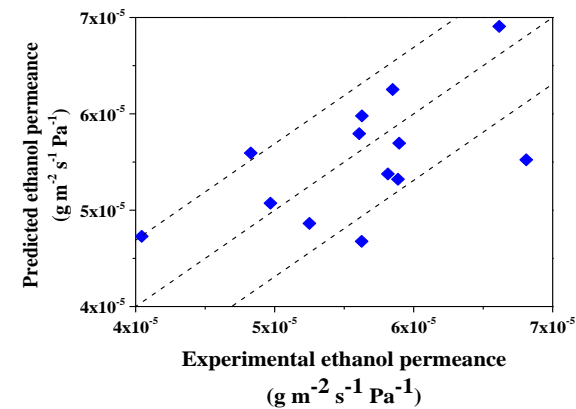
The results of these tables show the errors and the standard deviations for the three models. These results also support the aforementioned statement which made reference to the good fit of all the models used in this work. However, and as seen in Figures 4.8 and 4.9, the results for Eq. 4.5 are closer to the experimental data and when those results are combined with the statistical analysis provided in Table 4.8, one can conclude that this model is accurate enough to describe the permeation of ethanol through the organophilic membrane within the operating conditions at which these models are restricted.



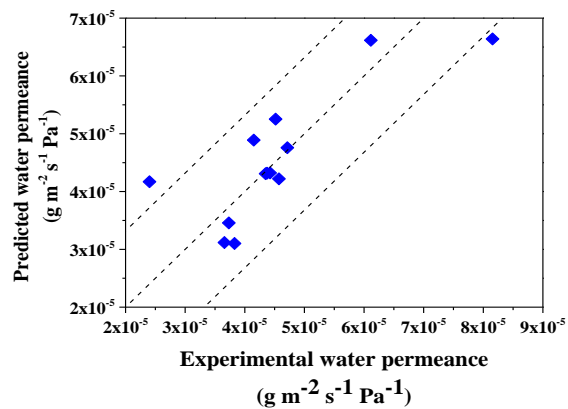
(a)



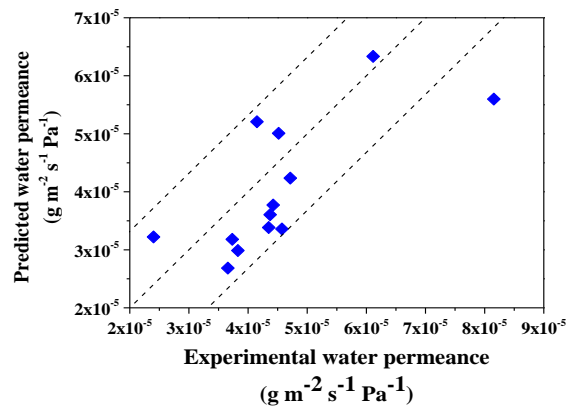
(b)



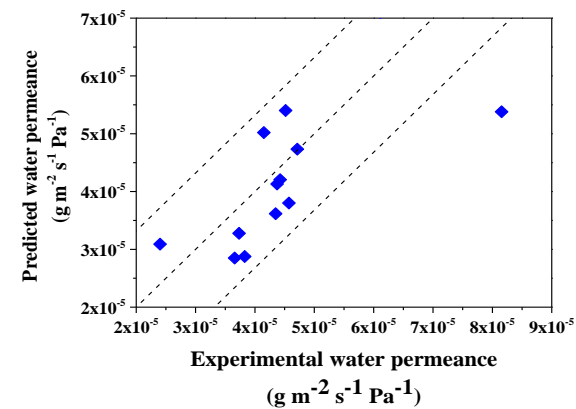
(c)



(d)



(e)



(f)

Figure 4.9: Parity plots with the fitted parameters for ethanol (top) and water (bottom) using: (a) Eq. 4.3, (b) Eq. 4.4, (c) Eq. 4.5, (d) Eq. 4.3, (e), Eq. 4.4, (f) Eq. 4.5

Table 4.9: Parameter estimation problem for the permeance of ethanol and water using Eq. 4.3

Ethanol					Water				
Permeance ethanol ($g\ m^{-2}\ s^{-1}\ Pa^{-1}$)		Deviation			Permeance water ($g\ m^{-2}\ s^{-1}\ Pa^{-1}$)		Deviation		
Experimental Measurement 10^5	Model Prediction 10^5	Absolute 10^7	Percentage (%)	Weighted	Experimental Measurement 10^5	Model Prediction 10^5	Absolute 10^7	Percentage (%)	Weighted
5.63	5.53	9.20	1.63	0.13	4.42	4.32	9.76	2.41	0.04
5.61	5.53	7.30	1.30	0.11	4.37	4.31	5.23	1.28	0.04
5.89	5.49	39.6	6.73	0.43	4.57	4.22	34.9	7.13	0.26
4.97	5.53	-5.61	-11.3	-0.96	4.35	4.31	3.97	-0.04	0.03
4.04	5.47	-143	-35.5	-2.23	2.40	4.17	-177	-78.1	-1.34
5.85	5.68	16.9	2.88	0.10	4.71	4.76	-4.81	-0.16	-0.04
5.81	5.25	55.8	9.61	0.89	3.73	3.45	27.2	5.25	0.21
5.25	5.18	6.64	1.26	0.34	3.83	3.10	72.7	15.8	0.55
5.63	5.19	43.5	7.73	0.87	3.66	3.11	54.2	11.3	0.41
6.62	6.00	61.9	9.35	0.71	6.11	6.61	-50.8	-5.1	-0.38
5.90	5.71	18.7	3.18	0.49	4.15	4.89	-74.1	-19.6	-0.56
6.81	6.00	80.7	11.8	0.96	8.16	6.64	151	19.1	1.15
4.83	5.76	-93.4	-19.3	-1.12	4.52	5.25	-73.2	-16.5	-5.55

Table 4.10: Parameter estimation problem for the permeance of ethanol and water using Eq. 4.4

Ethanol					Water				
Permeance ethanol ($g\ m^{-2}\ s^{-1}\ Pa^{-1}$)		Deviation			Permeance water ($g\ m^{-2}\ s^{-1}\ Pa^{-1}$)		Deviation		
Experimental Measurement 10^5	Model Prediction 10^5	Absolute 10^7	Percentage (%)	Weighted	Experimental Measurement 10^5	Model Prediction 10^5	Absolute 10^7	Percentage (%)	Weighted
5.63	5.77	-13.7	-2.43	-0.19	4.42	4.11	30.4	6.88	0.23
5.61	5.56	4.91	0.88	0.07	4.37	4.24	13.4	3.06	0.10
5.89	5.33	55.5	9.42	0.80	4.57	4.26	31.2	6.82	0.24
4.97	5.29	-32.4	-6.52	-0.47	4.35	4.40	-4.92	-1.13	-0.04
4.04	5.18	-114	-28.3	-1.66	2.40	4.29	-189	-78.8	-1.45
5.85	5.93	-8.24	-1.41	-0.12	4.71	4.53	17.8	3.77	1.36
5.81	5.45	35.9	6.17	0.52	3.73	3.32	41.0	10.9	3.15
5.25	5.29	-4.16	-0.79	-0.06	3.83	3.05	78.3	20.4	0.60
5.63	4.83	79.2	14.1	1.15	3.66	3.31	35.4	9.67	0.27
6.62	6.37	25.1	3.79	0.36	6.11	6.27	-15.9	-2.61	-0.12
5.90	5.92	-2.29	-0.39	-0.03	4.15	4.83	-68.0	-16.4	-0.52
6.81	5.73	107	15.8	1.56	8.16	6.85	131	16.10	1.01
4.83	5.42	-59.4	-12.3	-0.86	4.52	5.57	-105	-23.3	-0.81

Table 4.11: Parameter estimation problem for the permeance of ethanol and water using Eq. 4.5

Ethanol					Water				
Permeance ethanol ($g\ m^{-2}\ s^{-1}\ Pa^{-1}$)		Deviation			Permeance water ($g\ m^{-2}\ s^{-1}\ Pa^{-1}$)		Deviation		
Experimental Measurement 10^5	Model Prediction 10^5	Absolute 10^8	Percentage (%)	Weighted	Experimental Measurement 10^5	Model Prediction 10^5	Absolute 10^7	Percentage (%)	Weighted
5.63	5.62	5.18	0.09	0.01	4.42	4.31	10.7	2.41	0.08
5.61	5.63	-15.4	-0.27	-0.22	4.37	4.31	5.59	1.28	0.04
5.89	5.59	298	5.06	0.43	4.57	4.24	32.6	7.13	0.25
4.97	5.64	-666	-13.4	-0.96	4.35	4.35	-0.16	-0.04	-0.001
4.04	5.58	-1540	-38.0	-2.23	2.40	4.27	-187	-78.1	-1.44
5.85	5.78	72.8	1.24	0.10	4.71	4.72	-0.76	-0.16	-0.01
5.81	5.19	619	10.6	0.89	3.73	3.53	19.6	5.25	0.15
5.25	5.02	235	4.47	0.34	3.83	3.22	60.5	15.8	0.47
5.63	5.03	601	10.7	0.87	3.66	3.25	41.5	11.3	0.32
6.62	6.13	490	7.41	0.71	6.11	6.43	-31.5	-5.1	-0.24
5.90	5.56	342	5.79	0.49	4.15	4.96	-81.2	-19.6	-0.62
6.81	6.15	664	9.74	0.96	8.16	6.60	156	19.1	1.20
4.83	5.61	-7.76	-16.1	-1.12	4.52	5.27	-74.7	-16.5	-0.58

4.6 Conclusions

This chapter presented an experimental design for the formulation of an empirical model that could be used to describe the permeation of ethanol from aqueous solutions using a PERVAP™ 4060 organophilic membrane. Several works have assessed the benefits of using this particular membrane for different organic solvents but none of them has explored its application for the ethanol production process from lignocellulosic biomass or even formulated a mathematical model to predict the partial fluxes. These experiments consisted of the variation of different operating conditions during the pervaporation process in which the ethanol was expected to be removed from the aqueous solutions on the permeate side of the membrane module.

The results of the experiments showed that the operating conditions had a significant influence over the performance of membrane. The partial fluxes for ethanol and water increased as the feed temperature (T_{feed}) and the feed concentration of ethanol (W_{feed}) increased. Conversely, it was observed that the partial fluxes decreased along with the increase of the permeate pressure (P_{perm}) (see Table 4.4). These trends were consistent with the observations reported by several authors who had used the same membrane in the separation of other organic solvents from aqueous solutions.

The results of the experiments were used to evaluate the parameters of an empirical model using gPROMS. Three different mathematical models for the calculation of the permeance of ethanol and water were considered (see Eq. 4.3 to 4.5). The first approach (Eq. 4.3) considered the product of an Arrhenius-type term for the influence of temperature and the feed concentration powered to a parameter (A_i). The second approach (Eq. 4.4) added another term to the model presented in Eq. 4.3, which considers a ratio between the vapour pressure and the permeate pressure powered to a term (B_i).

The third approach (Eq. 4.5) considers a different term for the influence of the permeate pressure in the pervaporation. The results showed that Eq. 4.4 had a good fit for the experimental results. However, Eq. 4.5 had a better fit since the curves for partial fluxes under the influence of feed temperature (see Figure 4.8) were closer to

the experimental data and the error percentages were smaller than in Eq. 4.3 and 4.4. A statistical analysis was conducted in this chapter in order to quantify the errors obtained during the collection of samples and the measurements. This analysis showed that all the models presented small deviations from the experimental data and low errors.

However, the errors obtained with Eq. 4.5 were less significant than the errors obtained with the other two equations. Additional experiments were conducted using common fermentation by-products such as glucose, xylose, glycerol and acetic acid. These results were not included in the parameter estimation due to the limited number of experiments. However, an increase in the total flux could be appreciated when the concentration of the impurities was increased. Acetic acid was the only component detected in the permeate stream. The presence of acetic acid in the permeate side suggested that a more rigorous experimental design for a more detailed mathematical model might be required. The implementation of the mathematical model into the ethanol production process from lignocellulosic biomass and the optimisation and energy evaluation will be presented in Chapter 5.

Chapter 5 – Optimisation of the separation section of the ethanol production process

Abstract

The ethanol production process from lignocellulosic biomass shows high levels of energy demand (mainly in the separation section) making its implementation in industry less profitable. This chapter focuses on the optimal design and operation of the separation section of the ethanol production process from corn stover. In particular, the chapter provides an assessment of the impact of the implementation of the organophilic membrane before the distillation column.

5.1 Introduction

Ethanol production has been studied extensively for its potential to generate energy from renewable sources. However, much is still needed to be done in terms of energy efficiency to make this process profitable and competitive against traditional fuels such as coal and oil. In this work, ethanol is produced from corn stover, a lignocellulosic residue with high organic content (Bhandari et al., 1984; Liu and Chen, 2016). The separation section of the ethanol production process from corn stover shown in Chapter 3 consists of two distillation columns and a pervaporation network (Cardona et al., 2010; Drapcho et al., 2008; Garcia et al., 2010; Morales-Rodriguez et al., 2011). Different publications have concluded that one of the main obstacles for the implementation of the ethanol production from lignocellulosic biomass in industry is the energy consumption associated with the separation of this alcohol from the fermentation medium (Baeyens et al., 2015; Karlsson et al., 2014; Kiss and Suszwalak, 2012; Kravanja et al., 2013; Triana et al., 2015).

Alternative configurations to distillation techniques for ethanol separation such as double effect distillation, pressure-swing distillation, heat-integrated distillation

columns, etc., seek to reduce the heat duty in the reboiler and increase the concentration of ethanol in distillate as close as possible to the azeotrope (Kiss and Olujic, 2014; Knapp and Doherty, 1992; Pohlmeier and Rix, 1996). In the case of pressure-swing distillation and extractive distillation, the primary goal is to overcome the azeotrope more than reduce energy consumption (Towler and Sinnott, 2013). These configurations have shown to be very successful in the purification of ethanol from aqueous solutions (Caballero, 2015; Kookos, 2003; Sudhoff et al., 2015). However, their implementation may incur in additional operating costs such as controllability of the column and operating conditions, solvent recovery, compression, etc. (Kiss and Olujic, 2014). In this thesis, only simple distillation will be considered since this work seeks to evaluate simpler technologies rather than embarking in more elaborate configurations. The optimal arrangement of the separation section (i.e. number of distillation columns, number of trays in the distillation columns, reflux ratio, the number of pervaporation stages, permeate pressure, etc.), which minimises the total annualised cost (TAC), will be obtained by using rigorous optimisation methods.

This chapter will focus on the implementation of a practical methodology for the optimisation of the entire separation section of the ethanol production process. This methodology consists of using optimisation results of individual units (i.e. distillation column or pervaporation modules) as initial guesses for the overall separation sections since this will narrow the feasibility region in which the optimum solution may be located and will help reduce computational times as the set of algebraic-differential equations is highly non-linear. This chapter presents initially the optimisation of the individual units and will lead to the solution and analysis of the different configurations.

5.2 Design of distillation columns

The number of trays required in a distillation column to achieve a separation with a specific concentration of product can be determined in several ways. Some of these methods include shortcut methods, group methods, aggregated methods, rigorous

tray-by-tray optimisation methods, among others. This section will briefly introduce some of these methods.

5.2.1 Shortcut methods

One of the most recognised methods for the design of distillation columns is the method of Fenske-Underwood-Gilliland (FUG). The FUG method presents the assumptions of constant molar overflow and constant relative volatilities in all the trays along the distillation column. This method considers two extremely ideal assumptions (Sorensen, 2014; Towler and Sinnott, 2013):

1. The distillation column operates at total reflux (i.e. no lateral or additional feed is entering or exiting from the column), which allows the calculation of the minimum number of trays for a given separation of two key components
2. The column operates at infinite number of trays, which allows calculating the minimum reflux

The optimal solution of a single distillation column will lie between these two extreme cases. Although this method can be applied for the separation of different mixtures, it is not recommended for systems with highly non-ideal nature like those that present azeotropes (Sorensen, 2014).

5.2.2 Group methods

Group methods are equation-based methods that can be easily implemented in mathematical programming. Group methods (GM) use approximate calculations to relate the outlet stream properties to the thermodynamic state of the inlet stream and number of equilibrium trays (Caballero and Grossmann, 2014a; Dünnebier and Pantelides, 1999). These approximation procedures are called group methods because they provide only an overall treatment of the trays in the cascade without considering detailed changes in the temperature and composition of individual trays. However, they are easy to solve because they involve few variables and constraints. They can be represented as a cascade of trays in counter-current operations like

absorption, stripping, distillation, leaching or extraction (Dünnebier and Pantelides, 1999; Kamath et al., 2010; Kiss and Olujic, 2014) .

5.2.3 Rigorous tray-by-tray optimisation models

As previously mentioned, the economic optimisation of a distillation column involves the selection of the number of trays and feed location, as well as the operating conditions, to minimise the total investment and operating costs. Continuous decisions are related to the operational conditions and energy involved in the separation, while discrete decisions are related to the design of the unit (i.e. total number of trays, and the tray positions of each feed and product streams). A major challenge is to perform the optimisation using tray-by-tray models that assume phase equilibrium because of non-linearity of the thermodynamic models and the equations of state used therein (Caballero & Grossmann 2014a ;Caballero & Grossmann 2014b; Gomez-Castro et al. 2011; Viswanathan & Grossmann 1993).

5.3 Optimisation of a distillation system

Section 2.7 presented a brief introduction to the definition of MINLP problems for systems with both continuous and discrete variables. In this work, the system consists of a distillation column divided in three sections as shown in Figure 5.1. The first section is rectification. This part of the column comprises the upper trays of the column, the condenser and reflux. The second section of the column is the feed which consists of three fixed trays where the feed stream is fed into the column. There is no restriction as to how many trays there should be in the feed section (i.e. there could be higher than three).

However, a higher number of trays in the feed section could lead to unfeasible results, especially regarding the feed location since it may not represent a physically realistic solution. On the other hand, fewer trays in the feed section may result in convergence issues during the solution of the optimisation problem, especially if a concentration close to the azeotrope is specified. The third section is stripping where the liquid passes through a partial reboiler to generate the vapour for the mass and heat transfer within the upper stages (Caballero and Grossmann, 2014a).

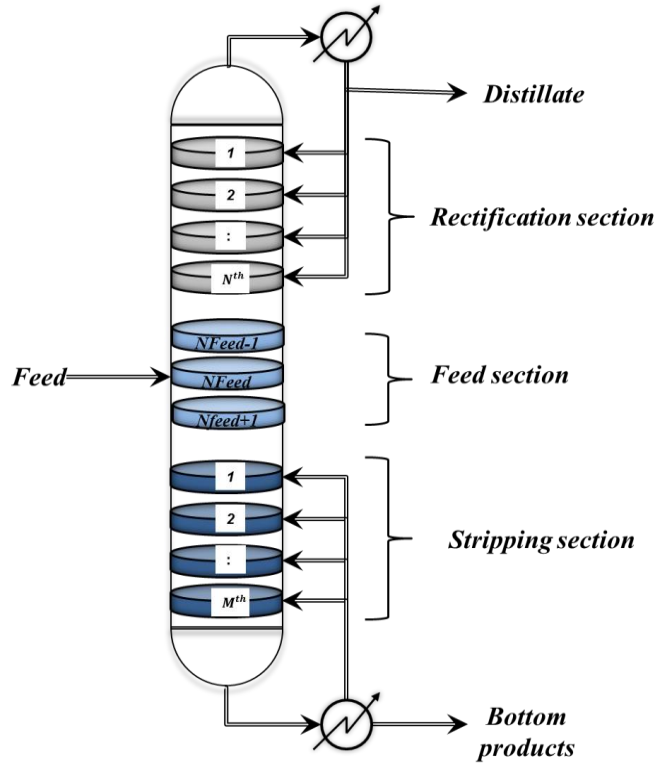


Figure 5.1: Sections of the distillation column used in the rigorous tray-by-tray optimisation

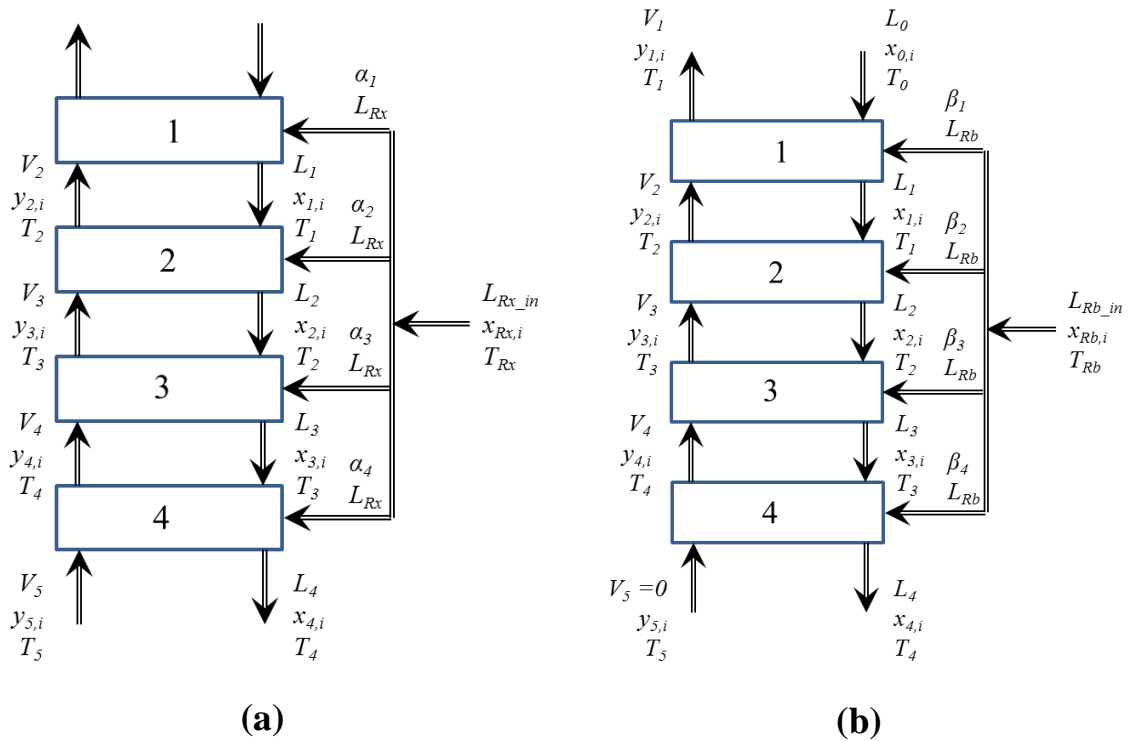


Figure 5.2: a) Rectification section with side reflux stream and b) stripping section with side boilup stream

The multiple recycles in both the rectification and stripping sections will determine the trays into which the reflux and the boilup streams are fed. The total number of trays in the column is calculated as the summation of all the active trays in rectification, stripping and feed. Figure 5.2 shows the configurations and variables used in both rectification and stripping sections in finding the optimal number of trays in the distillation column. The tray-by-tray method is a very useful method for the evaluation of the optimal parameters of a distillation column given fixed operating conditions for feed. However, the implementation of this methodology entails longer CPU times than shortcut methods given the highly non-linear nature of the system of equations (i.e. mass and energy balances, equation of state, activity coefficient models, etc.).

The streams and the mole fractions presented in Figure 5.2 are described next:

- L_j : Liquid flow rate leaving tray j (mole/sec)
- x_{ij} : Liquid mole fraction of component i leaving tray j
- T_j : Outlet temperature tray j (K)
- V_j : Vapour flow rate leaving tray j (mole/sec)
- y_{ij} : Vapour mole fraction of component i leaving tray j
- α_j : Binary variable used to determine the position of the reflux stream
- β_j : Binary variable used to determine the position of the boilup stream

The objective function to be minimised is presented in Eq. 5.1. This function comprises the capital investment which is the cost of the different units included in the distillation system (e.g. cost of condenser, reboiler, trays and column shell) within a payback period that may go between 3 and 10 years, depending on the projections of production and earnings in order to recover the money invested in the project (Peters et al., 2003).

$$TAC = \sum \text{Annual operating cost} + \sum \frac{\text{Capital investment}}{\text{payback period}} \quad \text{Eq. 5.1}$$

However, some authors suggest that for separation units such as distillation a payback period of four years is recommended (Caballero and Grossmann, 2014a; Dünnebier and Pantelides, 1999; Koch et al., 2013; Luyben, 2006).

The objective function also features the annual operating cost which represents the costs related to the utilisation of services such as steam, cooling water and electricity. The objective function is the sum of all the different costs for operation and equipment and the optimisation will find the minimum value of this function. The solution of this problem also requires additional constraints to guarantee the viability of the process in terms of purity and design. The constraints of the optimisation problem considered in this work are shown in Equations 5.2 to 5.5 (Caballero and Grossmann, 2014a; J Viswanathan and Grossmann, 1993; Viswanathan and Grossmann, 1990). Figure 5.3 presents the two configurations considered in the solution of the optimisation problem.

Eq. 5.2 presents the constraint related to the purity specifications at the top of the distillation column in order to obtain a concentration of ethanol that meets the feed requirements for the pervaporation system. Equations 5.3 and 5.4 ensure that the reflux and the steam leaving the reboiler only enter into one tray.

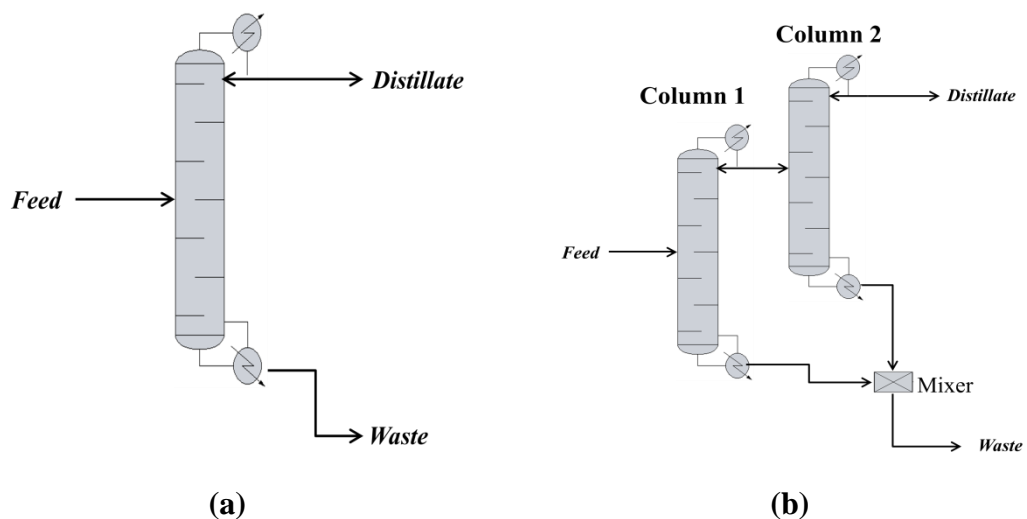


Figure 5.3: Configurations for the distillation system considered in this work: a) single distillation column and b) double distillation system with mixed waste

$$W_{D,Eth} \geq W_{D,eth}^{Spec} \quad \text{Eq. 5.2}$$

Equations 5.3 and 5.4 refer to the constraints necessary to ensure that the recycles in both sides of the column (e.g rectification and stripping) are fed into one single tray.

$$\sum_{j=1}^{N_{tray_rc}} \alpha_j = 1 \quad j = 1, 2, \dots, \text{Number of trays in rectification} \quad \text{Eq. 5.3}$$

$$\sum_{k=1}^{N_{trays_st}} \beta_k = 1 \quad k = 1, 2, \dots, \text{Number of trays in stripping} \quad \text{Eq. 5.4}$$

One the other hand, Equations 5.5 and 5.6 represent the number of active trays that can be counted in both sections of the column and are used in the calculation of its height.

$$N_{Rec}^{total} = \sum_j \alpha_j Rct_j \quad Rct_j = \{1, 2, 3 \dots N_{tray_rc}\} \quad \text{Eq. 5.5}$$

$$N_{Str}^{total} = \sum_k \beta_k Str_k \quad Str_k = \{N_{tray_st}, N_{tray_st-1}, \dots, 2, 1\} \quad \text{Eq. 5.6}$$

The set of constraints that correlate the continuous variables of the system with the discrete variables used to identify the recycle of both distillate and steam into the column are defined as follows (Caballero and Grossmann, 2014a):

$$RF_T = \{j \mid \text{Candidate tray of reflux return}\} \quad \text{Eq. 5.7}$$

$$RB_T = \{k \mid \text{Candidate tray of reboil return}\} \quad \text{Eq. 5.8}$$

Let L_{Rx} , L_{Rb} be the reflux and reboil flow rate returned to the column, respectively. Let α_j $j \in RF_T$; β_k $k \in RB_T$ be binaries that take the value 1 if the reflux/reboil is returned to tray j and k , respectively. Equations

$$ref_{tr} \leq L_{Rx} \alpha_j \quad j \in RF_T \quad \text{Eq. 5.9}$$

$$reb_{tr} \leq L_{Rb} \beta_k \quad k \in RB_T \quad \text{Eq. 5.10}$$

$$ref_{tr} \geq 0, \quad \alpha_j \in \{0,1\} \quad \forall j \in RF_T \quad \text{Eq. 5.11}$$

$$reb_{tr} \geq 0, \quad \beta_k \in \{0,1\} \quad \forall k \in RB_T \quad \text{Eq. 5.12}$$

Equations 5.13 and 5.14 correlate the vectors of recycles with the actual flow rate to be fed into the column.

$$L_{Rx_in} = \sum_{j \in RF_T} ref_{tr} \quad \text{Eq. 5.13}$$

$$L_{Rb_in} = \sum_{k \in RB_T} reb_{tr} \quad \text{Eq. 5.14}$$

An additional constraint is introduced for the double-column system, which represents the amount of ethanol lost during the separation as shown in Figure 5.3.b.

$$W_{Loss.Eth}^{min} \leq W_{Loss.Eth} \leq W_{Loss.Eth}^{max} \quad \text{Eq. 5.15}$$

Several authors have presented the cost estimating formulae and values of the parameter for the evaluation of the annual cost for the different parts of the distillation column as well as the costs for utilities such as cooling water and steam (Kiran and Jana, 2015). These equations are also presented in the works of Chung et al. (2015), Kookos (2003), Olujić et al. (2006), Szitkai et al. (2002), Wei et al. (2013), etc.

$$\text{Cost column shell} = \left(\frac{M\&S}{280}\right) 101.9 D_c^{1.066} L_c^{0.802} (c_{in} + c_m c_p) \quad \text{Eq. 5.16}$$

< US\$ >

where D_c is the column diameter (ft), L_c the column height (ft), the *M&S* (the Marshal & Swift index for 2015) is 1625.9 and the coefficients $c_{in} = 2.18$, $c_m = 3.67$ and $c_o = 1.2$.

$$\text{Cost column tray} = \left(\frac{M\&S}{280}\right) 4.7 D_c^{1.55} L_c (c_s + c_t + c_m) \quad \text{Eq. 5.17}$$

< US\$ >

where coefficients $c_s = 1$, $c_t = 0$ and $c_m = 1.7$

The cost function used for both the condenser and reboiler are presented in the works of Luyben (2006).

$$\text{Cost condenser} = 7296 (A_{cond})^{0.65} \quad \text{Eq. 5.18}$$

$$\text{Cost reboiler} = 7296 (A_{reboiler})^{0.65} \quad \text{Eq. 5.19}$$

The area for both condenser and reboiler can be determined as follows:

$$Q_{trans} = U A LMTD \quad \text{Eq. 5.20}$$

Log Mean Temperature Difference (LMTD) is calculated for counter-current heat exchanging processes. The average overall heat transfer coefficients (U) for the condenser and reboiler are 852 and 568 $W/K m^2$, respectively, (Luyben, 2006). These overall heat transfer coefficients are suggested based on the materials normally used in condensers and reboilers and the types of fluids used therein. The costs of services such as cooling water, low pressure steam (≤ 6 bar), high pressure steam (≥ 10 bar) and electricity for an annual operating period of 8000 hours, are 0.16 US\$/GJ, 7.78 US\$/GJ, 9.98 US\$/GJ and 16.8 US\$/GJ, respectively (Caballero, 2015; Wang et al., 2015).

5.3.1 Specifications of the distillation columns

This section presents the specifications used in the optimisation of the distillation column system including: feed flow rate, feed concentration, concentration of distillate, number of trays in both rectification and stripping, pressure and, in the case of a double-column system, the losses of ethanol in the waste stream (see Figure 5.3.b).

The optimisation of a single distillation column and an arrangement of two columns are carried out in order to determine which configuration has the minimum TAC (see Eq. 5.1). The MINLP problems are solved using gPROMS v.4.1.0 on a Dell OptiPlex 9010 Intel® Core™ i7-3770 CPU @3.40 GHz and 16 GB RAM running Windows 7® Enterprise (64-bit operating system). The tool known as gOPT allows solving optimisation problems using a dynamic approach. This tool includes several solvers whose effectiveness are dependent on the nature of the system of equations (i.e. the complexity in terms the number of variables, constraints, application, etc.).

The solver used in this work for the integration of the algebraic and ordinary differential equations is called DASOLV and uses a *Backward Finite Difference* (BFD) formulation. gPROMS uses an Outer Approximation (OA) algorithm for the solution of the MINLP problem and the steps it follows are shown in Figure 5.4. This algorithm is implemented in the optimisation of both the distillation systems as well as the pervaporation network (Process System Enterprises, 2015). The input variables are shown in Table 5.1.

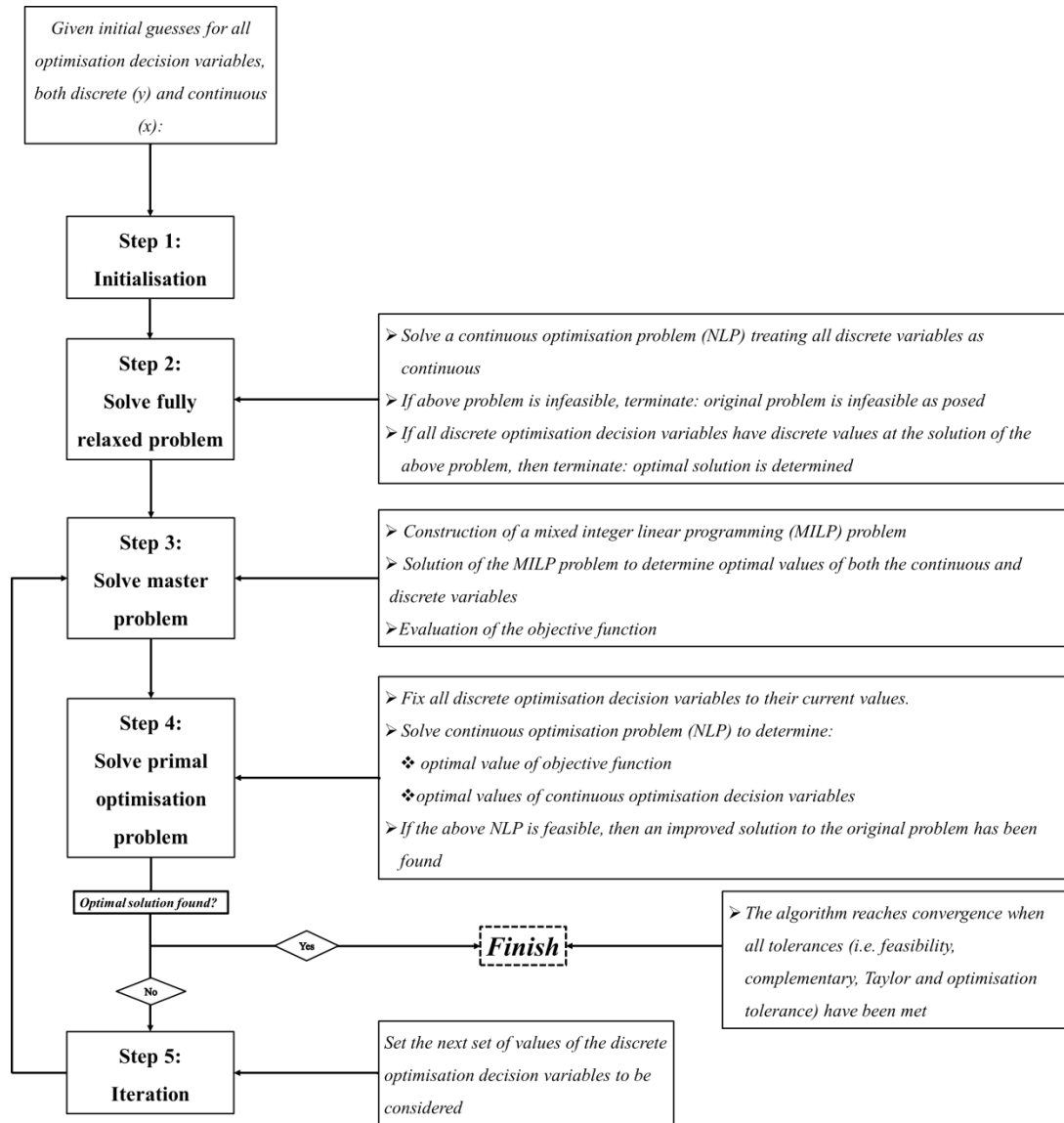


Figure 5.4: Outer Approximation (OA) algorithm for the solution of the MINLP problem using gPROMS (Process System Enterprises, 2015)

Table 5.1: Input variables used in the optimisation of the distillation systems

Feature	Value
Feed flow rate (mole/sec)	50
Conc. ethanol feed (% w/w)	5
Pressure (kPa)	101.3
Feed temperature (°C)	Saturated liquid at specified pressure

This work will consider the separation of 50 mole/sec (or 3344.63 kg/h) of a solution 5% (w/w) of ethanol. The concentration of ethanol in the feed stream has been set at 5 % (w/w) since this is the average concentration that is expected to be obtained during the fermentation of lignocellulosic hydrolysates using the genetically modified bacterium *Zymomonas mobilis* ZM4 (pZB5). Pressure inside the column has been set at atmospheric conditions in order to avoid the implementation of additional devices such as pumps since the feed stream comes out directly from the fermenter. The feed temperature corresponds to the temperature of saturated liquid at the operating pressure in the column in order to guarantee energy efficiency within the system (Kunnakorn et al., 2013).

5.3.2 Results of the optimisation of the distillation system

This section presents the results of the optimisation of the different units included in the separation stage of the ethanol production process from corn stover. These calculations are carried out using the tool in gPROMS known as gOPT. As previously mentioned, this chapter seeks to obtain the solution of each unit individually and later use these results as initial estimates for the solution of the overall problem. This methodology is a practical way of reducing the number of calculations and therefore reducing computational times since the system of equations featured in this problem possess a highly non-linear formulation. Appendix A presents the equations used in the formulation of a distillation column. Table 5.2 presents the initial guesses used in the optimisation of the distillation systems as well as the bounds of the optimisation variables considered in the solution of the MINLP problem.

Table 5.2: Initial guesses and bounds used in the optimisation of the distillation systems

Parameter	Single column	Two columns		Lower bound	Upper bound
		Column 1	Column 2		
Number of trays in rectification	25	20	20	1	25
Number of trays in stripping	25	20	20	1	25
Reflux ratio	2	1	3	0.01	100
Mass fraction distillate ($W_{D,Eth}$)	0.93	0.93*		0.93	1.0
Waste ($W_{Loss.Eth}$) % (W/W)	N/A	7		5	10

* Refers to the concentration of ethanol in the distillate stream of the second column

Table 5.3: Results of the optimisation of the distillation systems

Parameter	Single column	Two columns	
		Column 1	Column 2
Number of trays rectification	19	13	11
Number of trays stripping	12	15	1*
Total number of trays	34	31	15
Feed tray	21	15	13
Diameter column (m)	0.43	0.36	0.38
Height column (m)	20.7	18.9	9.15
Reflux ratio	3.81	1.29	2.89
Heat duty reboiler (kW)	224.6	217.9	160.6
Mass fraction distillate	0.93*	0.64	0.93*
Cost column shell (US\$/yr. 10^4)	4.15	3.48	2.11
Cost trays (US\$/yr. 10^3)	1.07	0.81	0.44
Cost reboiler (US\$/yr. 10^4)	1.25	1.22	1.01
Cost condenser (US\$/yr. 10^3)	7.03	7.10	5.71
Cost steam (US\$/yr. 10^4)	5.51	5.35	3.94
Cost cooling water (US\$/yr. 10^3)	1.06	1.08	0.77
CPU time (sec)	8912	20,852	
Payback period	4 years		
TAC (US\$/yr. 10^5)	1.18	1.87	

* Value on bound

Table 5.3 and Figures 5.5 and 5.6 show the results of the optimisation of the distillation column systems shown in Figure 5.3. The results suggest that the implementation of a single distillation column in the separation of ethanol from the fermentation broth can be more economical than having a double-column system for the same distillate concentration. This conclusion is also supported by the amount of energy required in the reboiler for both systems with heat requirements in the reboiler of 224.6 kW for a single column and 378.5 kW in total for the double-column system (savings of up to 41 %). In terms of economics, the configuration shown in Figure 5.6 reported a TAC of 1.87×10^5 US\$/year which is 42 % more expensive than the single distillation column.

In terms of the design, the number of trays in the single column is related to the concentration in the distillate stream. In binary mixtures that present azeotropes, the number of trays increase as the concentration in the distillate gets closer to the azeotropic point. The heat duty at the reboiler also increases as the concentration of ethanol increases, which directly correlates to the operating costs. The results of the optimisation of the double-column system show that the energy requirement in the first column accounts only for 97 % of the energy used in the reboiler of the single column, which makes the installation of the second column less practical from the point of view of the usage of utilities and controllability of additional units.

5.4 Optimisation of the pervaporation system using a PAN-B5 hydrophilic membrane

This section presents the optimisation of the membrane network for the pervaporation of the distillate stream from the distillation column chosen in the previous section. Similar to the case of the distillation column systems, the evaluation of the optimal arrangement of pervaporation modules will be based on the minimum TAC using the algorithm presented in Figure 5.4. For the subsequent analysis and optimisation of the pervaporation network, the values for feed flow rate, concentration of ethanol, feed temperature and feed pressure, will be taken from the values obtained in the distillate stream of the single distillation column configuration shown in Table 5.1 and Figure 5.5.

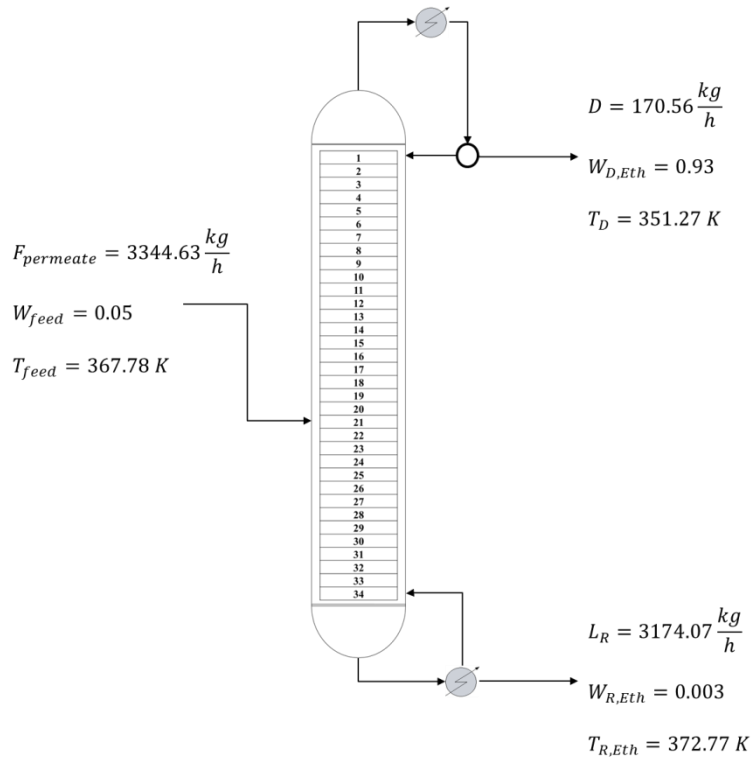


Figure 5.5: Streams and concentrations in a single distillation column using the results of the optimisation presented in Table 5.3

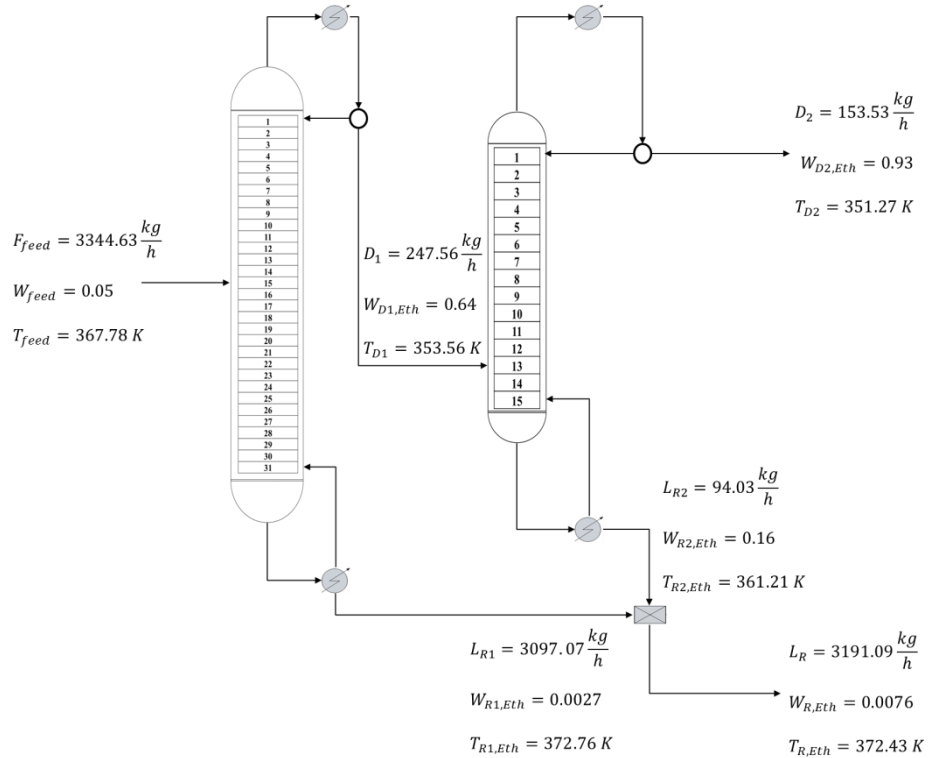


Figure 5.6: Streams and concentrations in a double-column distillation system using the results of the optimisation presented in Table 5.3

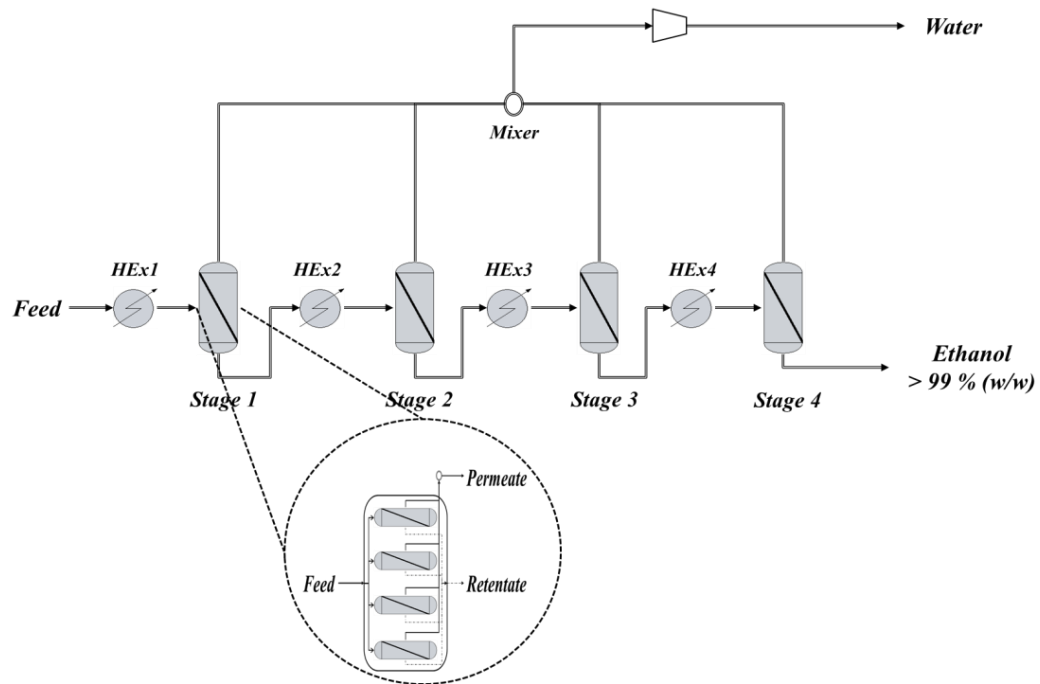


Figure 5.7: Pervaporation network design using PAN-B5 hydrophilic membrane

Figure 5.7 presents the general configuration of the membrane network. The methodology to find the optimal configuration consists of determining the optimal number of in-parallel modules and operating conditions for one stage. Then, the optimal conditions for two in-series stages is determined, then three stages, etc. The configuration with the minimum TAC is the configuration to be used for the overall optimisation along with the distillation column (Marriott and Sørensen, 2003; Marriott et al., 2001).

In industrial pervaporation processes, due to the evaporation of the components in the feed mixture and the permeation through the membrane into the permeate side, the temperature in the retentate side decreases (Baker, 2012). Since the flux has a high dependence on the feed temperature, operating temperatures within the system should be as high as possible, and temperature drops should be limited to a minimum. Hence, intermediate heating is required in the system to ensure that the feed temperature for all the stages is the same. This requirement has to be balanced against the additional costs for a larger number of sub-divisions of membrane compartments and for the heat exchangers (Baeyens et al., 2015; Kunnakorn et al., 2013; Sander and Soukup, 1988; Tusel and Brüschke, 1985). For the optimisation of

the pervaporation network, an objective function similar to Eq. 5.1 is required. This equation needs to have costs related to the size of the membrane, the installation of the modules, compression and heat exchangers:

$$Cost\ Compressor = \left(\frac{M\&S}{280}\right) 517.9\ BHP^{0.82}\ 3.11\ <US\$> \quad \text{Eq. 5.21}$$

BHP, which is also known as Brake horsepower, is the work done by the compressor over the vapour and is defined as:

$$BHP = \frac{hp}{\eta} \quad \text{Eq. 5.22}$$

Where *hp* is the work done by an isothermal compressor and η is the efficiency of the compressor assumed to be 0.95 (Marriott and Sorensen, 2003).

$$hp = \frac{F_{in}}{\rho^V} \frac{P_{in}}{\eta} \ln\left(\frac{P_{out}}{P_{in}}\right) \quad \text{Eq. 5.23}$$

The following constraints are required for the optimisation of the pervaporation network. Eq. 5.16 is the temperature difference allowed after the permeation of the mix through the membrane. This temperature difference constraint is only applicable for two pervaporation stages or more. For a single stage, this constraint does not apply since the flux through the membrane, in order to meet the desire specifications, is too high and the temperature will plummet beyond a difference of 20 K due to the evaporation heat.

$$\Delta T_{feed,retent}^{min} \leq \Delta T_{feed,retent} \leq \Delta T_{feed,retent}^{max} \quad \text{Eq. 5.24}$$

Eq. 5.17 is the constraint related to the purity of the product in the retentate stream which needs to meet biofuel standards (Drapcho et al., 2008; Palmarola-Adrados et al., 2005; Sánchez and Cardona, 2012):

$$W_{retent,eth}^{min} \leq W_{retent,eth} \leq W_{retent,eth}^{max} \quad \text{Eq. 5.25}$$

Eq. 5.18 is the permeate pressure range at which the PAN-B5 hydrophilic membrane model is valid. This is presented in the experimental work developed by Tsuyumoto et al., (1995), (1997):

$$P_{perm}^{min} \leq P_{perm} \leq P_{perm}^{max} \quad \text{Eq. 5.26}$$

The cost of the PAN-B5 hydrophilic membrane is 217.4 US\$/m², the cost of each membrane module is 140.2 US\$/m² and their replacement takes place every four years (Kiran and Jana, 2015).

5.4.1 Specifications of the pervaporation network using a hydrophilic membrane

The flow rate obtained in the distillate of the distillation column shown in Figure 5.5 will be used as the feed flow rate for the pervaporation network presented in Figure 5.7. The distillate stream is initially cooled down to operating feed temperature of the membrane and the passed through the pervaporation stages in order to remove water from the mixture.

Table 5.4: Input variables used in the optimisation of the pervaporation system using the PAN-B5 hydrophilic membrane

Feature	Value
Feed flow rate (mole/sec)	Distillate flow rate
Conc. ethanol feed (% w/w)	93
Pressure (kPa)	101.3
Feed temperature (°C)	Saturated liquid at specified pressure

Table 5.5: Initial guesses and bounds used in the optimisation of the PAN-B5 hydrophilic membrane

Parameter	Stage 1	Stage 2	Stage 3	Stage 4	Stage 5	Lower bound	Upper bound
Number of in-parallel modules	1	1	1	1	1	1	25
Permeate pressure (Pa)	4000	2000	400	400	400	10	10,000
Conc. retentate ($W_{retent,Eth}$)	0.993	0.993	0.993	0.993	0.993	0.993	0.998
$\Delta T_{feed,retent}$	20	20	20	20	20	10	20

Table 5.4 presents the input variables used in the optimisation of the pervaporation system using the PAN-B5 hydrophilic membrane. Table 5.5 presents the initial guesses and boundaries used in the solution of the MINLP problem.

5.4.2 Results of the optimisation of the pervaporation network using a hydrophilic membrane

Figure 5.8 presents the results of the optimisation of the pervaporation network for different in-series membrane stages. Figure 5.8 shows a decrease of the TAC as the number of in-series stages increases and after three stages, the TAC increases for four and five stages meaning that the optimal configuration for the pervaporation network may have three stages. However, for this particular case study, the curves for three and four stages present a narrow gap, and in some cases they overlap making this comparison more difficult. Therefore, another criterion should be taken into consideration in order to determine the optimal number of pervaporation stages and their membrane area.

Figure 5.9 shows a trade-off between the TAC and energy consumption for the arrangements of three and four in-series pervaporation stages in order to find an optimal configuration that can be considered in the optimisation of the whole separation section. For membrane areas between 100 and 150 m², the energy consumption is high for both arrangements and then decreases until 400 m².

Table 5.6 presents the results of the optimisation of the different arrangements for the pervaporation network in the dehydration of ethanol. It can be observed that the total

number of in-parallel modules decreases as the area increases. For membrane areas larger than 250 m², the number of stages remains constant. This suggests that configurations with larger membrane areas are economically inviable as they only represent an increment in the capital and operating costs with similar performance as those configurations with smaller membrane areas. For instance, for four and five stages, the number of models remains constant after a membrane area of 250 m². The only difference between these arrangements is the permeate pressure which increases as the membrane area increases.

However, the partial fluxes and the separation rates of ethanol through the permeate side in these configurations with larger areas do not differ from those with smaller areas. Moreover, for larger areas in the configuration consisting of five stages, a permeate pressure higher than 10,000 Pa is required in order to find an optimal (see Eq. 5.16 for the boundaries of permeate pressure used in the membrane module). These results are marked with an asterisk in Table 5.6.

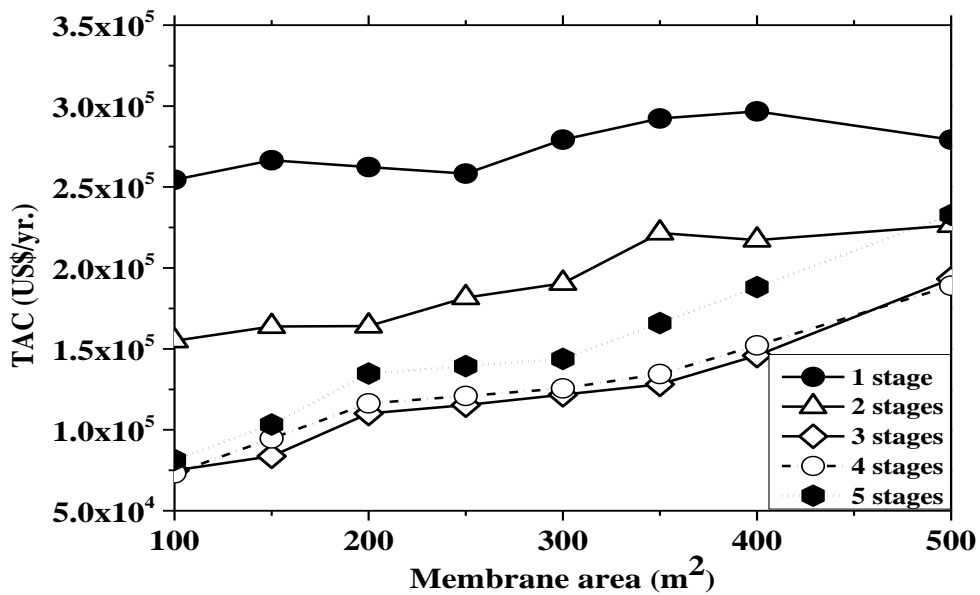


Figure 5.8: Optimisation of the hydrophilic pervaporation system at different membrane areas for the system consisting of a single distillation column shown in Figure 5.5

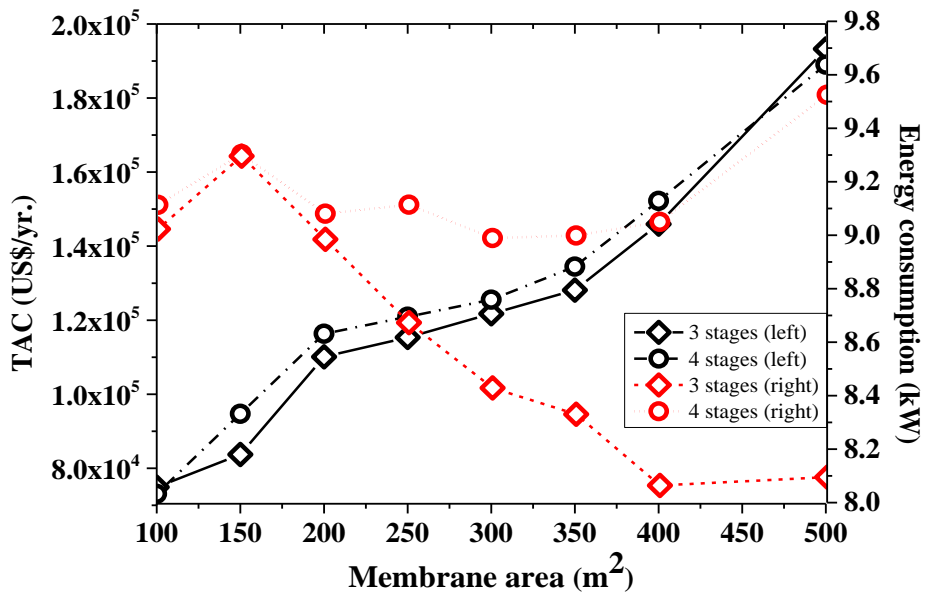


Figure 5.9: Comparison of total annualised cost vs. energy consumption for three and four in-series pervaporation stages shown in Figure 5.8

For four stages, for instance, the energy consumption starts to increase along with the TAC from 400 m² onwards. This supports the conclusion previously stated that having more than three stages with larger areas is inefficient not only in terms of separations rates but also in terms of energy requirements. This energy assessment also shows that for three stages, with areas between 150 and 300 m², both the TAC and the energy consumption are lower than for four stages. It can be concluded based on this analysis that the optimal configuration for the dehydration of ethanol using a hydrophilic membrane should consist of three stages with a membrane area of 250 m².

Table 5.6: Optimal parameters for a minimum TAC in the PAN-B5 hydrophilic membrane system

Stage	Parameters	Membrane Area (m ²)							
		100	150	200	250	300	350	400	500
One Stage									
	TAC (US\$/yr.)	254,470	266,503	262,350	258,307	279,299	292,345	296,724	279,299
1	Number of modules	27	19	14	11	10	9	8	6
	Permeate pressure (Pa)	57	138	112	85	211	278	298	211
Two Stages									
	TAC (US\$/yr.)	155,013	163,849	164,090	181,613	190,517	221,635	217,225	226,200
1	Number of modules	1	1	1	1	1	1	1	1
	Permeate pressure (Pa)	3324	5139	5972	6495	6880	7190	7456	7915
2	Number of modules	15	10	8	6	6	5	4	4
	Permeate pressure (Pa)	59	46	133	21	276	227	86	374
Three Stages									
	TAC (US\$/yr.)	74,898	83,737	110,095	<u>115,339</u>	121,720	128,102	145,958	193,282
1	Number of modules	1	1	1	<u>1</u>	1	1	1	1
	Permeate pressure (Pa)	3324	5139	5972	<u>6495</u>	6880	7190	7456	7915
2	Number of modules	2	2	1	<u>1</u>	1	1	1	1
	Permeate pressure (Pa)	74	1134	480	<u>243</u>	1232	1880	2369	3122
3	Number of modules	5	3	3	<u>2</u>	2	2	3	3
	Permeate pressure (Pa)	74	71	251	<u>243</u>	415	538	1073	1215

Underlined values in bold and italic font represent the optimal solution of the pervaporation network

Table 5.6: Optimal parameters for a minimum TAC in the PAN-B5 hydrophilic membrane system (cont.)

Stage	Parameters	Membrane Area (m ²)							
		100	150	200	250	300	350	400	500
Four Stages									
	TAC (US\$/yr.)	73,077	94,715	116,354	120,948	125,541	134,469	152,206	188,999
1	Number of modules	1	1	1	1	1	1	1	1
	Permeate pressure (Pa)	3324	5365	5972	8044	8059	8064	8060	8500
2	Number of modules	1	1	1	1	1	1	1	1
	Permeate pressure (Pa)	325	316	1097	2360	2670	2880	3032	6000
3	Number of modules	3	2	3	1	1	1	1	1
	Permeate pressure (Pa)	325	316	1097	437	754	991	1187	800
4	Number of modules	2	1	1	1	1	1	1	1
	Permeate pressure (Pa)	325	316	1097	437	754	991	1187	800
Five Stages									
	TAC (US\$/yr.)	81,436	103,279	134,778	139,321	143,863	165,940	188,166	232,798
1	Number of modules	1	1	2	1	1	1	1	1
	Permeate pressure (Pa)	8079	8845	10,702	9735	10,102*	10,441*	10,770*	11,427*
2	Number of modules	1	1	1	1	1	1	1	1
	Permeate pressure (Pa)	3720	4848	7376	7726	8178	8562	8934	9063
3	Number of modules	1	1	1	1	1	1	1	1
	Permeate pressure (Pa)	494	800	1125	3602	3046	3085	3111	3242
4	Number of modules	3	3	2	1	1	1	1	1
	Permeate pressure (Pa)	494	800	814	973	762	1000	1196	1524
5	Number of modules	2	1	1	1	1	1	1	1
	Permeate pressure (Pa)	494	800	814	17	762	1000	1196	1524

* Indicates values of permeate pressure out of the boundaries of the mathematical model for the membrane the PAN-B5 developed by Tsuyumoto et al., (1997)

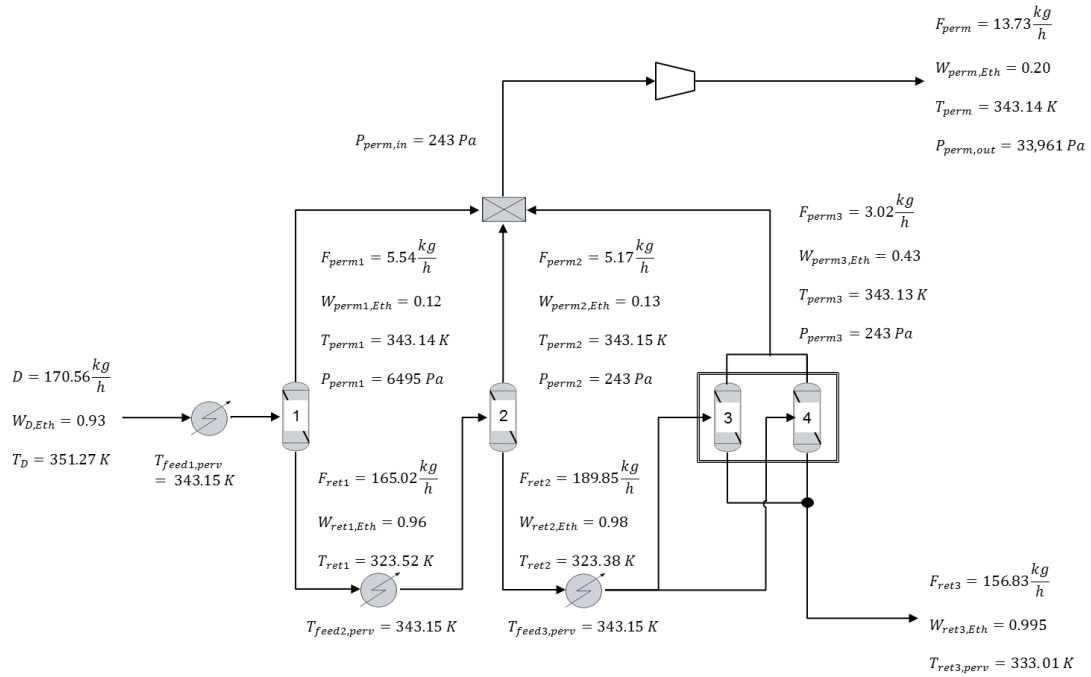


Figure 5.10: Results of the optimisation of the pervaporation network using PAN-B5 hydrophilic membrane and a membrane area of 250 m² for the distillation system shown in Figure 5.5

The results of the optimisation and simulation of the configuration illustrated in Figure 5.10 show that a 98 % of the ethanol fed into the system is recovered in the retentate stream from the last stage. In terms of operating conditions, the results show a temperature drop for the first and the second stages of almost 20 K which is necessary in order to remove as much water as possible from the mix.

This optimisation problem is mainly influenced by the concentration at the end of the pervaporation plant. If concentrations of ethanol higher than 99.8 % (w/w) were fixed, the number of in-parallel modules and the total membrane area would increase. The operating costs of the plant would increase as well since lower permeate pressures would be required in order to increase the concentration of ethanol in the retentate, which will impact on the consumption of energy in the compressor and the amount of steam to provide heat to the intermediate heat exchangers.

5.5 Optimisation of the pervaporation system using a PERVAP™ 4060 organophilic membrane

Chapter 4 presented the formulation of a mathematical model, based on experimentation, of an organophilic membrane for the removal of ethanol from the fermentation broth. This mathematical model (see Eq. 4.5) describes the permeation of ethanol through the membrane into the permeate side for a specific range of operating conditions (see Table 4.1).

As explained in Chapter 4, the reason to use the organophilic membrane is to reduce the energy consumption in the distillation column as well as the size of some units in the plant by reducing the feed flow rate into the column and increasing the concentration of ethanol. The pervaporation network with the PERVAP™ 4060 organophilic membrane will be optimised in the same fashion as the PAN-B5 hydrophilic membrane shown in Figure 5.7.

Unlike the pervaporation network using the hydrophilic membrane, the removal of ethanol using PERVAP™ 4060 will require an additional heat exchanger that will heat the permeate stream to a temperature corresponding to the dew point of the mixture at atmospheric conditions (i.e. 101.3 *kPa*). Once the mixture has reached the desired temperature, the vapour is passed through a compressor to increase the pressure from the vacuum pressure of the pervaporation module to atmospheric conditions before entering the distillation column as saturated vapour to reduce heat losses and improve energy efficiency. Figure 5.11 illustrates this configuration.

The feed conditions are 50 mole/sec (or 3344.63 kg/h) of a solution 5% (w/w) of ethanol which is the concentration expected to be obtained at the end of the fermentation stage at 50 °C. The cost of the PERVAP™ 4060 organophilic membrane is 214.53 US\$/m² and its replacement takes place every three years (Sulzer Chemtech, 2014). The cost of the each membrane module is 140.2 US\$/m² (Gaykawad et al., 2013; Kiran and Jana, 2015).

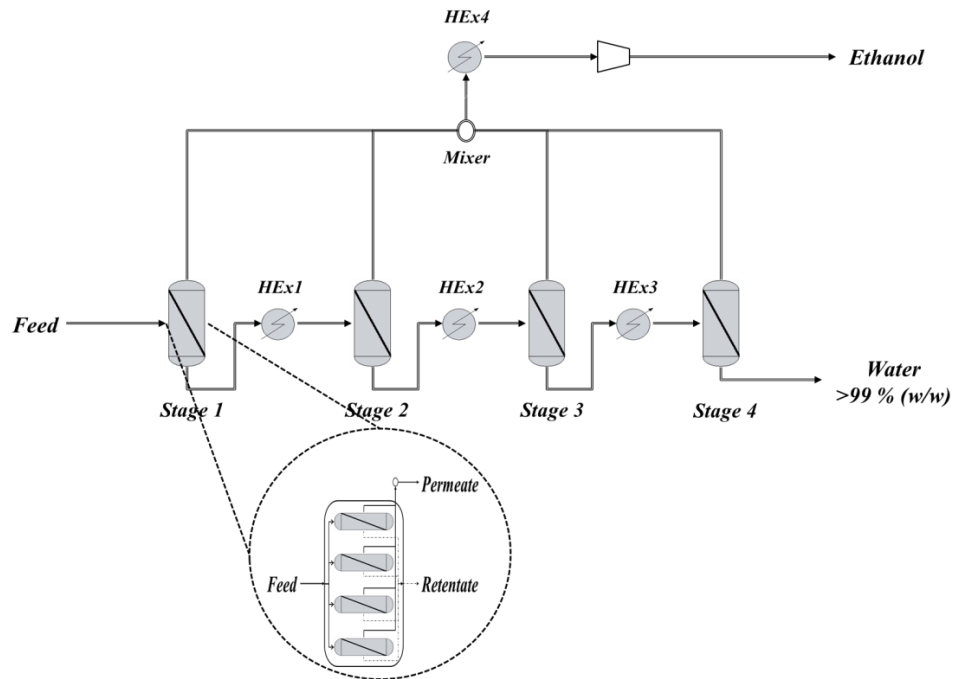


Figure 5.11: Pervaporation network design using PERVAP™ 4060 organophilic membrane

Similar to the optimisation of the hydrophilic membrane, a set of constraints need to be included in the formulation of the MINLP problem. Eq. 5.19 can be applied for two or more pervaporation stages, unlike a single stage in which the evaporation heat transferred from the feed side to the permeate side can cause a sharp decrease in the retentate temperature lower than these limits. The following are the constraints for the optimisation of the pervaporation network using an organophilic membrane:

$$\Delta T_{feed,retent}^{min} \leq \Delta T_{feed,retent} \leq \Delta T_{feed,retent}^{max} \quad \text{Eq. 5.27}$$

Eq. 5.20 is presents the desired concentration of ethanol in the retentate stream. In other words, all the ethanol present in the feed stream is expected to permeate and be fed to the distillation system.

$$W_{retent,eth}^{min} \leq W_{retent,eth} \leq W_{retent,eth}^{max} \quad \text{Eq. 5.28}$$

Table 5.7: Input variables used in the optimisation of the pervaporation system using the PAN-B5 hydrophilic membrane

Feature	Value
Feed flow rate (mole/sec)	50
Conc. ethanol feed (% w/w)	5.0
Pressure (kPa)	101.3
Feed temperature ($^{\circ}C$)	50

Table 5.8: Initial guesses and bounds used in the optimisation of the PAN-B5 hydrophilic membrane

Parameter	Stage 1	Stage 2	Stage 3	Lower bound	Upper bound
Number of in-parallel modules	1	1	1	1	25
Permeate pressure (Pa)	3500	2000	400	400	3500
Conc. retentate ($W_{retent,Eth}$)	0.001	0.001	0.001	0.0001	0.001
$\Delta T_{feed,retent}$	20	20	20	10	20

Eq. 5.21 is the range of permeate pressure used in the formulation of the mathematical model of the membrane (see Chapter 4, sections 4.4 and 4.5).

$$P_{perm}^{min} \leq P_{perm} \leq P_{perm}^{max} \quad \text{Eq. 5.29}$$

5.5.1 Specifications for the pervaporation network using an organophilic membrane

Following a similar approach as in the specifications for the hydrophilic membrane, Table 5.7 presents the input variables used in the optimisation of the pervaporation system using the organophilic membrane. The feed flow rate and the feed concentration are set as in the distillation systems (see Table 5.3), which are expected to be the outlet stream conditions from the fermentation stage. Table 5.8 presents the initial guesses and the bounds used in the solution of the optimisation problem.

5.5.2 Results of the optimisation of the pervaporation network using an organophilic membrane

Table 5.9 and Figure 5.12 present the results of the optimisation of the pervaporation network using the organophilic membrane. The results show that the TAC increases with the number of stages in the pervaporation network. Similar to the case of the hydrophilic membrane, for larger areas, higher permeate pressures are required. For one, two and three stages, and membrane areas of 200 m², the optimal permeate pressures are above 3500 Pa which rules out any implementation of these configurations into the main process since the operating conditions are out of the bounds in which the mathematical model of the membrane was formulated.

The TAC for all the cases decreases at 200 m² which can be attributed to the reduction in the energy consumption in the compressor that increases the pressure to atmospheric conditions. Also notice that for all the cases, the permeate pressures are higher than 1000 Pa and as seen in Section 4.5, the higher the permeate pressure the lower the separation rates in the pervaporation sections.

The results of permeate pressure also suggest that for two and three stages and membrane areas of 50 m² and above, the flux rates in the first two stages are expected to be lower (as shown in Table 4.4, the partial fluxes decrease as permeate pressure increases) which basically means that the last stage would do all the work in the pervaporation plant. This trend in the partial fluxes through the membrane supports the implementation of just one stage with multiple in-parallel modules since it is more practical from the point of view of controllability, size of the units, intermediate heating and maintenance. Hence, for the optimisation of the overall process, a membrane area of 20 m² and one pervaporation stage will be considered. Figure 5.12 shows the results of the optimisation of the pervaporation network using the PERVAPTM organophilic membrane for the removal of ethanol from the fermentation broth.

Table 5.9: Optimal parameters for a minimum TAC in the PERVAP 4060™ organophilic membrane system

Stage	Parameters	Membrane area (m ²)						
		20	50	80	100	150	180	200
One Stage								
	TAC (US\$/yr.)	<i>206,516</i>	231,248	181,064	197,388	177,431	181,831	197,388
1	Number of modules	<i>19</i>	7	5	4	4	4	2
	Permeate pressure (Pa)	<i>3431</i>	1988	6959*	4223*	8579*	9829*	4223*
Two Stages								
	TAC (US\$/yr.)	231,584	236,389	223,821	250,206	229,312	225,983	226,133
1	Number of modules	3	1	2	1	1	1	1
	Permeate pressure (Pa)	3500	3500	8329*	3500	7891*	9063*	10,000*
2	Number of modules	19	8	7	4	4	3	3
	Permeate pressure (Pa)	3758*	4453*	8011*	4652*	8526*	7713*	8509*
Three Stages								
	TAC (US\$/yr.)	257,363	261,168	267,632	293,957	276,321	273,654	270,952
1	Number of modules	3	1	1	1	1	1	1
	Permeate pressure (Pa)	3500	3500	8169*	3500	10,000*	12,109*	10,000*
2	Number of modules	3	1	1	1	1	1	1
	Permeate pressure (Pa)	5828*	3500	8022*	3500	10,000*	11,740*	10,000*
3	Number of modules	18	7	7	4	4	2	3
	Permeate pressure (Pa)	3164	2669	8028*	4975*	8493*	3078*	8455*

* Indicates permeate pressure out of the boundaries of the empirical model

Underlined values in bold and italic font represent the optimal solution of the pervaporation network

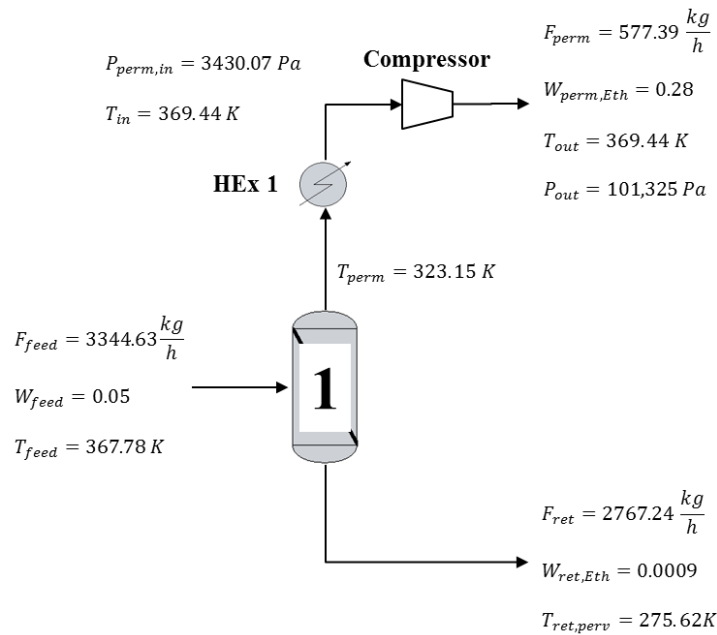


Figure 5.12: Results of the optimisation of the pervaporation network using PERVAPTM 4060 organophilic membrane and a membrane area of 20 m² and 19 in-parallel modules

Table 5.10: Input variables used in the optimisation of the distillation column linked to the organophilic membrane system

Feature	Value
Feed flow rate (mole/sec)	Permeate flow rate leaving the compressor (see Figure 5.12)
Conc. ethanol feed (% w/w)	Conc. of permeate leaving the pervaporation module
Pressure (kPa)	101.32
Feed temperature (°C)	Saturated vapour at specified pressure

Table 5.10 presents the list of input variables used in the solution of the optimisation problem of the distillation column using the permeate stream from the PERVAPTM 4060 organophilic membrane system. Table 5.11 presents the results optimisation of the distillation column using the outlet stream of the pervaporation stage with the organophilic membrane. These results show a noticeable reduction in the energy consumption in comparison with the results shown in Table 5.3 and this is due to the conditions at which the feed stream is fed (saturated vapour). The size of the trays and the shell of the column are also smaller than the single column in Figure 5.5.

Table 5.11: Results of the optimisation of the distillation systems using the permeate stream of the pervaporation system shown in Figure 5.15 as feed

Parameter	Single column
Number of trays rectification	21
Number of trays stripping	1*
Total number of trays	25
Feed tray	23
Diameter column (m)	0.35
Height column (m)	15.3
Reflux ratio	2.08
Heat duty reboiler (kW)	144.1
Mass fraction distillate	0.93*
Cost column shell (US\$/yr. 10⁴)	2.59
Cost trays (US\$/yr. 10²)	5.67
Cost reboiler (US\$/yr. 10³)	9.37
Cost condenser (US\$/yr. 10³)	5.19
Cost steam (US\$/yr. 10⁴)	3.54
Cost cooling water (US\$/yr. 10²)	6.68
CPU time (sec)	29,182
Payback period	4 years
TAC (US\$/yr. 10⁴)	7.71

* Value on bound

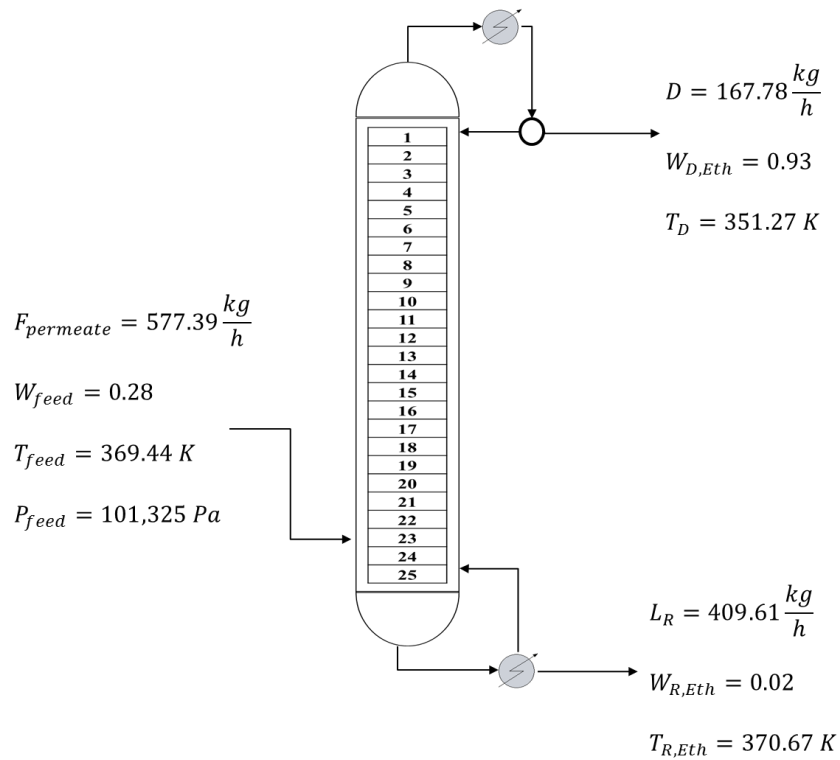


Figure 5.13: Results of the optimisation of the distillation column under the specifications presented in Table 5.10

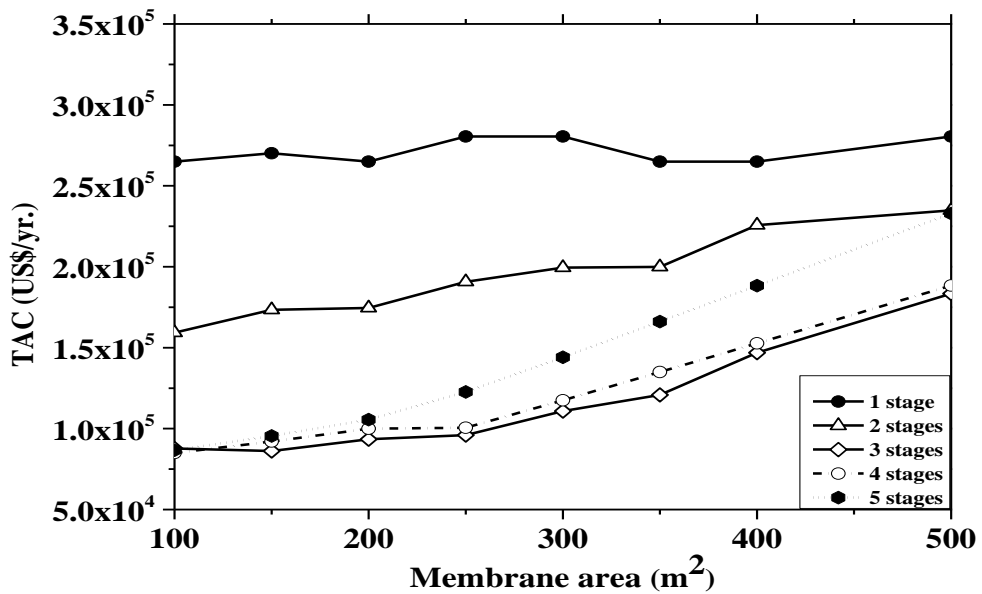


Figure 5.14: Optimisation of the hydrophilic pervaporation system at different membrane areas for the system consisting of a single distillation column shown in Figure 5.13

Figure 5.14 presents the results optimisation of the pervaporation section using the distillate stream of the distillation column shown in Figure 5.13. A similar trend as in

Figure 5.8 can be observed in Figure 5.14. The TAC decreases for the first three stages and starts to increase after four stages. However, in this case, an energy analysis is not necessary since there is a clear distinction between the curve that represents three stages and the one for four stages.

Similarly to the case shown in Figure 5.8, for five stages and membrane areas larger than 350 m^2 , the permeate pressure is higher than the upper bound in Eq. 5.16 which means that these configurations are not viable for implementation into the main process since the mathematical model has not validity beyond $10,000 \text{ Pa}$.

A minimum TAC is also obtained for a configuration consisting of three stages and a membrane area of 150 m^2 (see Table 5.14). This configuration will serve as initial estimate for the solution of the optimisation of the overall separation process. Figure 5.15 shows the simulation of the optimal configuration which consists of three in-series stages of pervaporation and their respective operating conditions.

Table 5.12: Initial guesses and bounds used in the optimisation of the PAN-B5 hydrophilic membrane in the configuration with the organophilic membrane

Parameter	Stage 1	Stage 2	Stage 3	Lower bound	Upper bound
Number of in-parallel modules	1	1	1	1	25
Permeate pressure (Pa)	3500	2000	400	400	3500
Conc. retentate ($W_{retent,Eth}$)	0.001	0.001	0.001	0.0001	0.001
$\Delta T_{feed,retent}$	20	20	20	10	20

Table 5.13: Initial guesses and bounds used in the optimisation of the PAN-B5 hydrophilic membrane

Parameter	Stage 1	Stage 2	Stage 3	Stage 4	Stage 5	Lower bound	Upper bound
Number of in-parallel modules	1	1	1	1	1	1	25
Permeate pressure (Pa)	4000	2000	400	400	400	10	10,000
Conc. retentate ($W_{retent,Eth}$)	0.993	0.993	0.993	0.993	0.993	0.993	0.998
$\Delta T_{feed,retent}$	20	20	20	20	20	10	20

Table 5.14: Optimal parameters for a minimum TAC in the pervaporation network using the distillate stream of the single distillation column shown in Figure 5.13

Stage	Parameters	Membrane Area (m ²)							
		100	150	200	250	300	350	400	500
One Stage									
	TAC (US\$/yr.)	264,961	270,127	264,961	280,459	280,459	264,961	264,961	280,459
1	Number of modules	28	15	14	12	10	8	7	6
	Permeate pressure (Pa)	32	10	32	137	137	32	32	137
Two Stages									
	TAC (US\$/yr.)	159,234	173,387	174,572	190,685	199,444	199,922	225,689	234,805
1	Number of modules	1	1	1	1	1	1	1	1
	Permeate pressure (Pa)	2984	4958	5836	6379	6772	7085	7351	7804
2	Number of modules	15	11	8	7	6	5	5	4
	Permeate pressure (Pa)	10	115	56	179	208	157	330	311
Three Stages									
	TAC (US\$/yr.)	87,755	<u>86,200</u>	93,478	95,972	110,833	120,788	146,919	183,405
1	Number of modules	1	<u>1</u>	1	1	1	1	1	1
	Permeate pressure (Pa)	2984	<u>4958</u>	5836	6379	6772	7085	7351	7804
2	Number of modules	1	<u>2</u>	1	1	1	1	1	1
	Permeate pressure (Pa)	75	<u>649</u>	179	137	978	1672	2182	2948
3	Number of modules	8	<u>3</u>	3	2	2	2	2	2
	Permeate pressure (Pa)	56	<u>80</u>	179	137	371	498	597	746

Underlined values in bold and italic font represent the optimal solution of the pervaporation network

Table 5.14: Optimal parameters for a minimum TAC in the pervaporation network using the distillate stream of the single distillation column shown in Figure 5.13 (cont.)

Stage	Parameters	Membrane Area (m ²)							
		100	150	200	250	300	350	400	500
Four Stages									
	TAC (US\$/yr.)	84,926	92,058	99,983	100,545	117,462	134,980	152,678	188,385
1	Number of modules	1	1	1	1	1	1	1	1
	Permeate pressure (Pa)	2995	8643	6686	8038	8056	8063	8063	8085
2	Number of modules	1	1	1	1	1	1	1	1
	Permeate pressure (Pa)	511	1656	3113	2255	2589	2814	2976	3255
3	Number of modules	2	1	1	1	1	1	1	1
	Permeate pressure (Pa)	10	214	448	334	668	913	1111	1411
4	Number of modules	3	3	2	1	1	1	1	1
	Permeate pressure (Pa)	401	214	448	334	668	913	1111	1365
Five Stages									
	TAC (US\$/yr.)	86,657	95,430	105,551	122,670	144,097	166,111	188,310	232,917
1	Number of modules	1	1	1	1	1	1	1	1
	Permeate pressure (Pa)	5827	8059	9215	9647	9995	10,322*	10,636*	11,259
2	Number of modules	1	1	1	1	1	1	1	1
	Permeate pressure (Pa)	4325	6008	7116	7658	8056	8426	8783	9114
3	Number of modules	1	1	1	1	1	1	1	1
	Permeate pressure (Pa)	66	1597	2581	2974	3031	3073	3102	3200
4	Number of modules	3	2	1	1	1	1	1	1
	Permeate pressure (Pa)	20	22	10	342	676	921	1120	1446
5	Number of modules	2	1	1	1	1	1	1	1
	Permeate pressure (Pa)	20	22	37	342	676	921	1120	1446

* Indicates values of permeate pressure out of the boundaries of the mathematical model for the membrane the PAN-B5 developed by Tsuyumoto et al., (1997)

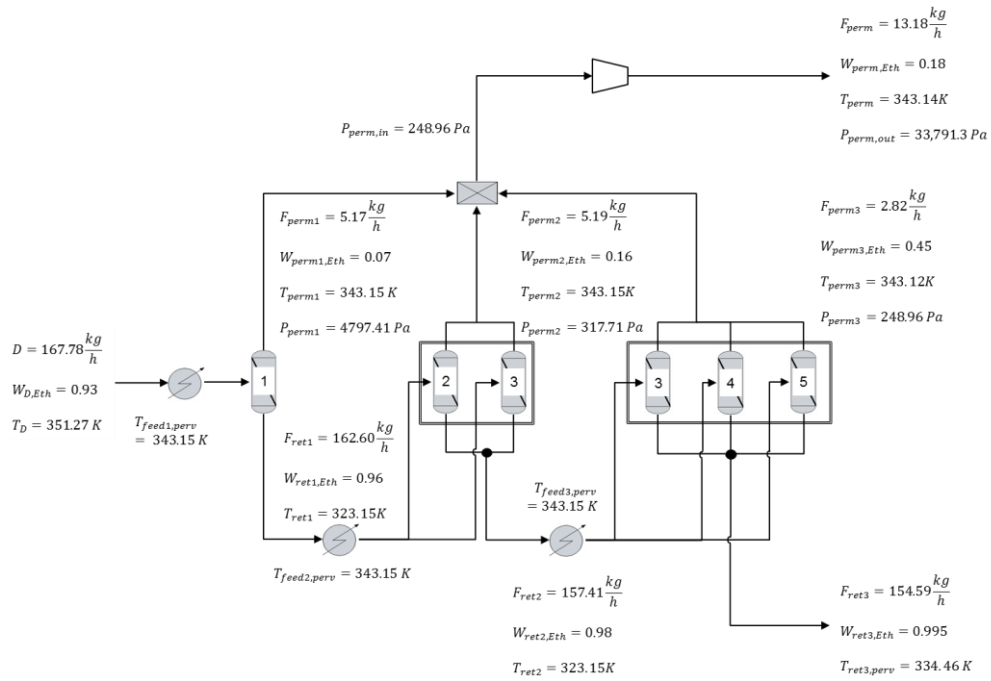


Figure 5.15: Results of the optimisation of the pervaporation network using PAN-B5 hydrophilic membrane and a membrane area of 150 m² for the distillation system shown in Figure 5.14

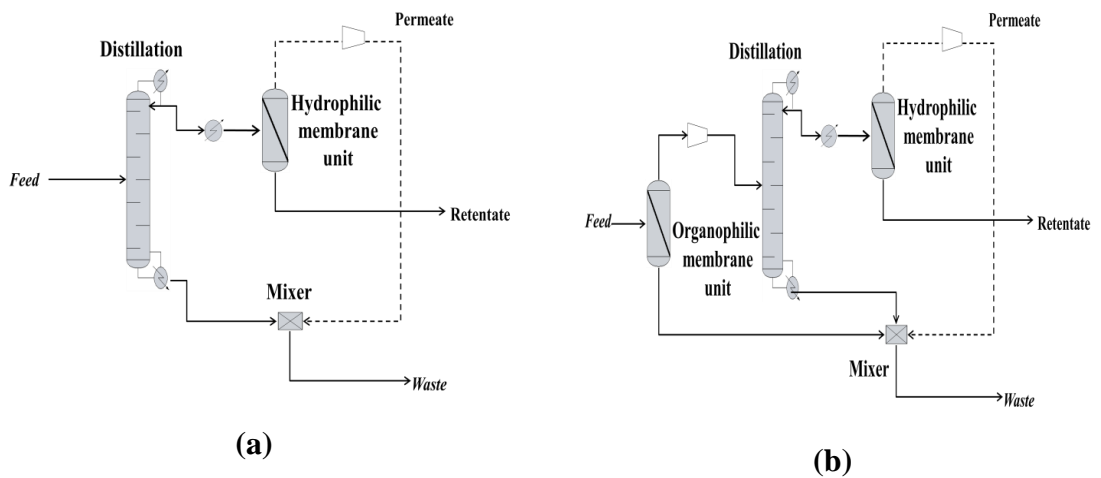


Figure 5.16: Superstructure of the separation section of the ethanol production process: a) single distillation and pervaporation network with PAN-B5 hydrophilic and b) pervaporation network with PERVAPTM organophilic membrane linked to a single distillation column and a pervaporation network with PAN-B5 hydrophilic membrane

Table 5.15: Input variables used in the optimisation of the separation section with and without the organophilic membrane

Feature	Value
Feed flow rate (mole/sec)	50
Conc. ethanol feed (% w/w)	5.0
Pressure (kPa)	101.3
Feed temperature without organophilic membrane ($^{\circ}C$)	Saturated liquid at specified pressure
Feed temperature with organophilic membrane ($^{\circ}C$)	50

5.6 Optimisation of the complete separation section – Case study

Figure 5.16 presents the schematics of the two different cases of separation stages considered in this chapter. As mentioned before, the results of the optimisation of the individual units of the separation section (i.e. distillation, hydrophilic pervaporation network and organophilic pervaporation network) are used in the solution of the optimisation problem in the superstructures presented in Figure 5.16 as initial estimates.

5.6.1 Specifications of the separation section

The specifications for the complete separation sections are the same as for the individual units. Table 5.15 presents the input variables for the optimisation of the complete separation section used in the solution of the MINLP problem. The initial guesses for the superstructure without the organophilic membrane are taken from the results presented in Tables 5.3 and 5.6. The initial guesses for the superstructure featuring the organophilic membrane are taken from the results presented in Tables 5.9, 5.11 and 5.14. The lower and upper bounds and the specifications of purity for the complete system are the same as used in the individual units (see Tables 5.2, 5.5 and 5.8).

For the optimisation of the complete separation stage, an additional constraint needs to be included in the formulation of the solution of the optimisation problem. That constraint represents the amount of ethanol removed in the waste stream as shown in Figure 5.16 and is presented in Eq. 5.22:

$$W_{Loss.Eth}^{min} \leq W_{Loss.Eth} \leq W_{Loss.Eth}^{max}$$

Eq. 5.30

This section presents the optimisation of the separation sections with and without the organophilic membrane. As previously mentioned, the combined process will use the optimisation results of the individual units as initial guess in order to narrow the feasibility region in which the optimal solutions can be found.

5.6.2 Results of the separation sections

For the structure presented in Figure 5.17, the results of each unit present similarities to those obtained individually. For instance, the total number of trays in the distillation column is 34, which is the same solution obtained for the individual case (see Figure 5.5). For the superstructure, the feed stream is located at tray 20 whereas in the individual column it was located at tray 21. The number of in-parallel modules is slightly different since in the individual solution (see Figure 5.10) the total number of modules is 4 whereas the superstructure presents 5. These small variations indicate that the superstructure can be considered as a completely new and different system of equations with different behaviour and possibly different solutions. However, these comparisons also suggest that using the individual solution as an initial guess for the optimisation of the overall separation section does facilitate the solution of the MINLP.

A similar comparison can be applied to the distillation column systems in Figure 5.13 and Figure 5.19. The feed tray in both cases is close to the bottom of the column and the number of trays is 25 and 24 for the individual solution and the superstructure, respectively. Other similarities can be observed in the permeate pressures, which decrease as the concentration of ethanol in the retentate increases in both the individual solution of the dehydration section and the superstructure. Table 5.16 presents a summary of the results of the optimisation for both superstructures, including the TAC and the energy requirements.

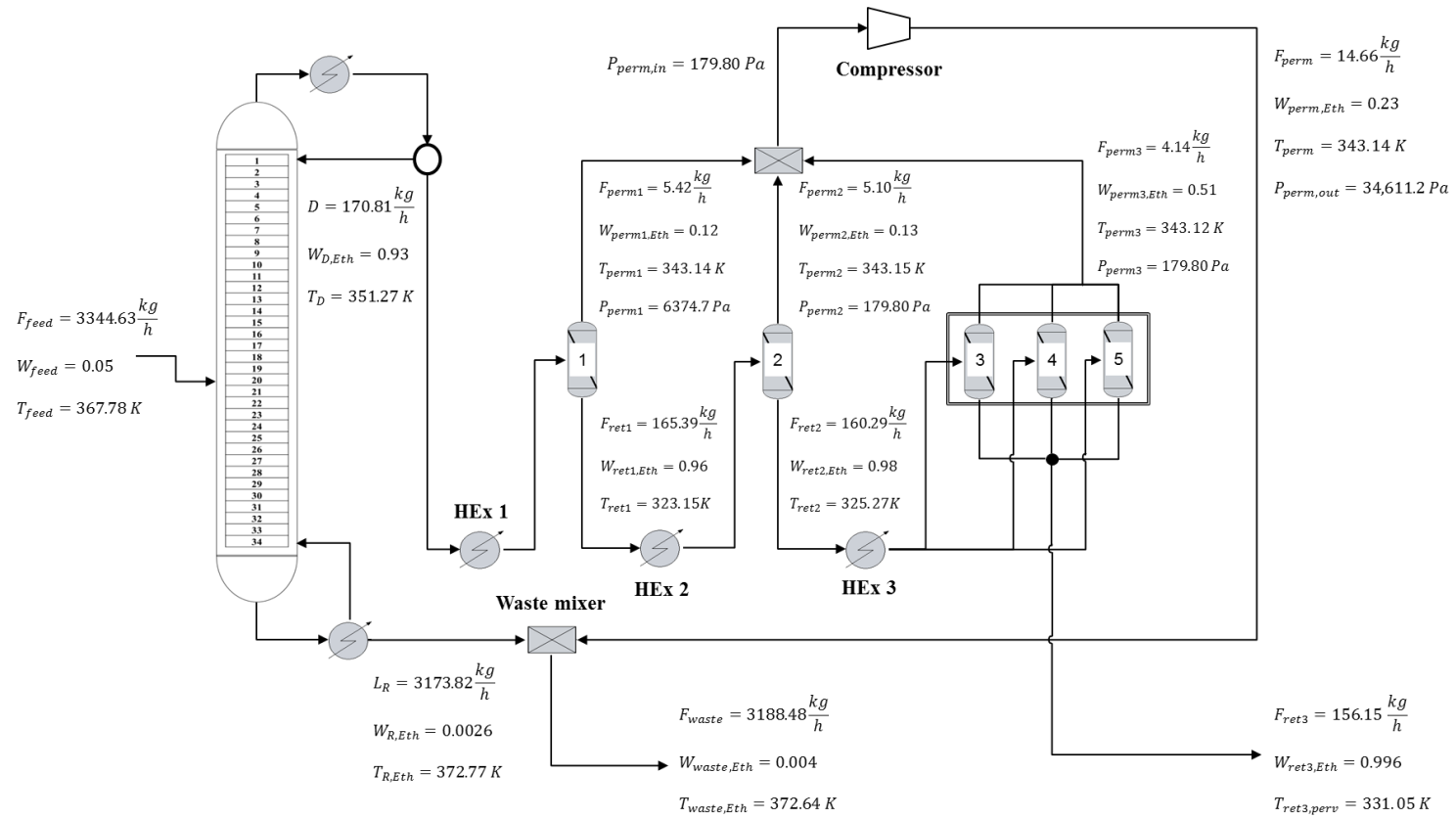


Figure 5.17: Results of the optimisation of the separation section with a PAN-B5 hydrophilic membrane area of 250 m²

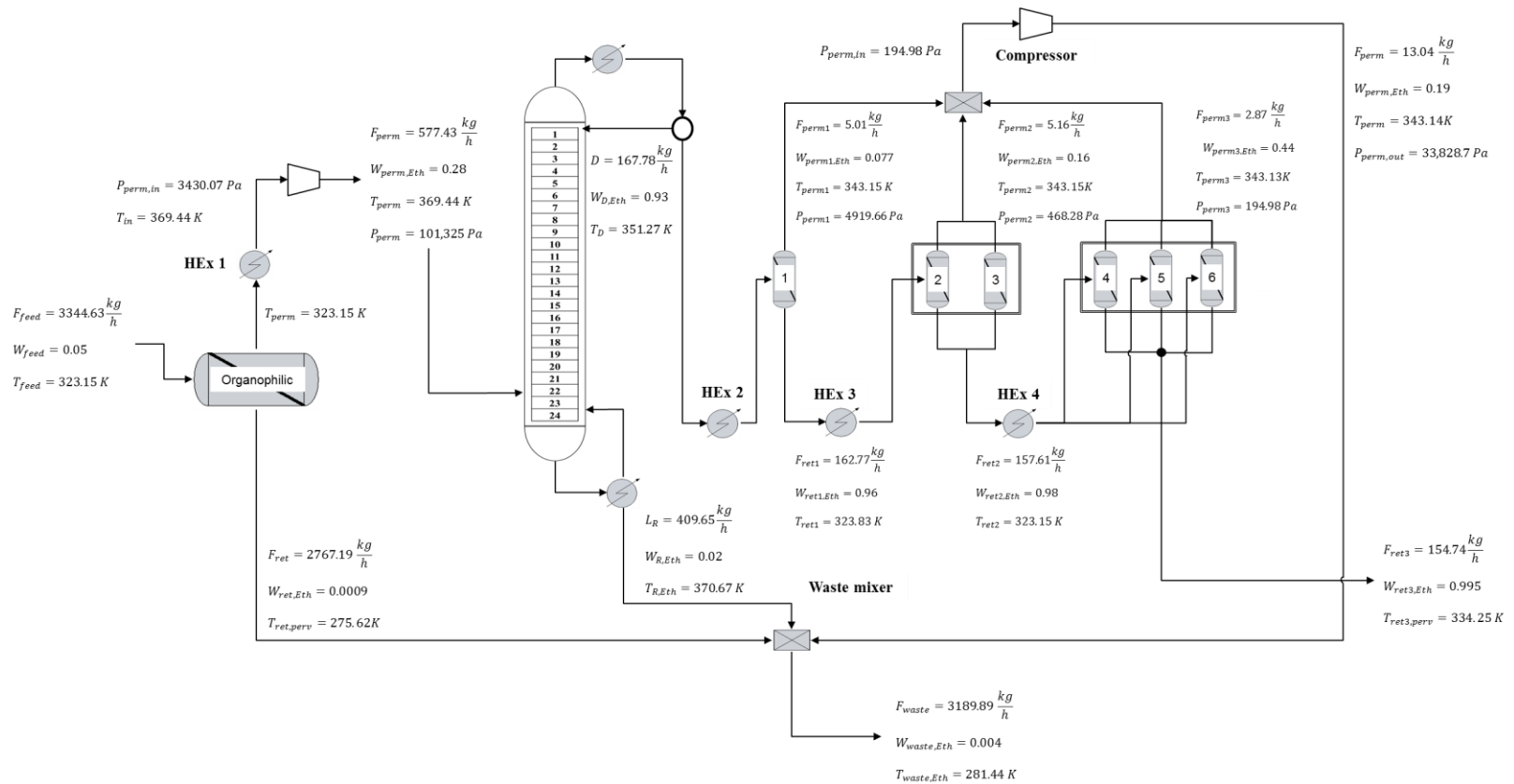


Figure 5.18: Results of the optimisation of the separation section including a PERVAP™ 4060 organophilic membrane with 19 in-parallel membrane modules with an area of 20 m² and a PAN-B membrane with a membrane area of 150 m²

Table 5.16: Results of the optimisation of the superstructures of the separation stages of the ethanol production process

Parameters	Superstructure 1	Superstructure 2
Number of trays	34	24
Feed tray	20	22
Reflux ratio	3.80	2.08
Organophilic membrane area (m²)	N/A	20
Hydrophilic membrane area (m²)	250	150
Electricity (kW)	3.23	87.9
Heat duty reboiler (kW)	224.1	144.3
Total energy consumption (kW)	233.5	271.2
Ethanol losses in waste (%)	7.06	9.06
CPU time (sec)	54,720	106,672
TAC (US\$/yr. 10⁵)	2.56	3.68

Table 5.16 presents the results of the optimisation of both superstructures, providing an evaluation of the overall energy consumption within the process as well as the minimum TAC. For instance, the distillation column in Superstructure 2 presents fewer trays and lower reflux ratio. The optimal design of this column shows that the feed stream should be fed in stages close to the reboiler to guarantee higher mass and heat transfer between phases in upper trays in order to increase the separation ethanol with lower energy demands.

The number of in-parallel modules in Superstructure 2 increases as the result of a lower flow rate from the distillate stream which directly translates into smaller total membrane areas (900 m² in Superstructure 2 against 1250 m² in Superstructure 1) and high separation rates.

Superstructure 2 also reports a reduction in the heat duty at the reboiler of the distillation column. In the case of the energy demand, the reboiler in Superstructure 2 shows a reduction of 36 % in comparison to the results obtained in Superstructure 1. This reduction can be attributed to the thermodynamic state, the feed flow rate and

the concentration of ethanol in the feed as well as the feed location in the distillation column.

However the overall energy consumption of Superstructure 2 is 16 % higher than Superstructure 1, which is mainly caused by the implementation of additional units such as heat exchangers to heat the permeate stream until saturation conditions and compressors to increase the pressure of the permeate stream from 3430 *Pa* to atmospheric conditions (i.e. 101,325 *Pa*). These results have also influenced the TAC, making Superstructure 2 more expensive than Superstructure 1 (an increment of 44 %). Although several aspects like the lower energy consumption in the reboiler and the smaller membrane areas in the dehydration section are appealing for some units of the separation section with the organophilic membrane, the overall results suggest that this membrane is not suitable for the separation of ethanol from the fermentation broth.

5.7 Sensitivity analysis

The results presented in Figures 5.17 and 5.18 are obtained for a case study where the concentration of ethanol in the feed stream is fixed at 5 % (w/w) and a distillate concentration close to 93 % (w/w). However, the concentration of ethanol in the feed is subject to variations due to changes in the chemical composition of the raw material, the conversion of hemicellulose and cellulose during the pretreatment stages, the operating conditions and performance of the fermenting strain during the fermentation, among other aspects.

Therefore, this section will focus on the variations of the concentration of ethanol in the feed and the distillate stream and their effect on the design of the overall separation section with and without the organophilic membrane. Table 5.17 presents the different case studies considered in the sensitivity analysis.

Table 5.17: Case studies considered in the optimisation of the separation section

	Characteristics
Base case	5 % (w/w) feed and 93 % (w/w) distillate
Case 1	4 % (w/w) feed and 93 % (w/w) distillate
Case 2	6 % (w/w) feed and 93 % (w/w) distillate
Case 3	5 % (w/w) feed and 90 % (w/w) distillate

Table 5.18 presents the results of the optimisation problem for three different cases in which both the concentration of the feed stream and distillate are modified in order to evaluate the optimal design of Superstructures 1 and 2. In Superstructure 1, the number of distillation columns is one and the number of in-series pervaporation stages is fixed at three with a membrane area of 250 m². On the other hand, Superstructure 2 presents a single pervaporation module for the organophilic membrane with an area of 20 m², a single distillation column and three in-series pervaporation stages with an area of 150 m². These specifications are taken from the results presented in the previous sections.

The results in Table 5.18 suggest that a decrease in the concentration of ethanol in the feed stream reduces the amount of ethanol in the distillate and therefore the energy required to recover it at the top of the column. Conversely, the number of trays in the distillation column increases alongside the reflux ratio in order to obtain the concentration of ethanol specified in Table 5.17. The economic evaluation shows a reduction in the TAC of 6 % and 7 % for Superstructure 1 and Superstructure 2, respectively. These savings are the result of a reduction in the utilisation of steam and electricity in the process as well as the cost of the membrane modules.

Case 2 presents an increment of the concentration of ethanol in the feed (from 5 % to 6 %). Unlike the results presented for Case 1, in Case 2 the TAC and the total energy consumption are higher than in the base case, which is mainly due to the cost of membranes, steam and electricity. The number of in-parallel membrane modules in both superstructures increase since the flow rate of the distillate stream increase with the feed concentration, which can also be observed in Figures 5.19 to 5.21.

When the concentration of ethanol in the distillate stream changes from 93 % to 90 % (Case 3 in Table 5.17), the energy consumption increases 3% and 5% in Superstructures 1 and 2, respectively. However, the most noticeable change in this case is the size of distillation column and the pervaporation network. Since the concentration of distillate is lower than in the base case, the number of trays is expected to be lower. This results in lower costs for the distillation column, especially in Superstructure 2 where savings of up to 28 % are reported. In the pervaporation section, the number of in-parallel modules is higher than in Cases 1 and 2.

The partial flux of water through the membrane increases when the distillate concentration of ethanol in the distillate decreases, causing a sharp decline in the temperature of the retentate stream. Since the constraints used in the solution of the optimisation problem allow a maximum temperature drop of 20 K, the first two stages of pervaporation will attempt to increase the concentration in the retentate side without letting the temperature drop below the maximum bound. This behaviour has a clear effect on the last stage where basically more in-parallel modules and lower permeate pressures are required in order to reach the desired concentration. In Superstructure 1, there are 8 in-parallel membrane modules whereas Superstructure 2 presents 12.

The minimum TAC for each case can also be observed in Figure 5.22. The results illustrated in Figure 5.22 showed that in all case studies, Superstructure 2 has the highest TAC which is likely to be caused by the compression done over the permeate stream before the distillation column and as seen in Table 5.18, the costs associated with compression go from 1000 to 38,000 US\$/yr.

Table 5.18: Sensitivity analysis of the separation section

Feature	Without the organophilic membrane				With the organophilic membrane			
	Base case	Case 1	Case 2	Case 3	Base case	Case 1	Case 2	Case 3
Number of trays	34	43	33	31	24	21	21	11
Feed location	20	30	27	22	22	17	18	6
Reflux ratio	3.80	4.71	3.51	3.55	2.08	2.20	1.95	2.08
Organophilic membrane								
Number of modules stage 1	N/A	N/A	N/A	N/A	19	19	19	19
Permeate pressure stage 1 (<i>Pa</i>)	N/A	N/A	N/A	N/A	3430.1	3375.7	3441.7	3430.1
Hydrophilic membrane								
Number of modules stage 1	1	1	1	1	1	1	1	1
Permeate pressure stage 1 (<i>Pa</i>)	6374.7	8194.1	8181.0	10,000	4919.7	6028.9	4984.9	9892.2
Number of modules stage 2	1	1	1	1	2	1	2	1
Permeate pressure stage 2 (<i>Pa</i>)	179.8	2849.0	521.2	7162.4	468.3	392.7	987.1	5789.1
Number of modules stage 3	3	3	4	8	3	4	5	12
Permeate pressure stage 3 (<i>Pa</i>)	179.8	393.2	521.2	198.6	194.9	392.7	194.6	107.8
Ethanol losses in waste (% w/w)	7.06	7.55	7.03	9.00	9.06	9.06	8.04	10.0
Total energy consumption (kW)	233.5	218.70	261.0	241.0	271.2	235.6	307.3	285.6

Table 5.18: Sensitivity analysis of the separation section (cont.)

Feature	Without the organophilic membrane				With the organophilic membrane			
	Base case	Case 1	Case 2	Case 3	Base case	Case 1	Case 2	Case 3
Total cost of the distillation system (US\$/yr. 10⁵)	0.62	0.69	0.66	0.59	0.40	0.34	0.42	0.29
Total cost of the organophilic membrane system (US\$/yr. 10⁵)	N/A	N/A	N/A	N/A	0.34	0.34	0.34	0.34
Total cost of the hydrophilic membrane system (US\$/yr. 10⁵)	1.28	1.12	1.34	2.23	0.81	0.80	1.07	1.84
Cost of heat exchanger 1 (US\$/yr. 10⁵)	0.002	0.002	0.002	0.002	0.02	0.02	0.02	0.02
Cost of heat exchanger 2 (US\$/yr. 10⁵)	0.002	0.001	0.001	0.001	0.002	0.002	0.002	0.002
Cost of heat exchanger 3 (US\$/yr. 10⁵)	0.001	0.001	0.002	0.001	0.002	0.001	0.002	0.002
Cost of heat exchanger 4 (US\$/yr. 10⁵)	N/A	N/A	N/A	N/A	0.001	0.001	0.002	0.001
Total cost of compressors (US\$/yr. 10⁵)	0.08	0.06	0.08	0.12	1.32	1.23	1.41	1.37
Cost of cooling water (US\$/yr. 10⁵)	0.01	0.01	0.01	0.01	0.01	0.006	0.008	0.007
Cost of steam (US\$/yr. 10⁵)	0.56	0.52	0.63	0.57	0.43	0.36	0.50	0.45
Cost of electricity (US\$/yr. 10⁵)	0.01	0.01	0.01	0.02	0.35	0.33	0.38	0.36
TAC (US\$/yr. 10⁵)	2.56	2.41	2.73	3.54	3.68	3.43	4.15	4.68

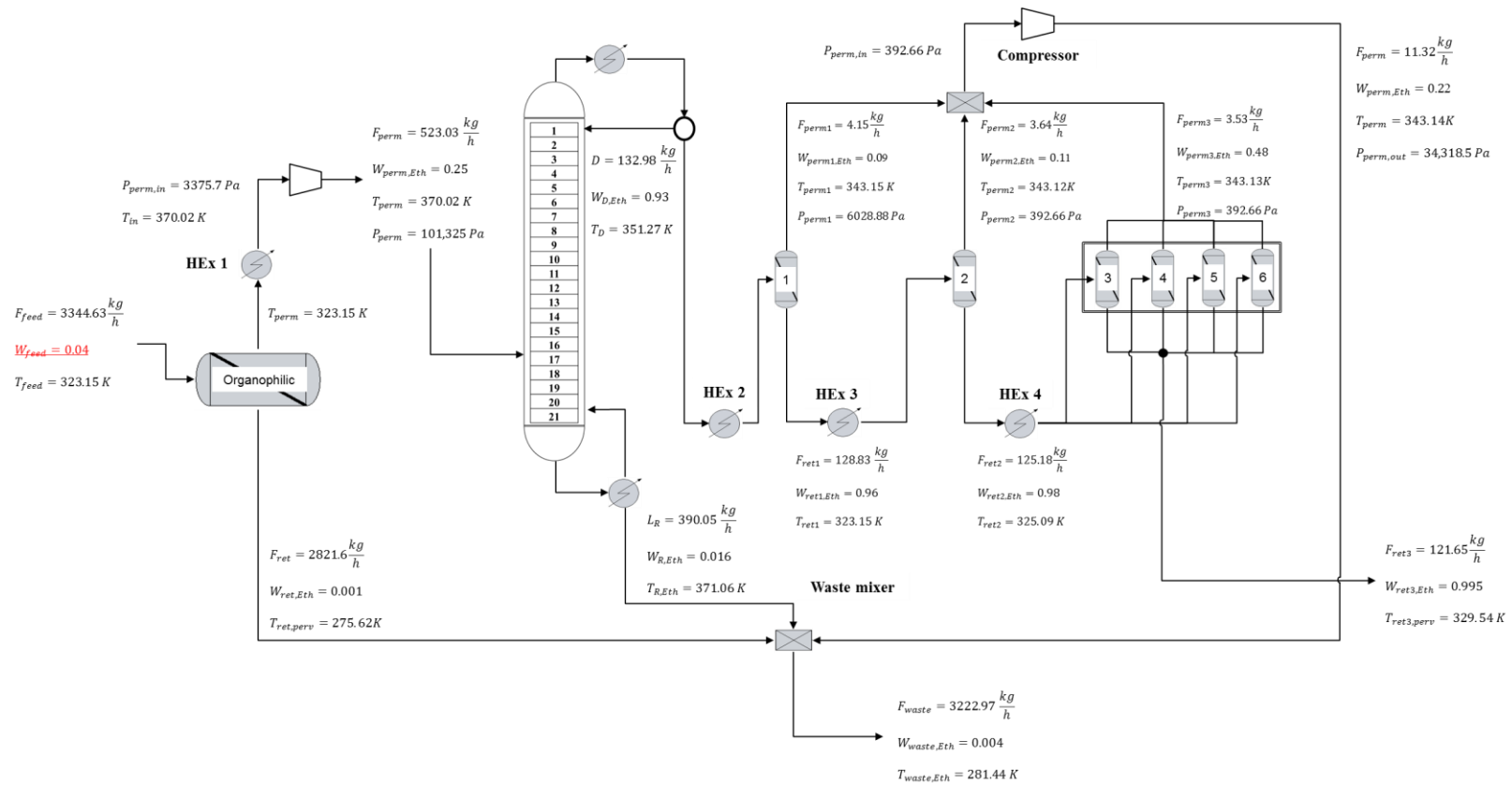


Figure 5.19: Case 1 - Results of the optimisation of the separation section of the ethanol production process with the PERVAP™ 4060 organophilic membrane considering a feed concentration of ethanol of 4 % (w/w)

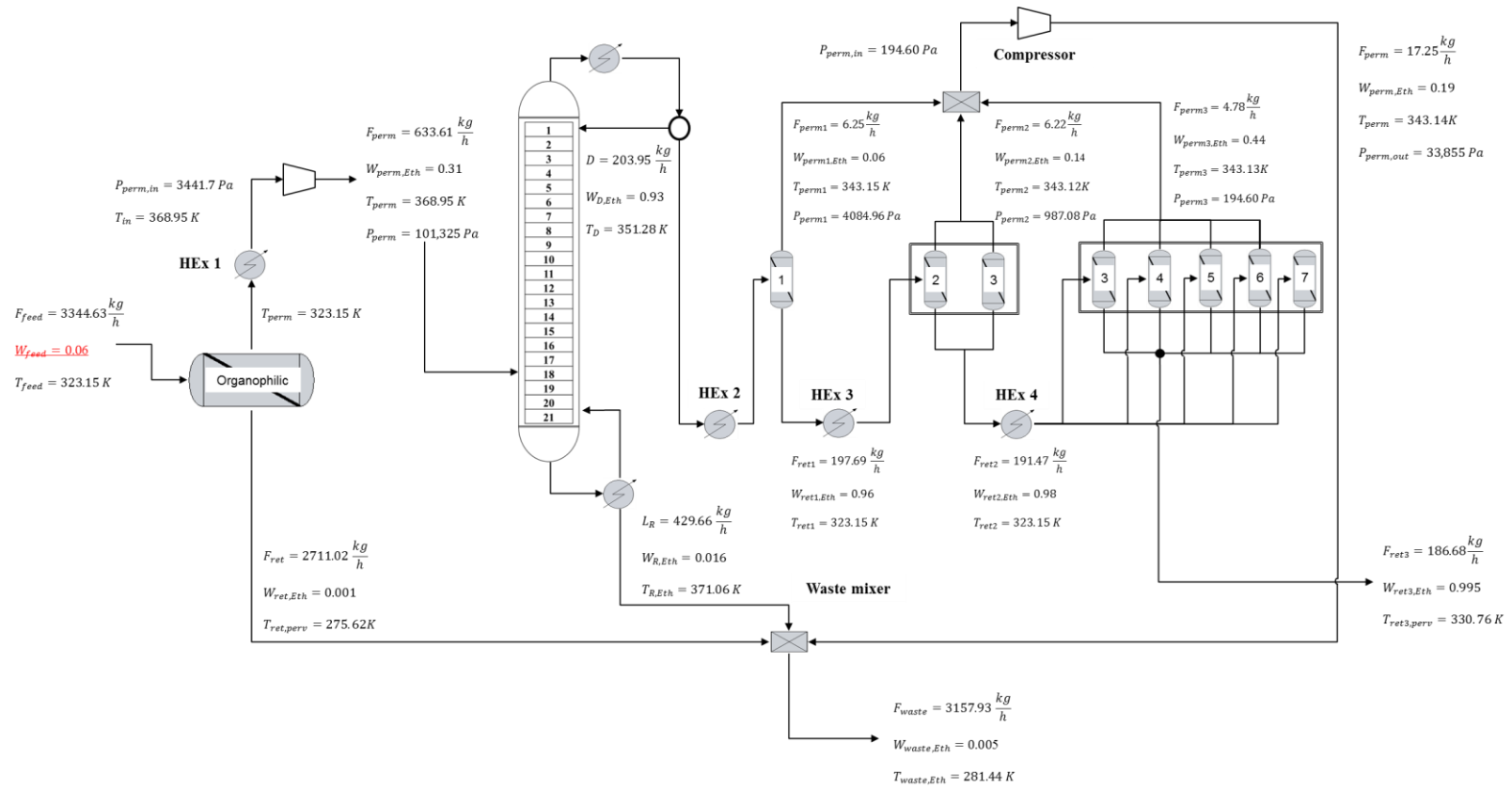


Figure 5.20: Case 2 - Results of the optimisation of the separation section of the ethanol production process with the PERVAP™ 4060 organophilic membrane considering a feed concentration of ethanol of 6 % (w/w)

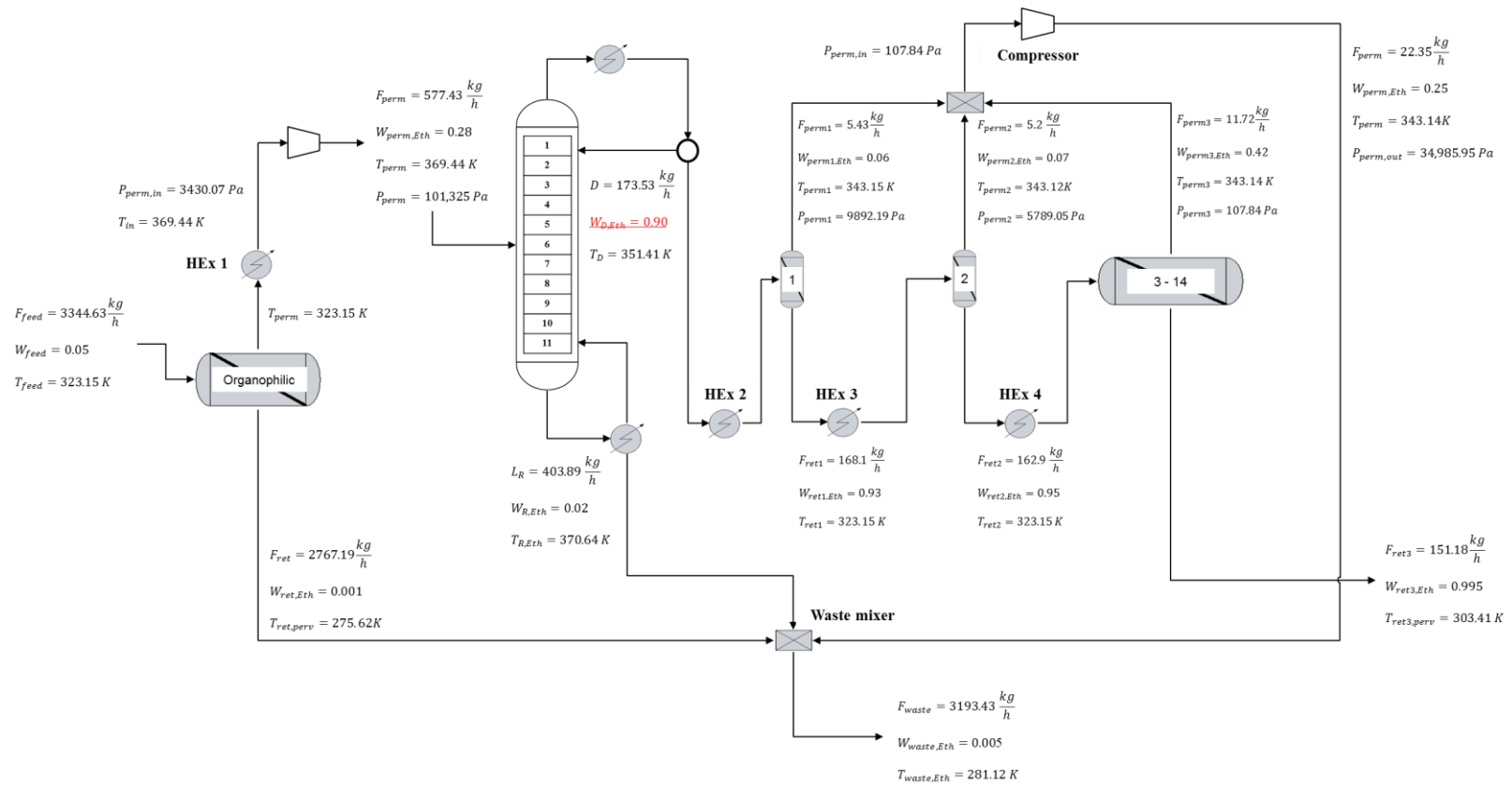


Figure 5.21: Case 3 - Results of the optimisation of the separation section of the ethanol production process with the PERVAP™ 4060 organophilic membrane considering a concentration of ethanol in the distillate stream of 90 % (w/w)

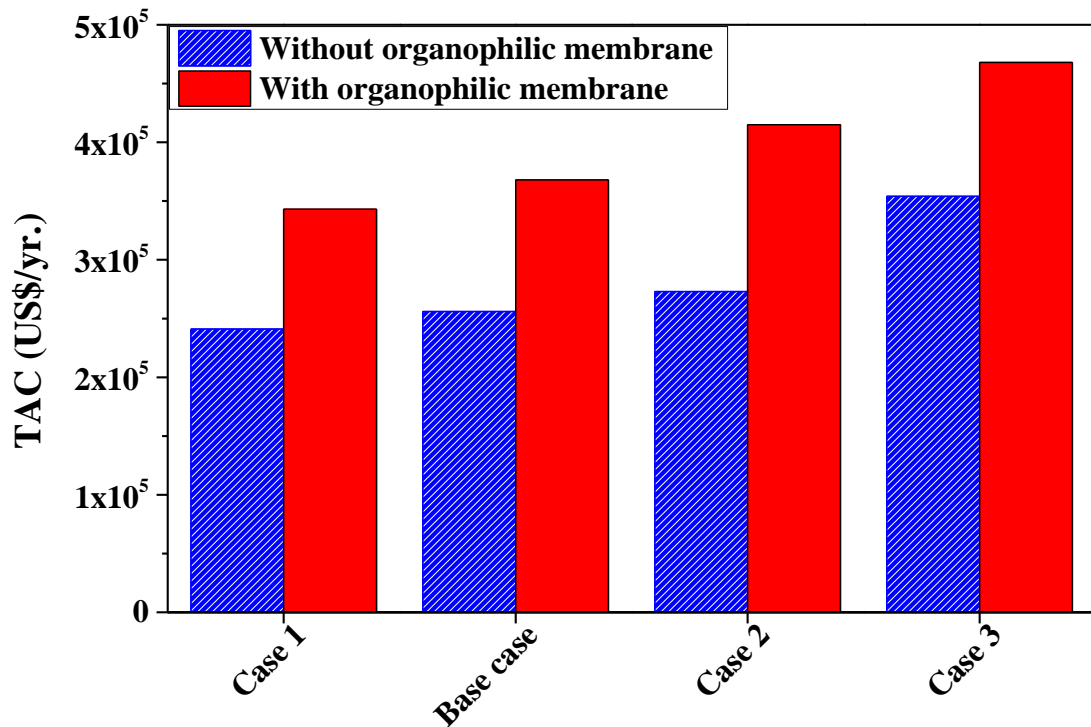


Figure 5.22: Evaluation of the minimum TAC of the separation section with and without the organophilic membrane considering different cases studies

5.8 Conclusions

This chapter presented the optimisation of two different configurations of the separation section of the ethanol production process from lignocellulosic biomass using a deterministic approach. The first configuration comprised a distillation system linked to a pervaporation network with a hydrophilic membrane (PAN-B5). The second configuration included the organophilic membrane (PERVAP™ 4060) introduced in Chapter 4 in the overall process, located before the distillation column. This pervaporation network is linked to a distillation column and a hydrophilic membrane system.

The optimisation of both superstructures consisted in first optimising each unit individually. Using specific feed conditions, the optimal design with the minimum total annualised cost was determined. The first unit to be analysed was the distillation column using a tray-by-tray approach presented by Caballero and Grossmann, (2014a). With this approach, the total number of trays and the optimal feed location that minimised the TAC could be determined. In fact, two arrangements for the

distillation section were optimised: a single distillation column and double-distillation system. The results of this optimisation showed that a single distillation column was more economically viable for the separation of a solution 5% (w/w) of ethanol and a distillate concentration of 93 % (w/w). The single column was 42 % cheaper than the double-column arrangement and reported energy savings of 41%.

The following step was to determine the design of the pervaporation network for both membranes. The optimisation showed that for the PAN-B5 hydrophilic membrane system, for both superstructures, a configuration of three in-series stages was required. In the case of the PERVAPTM 4060 membrane, only one stage was required in order to remove most of the ethanol from the feed. Once all the units involved in the separation of ethanol from the fermentation broth were optimised, the result were used in the solution of the superstructure as initial estimates as a way to narrow down the feasibility region in which the solution might be found.

The results of these calculations showed that the implementation of the organophilic membrane reduced the energy required in the reboiler of the distillation column in Superstructure 2 by 36 % in comparison with distillation column in Superstructure 1. However, the overall energy consumption in Superstructure 2 was 16 % higher than in Superstructure 1. These results could be attributed to the use of a compressor unit for the permeate stream leaving the organophilic membrane which directly influenced the TAC in Superstructure 2. Table 5.16 showed that not only Superstructure 2 had higher energy consumption than Superstructure 1, this configuration was also more expensive and the implementation of additional units to provide the necessary operating conditions only increased the investment costs.

A sensitivity analysis was also carried out in this chapter. The purpose of this analysis was to determine the variations in the optimal design of both superstructures, focusing mainly on the structure with the organophilic membrane since this is the novelty of this work. The results showed that in all case studies, the implementation of the organophilic membrane is more expensive and more energy intensive than the configuration without said membrane. Chapter 6 will focus on the

heat integration of the entire plant as an additional step to reduce the usage of utilities and distribute all the sources of energy within the plant in a more efficient fashion.

Chapter 6 – Heat integration across an ethanol production process

Abstract

This chapter introduces a methodology for the implementation of heat storage systems for the ethanol production process from lignocellulosic biomass. Initially, this chapter presents the optimisation of the complete process without heat storage so it can be taken as a reference case for other arrangements with heat storage. Two arrangements with heat storage are considered in this work in which two tanks of equal size are used to store the heat transfer fluid. The first tank will initially contain the heat transfer fluid used to provide heat to the reactors and other units, and the second tank will receive the outlet streams coming out of the jackets of the units. The results of the optimisation of the process with heat storage show a decrease in the Total Annualised Cost as well as the energy consumption throughout the plant.

6.1 Introduction

In the design of a chemical process, there are several design variables that need to be considered such as size of the equipment, fouling, operating time, capital investment, etc., and operating variables such as purity of the product, waste, temperature, pressure, among others. One variable, of particular interest is energy consumption. Energy consumption makes reference to the heat provided from external sources to units in the process in order to function at the desired operating conditions. This heat can be transferred from sources such as steam or electricity (Yee et al., 1990a, 1990b; Yee and Grossmann, 1990). On the other hand, chemical processes may also require external cooling (e.g. cooling towers in power and nuclear plants) (Kiss and Olujic, 2014; Wang et al., 2015). The costs related to the usage of these external sources can have a significant impact on the profitability of a process. (Čuček et al., 2011; Grisales et al., 2008; Kiran and Jana, 2015; Kravanja et al., 2013). Hence, heat integration has emerged as a sophisticated way of reducing the energy demands by

distributing the different forms of heat (either supplied or released) that can be found in the process in order to make the entire plant more energy efficient (Modarresi et al., 2012; Rašković et al., 2010).

Batch operations are generally run on a smaller scale compared to continuous operations and utility requirements are therefore considered lower than their counterparts. Energy consumption in general is commonly estimated to be about 5% - 10% of total costs (Vaklieva-Bancheva et al., 1996). However, some batch industries have a much higher utility demands than others. For example, utility requirements in the food industry, breweries, dairies, meat processing facilities, biochemical plants and agrochemical facilities contribute largely to the total cost and heat integration has proved successful in improving energy efficiency in these sectors (Knopf et al., 1982; Rašković et al., 2010). In several chemical processes, for instance pharmaceuticals and pigments, due to the existence of large amounts of used solvents and volatile organic compounds to incinerate, there is an excess of available heat which can be utilised for heat integration.

Heat integration for improvement and reduction in energy consumption in a plant, may be achieved by one of the following paths: Direct Heat Integration (DHI) and Indirect Heat Integration (IHI). These methods for heat integration and their implementation depend on the type of production (e.g. continuous or batch) and the different components involved in the process (Krummenacher, 2002). These methods are discussed in more detail in the following section.

6.1.1 Direct heat integration (DHI)

In DIH, process streams can exchange heat with one another directly so the process can only experience heat transfer once. This aspect suggests that the amount of heat recovered in the process can be high due to a smaller temperature difference during heat integration. However, because process streams cannot be mixed, when the number of process streams involved in heat integration is large, a number of heat transfer loops are required (Kiran and Jana, 2015; Kravanja et al., 2013). DHI normally requires more heat exchange loops than in the indirect heat integration approach which may result higher capital costs, although this is also dependent on

the area of the heat exchangers and the amount of heat that can be recovered (Wang et al., 2015).

6.1.2 Indirect heat integration (IHI)

A second form of heat integration is Indirect Heat Integration (IHI). Energy may be stored in several forms, including chemical energy (e.g. in biomass and electrochemical batteries), mechanical energy (e.g. in pumped hydro, compressed air and flywheels) and as heat (Dinçer and Rosen, 2010). For the IHI method, the heat exchange between non-coexistent process streams becomes less limited so it is less schedule-sensitive and it could provide a great deal of operating flexibility (Krummenacher, 2002). IHI may sometimes be considered as an expensive form of heat integration. Heat storage has only been considered as an alternative mode for heat integration when opportunities of using DHI have been exhausted (Rodera and Bagajewicz, 2001). When energy is stored in the form of heat, this is known as thermal energy storage (TES) and such storage may further be in the form of either Sensible TES or Latent TES as shown next:

Latent energy storage: It uses phase change materials (e.g. hydrated salts) to store heat (generally by crystallization /melting). The temperature at which the phase change occurs depends on the selected material; therefore, unlike sensible heat storage, the operating temperature of Latent Heat Storage Units (*HSU*) has to be selected among a discrete set of values (Schröder and Gawron, 1981). Latent heat storage generally results in a significantly smaller volume when compared to sensible heat storage, and is particularly recommended when large amounts of heat must be stored with small temperature differences (Feczko et al., 2016; Schröder and Gawron, 1981; Sciacovelli et al., 2015; Zhang et al., 2016).

Sensible energy storage: Three main types of sensible heat storage systems may be distinguished:

- **Mixing heat storage:** the storage of heat is achieved by an increase of the overall mean temperature of the storage fluid in the tank. By construction, or by operation, the heat storage fluid features an almost homogenous temperature in the HSU (Krummenacher, 2002).

- Stratified heat storage: stratification results in a hot (or cold) fluid storage tank when different regions in the tank are at different temperatures. The density variations which result from those temperature differences will cause the hotter fluid masses to rise to the top and the cooler fluid masses to fall to the bottom of the storage tank, with a middle layer transition zone (the thermocline), separating the hot upper zone from the cold lower zone (Altuntop et al., 2005; Han et al., 2009).
- Fixed temperature / variable mass (FTVM) heat storage: FTVM heat storage operates in the same way as stratified heat storage, but prevents the temperature degradation problem by keeping the volumes presenting different temperatures in separate tanks (*HSU's*) (Sciacovelli et al., 2015; Zalba, 2003; Zhang et al., 2016).

For any of these three types, given a heat storage capacity, the required volume is inversely proportional to the temperature difference between the "charged state" and "empty state".

6.1.3 Mixed direct-indirect heat integration (MDIHI)

This mode of heat integration combines the approaches of both direct and indirect heat integration where process streams are initially stored in order to provide heat to other streams at different times. The indirect mode often implies higher capital costs, so in order to avoid these costs, process rescheduling is considered, which increases the potential of direct heat exchanges between process streams. Similarly, heat integration of multi-product and multi-purpose plants is often focused on the scheduling of batch operations accounting for direct heat exchanges opportunities.

6.2 Heat transfer fluids

Heat integration using heat storage often requires a fluid which must be carefully selected for a specific purpose. Table 6.1 presents a list of heat transfer fluids often used in industry for heat storage. Air and water in the form of steam are the cheapest and most accessible transfer fluids available. Their implementation usually requires larger volumes of *HSU's* which is very impractical from the point of view of costs and also the use of additional equipment such as compressors and more heat exchangers (Krummenacher, 2002; Zalba, 2003).

Table 6.1: List of heat transfer fluids (Vignarooban et al., 2015)

Name	Melting point (°C)	Stability limit (°C)	Heat capacity (kJ kg ⁻¹ K ⁻¹)	Average cost (\$/kg)
Air	-	-	1.03 (127 °C)	0
Water	0	-	1.90 (127 °C)	~0
Thermal oils				
Mineral oil	-20	300	1.67	0.3
Synthetic oil	-20	350	1.94	3.0
Silicone oil	-20	400	1.09	5.0
Organic				
Biphenyl/Diphenyl Oxide (Therminol VP-1)	12	393	1.93	100
Molten-salts				
Solar salt	220	650	1.60	0.50
Hitec	142	535	1.56	0.93
Na-K-Li nitrates	130	600	1.10	1.10
Liquid metals				
Na-K	-12	785	0.87 (600 °C)	2.00
Na	98	883	1.25 (600 °C)	2.00
Pb-Bi	125	1533	0.15 (600 °C)	13.0

Heat storage using water is limited by the operating conditions of the rest of the units of the process. For instance, units with high operating temperatures would require a transfer fluid with high heat capacities and, in the case of steam, pressurised tanks would be required which reflects negatively on the costs of the process and the controllability of the operating conditions. Furthermore, steam systems experience large heat losses due to condensation (Lienhard, 2010; Zalba, 2003).

Thermal oils are widely used to carry thermal energy in process heating, metal working and machine cooling applications. They are mainly used in high temperature process applications where the optimum bulk fluid operating temperatures (between 150°C and 400°C) are safer and more efficient than steam, electrical, or direct fire heating methods (Vignarooban et al., 2015; Zhang et al., 2016). Thermal oils allow the use of low pressure heat transfer systems to achieve high temperatures which would otherwise have necessitated high pressure steam systems (Mawire et al., 2014; Veses et al., 2016). Steam systems are subject to statutory and regulatory

requirements due to the inherent risk from pressure and the increased cost of installation and routine insurance inspection requirements (Mawire et al., 2014; Zhang et al., 2016).

Molten salts refer to the type of ionic liquids that are currently used for heat transfer and heat storage due to the elevated temperatures at which they can be operated. The growing interest in energy applications of molten salts is justified by several of their properties (Amusat et al., 2015; Serrano-López et al., 2013a). The advantages of molten salts as heat transfer fluid and thermal storage systems promise a great development during next decades. The cost for the required volume of heat exchangers and pumps are highly reduced by the use of liquid salts instead of other coolants due to their higher volumetric heat capacity without the need of pressurising (Vignarooban et al., 2015; Zhang et al., 2016). One of the most prominent applications for molten salts is solar thermal power which is a promising way of providing renewable electricity (Feczko et al., 2016; Serrano-López et al., 2013b). Unlike other renewable energy technologies, solar thermal power plants have the ability to store thermal energy (Zaversky et al., 2013).

Liquid Metals are a specific class of heat transfer fluid. Their basic advantage is a high molecular thermal conductivity which, for identical flow parameters, enhances heat transfer coefficients. Another characteristic of liquid metals is the low pressure of their vapours, which allows their use in power engineering equipment at high temperatures and low pressure, thus improving solution of mechanical strength problems (Zeigarnik, 2011). One of the major applications for liquid metals has been in nuclear industries which have been in development since the 1940's. Nowadays, liquid metals are currently being studied for use in solar thermal systems as energy storage media with purposes of green technologies and sustainability (Vignarooban et al., 2015).

Organic fluids are also used in the chemical industry for heat transfer and heat storage applications in processes within oil and gas, plastic processing, pharmaceuticals, solar energy, etc. (Eastman, 2016; Krummenacher, 2002; Schröder and Gawron, 1981; Zalba, 2003). The most known material is Therminol which is a mix of several organic compounds with high stability and relatively low prices

(Weiguo et al., 2016; Xu et al., 2016). Its implementation in the chemical industry has been reported by several authors showing promising results in terms of lower energy losses, lower fire risks and easier acquisition. Therefore, organic fluids will be considered in the development of a heat transfer configuration for the ethanol production process from corn stover.

Eastman Ltd has a variety of Therminol fluids for heat transfer purposes but has reported that the most successful in sales is Therminol 66 (Eastman, 2016; Weiguo et al., 2016). Table 6.2 presents the properties of Therminol 66 used in the calculations carried out in this chapter.

6.3 Simulation procedure

Heat integration can be used to reduce the consumption of utilities in processes such as ethanol production from lignocellulosic biomass considered in this work. The process has high heat demands in units such as the pretreatment reactor, the evaporator and the distillation system. For this work, heat integration will consider the implementation of heat storage units in which a heat transfer fluid will be used to substitute steam in order to reduce operating costs.

Chapter 5 presented the optimisation of the separation section of the ethanol production process based on a total annual cost function (TAC). Chapter 6 will follow a similar approach for the optimisation of the separation section, except that in this part of the work, the entire process considering heat storage will be optimised.

6.3.1 Configuration of the ethanol process without heat storage

The optimisation problem presented in Figure 6.1 is the production of ethanol from corn stover, and is based on the configuration illustrated in Figure 2.1. The steps of the production of ethanol from corn stover are the following:

Table 6.2: List properties of Therminol 66 (Eastman, 2016)

Item	Characteristics
Appearance	Clear, pale yellow liquid
Composition	Modified terphenyl
Boiling point	359°C (678°F)
Molecular weight	252
Autoignition temperature	374°C (705°F)
Cost (US\$/kg)	6.5*

*Taken from Rajkumar et al., 2015

1. The initial load of raw material is processed in the pretreatment reactor
2. The outlet stream is filtered and the liquid fraction is concentrated in an evaporator and detoxified with Calcium Hydroxide Ca(OH)_2 in the detoxification reactor
3. The solid fraction of the pretreatment and the detoxified stream are mixed and sent to the *Simultaneous Saccharification and Co-Fermentation* (SSCF) reactor where ethanol is produced using the cocktail of enzymes cellulase/ β -glucosidases and fermenting bacteria *Zymomonas mobilis* ZM4 (pZB5)
4. The solids of the SSCF process (i.e. unreacted cellulose and hemicellulose, cells, insoluble solids, etc.) are filtered and the liquid is pumped into the distillation column
5. The distillate stream from the distillation column is cooled down to 70 °C (maximum operating temperature at which the partial flux of water is the highest) before the hydrophilic membrane network
6. Ethanol is dehydrated to concentrations higher than 99 % (w/w) in the pervaporation network

This chapter introduces the implementation of heat integration into the ethanol process and the optimisation of the design and operation of the plant by minimising costs. In other words, the solution of the optimisation problem needs to show the optimal number of trays in the distillation column, the optimal number of in-parallel pervaporation modules, the optimal size of each reactor, the operating conditions of each unit, etc. The configuration shown in Figure 6.1 will be used as reference for the comparative analysis against the configurations featuring heat integration. The

optimisation variables for the process without heat integration (see Figure 6.1) are the following:

1. Pretreatment reactor volume (m^3)
2. Detoxification reactor volume (m^3)
3. SSCF reactor volume (m^3)
4. Inlet stream of inoculum of cells (kg/s)
5. Concentration of cells in inoculum (% (w/w))
6. Reflux ratio
7. Number of trays in the stripping and rectification sections of the distillation column
8. Number of in-parallel modules in each pervaporation stage
9. Permeate pressure (Pa)

This optimisation methodology assumes that the number of in-series pervaporation stages is fixed as well as the number of distillation columns. These assumptions come from the evaluation of the separation section presented in Chapter 5, which showed that two distillation columns are more energy intensive and more expensive than just one column for the same distillate mole fraction.

The optimisation of the entire process considers steady-state conditions in the operation of the pretreatment stages, assuming that all flow rates have average values. This facilitates the calculations of the optimal design variables and operating conditions which is the main scope of this work. This methodology is also implemented in the optimisation of the configurations with heat storage tanks.

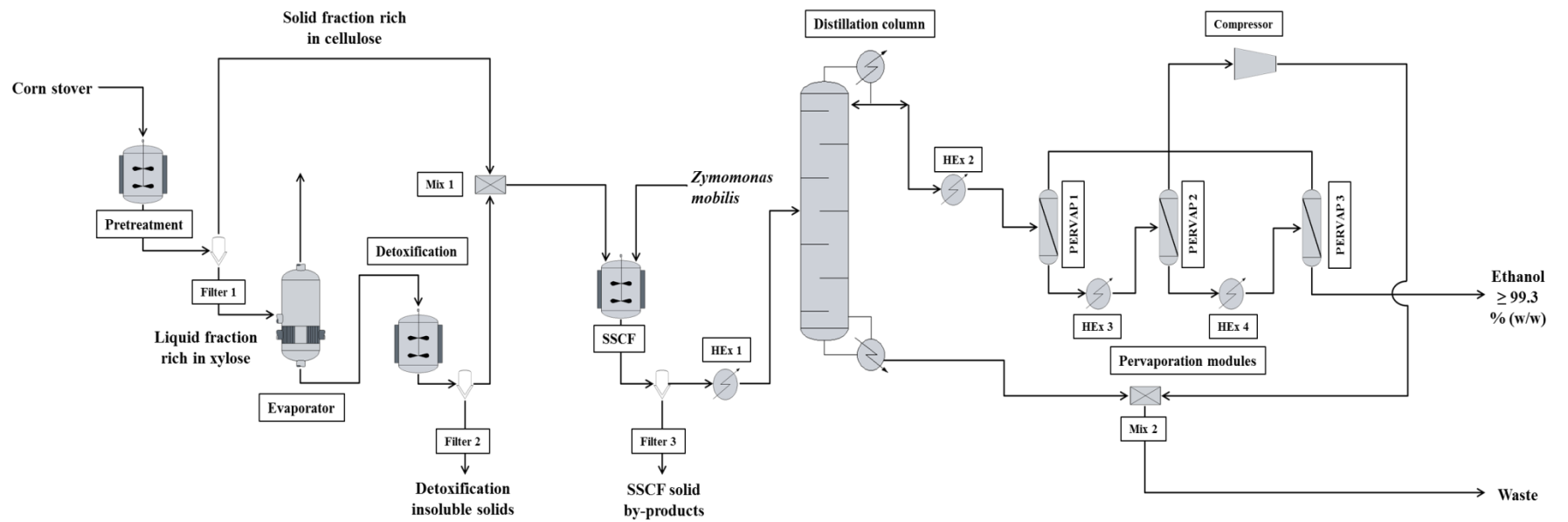


Figure 6.1: Flowsheet of the ethanol production process from corn stover without heat integration

The number of in-series pervaporation modules is assumed to be three since the results presented in Chapter 5 suggested that this arrangement presents the lowest total annual cost with a low energy consumption in the intermediate heaters as well as the low required area of each membrane module. The solution of an optimisation problem requires a set of constraints that will narrow down the convergence region to find an optimum under specifications of production rate and/or purity of ethanol. Equations 6.1 to 6.10 show the constraints used in the optimisation of the ethanol process without heat storage.

The range of conversion of hemicellulose during pretreatment is set as shown in Eq. 6.1. The reason for this choice is explained in the work of Esteghlalian et al., (1997) which states that higher conversions of hemicellulose could not only produce higher concentrations of xylose, but also higher concentrations of by-products which influence the performance of the detoxification stage. Therefore, the minimum conversion in the system should be 75 % (see Table 6.3):

$$X_{hemicellulose} \geq X_{hemicellulose}^{spec} \quad \text{Eq. 6.1}$$

The constraint for conversion of furfural in the detoxification stage is shown in Eq. 6.2. With this constraint, a higher degradation of by-products in the acid hydrolysates is expected. Given the parameters and the operating conditions obtained by Purwadi et al., (2004) the minimum conversion of by-products is the following:

$$X_{by-products} \geq X_{by-products}^{spec} \quad \text{Eq. 6.2}$$

The constraint for the production of ethanol during SSCF is shown in Eq. 6.3. This constraint seeks to maintain the concentration of other by-products such as cellobiose, xylose and cells to the lowest possible (Morales-Rodriguez et al., 2012, 2011):

$$W_{ethanol}^{min} \leq W_{ethanol} \leq W_{ethanol}^{max} \quad \text{Eq. 6.3}$$

Eq. 6.4 presents the constraint related to the maximum concentration achievable during the distillation process. This constraint is chosen in order to secure a feed composition in the pervaporation network applicable for the selected membranes (Tsuyumoto et al., 1997).

$$W_{D,eth} \geq W_{D,eth}^{Spec} \quad \text{Eq. 6.4}$$

Due to the evaporation of the volatile components in the feed which diffuse through the membrane, temperature drops in the retentate side. Feed temperature needs to be kept constant in all stages of the pervaporation network in order to maintain high rates of flux through the membrane. As seen in Figure 6.1, there are intermediate heat exchangers to maintain feed temperature at 70 °C. Equations 6.5 and 6.6 present the range of temperature difference between feed and retentate for the optimisation of the process (Baker, 2012; Marriott and Sorensen, 2003; Sander and Janssen, 1991):

$$\Delta T_{pervap_1}^{min} \leq \Delta T_{pervap_1} \leq \Delta T_{pervap_1}^{max} \quad \text{Eq. 6.5}$$

$$\Delta T_{pervap_2}^{min} \leq \Delta T_{pervap_2} \leq \Delta T_{pervap_2}^{max} \quad \text{Eq. 6.6}$$

In order to meet the standards of purity required for ethanol for energy generation purposes (Binod et al., 2010; Cardona and Sánchez, 2007; Drapcho et al., 2008), the concentration obtained in the retentate side of the last pervaporation stage is set as shown in Eq. 6.7 (see Table 6.3):

$$W_{retent,eth}^{min} \leq W_{retent,eth} \leq W_{retent,eth}^{max} \quad \text{Eq. 6.7}$$

The streams leaving the distillation column and the retentate of the third pervaporation stage are mixed. The constraint presented in Eq. 6.8 seeks to keep minimum losses of ethanol in this stream.

$$W_{Loss.Eth}^{min} \leq W_{Loss.Eth} \leq W_{Loss.Eth}^{max} \quad \text{Eq. 6.8}$$

For the optimisation of the distillation column, additional constraints are required for the evaluation of the total number of trays and feed location (see Figure 5.1). These constraints were discussed in more detail in Chapter 5 and are based on the tray-by-tray approach proposed by Caballero and Grossmann, (2014).

$$\sum_{j=1}^{N_{tray_rc}} \alpha_j = 1 \quad j = 1, 2, \dots, \text{Number of trays in rectification} \quad \text{Eq. 6.9}$$

$$\sum_{k=1}^{N_{trays_st}} \beta_k = 1 \quad k = 1, 2, \dots, \text{Number of trays in stripping} \quad \text{Eq. 6.10}$$

Equations 6.11 and 6.12 represent the number of active trays that can be counted in both sections of the column and are used in the calculation of its height, as shown in section 5.3.1.

$$N_{Rec}^{total} = \sum_j \alpha_j Rct_j \quad Rct_j = \{1, 2, 3 \dots N_{tray_rc}\} \quad \text{Eq. 6.11}$$

$$N_{Str}^{total} = \sum_k \beta_k Str_k \quad Str_j = \{N_{tray_st}, N_{tray_st-1}, \dots, 2, 1\} \quad \text{Eq. 6.12}$$

As presented in Section 5.3, the set of constraints that correlate the continuous variables of the system with the discrete variables used to identify the recycle of both distillate and steam into the column are defined as follows (Caballero and Grossmann, 2014a):

$$RF_T = \{j \mid \text{Candidate tray of reflux return}\} \quad \text{Eq. 6.13}$$

$$RB_T = \{k \mid \text{Candidate tray of reboil return}\} \quad \text{Eq. 6.14}$$

Let L_{Rx} , L_{Rb} be the reflux and reboil flow rate returned to the column, respectively. Let α_j $j \in RF_T$; β_k $k \in RB_T$ be binaries that take the value 1 if the reflux/reboil is returned to tray j and k , respectively. Equations

$$ref_{tr} \leq L_{Rx} \alpha_j \quad j \in RF_T \quad \text{Eq. 6.15}$$

$$reb_{tr} \leq L_{Rb} \beta_k \quad k \in RB_T \quad \text{Eq. 6.16}$$

$$ref_{tr} \geq 0, \quad \alpha_j \in \{0,1\} \quad \forall j \in RF_T \quad \text{Eq. 6.17}$$

$$reb_{tr} \geq 0, \quad \beta_k \in \{0,1\} \quad \forall k \in RB_T \quad \text{Eq. 6.18}$$

Equations 6.19 and 6.20 correlate the vectors of recycles with the actual flow rate to be fed into the column as previously presented in Chapter 5.

$$L_{Rx_in} = \sum_{j \in RF_T} ref_{tr} \quad \text{Eq. 6.19}$$

$$L_{Rb_in} = \sum_{k \in RB_T} reb_{tr} \quad \text{Eq. 6.20}$$

The objective function shown in Eq. 6.21 is the same used in Chapter 5. It presents the total annual cost or the total investment on the production of ethanol from lignocellulosic biomass and it covers the cost of all the equipment and the usage of utilities and services.

$$TAC = \sum \text{Annual operating cost} + \sum \frac{\text{Capital investment}}{\text{payback period}} \quad \text{Eq. 6.21}$$

6.3.2 First superstructure of the ethanol production process with heat storage

The heat integration of the ethanol process requires two heat storage tanks of equal size (HS1 and HS2). Heat storage tank 1 (HS1) initially contains the heat transfer fluid and distributes it to the reactors of the process. Heat storage tank 2 (HS2), collects the heat transfer fluid coming out of the jackets of the reactors and sends it to the separation section of the process. In Figure 6.2, the red lines denote the hot streams of Therminol 66 used in the transfer of heat to the units of the process. The

blue lines represent cooling water used in the detoxification reactor and the condenser of the distillation column.

Figure 6.2 presents the first configuration of the process using heat storage. This configuration is very similar to the one shown in Figure 6.1 but with a few differences. The first difference is the utilisation of a pump prior to the distillation system to increase the pressure inside the column. The second difference is the implementation of a heat exchanger (HEx 5) to use the heat from the stream leaving the reboiler to heat up the stream of Therminol 66 leaving HS2. The third difference is another heat exchanger (HEx 4) in which high-pressure steam is used to provide energy to the stream of Therminol 66 in order to increase its temperature to the same temperature as the outlet streams of HS1. The steps of the configuration shown in Figure 6.2 are summarised below:

1. The HS1 tank filled with Therminol 66 provides heat to the pretreatment, evaporation, SSCF stages through their jackets
2. The outlet of the jackets is collected in HS2 and sent to the other units in the process
3. The outlet of HS2 is passed through heat exchanger (HEx 5) where the bottom stream of the distillation column is used to heat the Therminol stream
4. The stream of Therminol heated in heat exchanger (HEx 5) is used in Heat Exchangers 2 and 3
5. The stream of Therminol is passed through Heat Exchanger 4 to increase the temperature of the heat transfer fluid before sending it back to HS1

The additional optimisation variables when considering heat storage are:

1. Distillation column pressure (Pa)
2. Outlet flowrates leaving HS1 and passed through the jackets of the different reactors (kg/s)
3. HS1 outlet temperature
4. Temperature difference between outlet streams in both shell and tube in Heat Exchanger 5 (Superstructure 1)

The assumptions for the simulation and optimisation of the ethanol production with and without heat storage process are the following:

1. Perfect mixing in all the reactors as well as in each tray of the distillation column and heat storage tanks (see Appendix A for mass and energy balances)
2. The HS tanks are adiabatic as in all the piping in the process. This assumption is supported by the reports presented by Zaversky et al., (2013) and Zhang et al., (2016), where insulation prevents heat losses higher than 0.5 %
3. There is no mixing between process streams and the transfer fluid Therminol 66
4. Solids or other soluble components in the feed of the distillation column are not considered
5. The strain *Zymomonas mobilis* used in these calculations is assumed to be thermotolerant and its capability is not diminished by the operating temperatures used in this case study (Baeyens et al., 2015; Hasunuma and Kondo, 2012)

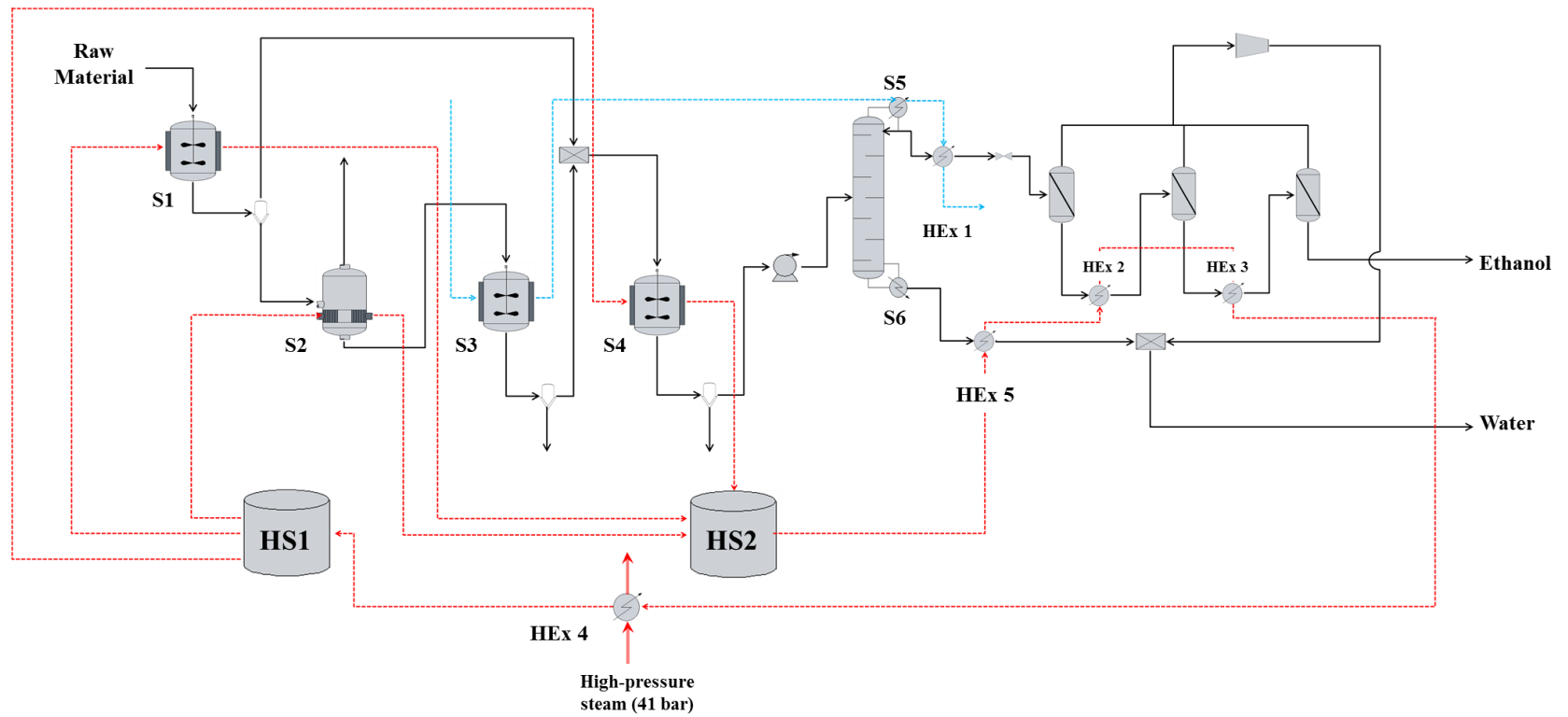


Figure 6.2: Superstructure 1 of the ethanol production process from corn stover with heat storage (using the bottom stream from the distillation column to heat the stream of Therminol 66)

Table 6.3: Initial guesses used in the optimisation of the process with and without heat integration

Variable	Initial guess	Lower bound	Upper bound
Conversion xylose	0.75	0.75	1
Temperature pretreatment (°C)	114	114	120
Volume pretreatment reactor (m³)	1	0.1	100
Conversion by-products	0.70	0.70	1
Volume detoxification reactor (m³)	1	0.1	100
Conc. ethanol fermentation (% w/w)	4	4	5
Intel flow rate cells (kg/sec)	1	0.01	100
Volume fermenter (m³)	1	0.1	100
Reflux ratio	3	1	100
Pressure column (kPa)	101.3	101.3	2026
Mass fraction ethanol in distillate	0.93	0.93	1
Number of membrane modules	1	1	25
Mass fraction ethanol in retentate	0.995	0.993	0.998
Permeate pressure (kPa)	400	0.01	10
Outlet temperature HS1 (°C)	114	114	350

Table 6.4: Operating conditions for the reactors and evaporator

Unit	Operating conditions
Pretreatment reactor	0.6 % (w/w) of acid in a solution 1:10 liquid/solid ratio
Evaporator	60 % of liquid evaporated
Detoxification reactor	30 °C and pH of 12
SSCF reactor	50 °C

6.3.3 Second superstructure of the ethanol production process with heat storage

The second superstructure with heat storage (see Figure 6.3) presents a similar configuration as in the previous section. The main difference lies in the usage of the Therminol 66 stream leaving HS2. Instead of using a heat exchanger to provide heat

from the stream leaving the bottom of the distillation column, the stream coming out of HS2 is heated by using the energy released from the condenser.

6.4 Results

The ethanol production system without heat integration (Figure 6.1) is going to be used as the base case for the comparative analysis with two systems with heat integration. Table 6.3 presents the initial guesses used in the solution of the optimisation problem and Table 6.4 shows the operating conditions considered for the different configurations for the pretreatment, detoxification, evaporation and SSCF stages.

6.4.1 Specifications

The specifications for the different models in each unit and the initial guesses use in the optimisation problem are listed in Tables 6.3 and 6.4 and are also described as follows:

1. For the pretreatment stage, the operating temperature and acid concentration were selected based on the findings by Esteghlalian et al., (1997) which state that, although higher temperatures and acid concentrations reduces the reaction times and increase the conversion of hemicellulose, they also increase the rate of degradation of xylose into by-products.
2. As stated in Section 3.8, the kinetic model for the detoxification of the acid hydrolysates is very limited in terms of the operating conditions. The parameters available in literature correspond to a temperature of 30 °C (Purwadi et al., 2004). However, the mathematical model was obtained as a function of the pH of the solution and, as seen in Section 3.8, the highest levels of conversion of furfural can be achieved at a pH of 12.
3. Similarly, the operating conditions of the SSCF stage are limited since only the enzymatic hydrolysis model is a function of temperature. The results presented by Kadam et al., (2004) show a high production of glucose at high temperatures. Morales-Rodriguez et al., (2011, 2012) suggest that the operating temperature for the SSCF should also be high only under the

assumption that the fermenting microorganisms can reproduce themselves at those conditions. Current research (see Chapter 2) has shown that thermotolerant strains are a viable option for the production of ethanol from lignocellulosic biomass.

4. The percentage of evaporation has been suggested by different companies that produce ethanol around the world to increase the concentration of sugars and to ensure a reduction in the concentration of other volatile compounds in the fermentation medium (BP, 2016b; Incauca, 2016).

6.4.2 Optimisation results – pretreatment stages

Table 6.5 presents the results of the optimisation of all the superstructures for the pretreatment stages. It can be seen from Table 6.5 that the configuration and design of the reactors and evaporator in all the configurations are very similar. This means that this part of the process is mainly governed by the mass balances rather than the energy. The largest reactor in the process is for SSCF which indicates that in order to obtain the necessary concentration of ethanol, the residence time during fermentation has to be long. Table 6.6 shows the results of the streams and concentrations of the optimal design of the pretreatment stages of ethanol production process.

The conversions in the pretreatment, detoxification and SSC stages are 76%, 90% and 83%, respectively. It can also be observed from Table 6.6 that components such as cellobiose, furfural and cells have low concentrations in their respective outlet streams. This indicates that, as expected, the operating conditions favoured the selectivity of the desired products for each stage.

Table 6.5: Optimal results of the pretreatment stages for all the configurations

Variable	Process without heat storage	Superstructure 1	Superstructure 2
Pretreatment reactor (m³)	3.21	3.20	3.21
Detoxification reactor (m³)	1.19	1.20	1.19
SSCF reactor (m³)	19.0	19.0	19.0
Inlet cells stream (kg/s)	0.17	0.16	0.16

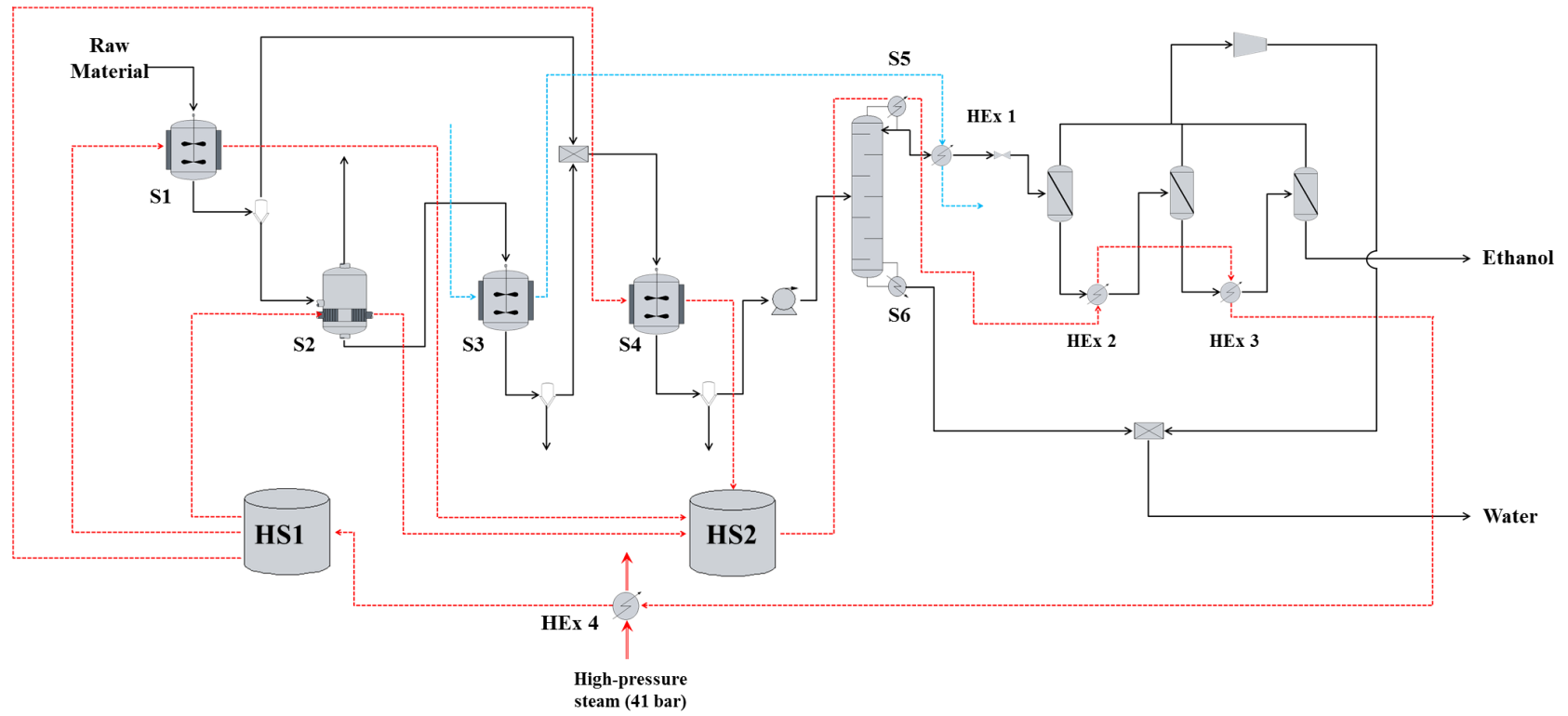


Figure 6.3: Superstructure 2 of the ethanol production process from corn stover with heat storage using the heat released in the condenser to heat the stream of Therminol 66

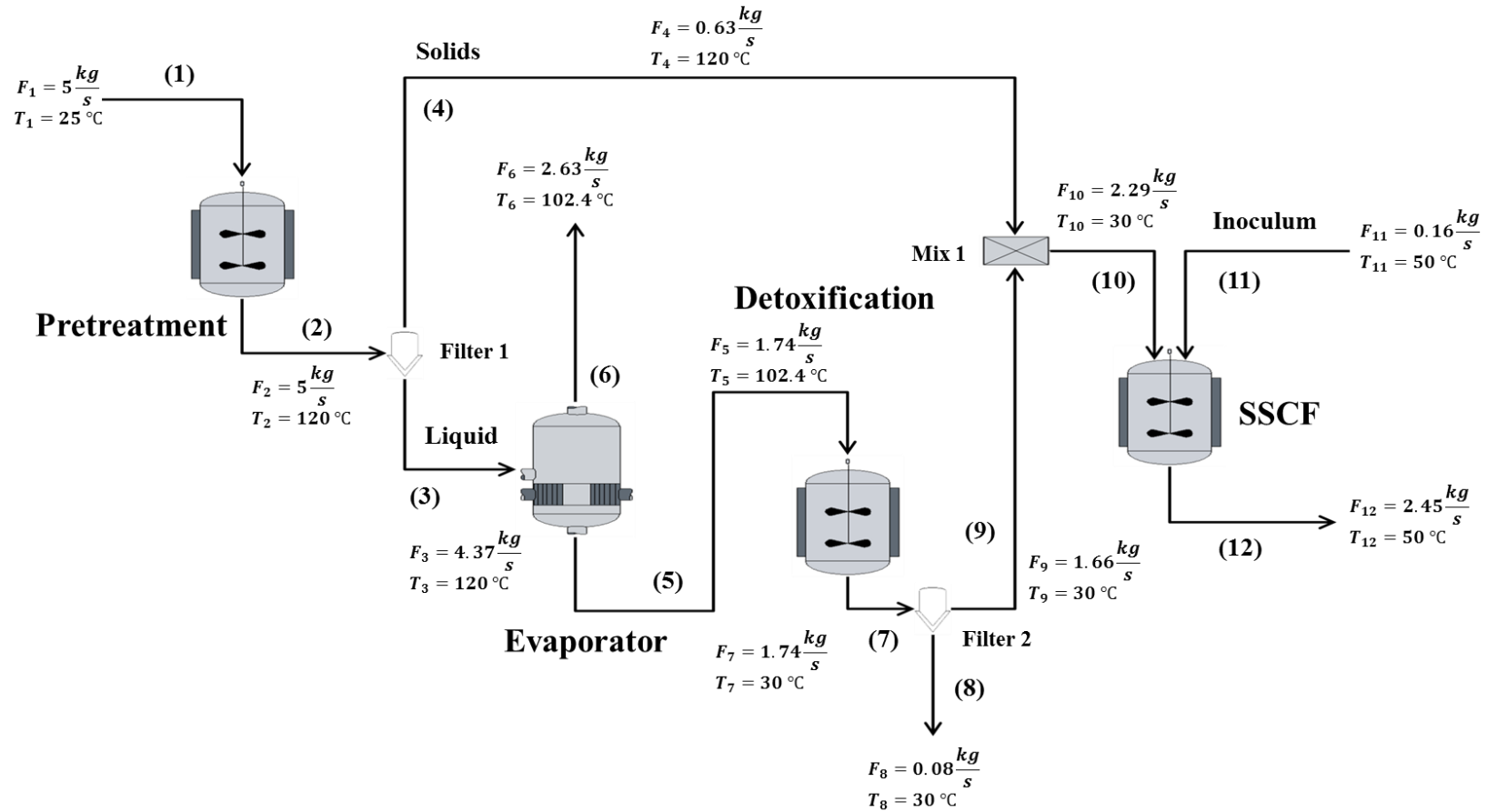


Figure 6.4: Results of the simulation and optimisation of the pretreatment stages of the ethanol production process

Table 6.6: Results of the optimisation of the pretreatment stages and composition of the process streams (% w/w)

Stream	Hemicellulose	Xylose	Furfural	Cellulose	Glucose	Cellobiose	Ethanol	Cells	Others*	Water
(1)	1.98	-	-	3.60	-	-	-	-	4.96	89.46
(2)	0.48	1.39	0.11	3.60	-	-	-	-	4.96	89.46
(3)	-	1.59	0.12	-	-	-	-	-	1.10	97.19
(4)	3.80	-	-	28.6	-	-	-	-	31.9	35.61
(5)	-	3.99	0.21	-	-	-	-	-	1.17	94.63
(6)	-	-	-	-	-	-	-	-	1.09**	98.91
(7)	-	3.98	0.02	-	-	-	-	-	9.37	94.63
(8)	-	-	-	-	-	-	-	-	3.76	96.24
(9)	-	4.19	0.02	-	-	-	-	-	1.24	94.55
(10)	1.04	3.04	0.02	7.86	-	-	-	-	9.66	78.38
(11)	-	-	-	-	-	-	-	25.0	-	75.00
(12)	0.41	-	0.02	0.75	0.19	0.68	4.5	1.87	11.9	79.69

* Refers to lignin, ashes other by-products in the process

** Volatile components such as Sulphuric Acid found in the vapour stream in the evaporator

Values below 0.001 have been ignored

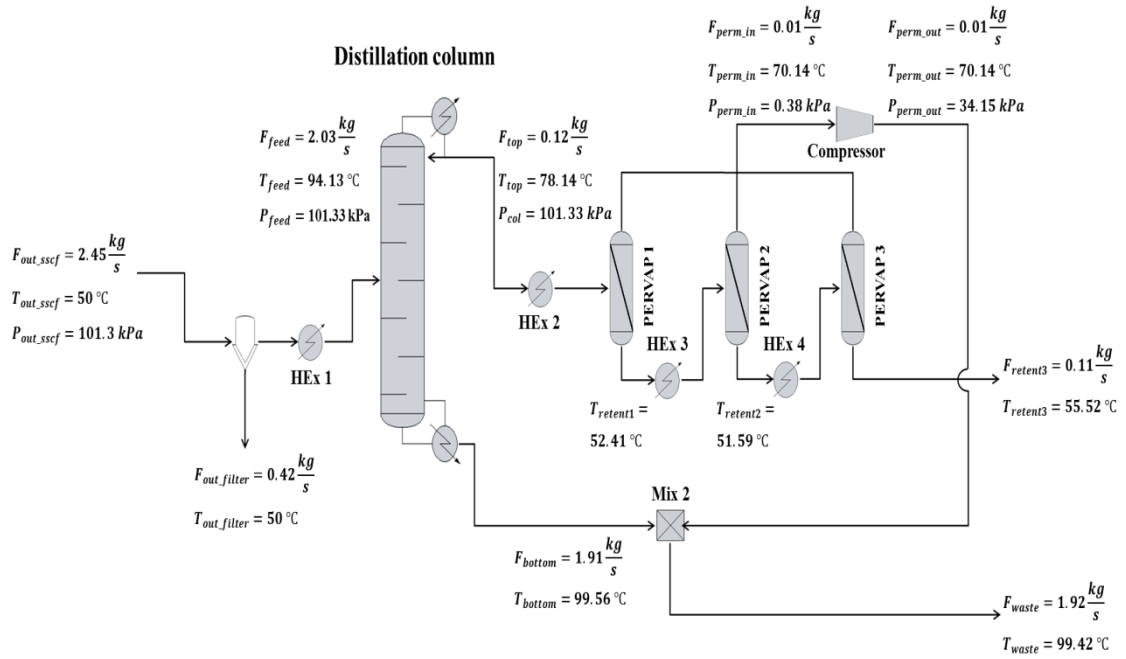


Figure 6.5: Results of the optimisation of the separation stages without heat storage

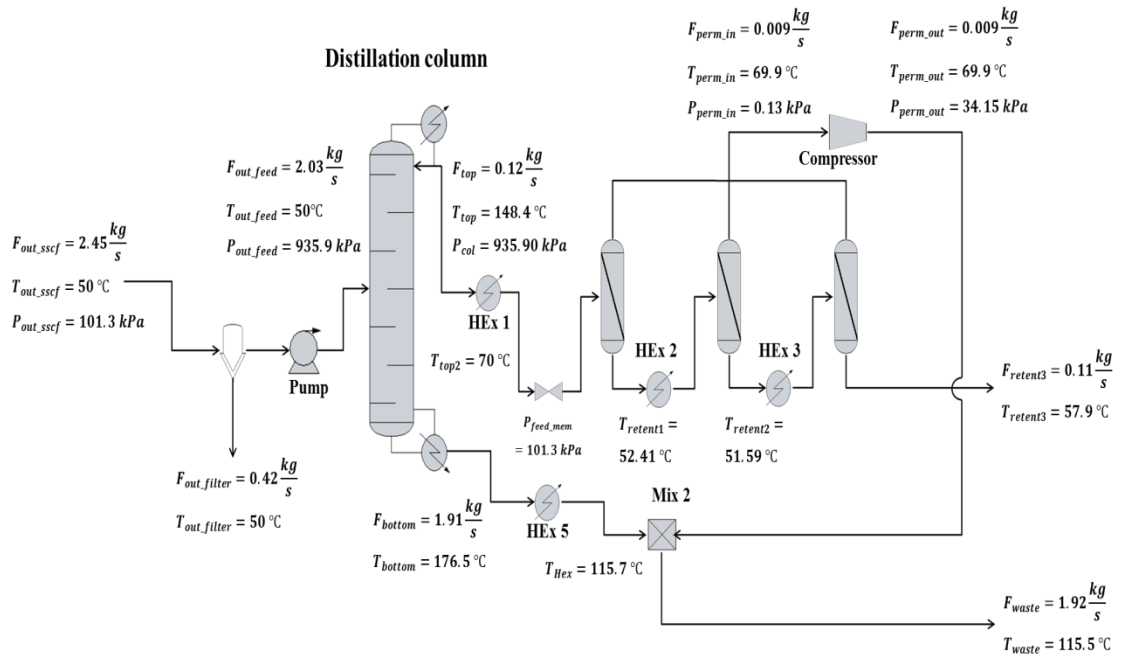


Figure 6.6: Results of the simulation and optimisation of the separation stages with heat storage (Superstructure 1)

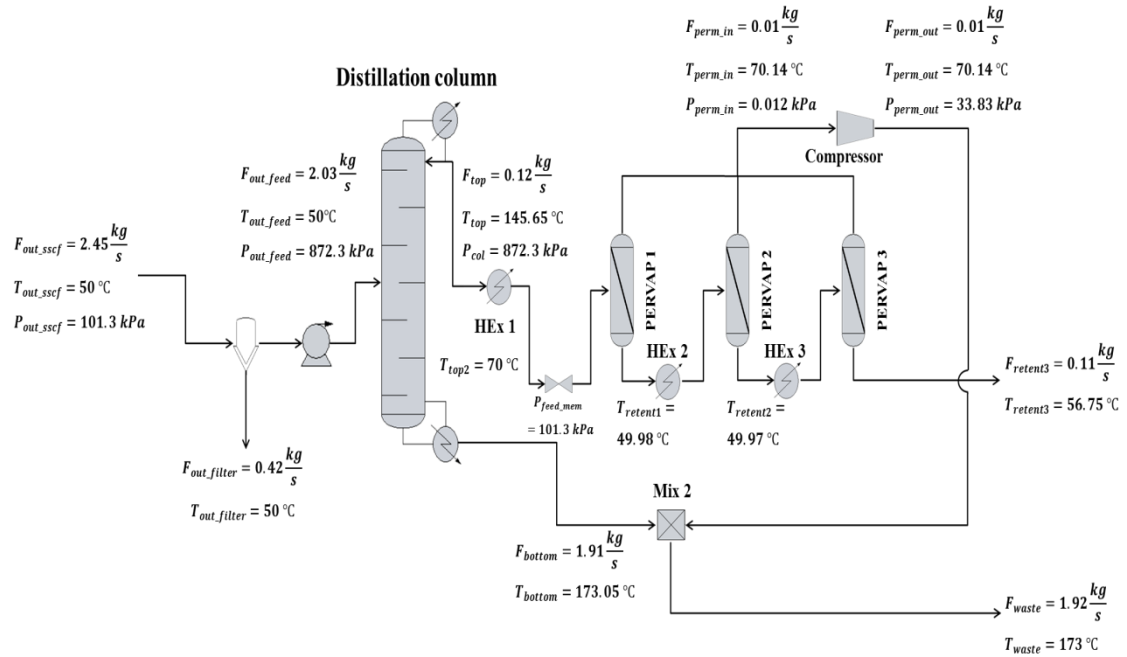


Figure 6.7: Results of the simulation and optimisation of the separation stages with heat storage (Superstructure 2)

6.4.3 Optimisation results – separation section

The results of the separation section are presented in Tables 6.7 to 6.9. These tables include the concentration of ethanol at the top and bottom of the column, number of trays in the distillation column, the feed tray location, the reflux ratio, the outlet pressure of the pump, the permeate pressures in the pervaporation network, the temperature of the retentate streams, and the final concentration of ethanol. The membrane area is chosen based on the results presented in Chapter 5 where 250 m^2 were used for a flow rate of 50 mole/sec. For all the configurations in this chapter the flow rate to the separation system is almost twice the capacity of the configurations in Chapter 5. Therefore, a membrane area of 500 m^2 will be considered for the pervaporation stages.

As presented in Chapter 5, the optimisation of the distillation column consists of three sections: rectification, feed and stripping. Rectification and stripping have initially 25 trays each as initial estimates. The feed section consists of three fixed trays being where the middle tray is where the feed stream is fed. The pervaporation network consists of three stages which were found to be less expensive according to the results presented in Section 5.4.2.

**Table 6.7: Results of the optimisation of the separation stages without heat storage
(membrane area of 500 m²)**

Variable	Distillation column	Pervaporation 1	Pervaporation 2	Pervaporation 3
Number of trays	40	-	-	-
Feed tray from top	32	-	-	-
Pressure column (kPa)	101.3	-	-	-
Heat duty reboiler (kW)	521.9	-	-	-
Reflux ratio	3.51	-	-	-
Ethanol concentration in distillate	0.93*	-	-	-
Ethanol concentration bottoms	0.003	-	-	-
Number of modules	-	1*	1*	4
Permeate pressure (Pa)	-	6767	545.1	381.5
Temperature in retentate (°C)	-	52.41	51.59	55.52
Ethanol mass fraction in retentate	-	0.95	0.98	0.995
Ethanol mass fraction in permeate	-	0.11	0.12	0.44

* Values on lower or upper bounds

**Table 6.8: Results of the optimisation of the separation stages in Superstructure 1
(membrane area of 500 m²)**

Variable	Distillation column	Pervaporation 1	Pervaporation 2	Pervaporation 3
Number of trays	36	-	-	-
Feed tray from top	26	-	-	-
Pressure column (kPa)	935.9	-	-	-
Heat duty reboiler (kW)	579.7	-	-	-
Reflux ratio	4.68	-	-	-
Ethanol concentration in distillate	0.93*	-	-	-
Ethanol concentration bottoms	0.003	-	-	-
Number of modules	-	1*	1*	3
Permeate pressure (Pa)	-	6313	134	134
Temperature in retentate (°C)	-	52.41	51.59	57.86
Ethanol mass fraction in retentate	-	0.96	0.98	0.995
Ethanol mass fraction in permeate	-	0.11	0.12	0.44

* Values on lower or upper bounds

**Table 6.9: Results of the optimisation of the separation stages in Superstructure 2
(membrane area of 500 m²)**

Variable	Distillation column	Pervaporation 1	Pervaporation 2	Pervaporation 3
Number of trays	38	-	-	-
Feed tray from top	13	-	-	-
Pressure column (kPa)	872.3	-	-	-
Heat duty reboiler (kW)	566.9	-	-	-
Reflux ratio	4.43	-	-	-
Ethanol concentration in distillate	0.93*	-	-	-
Ethanol concentration bottoms	0.003	-	-	-
Number of modules	-	1*	1*	3
Permeate pressure (Pa)	-	6701	356	12
Temperature in retentate (°C)	-	49.98	49.97	56.75
Ethanol mass fraction in retentate	-	0.95	0.98	0.995
Ethanol mass fraction in permeate	-	0.09	0.11	0.41

* Values on lower or upper bounds

Variables marked with an asterisk represent values on lower or upper bounds. In Table 6.7, the optimisation for the column without heat integration shows that the rectification section has 30 stages and the stripping section has 7 stages, giving a total of trays of 40 with the feed stream being located in tray number 32.

For the distillation column in superstructure 1 with heat integration (see Table 6.8), the number of trays is 36 with the feed location on tray 26. The design of this distillation column includes a pump before the distillation column instead of a heat exchanger. The state in which the feed enters the column is subcooled liquid whereas in the original configuration (see Figure 6.1), the feed enters as saturated liquid.

As seen in Table 6.8, Superstructure 2 with heat integration has 38 trays and the feed location is on tray 13. The design and operation of the distillation column is highly influenced by the pressure in the column, the thermodynamic state and concentration in which the feed stream enters the column.

Table 6.10: Energy requirements for the different configurations of the ethanol process (kW)

Unit	Without heat storage	With heat storage	
		Superstructure 1	Superstructure 2
Pretreatment	2386*	2386	2386
Evaporator	5806*	5806	5806
Detoxification	-609.5	-609.6	-609.6
SSCF	368.5*	368.5	368.5
Condenser	-489.9	-489.2	-481.7
Reboiler	521.9*	579.7*	566.9*
Heat exchanger 1	393.3*	-38.2	-37.1
Heat exchanger 2	-3.5	6.9	7.9
Heat exchanger 3	7.7*	6.8	7.5
Heat exchanger 4	7.4*	7995*	8094*
Heat exchanger 5	-	-578.8	-
Total energy demand	9491	8574	8660

* Heat sources that are considered in the calculation of the total energy demand

The pervaporation system for the configuration without heat integration (see Table 6.7) shows a total of 6 in-parallel module for a final concentration of ethanol of 99.5 % (w/w). The number of in-parallel modules in the pervaporation stages increases as the permeate pressure decreases from 6767 Pa to 381 Pa which agrees with what was presented in Chapter 4 (i.e. the lower the permeate pressure the higher the separation rate through the membrane).

Superstructures 1 (see Table 6.8) and 2 (see Table 6.9) with heat integration present similar behaviour compared with the base case without heat integration. One key difference between the base case and the two superstructures with heat integration is the number of in-parallel modules (only three modules in the last stage) which directly correlates to the permeate pressure in each stage. The concentration of ethanol in retentate for all the configurations is 99.5% (w/w) as specified.

Table 6.11: Economic analysis for equipment used in the ethanol production process 1×10^3 (US\$/year)

Unit	Without heat storage	With heat storage	
		Superstructure 1	Superstructure 2
Pretreatment	30.83	30.83	30.83
Evaporator	106.8	106.8	106.8
Detoxification	21.19	21.19	21.19
SSCF	89.79	89.79	89.79
Condenser	12.16	12.15	12.08
Reboiler	21.64	23.17	22.83
Column shell	73.89	79.89	79.92
Column trays	2.41	2.73	2.70
Pervaporation modules	268.2	223.5	223.5
Heat exchanger 1	2.49	0.87	0.82
Heat exchanger 2	0.20	0.21	0.23
Heat exchanger 3	0.13	0.21	0.23
Heat exchanger 4	0.13	16.79	13.64
Heat exchanger 5	-	7.81	-
Compressor	16.32	17.46	25.63
Pump	-	2.12	2.12
Heat storage tanks	-	6.01	6.01
Total cost	646.2	641.5	638.3

Table 6.12: Economic analysis for utilities and services used in the ethanol production process 1×10^3 (US\$/year)

Item	Without heat storage	Superstructure 1	Superstructure 2
Cost of steam	2700	2439	2464
Cost of cooling water	5.08	2.81	2.81
Cost of Therminol 66	-	14.21	14.71
Cost of electricity	3.4	5.16	7.54
Total cost	2708.5	2461.2	2489.1

Table 6.13: Area and cost for heat exchangers in all configurations

Unit	Without heat storage	With heat storage	
		Superstructure 1	Superstructure 2
Cost 1x10³ (US\$/yr.)			
Heat exchanger 1	2.49	0.87	0.82
Heat exchanger 2	0.20	0.21	0.23
Heat exchanger 3	0.13	0.21	0.23
Heat exchanger 4	0.13	16.79	13.64
Heat exchanger 5	-	7.81	-
Heat transfer area (m²)			
Heat exchanger 1	3.35	0.66	0.59
Heat exchanger 2	0.07	0.07	0.08
Heat exchanger 3	0.04	0.07	0.08
Heat exchanger 4	0.04	63.03	45.75
Heat exchanger 5	-	19.42	-

6.4.4 Optimisation results – energy demand and economic analysis

Additional calculations are required to assess the overall performance of the plant in terms of energy and cost. The results of energy demand in the process are shown in Table 6.10. The energy consumption is indicated by positive values, whilst energy released from a unit is represented by negative values. The total energy demand is calculated as the amount of heat transferred from steam into the system and is distinguished with an asterisk in Table 6.10. Therefore, the base case configuration (i.e. without heat storage) takes into account the amount of energy in the pretreatment reactor, evaporator, SSCF reactor, reboiler and intermediate heat exchangers, whereas superstructures 1 and 2 only consider the contribution from the reboilers and the heat exchanger where Therminol 66 needs to be re-heated.

A reduction in the energy requirements of 10 % and 8.7 % from the base case configuration can be observed for superstructures 1 and 2 due to the implementation of the heat storage tanks and the heat integration in the process. Figures 6.8 and 6.9 present the temperature of the heat transfer fluid and the flow rates across the

superstructures. Superstructure 2 operates at lower temperatures than Superstructure 1 and therefore requires higher flow rates (a total of 67.97 kg/sec against 39.36 kg/sec) in order to provide the necessary heat to the other units.

An economic analysis is presented in Tables 6.11 and 6.12 which will be helpful in determining the most appropriate configuration. Table 6.11 presents the economic evaluation of the equipment in the process, Table 6.12 shows an economic assessment of the utilities and services and Table 6.13 presents the information of the areas and costs of the heat exchangers. The total annual costs (TAC) for the base case configuration, Superstructure 1 and Superstructure 2 are 3355, 3103, 3127 k\$/year, respectively.

Compared to the original configuration, superstructure 1 reported a decrease in TAC of 6.9 %, whereas Superstructure 2 had a reduction of 6.2 %. The costs of equipment for the two superstructures are higher than the base case process since more units such as heat exchangers and heat storage tanks are included. In the case of heat exchangers, larger areas are required to heat up the stream of Therminol 66 that is recycled back to HS1 which has a direct impact in the overall costs of equipment. On the other hand, a reduction in the usage of utilities in both superstructures led to a reduction of 9 % in the costs of utilities and services.

6.5 Conclusions

This work presented a comparative study between three configurations of the process with and without heat integration using robust optimisation methods and dynamic mass and energy balances. The novelty of this work lies on the methodology to solve the system of equations and the optimisation of the process which had been introduced in Chapter 5 with applications on bioprocesses. The overall goal of this thesis was to prove that it was possible to reduce the energy consumption within the process and therefore the investment costs in order to make the production of ethanol for lignocellulosic biomass a more appealing alternative for energy generation from renewable sources.

The optimisation of the process without heat integration showed that for higher conversions, larger volumes were required. The results of operating conditions of the

units along with the corresponding constraints allowed obtaining low concentrations of furfural, cellobiose and cells throughout the production of ethanol. The optimisation also showed the arrangement of the separation section and the operating conditions necessary to achieve the desired concentration of ethanol. For Superstructure 1, the pressure inside the distillation column was higher than in Superstructure 2, which directly influenced the heat duty in the reboiler and the energy transferred to the stream of Therminol 66 leaving the reactor.

The implementation of the heat storage units showed a reduction of 6.9 % in the total annual cost for Superstructure 1 which can be attributed to the usage of the heat transfer fluid to substitute high pressure steam; and a reduction of TAC of 6.2 % was obtained in Superstructure 2. The difference between these two configurations lies on the recovery of heat in the stream of Therminol 66 coming out of HS2. For Superstructure 1, the total flow rate of Therminol was lower than its counterpart and the amount of heat transferred in Heat Exchanger 5 was higher.

Superstructure 1 is the optimal configuration for the ethanol production process since it reduced the energy consumption in the pretreatment reactors and reduced the costs related to equipment and usage of utilities in the process. Chapter 7 will summarise the achievements and main conclusions of this thesis and will present proposals for the future work for this project.

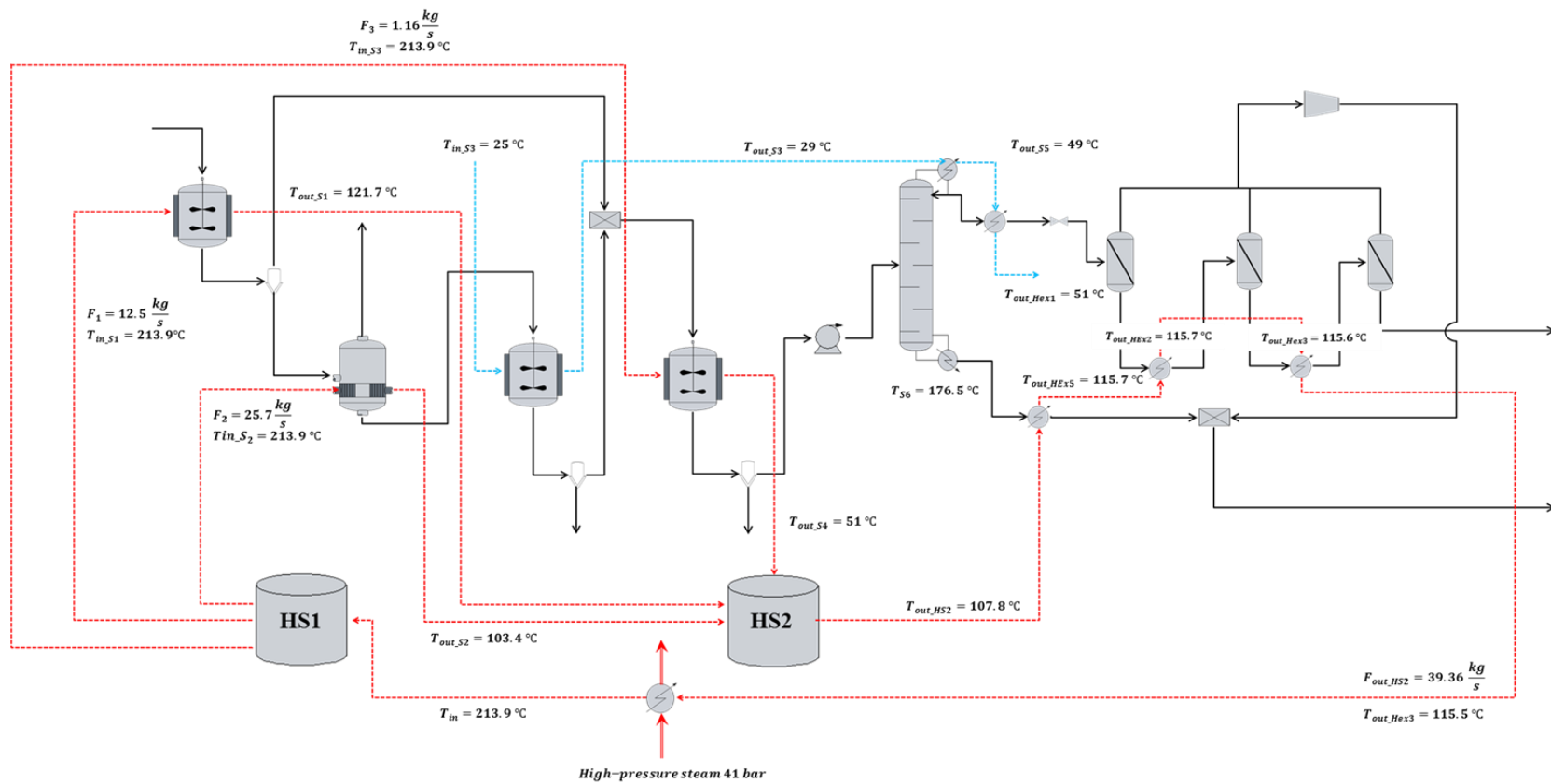


Figure 6.8: Temperatures of heat transfer fluid Therminol 66 across Superstructure 1

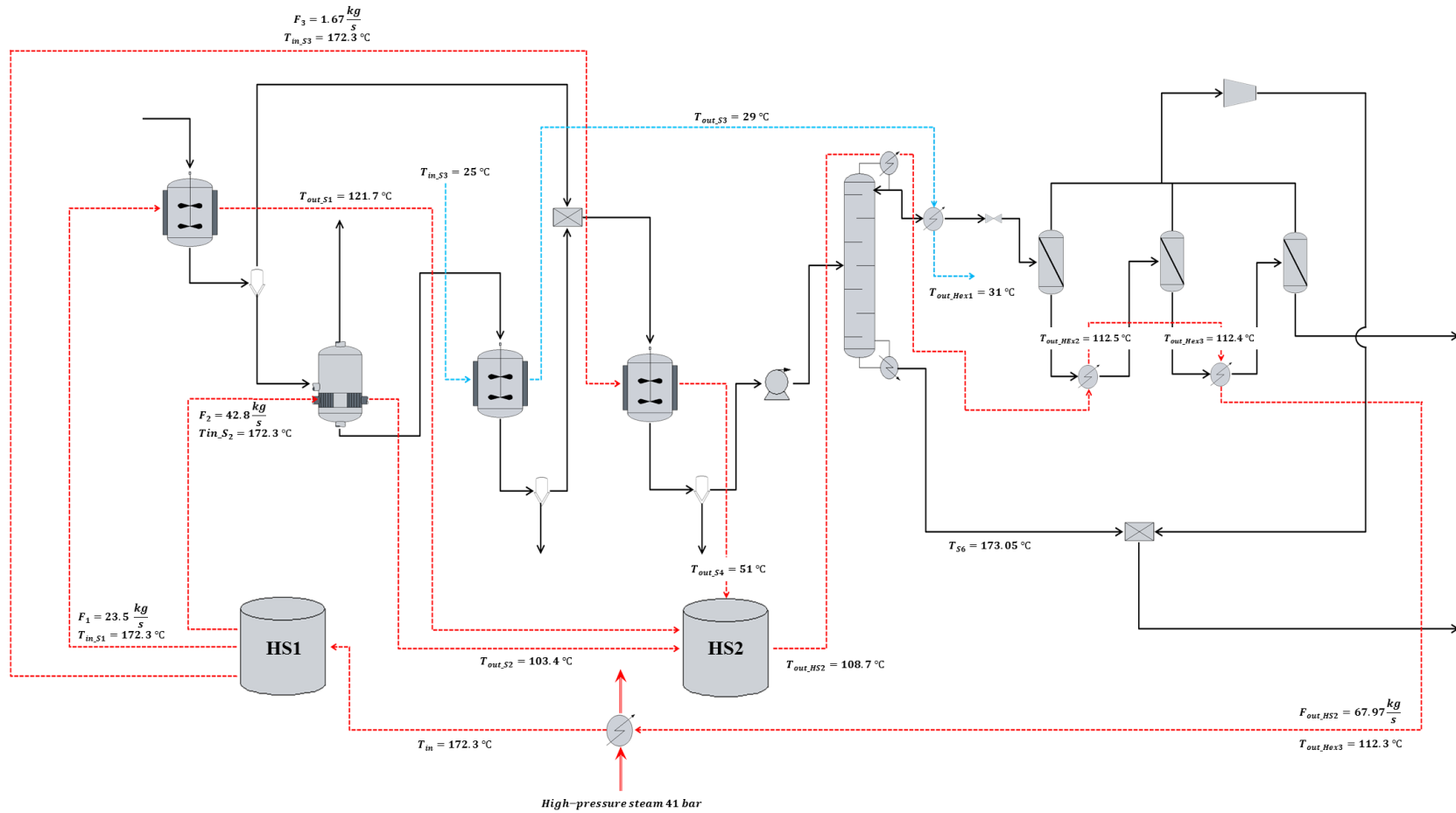


Figure 6.9: Temperatures of heat transfer fluid Therminol 66 across Superstructure 2

Chapter 7 – Conclusions and future work

Abstract

This chapter summarises the work that has been presented in this thesis. Section 7.1 presents the contributions of this research to the modelling of the ethanol production process, the formulation of the mathematical model of the organophilic membrane, the optimisation of the separation stage and the heat integration of the process. Section 7.2 presents the possible directions for future research and the application of this work into different processes.

7.1 Conclusions

This worked has focused on developing a complete dynamic model of the production of ethanol from lignocellulosic biomass and on the heat integration of this process using heat transfer fluids to reduce the usage of external sources of heat such as steam with the aims of finding more profitable and more efficient process configurations. This thesis covered several aspects which are summarised as follows:

A review of the current status of fuel consumption around the world was presented in Chapter 1. In this review, it could be seen that the consumption of crude oil and coal has been increasing in the last decades which signifies a problem for society giving that population and energy consumption go hand in hand. This chapter also presented the global production of biofuels and how they represent a sustainable alternative for energy generation from renewable sources. The chapter continued with the production of ethanol and the different routes from which it can be produced (e.g. hydration of ethylene and fermentation). In this work, the author opted for the production of ethanol from lignocellulosic biomass, more specifically, from corn stover. This raw material can be found in many countries and possess a high organic content and has the potential to be used in the production of high-added-value products of industrial interest.

In Chapter 2, a literature survey of the current state of the art on ethanol production was introduced. Some works included the implementation of new pretreatment methods, new strains, and new configurations for the separation stages. However, most of these works only focused on individual units and operating conditions rather than consider complete dynamic modelling and heat integration of the ethanol production process which is the main objective of this thesis. All the work available related to the optimisation of the process was only applicable to the design of the separation stages and individual reaction units.

This thesis presented complete mathematical models for all units of the process that were used in the calculations and subsequent simulations. In order to guarantee the reliability and consistency of the simulations, each model was validated against at least another source. In the cases of pretreatment, detoxification, enzymatic hydrolysis, fermentation and pervaporation, these stages were validated against experimental data. The distillation column was validated against simulations run in ChemCAD which is a commercially available simulation tool.

This work presented the formulation of a mathematical model for a membrane used in the separation of ethanol from the fermentation broth. This work, which was developed in collaboration with TU Dortmund in Germany, consisted of a series of experiments using a membrane called PERVAPTM 4060 provided by Sulzer. The parameters for three different mathematical models were estimated using gPROMS in order to evaluate the accuracy of different approaches. The results of these calculations generated a reliable model which was able to accurately describe the permeation of ethanol through the membrane which was later used in the optimisation of the complete separation section. It is important to establish that the implementation of membrane modules prior to the distillation system and their impact on the design and energy consumption of the process have not been investigated in the separation of ethanol from lignocellulosic hydrolysates.

A methodology for the optimisation of hybrid processes for the separation of ethanol was also developed in this thesis. This methodology took individual parts of the separation section (i.e. the pervaporation modules or the distillation column) and optimised their design and operating conditions to later use their results as initial

guesses to optimise the entire hybrid process. This methodology is very practical since it seeks for feasible regions in which the combined process can find a sensible solution that satisfies the specifications of purity and energy consumption. Two main configurations were compared: The first one consisted of a single distillation column linked to a network of hydrophilic membranes. The second one included the organophilic membrane before the distillation column. The results showed that having the organophilic membrane could indeed reduce the heat duty in the reboiler and the size of the distillation column and the pervaporation network. However, the overall energy consumption and the Total Annualised Cost (TAC) did not support the implementation of this membrane due to the requirement of additional units such as compressors and heat exchangers. A sensitivity analysis was also included in this work. The purpose of this analysis was to determine the variations in the optimal design of both superstructures focusing mainly on the structure with the organophilic membrane since this is the novelty of this work. The results showed that in all case studies, the implementation of the organophilic membrane was more expensive and more energy intensive than the configuration without said membrane.

Finally, the last section of this work focused on the optimisation and heat integration of the ethanol production process from corn stove and compared three configurations: The first configuration was a standard arrangement of the process as presented in Chapter 3. This configuration served as the base case for the results of the optimisation with heat integration.

The second configuration presented the introduction of heat storage units containing Therminol 66 to provide heat to the main reactors and to recover the energy from the stream at the bottom of the column. The third configuration also implemented heat storage units but it used the heat released by the condenser to recover heat with the transfer fluid.

The results of these optimisations showed that using heat transfer fluids reduced the energy consumption in the process by 10% and the Total Annualised Cost (TAC) by 7%. Although these numbers seemed relatively small, they do have an impact, especially in processes with high production rates. This thesis showed that biofuels can be a competitive source of energy in the mainstream energy market and the

usage of lignocellulosic biomass can still be an appealing alternative to reduce the consumption of oil and coal and to mitigate the harmful effects of global warming. This production route is still far from being successfully implemented in industry for sustainable energy generation and there are still issues that need to be addressed in the future and they are suggested in the following section.

7.2 Future work

This section focuses on the areas that this thesis did not cover and could potentially be interesting to address in future research. One of the most important aspects of the thesis was the optimisation of the separation stages for a binary mixture ethanol/water. However, the separation section of the process presented in this work did not consider other components in the purification of ethanol. This assumption was adopted because the concentration of most reducing sugars and soluble acids is very low in the outlet streams of the fermentation stage. However, these compounds could have a significant influence over the performance of some of the units in the separation section, especially in the pervaporation modules. Compounds such as acetic acid and other organic acids tend to reduce the lifetime of a membrane as seen in Chapter 4 for the PERVAP 4060TM organophilic membrane. This could represent an increase in the heat duty in the reboiler which also translates into more expensive operating conditions and design of the process. For the organophilic membrane model, it would be beneficial to include the effect of other by-products from the pretreatment. As seen in Chapter 4, by-products from pretreatment and fermentation influence the total flux through the membrane. The model would require more experimental data in order to estimate the parameters in the model to describe the separation between feed and permeate sides.

Another aspect that should be considered in the simulation of the separation stages is the presence of solids. Soluble and insoluble solids produced during the fermentation stage can also influence the design of the distillation columns as well as the heat duty in the reboiler. This aspect not only affects the design of the unit but also affects the maintenance and control of the distillation columns which are directly correlated to the components found in the feed stream.

methodology seems to be more practical, it is important to remember that the system of equations that describe the process is highly non-linear and the optimisation thereof could take longer computational times.

The heat integration process presented in Chapter 6 introduced the optimisation of the entire process using heat storage units. This methodology was implemented with aims to reduce the usage of utilities which have a significant effect in the minimisation of the total annualised costs. Something that should be considered for future work is the generation of energy from the unreacted lignocellulosic solids in the process. Several authors have presented works related to the generation of energy from the unreacted material in order to make the process more sustainable and more feasible for industrial applications. This approach will attempt to solve two issues in the production of ethanol: one is the reduction in the usage of utilities and the other one is the reduction and management of solids with high organic content coming out of the process. This will ensure a more efficient way to produce ethanol from any lignocellulosic material without risking the environment and natural sources.

Finally, this work could be expanded for the production of other metabolites of industrial applications such as butanol, biopolymers, biodiesel and organic acids from renewable materials. There is a demand for greener and more efficient technologies that can solve the problem of agroindustrial pollution as well as the management of solids or other residues that could potentially become into valuable chemicals. The work developed in this thesis follows a series of logical steps, in which every unit required is evaluated leading to a reliable simulation of a complete process with applicability into any metabolite from lignocellulosic biomass. This will ensure a reduction of energy consumption, costs of raw materials and an increase in the sustainability and profitability of the process.

List of publications and events

1. D Lorenzo, C Perez-Galvan, CF Triana, A Santos, A Romero, IDL Bogle, 2016, Modelling of a reactive distillation in the production process of high purity Cyclohexanone to produce Caprolactam. *Proceedings of ESCAPE 2016*. Portorož, Slovenia
2. CF Triana, ES Fraga & E Sorensen, 2015, Evaluation of the energy consumption of the production of bioethanol from lignocellulosic biomass. *Proceedings of ESCAPE 2015 and PSE 2015*. Copenhagen, Denmark
3. CF Triana, P Lutze, ES Fraga, E Sorensen, 2014, Implementation of an organophilic membrane system to remove ethanol from lignocellulosic biomass hydrolysates. *AIChE Annual Meeting*. Atlanta, GA, USA
4. CF Triana, ES Fraga & E Sorensen, 2014, Energy efficient separation alternatives for the production of ethanol from lignocellulosic biomass. 10th International Conference on Distillation & Absorption 2014. Friedrichshafen, Germany
5. 125th BASF International Summer School. Ludwigshafen, Germany
6. CF Triana, ES Fraga & E Sorensen, 2013, Optimal energy consumption in the production of bioethanol from lignocellulosic biomass. *AIChE Annual Meeting*. San Francisco, CA, USA

REFERENCES

- Abedinifar, S., Karimi, K., Khanahmadi, M., Taherzadeh, M.J., 2009. Ethanol production by *Mucor indicus* and *Rhizopus oryzae* from rice straw by separate hydrolysis and fermentation. *Biomass and Bioenergy* 33, 828–833.
- Agbogbo, F.K., Coward-Kelly, G., Torry-Smith, M., Wenger, K.S., 2006. Fermentation of glucose/xylose mixtures using *Pichia stipitis*. *Process Biochem.* 41, 2333–2336.
- Aguilar, R., Ramirez, J.A., Garrote, G., Vazquez, M., 2002. Kinetic study of the acid hydrolysis of sugar cane bagasse. *J. Food Eng.* 55, 309–318.
- Altuntop, N., Arslan, M., Ozceyhan, V., Kanoglu, M., 2005. Effect of obstacles on thermal stratification in hot water storage tanks. *Appl. Therm. Eng.* 25, 2285–2298.
- Amusat, O., Shearing, P., Fraga, E.S., 2015. System Design of Renewable Energy Generation and Storage Alternatives for Large Scale Continuous Processes, in: *Computer Aided Chemical Engineering*. pp. 2279–2284.
- AN, W., YU, F., DONG, F., HU, Y., 2008. Simulated Annealing Approach to the Optimal Synthesis of Distillation Column with Intermediate Heat Exchangers. *Chinese J. Chem. Eng.* 16, 30–35.
- Avci, A., Saha, B.C., Dien, B.S., Kennedy, G.J., Cotta, M.A., 2013. Response surface optimization of corn stover pretreatment using dilute phosphoric acid for enzymatic hydrolysis and ethanol production. *Bioresour. Technol.* 130, 603–612.
- Baeyens, J., Kang, Q., Appels, L., Dewil, R., Lv, Y., Tan, T., 2015. Challenges and opportunities in improving the production of bio-ethanol. *Prog. Energy Combust. Sci.* 47, 60–88.
- Bai, F.W., Anderson, W.A., Moo-Young, M., 2008. Ethanol fermentation technologies from sugar and starch feedstocks. *Biotechnol. Adv.* 26, 89–105.
- Baker, R., 2012. Pervaporation, in: *Membrane Technology and Applications*. Wiley, pp. 355–392.

- Balat, M., Balat, H., Öz, C., 2008. Progress in bioethanol processing. *Prog. Energy Combust. Sci.* 34, 551–573.
- Ballesteros, M., Oliva, J.M., Negro, M.J., Manzanares, P., Ballesteros, I., 2004. Ethanol from lignocellulosic materials by a simultaneous saccharification and fermentation process (SFS) with *Kluyveromyces marxianus* CECT 10875. *Process Biochem.* 39, 1843–1848.
- Balusu, R., Paduru, R.R., Kuravi, S.K., Seenayya, G., Reddy, G., 2005. Optimization of critical medium components using response surface methodology for ethanol production from cellulosic biomass by *Clostridium thermocellum* SS19. *Process Biochem.* 40, 3025–3030.
- Baños, R., Manzano-Agugliaro, F., Montoya, F.G., Gil, C., Alcayde, A., Gómez, J., 2011. Optimization methods applied to renewable and sustainable energy: A review. *Renew. Sustain. Energy Rev.* 15, 1753–1766.
- Bansal, P., Hall, M., Realff, M.J., Lee, J.H., Bommarius, A.S., 2009. Modeling cellulase kinetics on lignocellulosic substrates. *Biotechnol. Adv.* 27, 833–848.
- Beck, M., Johnson, R., Baker, C., 1990. Comparison of three commercial cellulases for production of glucose from acid-treated hardwood. *Appl. Biochem. Biotechnol.* 24–25, 407–414.
- Behera, S., Mohanty, R.C., Ray, R.C., 2010. Comparative study of bio-ethanol production from mahula (*Madhuca latifolia* L.) flowers by *Saccharomyces cerevisiae* and *Zymomonas mobilis*. *Appl. Energy* 87, 2352–2355.
- Ben Soltane, H., Roizard, D., Favre, E., 2013. Effect of pressure on the swelling and fluxes of dense PDMS membranes in nanofiltration: An experimental study. *J. Memb. Sci.* 435, 110–119.
- Berrin, J.-G., Herpoel-Gimbert, I., Ferreira, N.L., Margeot, A., Heiss-Blanquet, S., 2014. *Biotechnology and Biology of Trichoderma*, *Biotechnology and Biology of Trichoderma*. Elsevier.
- Bezerra, R., Dias, A., 2005. Enzymatic kinetic of cellulose hydrolysis. *Appl. Biochem. Biotechnol.* 126, 49–59.
- Bhandari, N., Macdonald, D.G., Bakhshi, N.N., 1984. Kinetic studies of corn stover

- saccharification using sulphuric acid. *Biotechnol. Bioeng.* 26, 320–327.
- Biegler, L.T., Grossmann, I.E., Westerberg, A.W., 1999. *Systematic methods of chemical process design*. Prentice-Hall.
- Binod, P., Sindhu, R., Singhania, R.R., Vikram, S., Devi, L., Nagalakshmi, S., Kurien, N., Sukumaran, R.K., Pandey, A., 2010. Bioethanol production from rice straw: An overview. *Bioresour. Technol.* 101, 4767–4774.
- Blum, C., Rol, A., Alba, E., 2005. *Parallel metaheuristics: a new class of algorithms*. Wiley.
- BP, 2016a. BP statistical review of world energy June 2016.
- BP, 2016b. Etanol da cana de acucar - BP Brazil [WWW Document].
- BP, 2012. BP statistical review of world energy June 2012.
- Bryson, A.E., Ho, Y.-C., 1975. *Applied optimal control: optimization, estimation and control*, 1st Editio. ed. CRC Press.
- Caballero, J.A., 2015. Logic hybrid simulation-optimization algorithm for distillation design. *Comput. Chem. Eng.* 72, 284–299.
- Caballero, J.A., Grossmann, I.E., 2014a. Chapter 11 - Optimization of Distillation Processes, in: Sorensen, A.G. (Ed.), *Distillation*. Academic Press, Boston, pp. 437–496.
- Caballero, J.A., Grossmann, I.E., 2014b. Optimal synthesis of thermally coupled distillation sequences using a novel {MILP} approach. *Comput. Chem. Eng.* 61, 118–135.
- Cara, C., Moya, M., I, B., José, M., 2007. Influence of solid loading on enzymatic hydrolysis of steam exploded or liquid hot water pretreated olive tree biomass. *Process Biochem.* 42, 1003–1009.
- Cardona, C.A., Quintero, J.A., Paz, I.C., 2010. Production of bioethanol from sugarcane bagasse: Status and perspectives. *Bioresour. Technol.* 101, 4754–4766.
- Cardona, C.A., Sánchez, Ó.J., 2007. Fuel ethanol production: Process design trends and integration opportunities. *Bioresour. Technol.* 98, 2415–2457.

- Carrasco, C., Baudel, H., Penarrieta, M., Solano, C., Tejada, L., Roslander, C., Galbe, M., Liden, G., 2011. Steam pretreatment and fermentation of the straw material Paja Brava using simultaneous saccharification and co-fermentation. *J. Biosci. Bioeng.* 111, 167–174.
- Chandel, A.K., Kapoor, R.K., Singh, A., Kuhad, R.C., 2007. Detoxification of sugarcane bagasse hydrolysate improves ethanol production by *Candida shehatae* NCIM 3501. *Bioresour. Technol.* 98, 1947–1950.
- Chemstations, 2015. ChemCAD.
- Chen, H.-G., Zhang, Y.-H.P., 2015. New biorefineries and sustainable agriculture: Increased food, biofuels, and ecosystem security. *Renew. Sustain. Energy Rev.* 47, 117–132.
- Cheng, J.-R., Liu, X.-M., Chen, Z.-Y., 2015. Methane Production from Rice Straw Hydrolysate Treated with Dilute Acid by Anaerobic Granular Sludge. *Appl. Biochem. Biotechnol.* 178, 9–20.
- Cho, D.H., Shin, S.J., Bae, Y., Park, C., Kim, Y.H., 2010. Enhanced ethanol production from deacetylated yellow poplar acid hydrolysate by *Pichia stipitis*. *Bioresour. Technol.* 101, 4947–4951.
- Chovau, S., Gaykawad, S., Straathof, A., der Bruggen, B., 2011. Influence of fermentation by-products on the purification of ethanol from water using pervaporation. *Bioresour. Technol.* 102, 1669–1674.
- Chung, Y.-H., Peng, T.-H., Lee, H.-Y., Chen, C.-L., Chien, I.-L., 2015. Design and Control of Reactive Distillation System for Esterification of Levulinic Acid and n-Butanol. *Ind. Eng. Chem. Res.* 54, 3341–3354.
- Claes, S., Vandezande, P., Mullens, S., De Sitter, K., Peeters, R., Van Bael, M.K., 2012. Preparation and benchmarking of thin film supported PTMSP-silica pervaporation membranes. *J. Memb. Sci.* 389, 265–271.
- Claes, S., Vandezande, P., Mullens, S., Leysen, R., De Sitter, K., Andersson, A., Maurer, F.H.J., Van den Rul, H., Peeters, R., Van Bael, M.K., 2010. High flux composite PTMSP-silica nanohybrid membranes for the pervaporation of ethanol/water mixtures. *J. Memb. Sci.* 351, 160–167.

- Čuček, L., Martín, M., Grossmann, I.E., Kravanja, Z., 2011. Energy, water and process technologies integration for the simultaneous production of ethanol and food from the entire corn plant. *Comput. Chem. Eng.* 35, 1547–1557.
- Davis, L., Jeon, Y.J., Svenson, C., Rogers, P., Pearce, J., Peiris, P., 2005. Evaluation of wheat stillage for ethanol production by recombinant *Zymomonas mobilis*. *Biomass and Bioenergy* 29, 49–59.
- Demirbas, A., 2007. Progress and recent trends in biofuels. *Prog. Energy Combust. Sci.* 33, 1–18.
- Diaz, A.B., Moretti, M.M. de S., Bezerra-Bussoli, C., Carreira Nunes, C. da C., Blandino, A., da Silva, R., Gomes, E., 2015. Evaluation of microwave-assisted pretreatment of lignocellulosic biomass immersed in alkaline glycerol for fermentable sugars production. *Bioresour. Technol.* 185, 316–23.
- Dien, B.S., Hespell, R.B., Wyckoff, H.A., Bothast, R.J., 1998. Fermentation of hexose and pentose sugars using a novel ethanologenic *Escherichia coli* strain. *Enzyme Microb. Technol.* 23, 366–371.
- Dieterle, F., Kieser, B., Gauglitz, G., 2003. Genetic algorithms and neural networks for the quantitative analysis of ternary mixtures using surface plasmon resonance. *Chemom. Intell. Lab. Syst.* 65, 67–81.
- Dinçer, İ., Rosen, M.A., 2010. Energy Storage Systems, in: *Thermal Energy Storage*. John Wiley & Sons, Ltd, pp. 51–82.
- Divne, C., Stahlberg, J., Tuula, T.T., TA., J., 1998. High-resolution crystal structures reveal how a cellulose chain is bound in the 50 Å long tunnel of cellobiohydrolase I from *Trichoderma reesei*. *J. Mol. Biol.* 275, 309–325.
- Drapcho, C.M., Nhuan, N.P., Walker, T.H., 2008. *Ethanol Production, Biofuels Engineering Process Technology*, The McGraw-Hill Companies. McGraw-Hill.
- Dünnebier, G., Pantelides, C.C., 1999. Optimal Design of Thermally Coupled Distillation Columns. *Ind. Eng. Chem. Res.* 38, 162–176.
- Eastman, 2016. *Therminol*.
- Elgharbawy, A.A., Alam, M.Z., Moniruzzaman, M., Goto, M., 2016. Ionic liquid pretreatment as emerging approaches for enhanced enzymatic hydrolysis of

- lignocellulosic biomass. *Biochem. Eng. J.* 109, 252–267.
- Engel, P., Krull, S., Seiferheld, B., Spiess, A.C., 2012. Rational approach to optimize cellulase mixtures for hydrolysis of regenerated cellulose containing residual ionic liquid. *Bioresour. Technol.* 115, 27–34.
- Erdei, B., Galbe, M., Zacchi, G., 2013. Simultaneous saccharification and co-fermentation of whole wheat in integrated ethanol production. *Biomass and Bioenergy* 56, 506–514.
- Escobar, J.C., Lora, E.S., Venturini, O.J., Yáñez, E.E., Castillo, E.F., Almazan, O., 2009. Biofuels: Environment, technology and food security. *Renew. Sustain. Energy Rev.* 13, 1275–1287.
- Esteghlalian, A., Hashimoto, A.G., Fenske, J.J., Penner, M.H., 1997. Modeling and optimization of the dilute-sulfuric-acid pretreatment of corn stover, poplar and switchgrass. *Bioresour. Technol.* 59, 129–136.
- Fan, S., Xiao, Z., Zhang, Y., Tang, X., Chen, C., Li, W., Deng, Q., Yao, P., 2014. Enhanced ethanol fermentation in a pervaporation membrane bioreactor with the convenient permeate vapor recovery. *Bioresour. Technol.* 155, 229–234.
- Feczko, T., Trif, L., Horák, D., 2016. Latent heat storage by silica-coated polymer beads containing organic phase change materials. *Sol. Energy* 132, 405–414.
- Felix, E., Tilley, D.R., 2009. Integrated energy, environmental and financial analysis of ethanol production from cellulosic switchgrass. *Energy* 34, 410–436.
- Fornell, R., Berntsson, T., 2012. Process integration study of a kraft pulp mill converted to an ethanol production plant – Part A: Potential for heat integration of thermal separation units. *Appl. Therm. Eng.* 35, 81–90.
- Freer, S.N., Detroy, R.W., 1983. Characterization of cellobiose fermentations to ethanol by yeasts. *Biotechnol. Bioeng.* 25, 541–557.
- Freer, S.N., Detroy, R.W., 1982. Direct fermentation of cellodextrins to ethanol by *Candida wickerhamii* and *C. Lusitaniae*. *Biotechnol. Lett.* 4, 453–458.
- Garcia, J.F., Cuevas, M., Bravo, V., Sanchez, S., 2010. Ethanol production from olive prunings by autohydrolysis and fermentation with *Candida tropicalis*. *Renew. Energy* 35, 1602–1608.

- García, V., Pongrácz, E., Phillips, P.S., Keiski, R.L., 2013. From waste treatment to resource efficiency in the chemical industry: recovery of organic solvents from waters containing electrolytes by pervaporation. *J. Clean. Prod.* 39, 146–153.
- Gaykawad, S.S., van der Wielen, L.A.M., Straathof, A.J.J., 2012. Effects of yeast-originating polymeric compounds on ethanol pervaporation. *Bioresour. Technol.* 116, 9–14.
- Gaykawad, S.S., Zha, Y., Punt, P.J., van Groenestijn, J.W., van der Wielen, L.A.M., Straathof, A.J.J., 2013. Pervaporation of ethanol from lignocellulosic fermentation broth. *Bioresour. Technol.* 129, 469–476.
- Geddes, C., Mullinnix, M., Nieves, I., Peterson, J., Hoffman, H., York, S., Yomano, L., Miller, E., Shanmugam, K., Ingram, L., 2011. Simplified process for ethanol production from sugarcane bagasse using hydrolysate-resistant *Escherichia coli* strain MM160. *Bioresour. Technol.* 102, 2702–2711.
- Gendreau, M., Potvin, J.-Y., 2010. *Handbook of metaheuristics*, Internatio. ed. Springer.
- Gil, I.D., Gómez, J.M., Rodríguez, G., 2012. Control of an extractive distillation process to dehydrate ethanol using glycerol as entrainer. *Comput. Chem. Eng.* 39, 129–142.
- Golias, H., Dumsday, G.J., Stanley, G.A., Pamment, N.B., 2002. Evaluation of a recombinant *Klebsiella oxytoca* strain for ethanol production from cellulose by simultaneous saccharification and fermentation: comparison with native cellobiose-utilising yeast strains and performance in co-culture with thermotolerant yeas. *J. Biotechnol.* 96, 155–168.
- Gomez-Castro, F.I., Rodriguez-Angeles, M.A., Segovia-Hernandez, J.G., Gutierrez-Antonio, C., Briones-Ramirez, A., 2011. Optimal Designs of Multiple Dividing Wall Columns. *Chem. Eng. Technol.* 34, 2051–2058.
- Gorak, A., Sorensen, E., 2014. Principles of binary distillation, in: *Distillation: Fundamentals and Principles*. Academic Press, pp. 145–186.
- Gorji-Bandpy, M., Yahyazadeh-Jelodar, H., Khalili, M., 2011. Optimization of heat exchanger network. *Appl. Therm. Eng.* 31, 779–784.

- Grisales, R., Cardona, C.A., Gutierrez, L.F., Sanchez, O.J., 2008. Heat integration of fermentation and recovery steps for fuel ethanol production from lignocellulosic biomass, in: 2nd Mercosur Congress on Chemical Engineering and 4th Mercosur Congress on Process Systems Engineering. Costa Verde, Rio De Janeiro.
- Haelssig, J.B., Tremblay, A.Y., Thibault, J., 2012. A new hybrid membrane separation process for enhanced ethanol recovery: Process description and numerical studies. *Chem. Eng. Sci.* 68, 492–505.
- Hahn-Hagerdal, B., Galbe, M., Gorwa-Grauslund, M.F., Liden, G., Zacchi, G., 2006. Bio-ethanol: the fuel of tomorrow from the residues of today. *Trends Biotechnol.* 24, 549–556.
- Han, Y.M., Wang, R.Z., Dai, Y.J., 2009. Thermal stratification within the water tank. *Renew. Sustain. Energy Rev.* 13, 1014–1026.
- Hasunuma, T., Kondo, A., 2012. Consolidated bioprocessing and simultaneous saccharification and fermentation of lignocellulose to ethanol with thermotolerant yeast strains. *Process Biochem.* 47, 1287–1294.
- Hoekman, S.K., 2009. Biofuels in the U.S. – Challenges and Opportunities. *Renew. Energy* 34, 14–22.
- Holtbruegge, J., Wierschem, M., Steinruecken, S., Voss, D., Parhomenko, L., Lutze, P., 2013. Experimental investigation, modeling and scale-up of hydrophilic vapor permeation membranes: Separation of azeotropic dimethyl carbonate/methanol mixtures. *Sep. Purif. Technol.* 118, 862–878.
- Holtzapple, M., Cognata, M., Shu, Y., Hendrickson, C., 1990. Inhibition of *Trichoderma reesei* cellulase by sugars and solvents. *Biotechnol. Bioeng.* 36, 275–287.
- Huang, C.-F., Lin, T.-H., Guo, G.-L., Hwang, W.-S., 2009. Enhanced ethanol production by fermentation of rice straw hydrolysate without detoxification using a newly adapted strain of *Pichia stipitis*. *Bioresour. Technol.* 100, 3914–3920.
- Huang, H.-J., Ramaswamy, S., Al-Dajani, W., Tschirner, U., Cairncross, R.A., 2009. Effect of biomass species and plant size on cellulosic ethanol: A comparative

- process and economic analysis. *Biomass and Bioenergy* 33, 234–246.
- Huang, Z., Guan, H., lee Tan, W., Qiao, X.-Y., Kulprathipanja, S., 2006. Pervaporation study of aqueous ethanol solution through zeolite-incorporated multilayer poly(vinyl alcohol) membranes: Effect of zeolites. *J. Memb. Sci.* 276, 260–271.
- Incauca, 2016. Incauca S.A. Alcohol carburante [WWW Document].
- Infochem, 2013. Multiflash.
- Ishola, M., Jahandideh, A., Haidarian, B., Brandberg, T., Taherzadeh, M., 2013. Simultaneous saccharification, filtration and fermentation (SSFF): A novel method for bioethanol production from lignocellulosic biomass. *Bioresour. Technol.* 133, 68–73.
- Jackson de Moraes Rocha, G., Martin, C., Soares, I.B., Souto Maior, A.M., Baudel, H.M., Moraes de Abreu, C.A., 2011. Dilute mixed-acid pretreatment of sugarcane bagasse for ethanol production. *Biomass and Bioenergy* 35, 663–670.
- Jamai, L., Ettayebi, K., Yamani, J.E., Ettayebi, M., 2007. Production of ethanol from starch by free and immobilized *Candida tropicalis* in the presence of amylase. *Bioresour. Technol.* 98, 2765–2770.
- Jeon, Y.J., Svenson, C.J., Joachimsthal, E.L., Rogers, P.L., 2002. Kinetic analysis of ethanol production by an acetate-resistant strain of recombinant *Zymomonas mobilis*. *Biotechnol. Lett.* 24, 819–824.
- Jervis, E.J., Haynes, C.A., Kilburn, D.G., 1997. Surface Diffusion of Cellulases and Their Isolated Binding Domains on Cellulose. *J. Biol. Chem.* 272, 24016–24023.
- Ji, X.J., Huang, H., Du, J., Zhu, J.G., Ren, L.J., Li, S., Nie, Z.K., 2009. Development of an industrial medium for economical 2,3-butanediol production through co-fermentation of glucose and xylose by *Klebsiella oxytoca*. *Bioresour. Technol.* 100, 5214–5218.
- Jin, M., Gunawan, C., Balan, V., Lau, M.W., Dale, B.E., 2012. Simultaneous saccharification and co-fermentation (SSCF) of AFEX(TM) pretreated corn stover for ethanol production using commercial enzymes and *Saccharomyces*

- cerevisiae* 424A(LNH-ST). *Bioresour. Technol.* 110, 587–94.
- Jin, M., Lau, M.W., Balan, V., Dale, B.E., 2010. Two-step SSCF to convert AFEX-treated switchgrass to ethanol using commercial enzymes and *Saccharomyces cerevisiae* 424A(LNH-ST). *Bioresour. Technol.* 101, 8171–8.
- Jung, Y.H., Kim, I.J., Kim, H.K., Kim, K.H., 2013. Dilute acid pretreatment of lignocellulose for whole slurry ethanol fermentation. *Bioresour. Technol.* 132, 109–14.
- Kadam, K.L., Forrest, L.H., Jacobson, W.A., 2000. Rice straw as a lignocellulosic resource: collection, processing, transportation, and environmental aspects. *Biomass and Bioenergy* 18, 369–389.
- Kadam, K.L., Rydholm, E.C., McMillan, J.D., 2004. Development and Validation of a Kinetic Model for Enzymatic Saccharification of Lignocellulosic Biomass. *Biotechnol. Prog.* 20, 698–705.
- Kadar, Z., Szengyel, Z., Reczey, K., 2004. Simultaneous saccharification and fermentation (SSF) of industrial wastes for the production of ethanol. *Ind. Crops Prod.* 20, 103–110.
- Kamath, R.S., Grossmann, I.E., Biegler, L.T., 2010. Aggregate models based on improved group methods for simulation and optimization of distillation systems. *Comput. Chem. Eng.* 34, 1312–1319.
- Karimi, K., Emtiazi, G., Taherzadeh, M.J., 2006. Production of ethanol and mycelial biomass from rice straw hemicellulose hydrolyzate by *Mucor indicus*. *Process Biochem.* 41, 653–658.
- Karimi, K., Emtiazi, G., Taherzadeh, M.J., 2006. Ethanol production from dilute-acid pretreated rice straw by simultaneous saccharification and fermentation with *Mucor indicus*, *Rhizopus oryzae*, and *Saccharomyces cerevisiae*. *Enzyme Microb. Technol.* 40, 138–144.
- Karlsson, H., Barjesson, P., Hansson, P., Ahlgren, S., 2014. Ethanol production in biorefineries using lignocellulosic feedstock-GHG performance, energy balance and implications of life cycle calculation methodology. *J. Clean. Prod.* 83, 420–427.

- Kim, Y., Hendrickson, R., Mosier, N.S., Ladisch, M.R., Bals, B., Balan, V., Dale, B.E., 2008. Enzyme hydrolysis and ethanol fermentation of liquid hot water and {AFEX} pretreated distillers' grains at high-solids loadings. *Bioresour. Technol.* 99, 5206–5215.
- Kiran, B., Jana, A.K., 2015. A hybrid heat integration scheme for bioethanol separation through pressure-swing distillation route. *Sep. Purif. Technol.* 142, 307–315.
- Kiss, A.A., Ignat, R.M., 2012. Innovative single step bioethanol dehydration in an extractive dividing-wall column. *Sep. Purif. Technol.* 98, 290–297.
- Kiss, A.A., Olujic, Z., 2014. A review on process intensification in internally heat-integrated distillation columns. *Chem. Eng. Process. Process Intensif.* 86, 125–144.
- Kiss, A.A., Suszwalak, D.J.-. P.C., 2012. Enhanced bioethanol dehydration by extractive and azeotropic distillation in dividing-wall columns. *Sep. Purif. Technol.* 86, 70–78.
- Klasson, K.T., Dien, B.S., Hector, R.E., 2013. Simultaneous detoxification, saccharification, and ethanol fermentation of weak-acid hydrolyzates. *Ind. Crops Prod.* 49, 292–298.
- Knapp, J.P., Doherty, M.F., 1992. A new pressure-swing-distillation process for separating homogeneous azeotropic mixtures. *Ind. Eng. Chem. Res.* 31, 346–357.
- Knopf, F.C., Okos, M.R., Reklaitis, G. V., 1982. Optimal design of batch/semicontinuous processes. *Ind. Eng. Chem. Process Des. Dev.* 21, 79–86.
- Koch, K., Gorak, A., 2014. Pervaporation of binary and ternary mixtures of acetone, isopropyl alcohol and water using polymeric membranes: Experimental characterisation and modelling. *Chem. Eng. Sci.* 115, 95–114.
- Koch, K., Sudhoff, D., Kreiß, S., Górak, A., Kreis, P., 2013. Optimisation-based design method for membrane-assisted separation processes. *Chem. Eng. Process. Process Intensif.* 67, 2–15.
- Koizumi, T., 2015. Biofuels and food security. *Renew. Sustain. Energy Rev.* 52,

829–841.

- Koltuniewicz, A., 2010. 4.05 - Integrated Membrane Operations in Various Industrial Sectors, in: Drioli, E., Giorno, L. (Eds.), *Comprehensive Membrane Science and Engineering*. Elsevier, Oxford, pp. 109–164.
- Kookos, I.K., 2003. Optimal Design of Membrane/Distillation Column Hybrid Processes. *Ind. Eng. Chem. Res.* 42, 1731–1738.
- Kravanja, P., Modarresi, A., Friedl, A., 2013. Heat integration of biochemical ethanol production from straw – A case study. *Appl. Energy* 102, 32–43.
- Kreis, P., Górak, A., 2006. Process Analysis of Hybrid Separation Processes. *Chem. Eng. Res. Des.* 84, 595–600.
- Krishnan, M., Ho, N., Tsao, G., 1999. Fermentation kinetics of ethanol production from glucose and xylose by recombinant *Saccharomyces 1400*(pLNH33). *Appl. Biochem. Biotechnol.* 78, 373–388.
- Krummenacher, P., 2002. Contribution to the heat integration of batch processes (with or without heat storage). *École polytechnique fédérale de Lausanne*.
- Kumar, P., Barrett, D.M., Delwiche, M.J., Stroeve, P., 2009. Methods for Pretreatment of Lignocellulosic Biomass for Efficient Hydrolysis and Biofuel Production. *Ind. Eng. Chem. Res.* 48, 3713–3729.
- Kumar, R., Wyman, C.E., 2008. An improved method to directly estimate cellulase adsorption on biomass solids. *Enzyme Microb. Technol.* 42, 426–433.
- Kunnakorn, D., Rirksomboon, T., Siemanond, K., Aungkavattana, P., Kuanchertchoo, N., Chuntanalerg, P., Hemra, K., Kulprathipanja, S., James, R.B., Wongkasemjit, S., 2013. Techno-economic comparison of energy usage between azeotropic distillation and hybrid system for water–ethanol separation. *Renew. Energy* 51, 310–316.
- Larran, A., Jozami, E., Vicario, L., Feldman, S.R., Podestá, F.E., Permingeat, H.R., 2015. Evaluation of biological pretreatments to increase the efficiency of the saccharification process using *Spartina argentinensis* as a biomass resource. *Bioresour. Technol.* 194, 320–5.
- Le, Q.-K., Halvorsen, I.J., Pajalic, O., Skogestad, S., 2015. Dividing wall columns

- for heterogeneous azeotropic distillation. *Chem. Eng. Res. Des.* 99, 111–119.
- Lee, H.J., Cho, E.J., Kim, Y.G., Choi, I.S., Bae, H.J., 2012. Pervaporative separation of bioethanol using a polydimethylsiloxane/polyetherimide composite hollow-fiber membrane. *Bioresour. Technol.* 109, 110–115.
- Leksawasdi, N., Joachimsthal, E., Rogers, P., 2001. Mathematical modelling of ethanol production from glucose/xylose mixtures by recombinant *Zymomonas mobilis*. *Biotechnol. Lett.* 23, 1087–1093.
- Lienhard, J.H., 2010. *Heat Transfer*. J. Heat Transfer, McGraw-Hill Higher Education 82, 198.
- Liguori, R., Ventrino, V., Pepe, O., Faraco, V., 2015. Bioreactors for lignocellulose conversion into fermentable sugars for production of high added value products. *Appl. Microbiol. Biotechnol.* 100, 597–611.
- Liu, L., Du, J., El-Halwagi, M.M., Ponce-Ortega, J.M., Yao, P., 2013. A systematic approach for synthesizing combined mass and heat exchange networks. *Comput. Chem. Eng.* 53, 1–13.
- Liu, Z.-H., Chen, H.-Z., 2016. Simultaneous saccharification and co-fermentation for improving the xylose utilization of steam exploded corn stover at high solid loading. *Bioresour. Technol.* 201, 15–26.
- Lutze, P., Gorak, A., 2013. Reactive and membrane-assisted distillation: Recent developments and perspective. *Chem. Eng. Res. Des.* 91, 1978–1997.
- Luyben, W.L., 2006. Distillation Economic Optimization, in: *Distillation Design and Control Using Aspen™ Simulation*. John Wiley & Sons, Inc., pp. 85–97.
- Mabee, W.E., McFarlane, P.N., Saddler, J.N., 2011. Biomass availability for lignocellulosic ethanol production. *Biomass and Bioenergy* 35, 4519–4529.
- Marriott, J., Sorensen, E., 2003. A general approach to modelling membrane modules. *Chem. Eng. Sci.* 58, 4975–4990.
- Marriott, J., Sørensen, E., 2003. The optimal design of membrane systems. *Chem. Eng. Sci.* 58, 4991–5004.
- Marriott, J.I., Sørensen, E., Bogle, I.D.L., 2001. Detailed mathematical modelling of membrane modules. *Comput. Chem. Eng.* 25, 693–700.

- Martinez, R., Sanz, M.T., Beltran, S., 2013. Concentration by pervaporation of brown crab volatile compounds from dilute model solutions: Evaluation of PDMS membrane. *J. Memb. Sci.* 428, 371–379.
- Mawire, A., Phori, A., Taole, S., 2014. Performance comparison of thermal energy storage oils for solar cookers during charging. *Appl. Therm. Eng.* 73, 1323–1331.
- Mielenz, J.R., Bardsley, J.S., Wyman, C.E., 2009. Fermentation of soybean hulls to ethanol while preserving protein value. *Bioresour. Technol.* 100, 3532–3539.
- Modarresi, A., Kravanja, P., Friedl, A., 2012. Pinch and exergy analysis of lignocellulosic ethanol, biomethane, heat and power production from straw. *Appl. Therm. Eng.* 43, 20–28.
- Mohagheghi, A., Ruth, M., Shell, D.J., 2006. Conditioning hemicellulose hydrolysates for fermentation: Effects of overliming pH on sugar and ethanol yields. *Process Biochem.* 41, 1806–1811.
- Morales-Rodriguez, R., Meyer, A.S., Gernaey, K. V., Sin, G., 2012. A framework for model-based optimization of bioprocesses under uncertainty: Lignocellulosic ethanol production case. *Comput. Chem. Eng.* 42, 115–129.
- Morales-Rodriguez, R., Meyer, A.S., Gernaey, K. V., Sin, G., 2011. Dynamic model-based evaluation of process configurations for integrated operation of hydrolysis and co-fermentation for bioethanol production from lignocellulose. *Bioresour. Technol.* 102, 1174–1184.
- Moreno, A., Tomas-Pejo, E., Ibarra, D., Ballesteros, M., Olsson, L., 2013. Fed-batch SSCF using steam-exploded wheat straw at high dry matter consistencies and a xylose-fermenting *Saccharomyces cerevisiae* strain: effect of laccase supplementation. *Biotechnol. Biofuels* 6, 1–10.
- Moreno, A.D., Tomás-Pejó, E., Ibarra, D., Ballesteros, M., Olsson, L., 2013. In situ laccase treatment enhances the fermentability of steam-exploded wheat straw in SSCF processes at high dry matter consistencies. *Bioresour. Technol.* 143, 337–43.
- Mosier, N., Wyman, C., Dale, B., Elander, R., Lee, Y.Y., Holtzapple, M., Ladisch, M., 2005. Features of promising technologies for pretreatment of lignocellulosic

- biomass. *Bioresour. Technol.* 96, 673–686.
- Mulakala, C., Reilly, P.J., 2005. Hypocrea jecorina (*Trichoderma reesei*) Cel7A as a molecular machine: A docking study. *Proteins Struct. Funct. Bioinforma.* 60, 598–605.
- Nagasawa, H., Matsuda, N., Kanezashi, M., Yoshioka, T., Tsuru, T., 2016. Pervaporation and vapor permeation characteristics of BTESE-derived organosilica membranes and their long-term stability in a high-water-content IPA/water mixture. *J. Memb. Sci.* 498, 336–344.
- Najafpour, G.D., Shan, C.P., 2003. Enzymatic hydrolysis of molasses. *Bioresour. Technol.* 86, 91–94.
- Niemisto, J., Kujawski, W., Keiski, R.L., 2013. Pervaporation performance of composite poly(dimethyl siloxane) membrane for butanol recovery from model solutions. *J. Memb. Sci.* 434, 55–64.
- Nigam, J.N., 2001. Ethanol production from wheat straw hemicellulose hydrolysate by *Pichia stipitis*. *J. Biotechnol.* 87, 17–27.
- Niu, H., Shah, N., Kontoravdi, C., 2016. Modelling of amorphous cellulose depolymerisation by cellulases, parametric studies and optimisation. *Biochem. Eng. J.* 105, 455–472.
- Nouredini, H., Byun, J., 2010. Dilute-acid pretreatment of distillers' grains and corn fiber. *Bioresour. Technol.* 101, 1060–1067.
- O'Brien, D.J., Senske, G.E., Kurantz, M.J., Craig, J.C., 2004. Ethanol recovery from corn fiber hydrolysate fermentations by pervaporation. *Bioresour. Technol.* 92, 15–19.
- Öhgren, K., Bura, R., Lesnicki, G., Saddler, J., Zacchi, G., 2007a. A comparison between simultaneous saccharification and fermentation and separate hydrolysis and fermentation using steam-pretreated corn stover. *Process Biochem.* 42, 834–839.
- Öhgren, K., Bura, R., Lesnicki, G., Saddler, J., Zacchi, G., 2007b. A comparison between simultaneous saccharification and fermentation and separate hydrolysis and fermentation using steam-pretreated corn stover. *Process Biochem.* 42,

834–839.

- Okoli, C.O., Adams, T.A., 2015. Design of dividing wall columns for butanol recovery in a thermochemical biomass to butanol process. *Chem. Eng. Process. Process Intensif.* 95, 302–316.
- Olofsson, K., Rudolf, A., Liden, G., 2008. Designing simultaneous saccharification and fermentation for improved xylose conversion by a recombinant strain of *Saccharomyces cerevisiae*. *J. Biotechnol.* 134, 112–120.
- Olujic, Ž., Sun, L., de Rijke, A., Jansens, P.J., 2006. Conceptual design of an internally heat integrated propylene-propane splitter. *Energy* 31, 3083–3096.
- Palmarola-Adrados, B., Choteborska, P., Galbe, M., Zacchi, G., 2005. Ethanol production from non-starch carbohydrates of wheat bran. *Bioresour. Technol.* 96, 843–850.
- Palmqvist, E., Hahn-Hagerdal, B., 2000a. Fermentation of lignocellulosic hydrolysates. II: inhibitors and mechanisms of inhibition. *Bioresour. Technol.* 74, 25–33.
- Palmqvist, E., Hahn-Hagerdal, B., 2000b. Fermentation of lignocellulosic hydrolysates. I: inhibition and detoxification. *Bioresour. Technol.* 74, 17–24.
- Patle, S., Lal, B., 2008. Investigation of the potential of agro-industrial material as low cost substrate for ethanol production by using *Candida tropicalis* and *Zymomonas mobilis*. *Biomass and Bioenergy* 32, 596–602.
- Peters, M.S., Timmerhaus, K.D., West, R.E., 2003. Profitability, alternative investments, and replacements, in: *Plant Design and Economics for Chemical Engineers*. Mc Graw Hill, pp. 324–330.
- Pettersson, A., Thomsen, M.H., Hauggaard-Nielsen, H., Thomsen, A.B., 2007. Potential bioethanol and biogas production using lignocellulosic biomass from winter rye, oilseed rape and faba bean. *Biomass and Bioenergy* 31, 812–819.
- Petrobras, 2016. Ethanol plants [WWW Document].
- Phisalaphong, M., Srirattana, N., Tanthapanichakoon, W., 2006. Mathematical modeling to investigate temperature effect on kinetic parameters of ethanol fermentation. *Biochem. Eng. J.* 28, 36–43.

- Pohlmeier, J., Rix, A., 1996. Interactive plant and control design of a double-effect distillation column. *Comput. Chem. Eng.* 20, 395–400.
- Prasad, S., Singh, A., Joshi, H.C., 2007. Ethanol as an alternative fuel from agricultural, industrial and urban residues. *Resour. Conserv. Recycl.* 50, 1–39.
- Process System Enterprises, 2015. gPROMS.
- Purwadi, R., Niklasson, C., Taherzadeh, M.J., 2004. Kinetic study of detoxification of dilute-acid hydrolyzates by Ca(OH)₂. *J. Biotechnol.* 114, 187–198.
- Rajkumar, P., Shankar, R., Srinivas, T., 2015. Economic analysis of solar collector with different thermic fluids of LiBr-water vapour absorption refrigeration system. *Int. J. Appl. Eng. Res.* 10, 1673–1675.
- Raman, S., Mohr, A., Helliwell, R., Ribeiro, B., Shortall, O., Smith, R., Millar, K., 2015. Integrating social and value dimensions into sustainability assessment of lignocellulosic biofuels. *Biomass and Bioenergy*.
- Ranjan, R., Thust, S., Gounaris, C.E., Woo, M., Floudas, C.A., Keitz, M. V, Valentas, K.J., Wei, J., Tsapatsis, M., 2009. Adsorption of fermentation inhibitors from lignocellulosic biomass hydrolyzates for improved ethanol yield and value-added product recovery. *Microporous Mesoporous Mater.* 122, 143–148.
- Rašković, P., Anastasovski, A., Markovska, L., Meško, V., 2010. Process integration in bioprocess industry: waste heat recovery in yeast and ethyl alcohol plant. *Energy* 35, 704–717.
- Rasmussen, M.L., Shrestha, P., Khanal, S.K., III, A.L.P., van Leeuwen, J. (Hans), 2010. Sequential saccharification of corn fiber and ethanol production by the brown rot fungus *Gloeophyllum trabeum*. *Bioresour. Technol.* 101, 3526–3533.
- Rattanachomsri, U., Tanapongpipat, S., Eurwilaichitr, L., Champreda, V., 2009. Simultaneous non-thermal saccharification of cassava pulp by multi-enzyme activity and ethanol fermentation by *Candida tropicalis*. *J. Biosci. Bioeng.* 107, 488–493.
- Reijnders, L., 2006. Conditions for the sustainability of biomass based fuel use. *Energy Policy* 34, 863–876.

- RESTEK, 2016. GC columns: Installation guide.
- Rivera, E.C., Costa, A.C., Atala, D.I.P., Maugeri, F., Maciel, M.R.W., Filho, R.M., 2006. Evaluation of optimization techniques for parameter estimation: Application to ethanol fermentation considering the effect of temperature. *Process Biochem.* 41, 1682–1687.
- Roberts, J.D., Caseiro, M.C., 1977. *Basic principles of organic chemistry*, Second. ed. W. A. Benjamin, Inc.
- Rocha, G.J.M., Gonçalves, A.R., Nakanishi, S.C., Nascimento, V.M., Silva, V.F.N., 2015. Pilot scale steam explosion and diluted sulfuric acid pretreatments: Comparative study aiming the sugarcane bagasse saccharification. *Ind. Crops Prod.* 74, 810–816.
- Rodera, H., Bagajewicz, M.J., 2001. Multipurpose Heat-Exchanger Networks for Heat Integration Across Plants. *Ind. Eng. Chem. Res.* 40, 5585–5603.
- Romaní, A., Pereira, F., Johansson, B., Domingues, L., 2015. Metabolic engineering of *Saccharomyces cerevisiae* ethanol strains PE-2 and CAT-1 for efficient lignocellulosic fermentation. *Bioresour. Technol.* 179, 150–8.
- Romero, I., Sanchez, S., Moya, M., Castro, E., Ruiz, E., Bravo, V., 2007. Fermentation of olive tree pruning acid-hydrolysates by *Pachysolen tannophilus*. *Biochem. Eng. J.* 36, 108–115.
- Roth, T., Kreis, P., Gorak, A., 2013. Process analysis and optimisation of hybrid processes for the dehydration of ethanol. *Chem. Eng. Res. Des.* 91, 1171–1185.
- Saha, B.C., Cotta, M.A., 2008. Lime pretreatment, enzymatic saccharification and fermentation of rice hulls to ethanol. *Biomass and Bioenergy* 32, 971–977.
- Saha, B.C., Cotta, M.A., 2007. Enzymatic saccharification and fermentation of alkaline peroxide pretreated rice hulls to ethanol. *Enzyme Microb. Technol.* 41, 528–532.
- Saha, B.C., Iten, L.B., Cotta, M.A., Wu, Y. V, 2005. Dilute acid pretreatment, enzymatic saccharification and fermentation of wheat straw to ethanol. *Process Biochem.* 40, 3693–3700.
- Saini, J.K., Anurag, R.K., Arya, A., Kumbhar, B.K., Tewari, L., 2013. Optimization

- of saccharification of sweet sorghum bagasse using response surface methodology. *Ind. Crops Prod.* 44, 211–219.
- Sanchez, O.J., Cardona, C.A., 2005. Produccion biotecnologica de alcohol carburante I: obtencion a partir de diferentes materias primas. *Interciencia* 30, 671–678.
- Sánchez, Ó.J., Cardona, C.A., 2012. Conceptual design of cost-effective and environmentally-friendly configurations for fuel ethanol production from sugarcane by knowledge-based process synthesis. *Bioresour. Technol.* 104, 305–314.
- Sanchez, S., Bravo, V., Moya, A.J., Castro, E., Camacho, F., 2004. Influence of temperature on the fermentation of d-xylose by *Pachysolen tannophilus* to produce ethanol and xylitol. *Process Biochem.* 39, 673–679.
- Sander, U., Janssen, H., 1991. Industrial application of vapour permeation. *J. Memb. Sci.* 61, 113–129.
- Sander, U., Soukup, P., 1988. Design and operation of a pervaporation plant for ethanol dehydration. *J. Memb. Sci.* 36, 463–475.
- Sasaki, K., Tsuge, Y., Sasaki, D., Teramura, H., Inokuma, K., Hasunuma, T., Ogino, C., Kondo, A., 2015. Mechanical milling and membrane separation for increased ethanol production during simultaneous saccharification and co-fermentation of rice straw by xylose-fermenting *Saccharomyces cerevisiae*. *Bioresour. Technol.* 185, 263–8.
- Sassner, P., Galbe, M., Zacchi, G., 2006. Bioethanol production based on simultaneous saccharification and fermentation of steam-pretreated *Salix* at high dry-matter content. *Enzyme Microb. Technol.* 39, 756–762.
- Sassner, P., Mårtensson, C.-G., Galbe, M., Zacchi, G., 2008. Steam pretreatment of H₂SO₄-impregnated *Salix* for the production of bioethanol. *Bioresour. Technol.* 99, 137–145.
- Saxena, R.C., Adhikari, D.K., Goyal, H.B., 2009. Biomass-based energy fuel through biochemical routes: A review. *Renew. Sustain. Energy Rev.* 13, 167–178.
- Schröder, J., Gawron, K., 1981. Latent heat storage. *Int. J. Energy Res.* 5, 103–109.

- Sciacovelli, A., Gagliardi, F., Verda, V., 2015. Maximization of performance of a PCM latent heat storage system with innovative fins. *Appl. Energy* 137, 707–715.
- Serrano-López, R., Fradera, J., Cuesta-López, S., 2013a. Molten salts database for energy applications. *Chem. Eng. Process. Process Intensif.* 73, 87–102.
- Serrano-López, R., Fradera, J., Cuesta-López, S., 2013b. Molten salts database for energy applications. *Chem. Eng. Process. Process Intensif.* 73, 87–102.
- Setlhaku, M., Heitmann, S., Gorak, A., Wichmann, R., 2013. Investigation of gas stripping and pervaporation for improved feasibility of two-stage butanol production process. *Bioresour. Technol.* 136, 102–108.
- Shuai, L., Yang, Q., Zhu, J.Y., Lu, F.C., Weimer, P.J., Ralph, J., Pan, X.J., 2010. Comparative study of SPORL and dilute-acid pretreatments of spruce for cellulosic ethanol production. *Bioresour. Technol.* 101, 3106–14.
- Siqueira, P.F., Karp, S.G., Carvalho, J.C., Sturm, W., Rodriguez-Leon, J.A., Tholozan, J.L., Singhania, R.R., Pandey, A., Soccol, C.R., 2008. Production of bio-ethanol from soybean molasses by *Saccharomyces cerevisiae* at laboratory, pilot and industrial scales. *Bioresour. Technol.* 99, 8156–8163.
- Sreenath, H.K., Jeffries, T.W., 2000. Production of ethanol from wood hydrolyzate by yeasts. *Bioresour. Technol.* 72, 253–260.
- Sreenath, H.K., Koegel, R.G., Moldes, A.B., Jeffries, T.W., Straub, R.J., 2001. Ethanol production from alfalfa fiber fractions by saccharification and fermentation. *Process Biochem.* 36, 1199–1204.
- Streitwieser, A., Heathcock, C.H., 1976. *Introduction to organic chemistry.* Macmillan.
- Stuart, P.R., El-Halwagi, M.M., 2012a. *Integrated Biorefineries: Design, Analysis, and Optimization.* CRC Press.
- Stuart, P.R., El-Halwagi, M.M., 2012b. *Integrated Biorefineries: Design, Analysis, and Optimization.*
- Su, R., Ma, Y., Qi, W., Zhang, M., Wang, F., Du, R., Yang, J., Zhang, M., He, Z., 2012. Ethanol Production from High-Solid SSCF of Alkaline-Pretreated

- Corncob Using Recombinant *Zymomonas mobilis* CP4. *BioEnergy Res.* 6, 292–299.
- Su, Y., Zhang, P., Su, Y., 2015. An overview of biofuels policies and industrialization in the major biofuel producing countries. *Renew. Sustain. Energy Rev.* 50, 991–1003.
- Sudhoff, D., Leimbrink, M., Schleinitz, M., Górak, A., Lutze, P., 2015. Modelling, design and flexibility analysis of rotating packed beds for distillation. *Chem. Eng. Res. Des.* 94, 72–89.
- Sukumaran, R.K., Singhanian, R.R., Mathew, G.M., Pandey, A., 2009. Cellulase production using biomass feed stock and its application in lignocellulose saccharification for bio-ethanol production. *Renew. Energy* 34, 421–424.
- Sulzer Chemtech, 2014. Membrane Technology [WWW Document].
- Swain, M.R., Krishnan, C., 2015. Improved conversion of rice straw to ethanol and xylitol by combination of moderate temperature ammonia pretreatment and sequential fermentation using *Candida tropicalis*. *Ind. Crops Prod.* 77, 1039–1046.
- Szitkai, Z., Lelkes, Z., Rev, E., Fonyo, Z., 2002. Optimization of hybrid ethanol dehydration systems. *Chem. Eng. Process. Process Intensif.* 41, 631–646.
- Tang, Y.Q., Koike, Y., Liu, K., An, M.Z., Morimura, S., Wu, X.L., Kida, K., 2008. Ethanol production from kitchen waste using the flocculating yeast *Saccharomyces cerevisiae* strain KF-7. *Biomass and Bioenergy* 32, 1037–1045.
- Teh, Y.S., Rangaiah, G.P., 2003. Tabu search for global optimization of continuous functions with application to phase equilibrium calculations. *Comput. Chem. Eng.* 27, 1665–1679.
- Telli-Okur, M., Eken-Saracoglu, N., 2008. Fermentation of sunflower seed hull hydrolysate to ethanol by *Pichia stipitis*. *Bioresour. Technol.* 99, 2162–2169.
- Tian, S., Zhou, G., Yan, F., Yu, Y., Yang, X., 2009. Yeast strains for ethanol production from lignocellulosic hydrolysates during in situ detoxification. *Biotechnol. Adv.* 27, 656–660.
- Toth, A.J., Mizsey, P., 2015. Methanol removal from aqueous mixture with

- organophilic pervaporation: experiments and modelling. *Chem. Eng. Res. Des.*
- Towler, G., Sinnott, R., 2013. Chapter 17 - Separation Columns (Distillation, Absorption, and Extraction), in: Towler, G., Sinnott, R. (Eds.), *Chemical Engineering Design (Second Edition)*. Butterworth-Heinemann, Boston, pp. 807–935.
- Triana, C.F., Fraga, E.S., Sorensen, E., 2015a. Energy assessment of different configurations for the ethanol production process from lignocellulosic biomass, in: *Computer Aided Chemical Engineering*. pp. 2285–2290.
- Triana, C.F., Fraga, E.S., Sorensen, E., 2015b. 12th International Symposium on Process Systems Engineering and 25th European Symposium on Computer Aided Process Engineering, *Computer Aided Chemical Engineering, Computer Aided Chemical Engineering*. Elsevier.
- Triana, C.F., Quintero, J.A., Agudelo, R.A., Cardona, C.A., Higuera, J.C., 2011. Analysis of coffee cut-stems (CCS) as raw material for fuel ethanol production. *Energy* 36, 4182–4190.
- Tsuyumoto, M., Akita, K., Teramoto, A., 1995. Pervaporative transport of aqueous ethanol: Dependence of permeation rates on ethanol concentration and permeate side pressures. *Desalination* 103, 211–222.
- Tsuyumoto, M., Teramoto, A., Mearns, P., 1997. Dehydration of ethanol on a pilot-plant scale, using a new type of hollow-fiber membrane. *J. Memb. Sci.* 133, 83–94.
- Tusel, G.F., Bruschke, H.E.A., 1985. Use of pervaporation systems in the chemical industry. *Desalination* 53, 327–338.
- U.S. Department of Energy, 2015. *International Energy Statistics* [WWW Document].
- Vaklieva-Bancheva, N., Ivanov, B.B., Shah, N., Pantelides, C.C., 1996. Heat exchanger network design for multipurpose batch plants. *Comput. Chem. Eng.* 20, 989–1001.
- Valentinyi, N., Csefalvai, E., Mizsey, P., 2013. Modelling of pervaporation: Parameter estimation and model development. *Chem. Eng. Res. Des.* 91, 174–

183.

- Vanderbei, R.J., 2010. Linear programming: foundations and extensions, Third Edit. ed. Springer.
- Vane, L.M., Alvarez, F.R., Rosenblum, L., Govindaswamy, S., 2013. Efficient Ethanol Recovery from Yeast Fermentation Broth with Integrated Distillation–Membrane Process. *Ind. Eng. Chem. Res.* 52, 1033–1041.
- Veses, A., Aznar, M., Callén, M.S., Murillo, R., García, T., 2016. An integrated process for the production of lignocellulosic biomass pyrolysis oils using calcined limestone as a heat carrier with catalytic properties. *Fuel* 181, 430–437.
- Vignarooban, K., Xu, X., Arvay, A., Hsu, K., Kannan, A.M., 2015. Heat transfer fluids for concentrating solar power systems – A review. *Appl. Energy* 146, 383–396.
- Viswanathan, J., Grossmann, I.E., 1993. Optimal feed locations and number of trays for distillation columns with multiple feeds. *Ind. Eng. Chem. Res.* 32, 2942–2949.
- Viswanathan, J., Grossmann, I.E., 1993. An alternate {MINLP} model for finding the number of trays required for a specified separation objective. *Comput. Chem. Eng.* 17, 949–955.
- Viswanathan, J., Grossmann, I.E., 1990. A combined penalty function and outer-approximation method for {MINLP} optimization. *Comput. Chem. Eng.* 14, 769–782.
- Wang, Y., Chang, C., Feng, X., 2015. A systematic framework for multi-plants Heat Integration combining Direct and Indirect Heat Integration methods. *Energy* 90, 56–67.
- Wei, H.-M., Wang, F., Zhang, J.-L., Liao, B., Zhao, N., Xiao, F., Wei, W., Sun, Y.-H., 2013. Design and Control of Dimethyl Carbonate–Methanol Separation via Pressure-Swing Distillation. *Ind. Eng. Chem. Res.* 52, 11463–11478.
- Wei, P., Cheng, L.H., Zhang, L., Xu, X.H., Chen, H.I., Gao, C.J., 2014. A review of membrane technology for bioethanol production. *Renew. Sustain. Energy Rev.* 30, 388–400.

- Weiguo, X., Depeng, R., Qing, Y., Guodong, L., Huilin, L., Shuai, W., 2016. Simulations and experiments of laminar heat transfer for Therminol heat transfer fluids in a rifled tube. *Appl. Therm. Eng.* 102, 861–872.
- Xiao, Z., Zhang, X., Gregg, D., Saddler, J., 2004. Effects of sugar inhibition on cellulases and glucosidase during enzymatic hydrolysis of softwood substrates. *Appl. Biochem. Biotechnol.* 115, 1115–1126.
- Xie, R., Tu, M., Carvin, J., Wu, Y., 2015. Detoxification of biomass hydrolysates with nucleophilic amino acids enhances alcoholic fermentation. *Bioresour. Technol.* 186, 106–13.
- Xu, J., Cheng, J.J., Sharma-Shivappa, R.R., Burns, J.C., 2010. Lime pretreatment of switchgrass at mild temperatures for ethanol production. *Bioresour. Technol.* 101, 2900–2903.
- Xu, W., Wang, S., Lu, H., Wang, Q., Zhang, Q., Lu, H., 2016. Thermo-hydraulic performance of liquid phase heat transfer fluid (Therminol) in a ribbed tube. *Exp. Therm. Fluid Sci.* 72, 149–160.
- Yakovlev, A. V, Shalygin, M.G., Matson, S.M., Khotimskiy, V.S., Teplyakov, V. V, 2013. Separation of diluted butanol-water solutions via vapor phase by organophilic membranes based on high permeable polyacetylenes. *J. Memb. Sci.* 434, 99–105.
- Yee, T.F., Grossmann, I.E., 1990. Simultaneous optimization models for heat integration—II. Heat exchanger network synthesis. *Comput. Chem. Eng.* 14, 1165–1184.
- Yee, T.F., Grossmann, I.E., Kravanja, Z., 1990a. Simultaneous optimization models for heat integration—I. Area and energy targeting and modeling of multi-stream exchangers. *Comput. Chem. Eng.* 14, 1151–1164.
- Yee, T.F., Grossmann, I.E., Kravanja, Z., 1990b. Simultaneous optimization models for heat integration—III. Process and heat exchanger network optimization. *Comput. Chem. Eng.* 14, 1185–1200.
- Zalba, B., 2003. Review on thermal energy storage with phase change: materials, heat transfer analysis and applications. *Appl. Therm. Eng.* 23, 251–283.

- Zaversky, F., García-Barberena, J., Sánchez, M., Astrain, D., 2013. Transient molten salt two-tank thermal storage modeling for CSP performance simulations. *Sol. Energy* 93, 294–311.
- Zeigarnik, Y., 2011. Liquid-Metal Heat Transfer. *Thermopedia*.
- Zhang, J., Xiongjun, S., Lynd, L.R., 2009. Simultaneous saccharification and co-fermentation of paper sludge to ethanol by *Saccharomyces cerevisiae* RWB222. Part II: Investigation of discrepancies between predicted and observed performance at high solids concentration. *Biotechnol. Bioeng.* 104, 932–938.
- Zhang, P., Ma, F., Xiao, X., 2016. Thermal energy storage and retrieval characteristics of a molten-salt latent heat thermal energy storage system. *Appl. Energy* 173, 255–271.
- Zhang, X., Wenjuan, Q., Michael, G.P., Saddler, J.N., 2009. High consistency enzymatic hydrolysis of hardwood substrates. *Bioresour. Technol.* 100, 5890–5897.
- Zhao, L., Zhang, X., Tan, T., 2008. Influence of various glucose/xylose mixtures on ethanol production by *Pachysolen tannophilus*. *Biomass and Bioenergy* 32, 1156–1161.
- Zhu, J.-Q., Qin, L., Li, W.-C., Zhang, J., Bao, J., Huang, Y.-D., Li, B.-Z., Yuan, Y.-J., 2015. Simultaneous saccharification and co-fermentation of dry diluted acid pretreated corn stover at high dry matter loading: Overcoming the inhibitors by non-tolerant yeast. *Bioresour. Technol.* 198, 39–46.
- Zhu, J.Y., Pan, X.J., 2010. Woody biomass pretreatment for cellulosic ethanol production: Technology and energy consumption evaluation. *Bioresour. Technol.* 101, 4992–5002.

NOMENCLATURE

A_{mem}	Membrane area	m^2
A_{fo}	Pre-exponential factor for fast hemicellulose (6.7×10^{16})	min^{-1}
A_{so}	Pre-exponential factor for slow hemicellulose (6.9×10^{19})	min^{-1}
A_{xo}	Pre-exponential factor for xylose (3.7×10^{10})	min^{-1}
C	Real concentration of sulphuric acid in the reactor	-
C_a	Actual concentration of sulphuric acid	-
C_{Cb}	Concentration of cellobiose	g/L
C_{cell}	Concentration of cellulose	g/L
C_{Eth}	Concentration of ethanol	g/L
$C_{Eth,ip,Gl}$	Threshold inhibition conc. of ethanol from glucose	g/L
$C_{Eth,is,Gl}$	Threshold conc. of ethanol from glucose that affects glucose uptake	g/L
$C_{Eth,ix,Gl}$	Threshold conc. of ethanol from xylose that causes inhibition	g/L
$C_{Eth,ip,XY}$	Threshold inhibition conc. of ethanol from xylose	g/L
$C_{Eth,is,XY}$	Threshold conc. of ethanol from xylose that affects xylose uptake	g/L
$C_{Eth,ix,XY}$	Threshold conc. of ethanol from xylose that causes inhibition	g/L
$C_{Eth,mp,Gl}$	Maximum inhibition conc. of ethanol from glucose	g/L
$C_{Eth,mp,XY}$	Maximum inhibition conc. of ethanol from xylose	g/L
$C_{Eth,ms,Gl}$	Maximum conc. of ethanol from glucose that affects glucose uptake	g/L
$C_{Eth,ms,XY}$	Maximum conc. of ethanol from glucose that affects xylose uptake	g/L
$C_{Eth,mx,Gl}$	Maximum conc. of ethanol from glucose that causes inhibition	g/L
$C_{Eth,mx,XY}$	Maximum conc. of ethanol from xylose that causes inhibition	g/L
C_{fur}	Concentration of furfural produced during pretreatment	g/L
C_{Gl}	Concentration of glucose	g/L
C_{hemi}	Total Concentration of hemicellulose	g/L
C_{hemi}^{fast}	Concentration of fast hemicellulose	g/L
C_{hemi}^{slow}	Concentration of slow hemicellulose	g/L
C_p	Concentration of insoluble salts	g/L
C_x	Concentration of cells	g/L
C_{xy}	Concentration of xylose	g/L
C_{ZA}	Concentration of Ca complex	g/L
$C_{Z,0}^N$	Concentration of $Ca(OH)_2$ to neutralise hydrolysates	g/L
DF_i	Gradient of activity through the membrane	Pa
E_i	Activation energy in organophilic membrane	$J mol^{-1} K^{-1}$
E_{fo}	Activation energy for fast hemicellulose conversion	kJ/mol
E_{iB}	Bound concentration of enzymes on the substrate	g/Kg

E_{iF}	Concentration of free enzymes in solution	g/Kg
E_{imax}	Maximum mass of active enzyme/substrate	$kg\ protein/$ $kg\ subst$
E_{iT}	Total enzyme concentration	g/Kg
E_{so}	Activation energy for slow hemicellulose conversion	$J/mole$
E_{xo}	Activation energy for xylose degradation	$J/mole$
F	Feed flow rate	kg/s
H^{liq}	Liquid enthalpy	$J/mole$
H^{vap}	Vapour enthalpy	$J/mole$
H^J	Enthalpy of permeate	$J/mole$
h^{liq}	Liquid enthalpy	J/sec
h^{vap}	Vapour enthalpy	J/sec
J_i	Partial flux of component i	$kg\ m^{-2}\ s^{-1}$
K_{iad}	Dissociation constant for absorption/desorption reaction i	$m^3/kg\ protein$
K_{ij}	Relative volatility	-
$K_{j:inh:k}$	Inhibition constants for the reactions $j = 1, 2, 3; k = cellobiose, glucose, xylose$	g/L
k_i	Reaction rate constants	min^{-1}
L	Liquid flow rate	kg/s
M_i	Liquid holdup of component i	Kg
M_t	Total liquid holdup	Kg
$M\&S$	Marshal and Swift Index	-
P	Pressure	Pa
P_{feed}	Feed pressure in pervaporation	Pa
P_{perm}	Permeate pressure in pervaporation	Pa
P_i^{sat}	Vapour pressure	Pa
Q_C	Heat released in the condenser	J/kg
Q_B	Heat duty in the reboiler	J/kg
Q_i	Permeance of the membrane	$mol\ m^{-2}\ s^{-1}Pa^{-1}$
$Q_{0,i}$	Pre-exponential factor for the evaluation of permeance in the membrane	$mol\ m^{-2}\ s^{-1}Pa^{-1}$
R	Reflux ratio	-
R_B	Boilup ratio	-
r_{bp}	Reaction rate of by-products produced during pretreatment	$g\ L^{-1}\ min^{-1}$
r_{fur}	Reaction rate of furfural	$g\ L^{-1}\ min^{-1}$
r_p	Reaction rate of insoluble salts	$g\ L^{-1}\ min^{-1}$
r_{ZA}	Reaction rate of Ca^{+2} complex	$g\ L^{-1}\ min^{-1}$
r_i	Reaction rates for equation 16 – 28	$g\ L^{-1}\ min^{-1}$
R_S	Substrate reactivity	-
r_{xy}	Reaction rate of xylose	$g\ L^{-1}\ min^{-1}$

u	Specific internal energy	J/kg
U	Internal energy	J
V	Vapour flow rate	kg/s
$W_{feed,i}$	Feed mass fraction in pervaporation	-
X_{ij}	Liquid mass fraction of component i in tray j	-
X_i^{feed}	Feed mole fraction in pervaporation	-
Y_{ij}	Vapour mass fraction of component i in tray j	-

Greek symbols

A	Weighting factor for glucose consumption	-
α_j	Binary variable used in the optimisation of the rectification section of tray j	-
β_j	Binary variable used in the optimisation of the stripping section of tray j	-
γ_i	Activity coefficient of component i in the mixture	-
δ_m	Membrane thickness	m
η	Efficiency of the compressor assumed to be 0.95	-
φ_i^{sat}	Fugacity coefficient of vapour at saturated conditions	-
φ_i^{vap}	Fugacity coefficient of vapour	-

Appendix A – Kinetic models, mass and energy balances for the production of ethanol from corn stover

Abstract

This section presents all the different kinetic models, mass and energy balances used in the simulation of the overall process. The kinetic models have been taken from literature. The modelling of the distillation column presents a Vapour-Liquid Equilibrium approach for the formulation of the mass and energy balances.

A.1. Pretreatment

The model proposed by Esteghlalian et al. (1997) presents a set of reaction rate expressions taking into account the formation of xylose from both fast and slow hemicellulose, and the production of by-products in an in-series reaction.

$$r_{hemi}^{fast} = -k_f C_{hemi}^{fast} \quad \text{Eq. A.1}$$

$$r_{hemi}^{slow} = -k_s C_{hemi}^{slow} \quad \text{Eq. A.2}$$

$$r_{xy} = k_f C_{hemi}^{fast} + k_s C_{hemi}^{slow} - k_x C_{xy} \quad \text{Eq. A.3}$$

$$r_{bp} = k_x C_{xy} \quad \text{Eq. A.4}$$

The initial conditions to solve this set of differential equations are given as the initial concentrations of hemicellulose (fast and slow), cellulose, lignin and other components found in the raw material (g/L). The initial concentration of the products (xylose, furfural and others) is assumed to be zero. The reaction rate constants (k_f , k_s and $k_x \text{ min}^{-1}$) are defined by an Arrhenius-type temperature dependence:

$$k_f = A_{fo} C_a^{1.5} \exp\left(-\frac{E_{fo}}{RT}\right) \quad \text{Eq. A.5}$$

$$k_s = A_{so} C_a^{1.6} \exp\left(-\frac{E_{so}}{RT}\right) \quad \text{Eq. A.6}$$

$$k_x = A_{2o} C_a^{0.5} \exp\left(-\frac{E_{xo}}{RT}\right) \quad \text{Eq. A.7}$$

Eq. A.8 determines the real concentration of sulphuric acid in the system taking into account the neutralising ability of the raw material:

$$C_a = C - (0.1 \text{ Neutralizing ability of the raw material}) \quad \text{Eq. A.8}$$

The mass balance for each component and the energy balance are used to describe the progress of the reaction in terms of operating conditions for the streams involved and the conversion of the reactants. Equations A.9 to A.12 show the mass balance for the components and Eq. A.13 presents the energy balance in the reactor. Figure A.1 presents the schematic of a jacketed reactor on which the mass and energy balances for pretreatment, detoxification and SSCF are based:

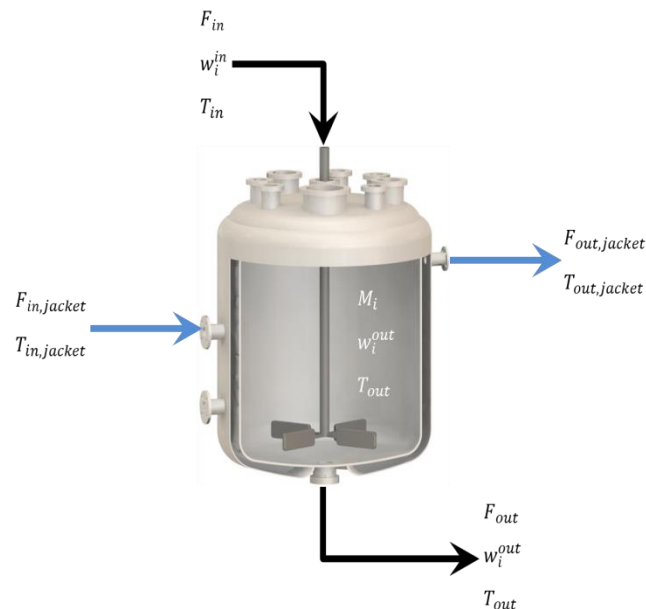


Figure A.1: Scheme of a jacketed reactor used in the formulation of the mass and energy balances

$$\frac{dM_{hemi}}{dt} = F_{in} w_{hemi}^{in} - F_{out} w_{hemi}^{out} - (r_{hemi}^{fast} + r_{hemi}^{slow}) V \quad \text{Eq. A.9}$$

$$M_{hemi} = M_{hemi}^{fast} + M_{hemi}^{slow} \quad \text{Eq. A.10}$$

$$\frac{dM_{xy}}{dt} = F_{in} w_{xy}^{in} - F_{out} w_{xy}^{out} + r_{xy} V \quad \text{Eq. A.11}$$

$$\frac{dM_{bp}}{dt} = F_{in} w_{bp}^{in} - F_{out} w_{bp}^{out} + r_{bp} V \quad \text{Eq. A.12}$$

The energy balance for the pretreatment reactor presents the heat of reaction which is define as the summation of the heat of reactions for equations A.9, A.11 and A.12.

$$\begin{aligned} \frac{dU}{dt} = L_{in} h_{in} - L_{out} h_{out} + \left((r_{hemic} + r_{xy} + r_{bp}) (-\Delta H^R) V \right) \\ + Q_{pret} \end{aligned} \quad \text{Eq. A.13}$$

Eq. A.14 presents the heat transferred from the jacket to the reactor taking into account overall heat transfer coefficients:

$$Q_{pret} = U_C A_{trans} \left(\frac{T_{jacket,in} + T_{jacket,out}}{2} - T_{out} \right) \quad \text{Eq. A.14}$$

A.2. Detoxification

The kinetic models that describe the process of detoxification of the lignocellulosic hydrolysates are the following (Purwadi et al., 2004):

$$r_{fur} = -k_1 C_{fur} (C_{Z,0} - C_{ZA}) + k_2 C_{ZA} \quad \text{Eq. A.15}$$

$$r_{ZA} = -(k_2 + k_3) C_{ZA} + k_1 C_{fur} (C_{Z,0} - C_{ZA}) \quad \text{Eq. A.16}$$

$$r_P = -k_3 C_{ZA} \quad \text{Eq. A.17}$$

With this model, the initial amount of cation $C_{Z,0}$ is related to the pH level, according to the Eq. A.13:

$$C_{Z,0} = k_Z \cdot 10^{-(14-pH)} + C_{Z,0}^N \quad \text{Eq. A.18}$$

Where $C_{Z,0}^N$ is $\text{Ca}(\text{OH})_2$ needed to neutralise the acidic hydrolysates, and k_Z is a constant which serves as a function of solubility of $\text{Ca}(\text{OH})_2$, affinity of the reactants to this ion and other unknown variables. See Purwadi et al., (2004) for the values of the parameters of the model.

$$\frac{dM_{fur}}{dt} = F_{in} w_{hemi}^{in} - F_{out} w_{fur}^{out} + r_{fur} V \quad \text{Eq. A.19}$$

$$\frac{dM_{ZA}}{dt} = F_{in} w_{ZA}^{in} - F_{out} w_{ZA}^{out} + r_{ZA} V \quad \text{Eq. A.20}$$

$$\frac{dM_P}{dt} = F_{in} w_P^{in} - F_{out} w_P^{out} + r_P V \quad \text{Eq. A.21}$$

The energy balance for the detoxification process is presented in Eq. A.21. The heat energy is assumed to be the heat of a neutralization reaction between a strong acid and a strong base:

$$\frac{dU}{dt} = F_{in} h_{in} - F_{out} h_{out} + \left((r_{fur} + r_{ZA} + r_P) (-\Delta H^R) V \right) - Q_{Detox} \quad \text{Eq. A.22}$$

Eq. A.23 presents the heat transferred from the jacket to the reactor taking into account overall heat transfer coefficients using cooling water as utility stream:

$$Q_{Detox} = U_C A_{trans} \left(T_{out} - \frac{T_{jacket,in} + T_{jacket,out}}{2} \right) \quad \text{Eq. A.23}$$

A.3. Evaporation

The evaporation stage is used in the concentration of xylose in the hydrolysate obtained from the pretreatment reaction. The approach considered in this work

consists of a dynamic mass balance, an energy balance and a VLE formulation for the concentration of the components in the vapour phase.

$$\frac{dM_i}{dt} = L_{in} x_i^{in} - L_{out} x_i^{out} - V_{out} y_i^{out} \quad \text{Eq. A.24}$$

$$\frac{dU}{dt} = L_{in} h_{in}^{liq} - L_{out} h_{out}^{liq} - V_{out} h_{out}^{vap} + Q_{Evap} \quad \text{Eq. A.25}$$

$$h_{out}^{vap} = \frac{Q_{Evap}}{\Delta H^{vap}} \quad \text{Eq. A.26}$$

$$y_i^{out} = x_i^{out} K_i \quad \text{Eq. A.27}$$

$i = 1, 2 \dots$ Number of components

Eq. A.28 presents the heat transferred from the jacket to the reactor taking into account overall heat transfer coefficients considering high-pressure steam as the utility of choice:

$$Q_{Evap} = U_C A_{trans} \left(\frac{T_{jacket,in} + T_{jacket,out}}{2} - T_{out} \right) \quad \text{Eq. A.28}$$

A.4. Simultaneous saccharification and co-fermentation (SSCF)

The parameters used in this work for the simulation of both enzymatic hydrolysis and co-fermentation are presented in the works of Kadam et al., (2004) and Leksawasdi et al., (2001).

A.4.1. Saccharification

The kinetic model for the enzymatic hydrolysis proposed by Kadam et al., (2004) is the following:

$$E_{iB} = \frac{E_{imax} K_{iad} E_{iF} C_{cell}}{1 + K_{iad} \cdot E_{iF}} \quad \text{Eq. A.29}$$

$$E_{iT} = E_{iF} + E_{iB} \quad \text{Eq. A.30}$$

$i = 1$ for cellulase; $i = 2$ for β -glucosidase

$$r_1 = \frac{k_1 E_{1B} R_s C_{cell}}{1 + \frac{C_{Cb}}{K_{1.inh.Cb}} + \frac{C_{Gl}}{K_{1.inh.Cb}} + \frac{C_{Xy}}{K_{1.inh.Cb}}} \quad \text{Eq. A.31}$$

$$r_2 = \frac{k_2 (E_{1B} + E_{2B}) R_s C_{cell}}{1 + \frac{C_{Cb}}{K_{2.inh.Cb}} + \frac{C_{Gl}}{K_{2.inh.Cb}} + \frac{C_{Xy}}{K_{2.inh.Cb}}} \quad \text{Eq. A.32}$$

$$r_3 = \frac{k_3 E_{2F} R_s C_{Cb}}{K_{3M} \left(1 + \frac{C_{Gl}}{K_{3.inh.Gl}} + \frac{C_{Xy}}{K_{3.inh.Xy}} \right) + C_{Cb}} \quad \text{Eq. A.33}$$

A variation for hemicellulose conversion into xylose and further degradation into furfural during the enzymatic hydrolysis has been proposed by Ballesteros et al., (2004).

$$r_4 = k_4 C_{hemi} \quad \text{Eq. A.34}$$

$$r_5 = k_5 C_{Xy} \quad \text{Eq. A.35}$$

A.4.2 Simultaneous saccharification and co-fermentation

Equations A.36 to A.42 show the growth rate of the strain from glucose and xylose and the reaction rate for ethanol production from both sugars.

$$r_{X,Gl} = \mu_{max,Gl} \left(\frac{C_{Gl}}{K_{sx,Gl} + C_{Gl}} \right) \left(1 - \frac{C_{Eth} - C_{Eth,ix,Gl}}{C_{Eth,mx,Gl} - C_{Eth,ix,Gl}} \right) \left(\frac{K_{ix,Gl}}{K_{ix,Gl} + C_{Gl}} \right) \quad \text{Eq. A.36}$$

$$r_{X,Xy} = \mu_{max,Xy} \left(\frac{C_{Xy}}{K_{sx,Xy} + C_{Xy}} \right) \left(1 - \frac{C_{Eth} - C_{Eth,ix,Xy}}{C_{Eth,mx,Xy} - C_{Eth,ix,Xy}} \right) \left(\frac{K_{ix,Xy}}{K_{ix,Xy} + C_{Xy}} \right) \quad \text{Eq. A.37}$$

$$r_X = [\alpha r_{X,Gl} + (1 - \alpha) r_{X,Xy}] C_X \quad \text{Eq. A.38}$$

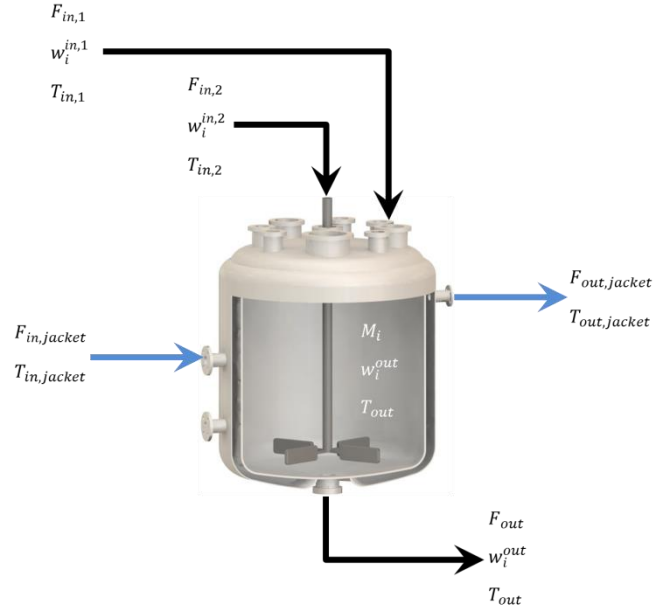


Figure A.2: Scheme of a jacketed reactor used in the formulation of the mass and energy balances

$$r_{Gl} = \alpha q_{S,max,Gl} \left(\frac{C_{Gl}}{K_{SS,Gl} + C_{Gl}} \right) \left(1 - \frac{C_{Eth} - C_{Eth,is,Gl}}{C_{Eth,ms,Gl} - C_{Eth,is,Gl}} \right) \left(\frac{K_{is,Gl}}{K_{is,Gl} + C_{Gl}} \right) C_X \quad \text{Eq. A.39}$$

$$r_{Xy} = (1 - \alpha) q_{S,max,Xy} \left(\frac{C_{Xy}}{K_{SS,Xy} + C_{Xy}} \right) \left(1 - \frac{C_{Eth} - C_{Eth,is,Xy}}{C_{Eth,ms,Xy} - C_{Eth,is,Xy}} \right) \left(\frac{K_{is,Xy}}{K_{is,Xy} + C_{Xy}} \right) C_X \quad \text{Eq. A.40}$$

$$r_{P,Gl} = q_{max,Gl} \left(\frac{C_{Gl}}{K_{Sp,Gl} + C_{Gl}} \right) \left(1 - \frac{C_{Eth} - C_{Eth,ip,Gl}}{C_{Eth,mp,Gl} - C_{Eth,ip,Gl}} \right) \left(\frac{K_{ip,Gl}}{K_{ip,Gl} + C_{Gl}} \right) \quad \text{Eq. A.41}$$

$$r_{P,Xy} = q_{max,Xy} \left(\frac{C_{Xy}}{K_{Sp,Xy} + C_{Xy}} \right) \left(1 - \frac{C_{Eth} - C_{Eth,ip,Xy}}{C_{Eth,mp,Xy} - C_{Eth,ip,Xy}} \right) \left(\frac{K_{ip,Xy}}{K_{ip,Xy} + C_{Xy}} \right) \quad \text{Eq. A.42}$$

$$r_P = [\alpha r_{P,Gl} + (1 - \alpha) r_{P,Xy}] C_X \quad \text{Eq. A.43}$$

Figure A.2 presents the schematic of a jacketed reactor used in the SSCF process. Notice the addition of a second inlet stream in which the inoculum of the fermenting microorganism is fed into the reaction medium. The mass balances are the combination of both the enzymatic saccharification and the co-fermentation for each component as shown below:

Hemicellulose:

$$\frac{dM_{hemi}}{dt} = F_{in,1} w_{hemi}^{in,1} + F_{in,2} w_{hemi}^{in,2} - F_{out} w_{hemi}^{out} + r_5 V \quad \text{Eq. A.44}$$

Xylose:

$$\begin{aligned} \frac{dM_{xy}}{dt} = F_{in,1} w_{xy}^{in,1} + F_{in,2} w_{xy}^{in,2} - F_{out} w_{xy}^{out} \\ + \left((1.136 r_4) - r_5 - r_{xy} \right) V \end{aligned} \quad \text{Eq. A.45}$$

Furfural:

$$\frac{dM_{fur}}{dt} = F_{in,1} w_{fur}^{in,1} + F_{in,2} w_{xy}^{in,2} - F_{out} w_{xy}^{out} + r_5 V \quad \text{Eq. A.46}$$

Cellulose:

$$\frac{dM_{cel}}{dt} = F_{in,1} w_{cel}^{in,1} + F_{in,2} w_{cel}^{in,2} - F_{out} w_{cel}^{out} - (r_1 + r_2) V \quad \text{Eq. A.47}$$

Cellobiose:

$$\frac{dM_{cb}}{dt} = F_{in,1} w_{cb}^{in,1} + F_{in,2} w_{cb}^{in,2} - F_{out} w_{hemi}^{out} + r_5 V \quad \text{Eq. A.48}$$

Glucose:

$$\begin{aligned} \frac{dM_{gl}}{dt} = F_{in,1} w_{gl}^{in,1} + F_{in,2} w_{gl}^{in,2} - F_{out} w_{gl}^{out} \\ + (1.111 r_2 + 1.053 r_3 - r_{gl}) V \end{aligned} \quad \text{Eq. A.49}$$

Ethanol:

$$\frac{dM_{Eth}}{dt} = F_{in,1} w_{Eth}^{in,1} + F_{in,2} w_{Eth}^{in,2} - F_{out} w_{Eth}^{out} + r_P V \quad \text{Eq. A.50}$$

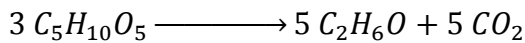
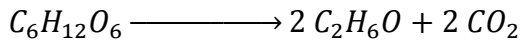
Cells:

$$\frac{dM_X}{dt} = F_{in,1} w_X^{in,1} + F_{in,2} w_X^{in,2} - F_{out} w_X^{out} + r_X V \quad \text{Eq. A.51}$$

Water:

$$\begin{aligned} \frac{dM_W}{dt} = F_{in,1} w_W^{in,1} + F_{in,2} w_X^{in,2} - F_{out} w_X^{out} \\ + (0.055 r_1 + 0.11 r_2 + 1.052 r_3 + 0.333 r_5) V \end{aligned} \quad \text{Eq. A.52}$$

The energy balance is similar to the other reactors in the process. However, the heat of reaction will be taken from the following stoichiometric reaction since the kinetic model does not specify the reactions and the stoichiometry in its formulation:



$$\begin{aligned} \frac{dU}{dt} = F_{in,1} h_{in,1} + F_{in,2} h_{in,2} - L_{out} h_{out} + \left(\sum r_j (-\Delta H^R) \right) V \\ + Q_{SSCF} \end{aligned} \quad \text{Eq. A.53}$$

The equation for the heat transferred from the jacket to the bulk consists of a difference between the average temperature in the jacket and the temperature in the bulk of the reactor.

$$Q_{SSCF} = U_C A_{trans} \left(\frac{T_{jacket,in} + T_{jacket,out}}{2} - T_{out} \right) \quad \text{Eq. A.54}$$

A.5. Distillation column

The distillation column comprises three main sub-units: the tray section, the top and the bottom of the column. The top is also composed by three units: the total condenser in which the vapour coming out from the tray section is completely condensed. The drum is used for the collection of the condensate. The splitter is the unit that serves as a recycle of the distillate. Finally, the reboiler that serves as vapour supplier to increase the mass and energy transfer within the tray section. This unit is a partial reboiler since one liquid stream and one vapour stream are produced. This is also known as a Kettle reboiler.

To solve the set of differential and algebraic equations that describe a tray section, condenser and reboiler in a distillation column, the following assumptions were taken into account since most of them have a negligible contribution in the solution of the system and, as shown in Section 3.7.1, the results were validated against ChemCAD (Chemstations, 2015).

1. Perfect mixing on each tray
2. Vapour holdup is neglected
3. Relative volatility is obtained with a $\gamma - \phi$ formulation
4. No chemical reaction
5. No pressure drop

A.5.1 Tray

For a single tray of the column, the following equations were formulated, according to the scheme shown in Figure A.3:

Mass balance:

$$\frac{dM_{ij}}{dt} = L_{in,j} x_{in,ij} + V_{in,j} y_{in,ij} + F_j z_{ij} - L_{out,j} x_{out,ij} - V_{out,j} y_{out,ij} \quad \text{Eq. A.55}$$

$$M_{ij} = X_{outij} M_{liq} \quad \text{Eq. A.56}$$

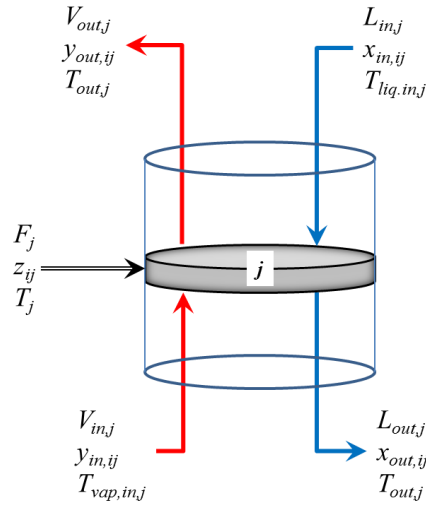


Figure A.3: Schematic of a distillation column tray

$$\sum_{i=1}^{Nc} X_{out,ij} = 1$$

Eq. A.57

$i = 1, 2, \dots$ Number of components $j = 1, 2, \dots$ Number of trays

Energy balance:

$$\frac{dU_j}{dt} = L_{in,j} h_{in,j}^{liq} + V_{in,j} h_{in,j}^{vap} + F_j h_{fj}^{liq} - L_{out,j} h_{out,j}^{liq} - V_{out,j} h_{out,j}^{vap}$$

Eq. A.58

$$U_j = M_{liq} h_{out,j}^{liq}$$

Eq. A.59

$j = 1, 2, \dots$ Number of trays

Vapour-Liquid Equilibrium:

$$y_{out,ij} = k_{ij} x_{out,ij}$$

Eq. A.60

$i = 1, 2, \dots$ Number of components $j = 1, 2, \dots$ Number of trays

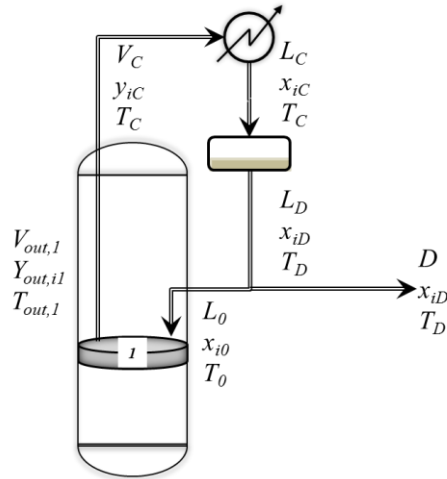


Figure A.4: Flowsheet of the top of the distillation column

Molar overflow:

$$L_{out,j} = L_{in,j} + F_j \quad \text{Eq. A.61}$$

$$V_{out,j} = V_{in,j} \quad \text{Eq. A.62}$$

$i = 1, 2, \dots$ Number of components $j = 1, 2, \dots$ Number of trays

A.5.2 Condenser

The condenser section is divided in three parts: Heat exchanger, drum and splitter. Figure A.4 describes the total condenser, drum and splitter used in this calculation. For the condenser, the vapour stream coming out of the first stage of the distillation column is totally condensed, giving as a result the following set of equations:

$$L_C = V_C \quad \text{Eq. A.63}$$

$$L_C h_C^{liq} + Q_C = V_C h_C^{vap} \quad \text{Eq. A.64}$$

$$x_{i,C} = y_{i,C} \quad \text{Eq. A.65}$$

$i = 1, 2, \dots$ Number of components

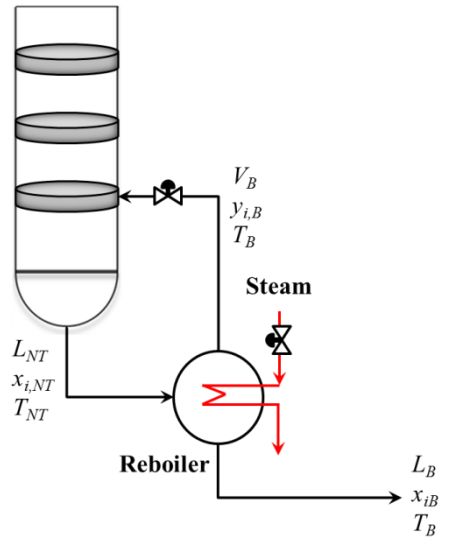


Figure A.5: Schematic of a Kettle reboiler

A.5.3 Drum

In the case of the drum, by using the same mass balance like in the tray section, and implementing the same assumptions, the following equation can be obtained:

$$\frac{dM_{iD}}{dt} = L_C x_{i,C} - L_D x_{iD} \quad \text{Eq. A.66}$$

$$M_{iD} = x_{iD} M_{liq,D} \quad \text{Eq. A.67}$$

$$\frac{dU_D}{dt} = L_C h_C^{liq} - L_D h_D^{liq} \quad \text{Eq. A.68}$$

$$U_D = M_{liq,D} h_D^{liq} \quad \text{Eq. A.69}$$

For the splitter and according to Figure A.2, the only equation considered is the reflux ratio defined by:

$$R = \frac{L_0}{D} \quad \text{Eq. A.70}$$

A.5.4 Reboiler

The reboiler has the same mathematical treatment as a single tray, except that this does not include an inlet vapour stream. The following equations are based on Figure A.5:

Mass balance:

$$\frac{dM_{iB}}{dt} = L_{NT} x_{NTj} - L_B x_{iB} - V_B y_{iB} \quad \text{Eq. A.71}$$

$$M_{iB} = x_{iB} M_{liq} \quad \text{Eq. A.72}$$

$$\sum_{i=1}^{NC} x_{iB} = 1 \quad \text{Eq. A.73}$$

$i = 1, 2, \dots$ Number of components

Energy balance:

$$\frac{dU_B}{dt} = L_{NT} h_{NT}^{liq} - L_B h_B^{liq} - V_B h_B^{vap} + Q_R \quad \text{Eq. A.74}$$

$$U_j = M_{liq} h_j^{liq} \quad \text{Eq. A.75}$$

Vapour-Liquid Equilibrium:

$$y_{iB} = K_{iB} x_{iB} \quad \text{Eq. A.76}$$

$i = 1, 2, \dots$ Number of components

Molar overflow:

$$L_{NT} = L_B + V_B \quad \text{Eq. A.77}$$

A.5.5 Tray section

Additional equations are required in the simulation and modelling of distillation systems with multiple trays. These equations allow connectivity between two trays inside the column and the different compositions and temperatures therein.

The liquid stream:

$$L_{in,j} = L_{out,j-1} \quad \text{Eq. A.78}$$

$$x_{in,ij} = x_{out,ij-1} \quad \text{Eq. A.79}$$

$$T_{liq,in} = T_{out,j-1} \quad \text{Eq. A.80}$$

The vapour stream:

$$V_{in,j} = V_{out,j+1} \quad \text{Eq. A.81}$$

$$y_{in,ij} = y_{out,ij+1} \quad \text{Eq. A.82}$$

$$T_{vap,in} = T_{out,j+1} \quad \text{Eq. A.83}$$

The following equations show the connections of the streams being recycled into the column and the other units in the distillation system (i.e. condenser and reboiler). Eq. A.84 to A.86 connect the outlet stream of the drum with reflux stream into the column.

$$L_D = L_0 + D \quad \text{Eq. A.84}$$

$$x_{i0} = x_{iD} \quad \text{Eq. A.85}$$

$$T_0 = T_D \quad \text{Eq. A.86}$$

Equations A.87 to A.89 connect the outlet stream of the splitter with the inlet liquid stream of the first tray of the column.

$$L_0 = L_{in,1} \quad \text{Eq. A.87}$$

$$x_{i0} = x_{in,i1} \quad \text{Eq. A.88}$$

$$T_0 = T_{liq,in,1} \quad \text{Eq. A.89}$$

Similarly, equations A.90 to A.92 connect the vapour outlet stream from the first tray with the inlet vapour stream of the condenser.

$$V_{out,1} = V_C \quad \text{Eq. A.90}$$

$$y_{out,i1} = y_{iC} \quad \text{Eq. A.91}$$

$$T_{out,1} = T_C \quad \text{Eq. A.92}$$

Other equations are required for the connection between the bottom of the column and the reboiler. These equations are the following:

$$L_{out,NT} = L_{NT} \quad \text{Eq. A.93}$$

$$x_{out,iNT} = x_{iNT} \quad \text{Eq. A.94}$$

$$T_{out,NT} = T_{NT} \quad \text{Eq. A.95}$$

$$V_{in,NT} = V_B \quad \text{Eq. A.96}$$

$$y_{in,iNT} = y_{iB} \quad \text{Eq. A.97}$$

$$T_{in,NT} = T_B \quad \text{Eq. A.98}$$

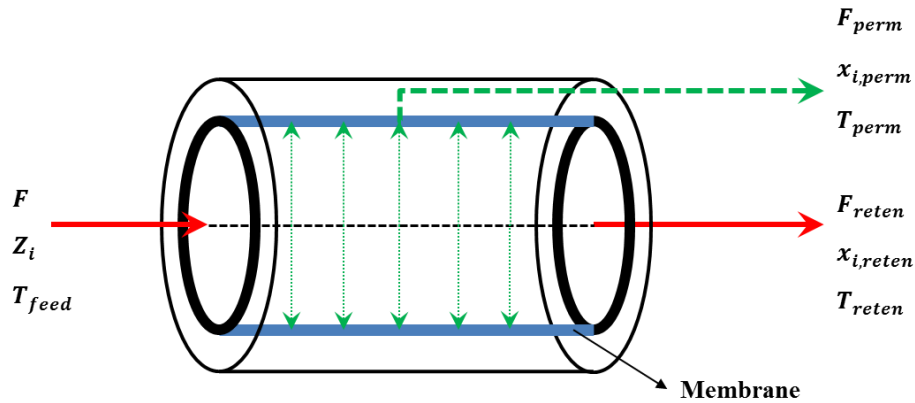


Figure A.6: Schematic of the membrane module (Marriott and Sorensen, 2003; Marriott et al., 2001; Tsuyumoto et al., 1997)

$$\frac{V_{j+1}}{L_B} = R_B \quad \text{Eq. A.99}$$

A.6. Membrane system

In this work, a membrane model is considered for the ethanol dehydration. The product from a simple distillation column reaches the azeotropic point, which at atmospheric pressure is around 94 % (w/w). The selective membrane removes the water by the principle of concentration gradient. In this case study, the model is described as a fibre-side fed co-current model. The module is composed by three sub-units: The fibre side, in which the inlet stream is fed and the shell side, which uses an inert gas or vacuum to remove the water. Finally, the membrane model is represented by the principle of Fick's law of mass transfer due to the concentration gradient. The scheme of the membrane system is shown in Figure A.6.

A.6.1. Fibre side

The fibre side is where the feed stream is passed through and separated into retentate and permeate. The mass balance for each component includes the inlet and outlet streams and the flux through the membrane. In similar way, the energy balance depicts the energy flows in the system with the particularity of considering the heat of vaporisation of the mix which is responsible for the decrease of the feed temperature.

$$\frac{dM_i}{dt} = F Z_i - F_{reten} x_{i,reten} - A_{mem} J_i \quad \text{Eq. A.100}$$

$$M_i = x_{i,reten} M_t \quad \text{Eq. A.101}$$

$$\frac{dU}{dt} = F h_{feed} - F_{reten} h_{reten}^{liq} - A_{mem} J H^J \quad \text{Eq. A.102}$$

$$U = u_{reten}^{liq} M_t \quad \text{Eq. A.103}$$

A.6.2 Shell side

The balances applied to this part of the system are similar to those described in equations A.79 to A.82, except that the terms $A_{mem} J_i$ and $A_{mem} J H^J$ are positive because vapour is permeating through the membrane into the permeate stream.

$$\frac{dM_i}{dt} = F Z_i - F_{perm} x_{i,perm} + A_{mem} J_i \quad \text{Eq. A.104}$$

$$M_i = x_{i,perm} M_t \quad \text{Eq. A.105}$$

$$\frac{dU}{dt} = -F_{perm} h_{perm}^{vap} + A_{mem} J H^J \quad \text{Eq. A.106}$$

$$U = u_{reten}^{vap} M_t \quad \text{Eq. A.107}$$

In this work, the mathematical model that describes the dehydration of ethanol in the pervaporation system was introduced by Tsuyumoto et al., (1997). This model considers the permeation of water and ethanol through the membrane taking into account operating conditions such as feed temperature, feed concentration and permeate pressure.

$$J_{Ethanol} = 1.72 \times 10^{-10} x_{Ethanol} (P_{feed} - P_{permeate}) \quad \text{Eq. A.108}$$

$$\begin{aligned}
J_{water} = & \frac{8.086 \times 10^6 \text{ EXP} \left(-\frac{11500}{T} \right)}{\delta_m} \left(y_{feed} x_{water} - \frac{P_{permeate}}{P_{Water}^{sat}} y_{water} \right) \\
& + \frac{3.441 \times 10^{-3} \text{ EXP} \left(-\frac{3390}{T} \right)}{2\delta_m} \left((y_{feed} x_{water})^2 \right. \\
& \left. - \left(\frac{P_{permeate}}{P_{Water}^{sat}} y_{water} \right)^2 \right)
\end{aligned}
\tag{Eq. A.109}$$

where:

- F : Feed flow rate (kg/sec)
- H^J : Enthalpy of permeate (J/kg)
- h : Enthalpy (J/kg)
- J_i : Flux of component i (kg. m⁻². s⁻¹)
- h : Enthalpy (J/kg)
- K_{ij} : Relative volatility
- L : Liquid flow rate (kg/sec)
- M_i : Liquid holdup of component i (kg)
- M_t : Total liquid holdup (kg)
- P_{feed} : Feed pressure (Pa)
- P_{perm} : Permeate pressure (Pa)
- Q_C : Heat released in the condenser (J/kg)
- Q_B : Heat duty in the reboiler (J/kg)
- R : Reflux ratio
- R_B : Boilup ratio
- u : Specific internal energy (J/kg)
- U : Internal energy (J)

- V : Vapour flow rate (kg/sec)
- X_{ij} : Liquid mass fraction of component i in tray j
- x_i : Liquid mole fraction of component i
- Y_{ij} : Vapour mass fraction of component i in tray j
- y_i : Vapour mole fraction of component i
- Z_{ij} : Feed mass fraction of component i in tray j